

This document was produced
by scanning the original publication.

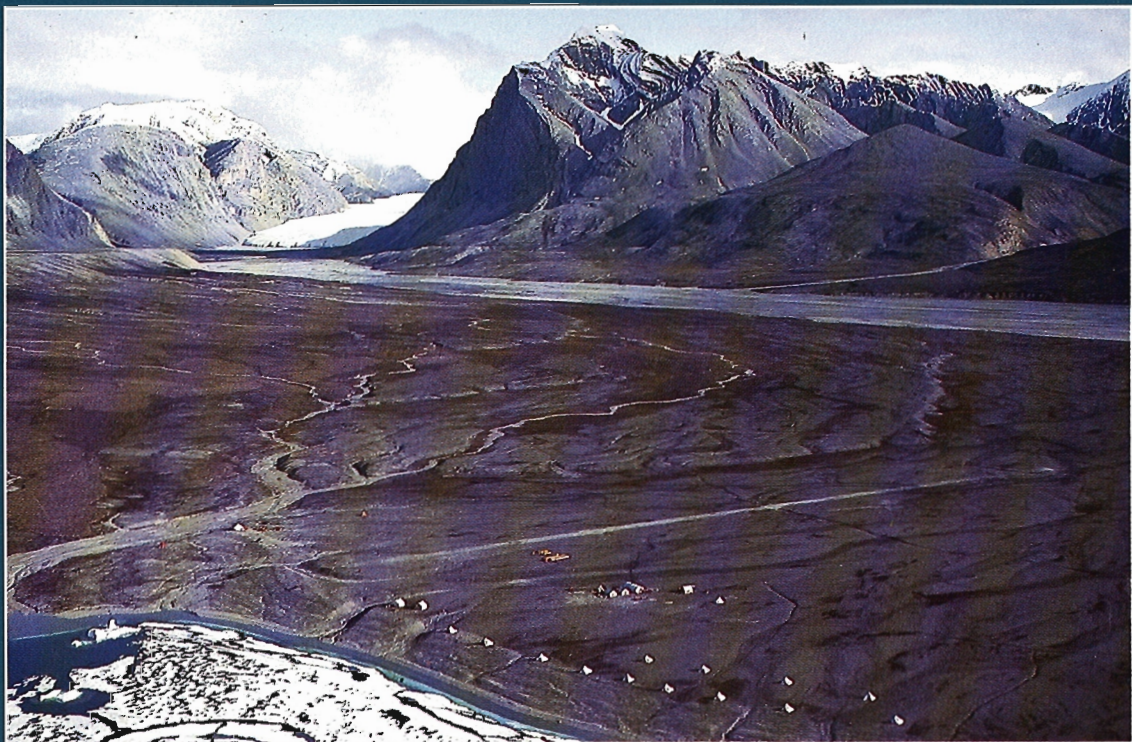
Ce document est le produit d'une
numérisation par balayage
de la publication originale.



**GEOLOGICAL SURVEY OF CANADA
COMMISSION GÉOLOGIQUE DU CANADA**

**CURRENT RESEARCH 1995-B
INTERIOR PLAINS AND ARCTIC CANADA**

**RECHERCHES EN COURS 1995-B
PLAINES INTÉRIEURES ET RÉGION
ARCTIQUE DU CANADA**



1995



Natural Resources Canada
Ressources naturelles Canada

Canada

GEOLOGICAL SURVEY OF CANADA
COMMISSION GÉOLOGIQUE DU CANADA

CURRENT RESEARCH 1995-B
INTERIOR PLAINS AND ARCTIC CANADA

RECHERCHES EN COURS 1995-B
PLAINES INTÉRIEURES ET RÉGION
ARCTIQUE DU CANADA

1995

©Minister of Energy, Mines and Resources Canada 1995

Available in Canada from

Geological Survey of Canada offices:

601 Booth Street
Ottawa, Canada K1A 0E8

3303-33rd Street N.W.,
Calgary, Alberta T2L 2A7

100 West Pender Street
Vancouver, B.C. V6B 1R8

or from

Canada Communication Group - Publishing
Ottawa, Canada K1A 0S9

and through authorized bookstore agents
and other bookstores

A deposit copy of this publication is also available for reference
in public libraries across Canada

Cat. No. M44-1995/3E
ISBN 0-660-15810-8

Price subject to change without notice

Cover description

Silicified pillow basalt, semi-conformable alteration zone, near Spi Lake, Kaminak Lake map area (55L/4), Northwest Territories. See report in this volume by Miller and Tella. (Photo by A.R. Miller; GSC 1994-791).

Description de la photo couverture

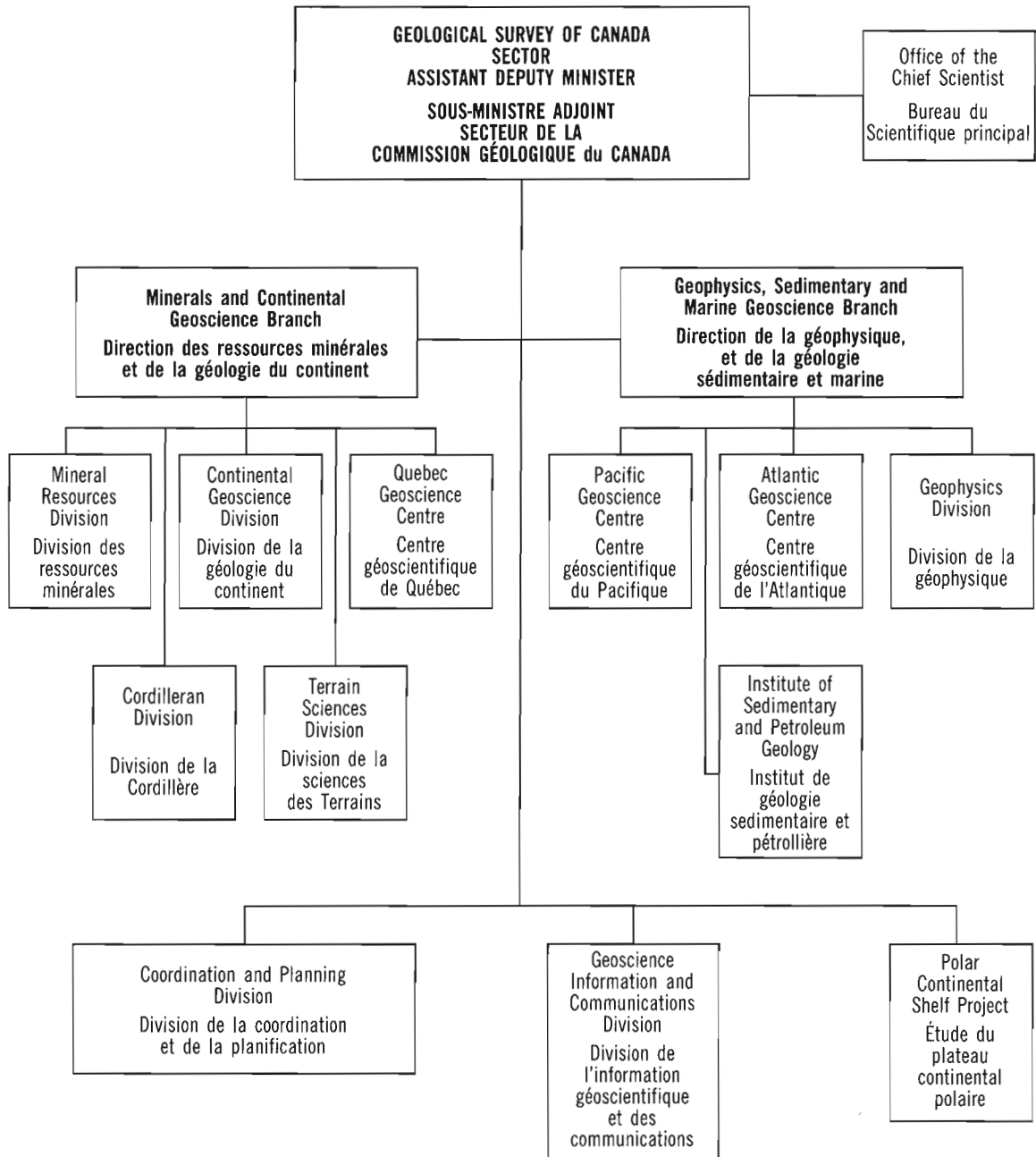
Basalte en coussin silicifié, zone d'altération semi-concordante, près du lac Spi, région cartographique du lac Kaminak (55L/4), Territoires du Nord-Ouest. Voir le rapport de Miller et Tella dans ce volume. (Photo prise par A.R. Miller; GSC 1994-791).

ERRATUM

Current Research 1995-C

The caption for Figure 1 on page 78 in the report by J.B. Henderson and T. Chacko was omitted. The caption is:

Figure 1. Geology of the southwestern Slave Province showing the location of the Paleoproterozoic uplift as expressed by the aeromagnetic anomaly pattern. The uplift has resulted in the exposure of unusually high metamorphic grade Archean rocks at the present erosion level. Geology modified after McGlynn (1977), Hoffman and Hall (1993), and Stubbley et al., (1994).



Separates

A limited number of separates of the papers that appear in this volume are available by direct request to the individual authors. The addresses of the Geological Survey of Canada offices follow:

601 Booth Street
OTTAWA, Ontario
K1A 0E8
(FAX: 613-996-9990)

Institute of Sedimentary and Petroleum Geology
3303-33rd Street N.W.
CALGARY, Alberta
T2L 2A7
(FAX: 403-292-5377)

Cordilleran Division
100 West Pender Street
VANCOUVER, B.C.
V6B 1R8
(FAX: 604-666-1124)

Pacific Geoscience Centre
P.O. Box 6000
9860 Saanich Road
SIDNEY, B.C.
V8L 4B2
(Fax: 604-363-6565)

Atlantic Geoscience Centre
Bedford Institute of Oceanography
P.O. Box 1006
DARTMOUTH, N.S.
B2Y 4A2
(FAX: 902-426-2256)

Québec Geoscience Centre
2700, rue Einstein
C.P. 7500
Ste-Foy (Québec)
G1V 4C7
(FAX: 418-654-2615)

When no location accompanies an author's name in the title of a paper, the Ottawa address should be used.

Tirés à part

On peut obtenir un nombre limité de «tirés à part» des articles qui paraissent dans cette publication en s'adressant directement à chaque auteur. Les adresses des différents bureaux de la Commission géologique du Canada sont les suivantes:

601, rue Booth
OTTAWA, Ontario
K1A 0E8
(facsimilé : 613-996-9990)

Institut de géologie sédimentaire et pétrolière
3303-33rd St. N.W.,
CALGARY, Alberta
T2L 2A7
(facsimilé : 403-292-5377)

Division de la Cordillère
100 West Pender Street
VANCOUVER, British Columbia
V6B 1R8
(facsimilé : 604-666-1124)

Centre géoscientifique du Pacifique
P.O. Box 6000
9860 Saanich Road
SIDNEY, British Columbia
V8L 4B2
(facsimilé : 604-363-6565)

Centre géoscientifique de l'Atlantique
Institut océanographique Bedford
B.P. 1006
DARTMOUTH, Nova Scotia
B2Y 4A2
(facsimilé : 902-426-2256)

Centre géoscientifique de Québec
2700, rue Einstein
C.P. 7500
Ste-Foy (Québec)
G1V 4C7
(facsimilé : 418-654-2615)

Lorsque l'adresse de l'auteur ne figure pas sous le titre d'un document, on doit alors utiliser l'adresse d'Ottawa.

CONTENTS

Geological map of Carboniferous and Permian units on Hvitland Peninsula and adjacent areas, northwestern Ellesmere Island, Arctic Canada U. Mayr, J.C. Harrison, and B. Beauchamp	1
Preliminary observations on the structural geology of Hvitland Peninsula, northwestern Ellesmere Island, Arctic Canada J.C. Harrison, U. Mayr, and B. Beauchamp	9
Carboniferous and Permian stratigraphic sequences on Hvitland Peninsula and adjacent areas, northwestern Ellesmere Island, Arctic Canada B. Beauchamp, U. Mayr, and J.C. Harrison	19
Serpukhovian and Bashkirian (Carboniferous) stratigraphy (Borup Fiord and Otto Fiord formations; Unit C1), Hvitland Peninsula and adjacent areas, northwestern Ellesmere Island, Arctic Canada P. Thériault, B. Beauchamp, J.C. Harrison, U. Mayr, and R. Steel	29
Moscovian (Upper Carboniferous) to Sakmarian (Lower Permian) stratigraphy (Nansen and Hare Fiord formations; Unit C2), Hvitland Peninsula, northwestern Ellesmere Island, Arctic Canada B. Beauchamp, C.T. Sherry, U. Mayr, J.C. Harrison, and A. Desrochers	37
Artinskian-Kungurian (Lower Permian) stratigraphy (Raanes, Great Bear Cape, and Trappers Cove formations), Hvitland Peninsula and adjacent areas, northwestern Ellesmere Island, Arctic Canada M.P. Kells, B. Beauchamp, and A. Desrochers	47
Ufimian-Kazanian (Lower and Upper Permian) stratigraphy (Van Hauen and Degerbøls formations), Hvitland Peninsula and adjacent areas, northwestern Ellesmere Island, Arctic Canada A. Desrochers and B. Beauchamp	57
Uppermost Permian stratigraphy (Unit P6), Hvitland Peninsula and adjacent areas, northwestern Ellesmere Island, Arctic Canada B. Beauchamp, U. Mayr, J.C. Harrison, and A. Desrochers	65
Establishing the chronology of snow and pollen deposition events on Agassiz Ice Cap (Ellesmere Island, Northwest Territories) from autostation records B.T. Alt and J.C. Bourgeois	71

Estimates of methane hydrate volumes in the Beaufort-Mackenzie region, Northwest Territories S.L. Smith and A.S. Judge	81
Field measurements of n-factors for natural forest areas, Mackenzie Valley, Northwest Territories A.E. Taylor	89
Active layer monitoring in natural environments, lower Mackenzie Valley, Northwest Territories F.M. Nixon, A.E. Taylor, V.S. Allen, and F. Wright	99
Cretaceous and Tertiary fossils discovered in kimberlites at Lac de Gras in the Slave Province, Northwest Territories W.W. Nassichuk and D.J. McIntyre	109
Thermal history and petrology of wood and other organic inclusions in kimberlite pipes at Lac de Gras, Northwest Territories L.D. Stasiuk and W.W. Nassichuk	115
Mineral occurrences in Middle Devonian carbonates, Salt River and Stony Islands (Slave River) areas, northeastern Alberta M.R. McDonough and H.J. Abercrombie	125
Recent and late Holocene sand dune activity in southwestern Saskatchewan S.A. Wolfe, D.J. Huntley, and J. Ollerhead	131
A preliminary assessment of remote sensing as a tool for mapping surficial sediments in the southern Canadian Prairies A. Blais, W.R. Stevens, D.F. Graham, and V.H. Singhroy	141
Stress orientation indicators (neotectonic plucking fractures) in bedrock of glacier forefields, southeastern Cordillera, western Canada J.S. Bell and G.H. Eisbacher	151

Geological map of Carboniferous and Permian units on Hvitland Peninsula and adjacent areas, northwestern Ellesmere Island, Arctic Canada

U. Mayr, J.C. Harrison, and B. Beauchamp

Institute of Sedimentary and Petroleum Geology, Calgary

Mayr, U., Harrison, J.C., and Beauchamp, B., 1995: Geological map of Carboniferous and Permian units on Hvitland Peninsula and adjacent areas, northwestern Ellesmere Island, Arctic Canada; in Current Research 1995-B; Geological Survey of Canada, p. 1-7.

Abstract: During the 1994 field season, Carboniferous and Permian, and to a lesser extent, Triassic and Cretaceous-Tertiary formations and units were mapped in the northern part of Ellesmere Island. About 20 map units, ranging from shallow-water carbonates to basinal shale and chert, were identified. The map area is characterized by a large number of thrusts with a diminishing amount of shortening from west to east.

Résumé : Au cours de la campagne 1994 sur le terrain, les formations et les unités du Carbonifère et du Permien et, dans une moindre mesure, du Trias et du Crétacé-Tertiaire, ont été cartographiées dans le nord de l'île d'Ellesmere. Environ 20 unités cartographiques, allant de roches carbonatées d'eau peu profonde à des shales et chert de bassin, ont été identifiées. La région cartographique se caractérise par un grand nombre de chevauchements avec diminution du raccourcissement d'ouest en est.

INTRODUCTION

The map area is situated on Hvitland Peninsula, part of northwestern Ellesmere Island, and straddles the area shown on topographic mapsheets of Otto Fiord (340 C) and Cape Stallworthy (560 D) (Fig. 1, 2). For the past four years, the Geological Survey of Canada has been investigating the upper Paleozoic stratigraphy and the structure of Hvitland Peninsula and adjacent areas of northwestern Ellesmere Island. Helicopter supported field work, carried out from a base camp at the north shore of Otto Fiord, was conducted in 1991, 1992 and 1994. The field activity revolved around two main programs: the basin analysis of the northeastern part of the hydrocarbon-prone Sverdrup Basin; and as a later phase, the mapping and structural interpretation of the bedrock geology. Over 70 stratigraphic sections were measured and examined by various GSC officers, university graduate students and their professors, and industry experts, including a contingent of specialists from Norway, where strata identical to those of the Sverdrup Basin are currently being explored for oil and gas in the Barents Sea. The area straddles a region of very complex and very well exposed facies changes. In the western Arctic Islands, on the Barents Shelf and probably in other areas, these facies changes are associated with major hydrocarbon potential.

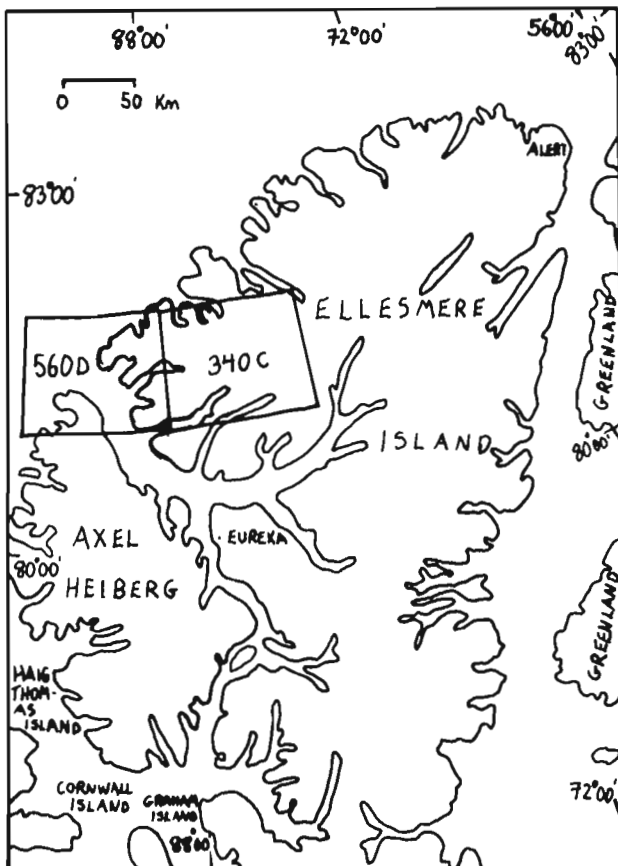


Figure 1. Index map, showing the outline of the 1:250 000 mapsheets (560 D and 340 C).

The GSC-lead effort on northwestern Ellesmere Island resulted in a great variety of collaborative studies, the most significant of which include: paleontological studies by C.M. Henderson (University of Calgary), A. Baude (Musée cantonal de Géologie, Lausanne, Switzerland), I. Nilsson (Saga Petroleum, Harstad, Norway), A. Lønøy (Norsk Hydro, Harstad, Norway), B. Lepage (University of Alberta, Edmonton), E.W. Bamber, J. Utting, R. Lin, S. Pinard, and W.W. Nassichuk (Institute of Sedimentary and Petroleum Geology); sedimentological studies by P. Thériault, R.L. Steel (Geological Institute, University of Bergen, Norway), A. Desrochers, M.P. Kells, C.T. Sherry, K. Besemann (University of Ottawa), G. Elvebakk (Saga Petroleum, Harstad, Norway), F. Brunton and N.P. James (Queen's University, Kingston); geochemical and diagenetic studies by M. Savard (Centre géoscientifique de Québec) and F. Mutunguti (University of Ottawa); fission track analyses by D. Arne (Dalhousie University, Halifax); structural geology and mapping by U. Mayr and J.C. Harrison (Institute of Sedimentary and Petroleum Geology); and stratigraphic studies by H.P. Trettin, A.F. Embry and B. Beauchamp (Institute of Sedimentary and Petroleum Geology).

The findings have changed the way one should envision the geology of this area. This quantum leap in our understanding is best expressed by the production of a new map of the area, one that contains over 15 different units, the distribution of which provides evidence for a complex stratigraphic and structural history that spans the greater portion of the Phanerozoic.

This paper introduces a series of eight reports that summarize the geological discoveries made on northwestern Ellesmere Island over the last four years. Other papers in the series deal with the structural geology of the area (Harrison et al., 1995), the Carboniferous and Permian stratigraphic sequences in general (Beauchamp et al., 1995a), and individual depositional sequences (Thériault et al., 1995; Beauchamp et al., 1995b, c; Kells et al., 1995; Desrochers et al., 1995).

Until the present investigation, the area was poorly known and the available A-series geological maps did not portray the unique features of the area. Previously available geological maps in the area comprise maps of Cape Stallworthy and Otto Fiord (1305A and 1309A in Thorsteinsson, 1974) and Open File maps by Trettin and Mayr (1981). A-series maps detailing the geology of the Cambrian to Silurian units are at present in preparation (Trettin, pers. comm., 1994). Thorsteinsson's maps of the areas north of Otto Fiord are of reconnaissance nature only, while Trettin and Mayr's open file map covers the upper Paleozoic succession only in the extreme north-eastern corner of the Otto Fiord map area.

Hvitland Peninsula lies between Otto and Emma fiords. The west end of the peninsula extends into Nansen Sound and faces the northernmost portion of Axel Heiberg Island. The eastern boundary of the investigated area includes Otto Glacier, a major tidewater icestream draining an extensive unnamed icecap to the east. Land lying north of the head of Otto Fiord is mountainous and, at higher elevations, includes icefields, valley glaciers and classic alpine scenery. This part of the report area is underlain by carbonate formations and local

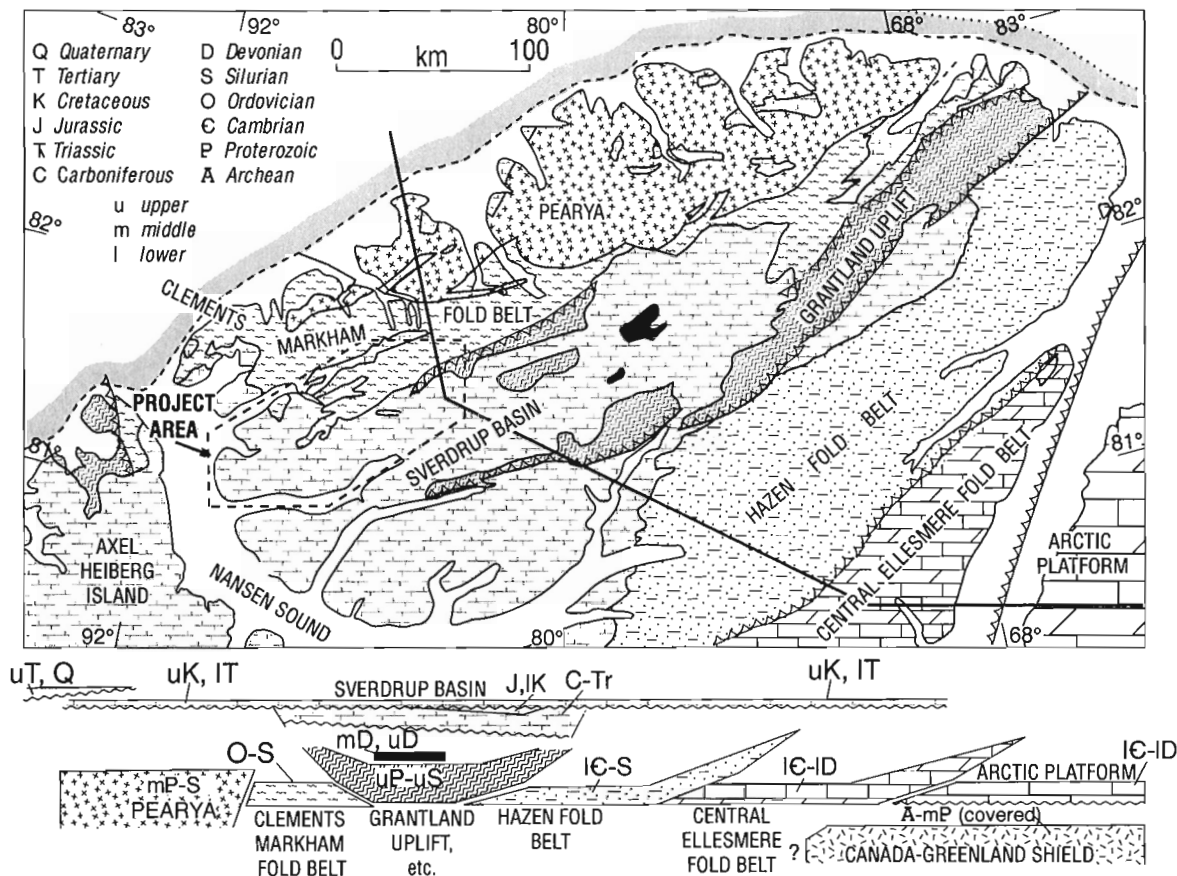


Figure 2. The geological provinces of northern Ellesmere and Axel Heiberg islands and the location of the Hvitland Peninsula map area (adapted from Okulitch, 1991; Okulitch and Trettin, 1991; Trettin, 1994). The geological contacts have been projected locally through onland ice cover.

relief exceeds 1200 m (Fig. 3). As relief on the peninsula diminishes progressively to the west, lower mountain ranges, free of ice cover, give way to felsenmeer-covered hills and sparsely-vegetated valleys mantled in glaciofluvial gravels. Shaly units dominate in the westernmost part of the area and the area of Hvitland Peninsula adjacent to Jugeborg Fiord consists of wide plains devoid of outcrops. Because of open water in Nansen Sound during the summer, the westernmost part of Hvitland Peninsula is under fog or low clouds during most of that time.

GEOLOGICAL SETTING

Geological provinces within the northernmost part of Canada’s Arctic Islands (Fig. 2) include: the Archean and Proterozoic Canada-Greenland shield to the southeast, which underlies continuous cover of undeformed lower Paleozoic strata; accreted terrains of Pearya to the north; intensely tectonized strata of the lower Paleozoic Franklinian Mobile Belt; and Lower Carboniferous to Paleogene strata of the Sverdrup Basin. All the provinces were, more or less, involved in the Eureka Orogeny and the related Tertiary convergence of



Figure 3. Northeast-trending valley just north of the head of Otto Fiord. Very dark grey-green Triassic shale with extensive sills is overthrust from the right (southeast) by dark grey, thin bedded limestone of the Hare Fiord Formation, and from the left (northwest) by massive, light grey limestone of the Nansen Formation. Elevation differences on the photo are in the order of 800 m.

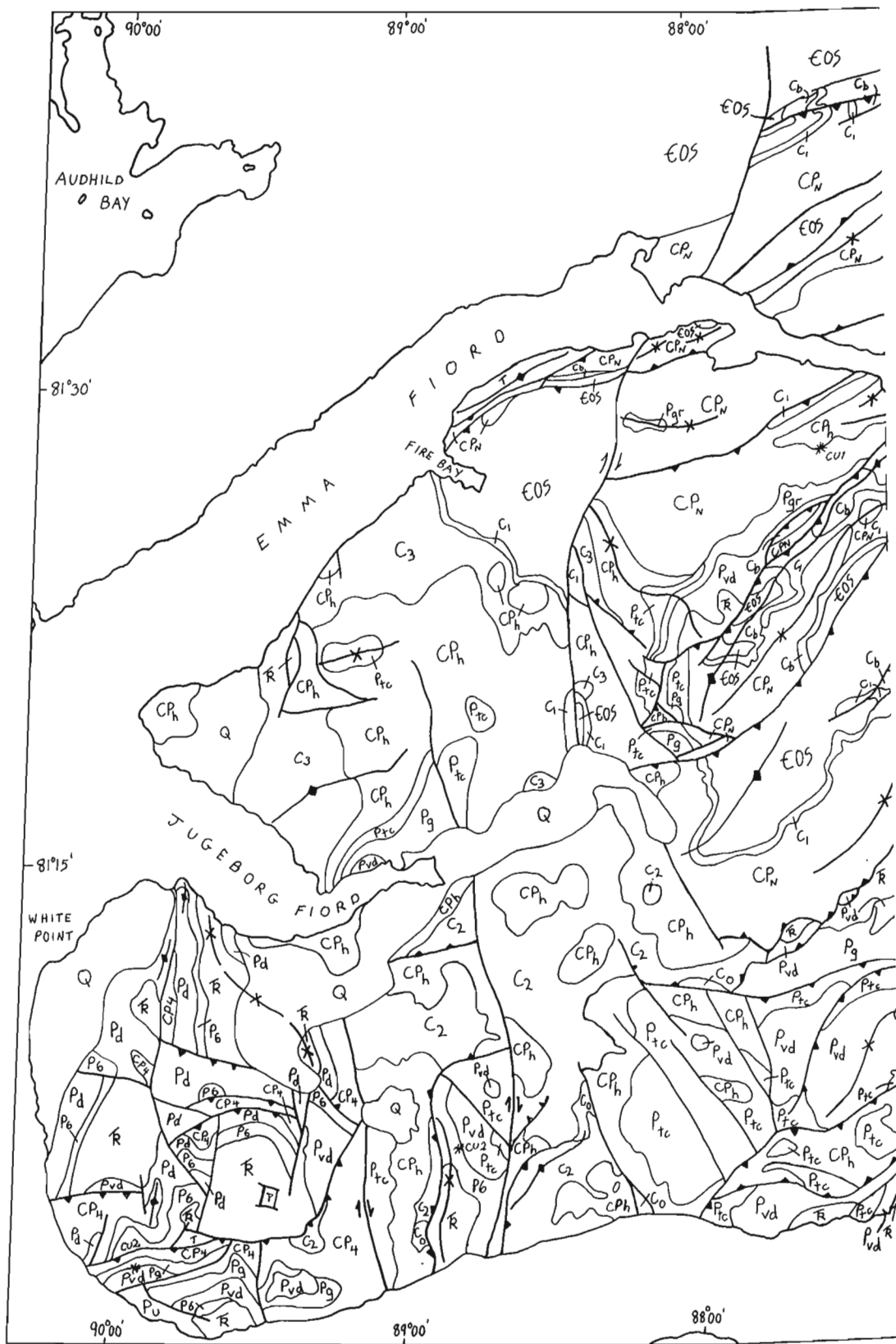


Figure 4. Simplified geological map of Hvitland Peninsula and adjacent areas.



Map units (Fig. 4)

- Q** Unconsolidated fluvial and glacial gravel and dirt
- T** Western Hvitland Peninsula: Paleocene coal, sand and sandstone, shale; south coast of Emma Fiord: Eocene(?) cobble conglomerate, underlain by Paleocene-Eocene sandstone and shale
- TR** Undivided Triassic unit: mostly Blind Fiord Formation, the highest formation is the Hoyle Bay Formation (Embry, 1991)
- P6** Unnamed Permian unit: best developed, though discontinuously, in the western part of the map area, very dark grey and brown chert and minor shale
- P5** Unnamed Permian unit in the northeastern part of the map area: carbonates and sandstone
- Pd** Degerbøls Formation on western Hvitland Peninsula: in that particular area the van Hauen Formation has been included in map unit CP4
- Pvd** Degerbøls and van Hauen formations, undivided
- Pg** Great Bear Cape Formation
- Pgr** Great Bear Cape and Raanes formations, undivided
- Ptc** Trappers Cove Formation
- Pu** Undivided Permian formations (P6 to Trappers Cove Formation): the stratigraphy is too detailed for the map's scale; the unit is present only at the southwestern coast of Hvitland Peninsula
- CPn** Nansen Formation
- CPh** Hare Fiord Formation
- CP4** Unnamed Carboniferous and Permian unit on western Hvitland Peninsula: includes equivalents of the van Hauen, Trappers Cove and Hare Fiord formations, where these units cannot be distinguished
- C3** Unnamed Carboniferous carbonate unit north of Jugeborg Fiord: probably correlative with the lower part of Nansen Formation
- C2** Unnamed Carboniferous carbonate unit on the Hvitland Peninsula ("Televak Limestone")
- Co** Otto Fiord Formation
- C1** Unnamed Carboniferous carbonate and evaporite unit: probably correlative with the Otto Fiord Formation
- Cb** Borup Fiord Formation
- COS** Cambrian to Silurian basement, undivided: includes intrusive rocks of Devonian(?) age

Copper mineralization

- *cu1** Malachite staining and disseminated copper sulphides in bivalve coquina of the Nansen Formation
- *cu2** Malachite spotting and disseminated copper sulphides in the highest limestone beds (crinoidal grainstone) of Degerbøls Formation. Small amounts of malachite are also common elsewhere in the Degerbøls Formation

Canada with northern Greenland (Okulitch and Trettin, 1991). Thick post-orogenic Neogene and Quaternary strata are assumed to exist in offshore areas to the northwest.

A profound angular unconformity exists throughout northern Ellesmere and Axel Heiberg islands and separates Devonian and older rocks below from Lower Carboniferous and younger strata above. The geology of the older succession (referred to as the "basement" in this account) is complex and beyond the scope of the present study. However, a few comments will provide the reader with some understanding of the tectonic fabric that has influenced the orientation and distribution of younger rocks and structures within the project area.

The Franklinian Mobile Belt embraces four major structural regions. From southeast to northwest on Ellesmere Island these regions are: 1) Lower Cambrian to Silurian shelf-associated strata of the Central Ellesmere fold belt, transported to the southeast over age- and facies-equivalent strata of the Arctic Platform; 2) Lower Cambrian through Silurian basin facies strata (part of the Hazen Fold Belt, Trettin, 1994) transported to the southeast over correlative shelf deposits; 3) a central high (including the Grantland Uplift) featuring extensive exposures of Upper Proterozoic, Lower Cambrian and some younger strata thrust over adjacent belts located both to the southeast and northwest; and 4) a belt of lower Paleozoic basin facies strata and volcanic rocks (embracing part of Clements Markham Fold Belt), the youngest portions of which unconformably overlie the accreted Pearya composite terrane. Although some uncertainty exists as to the relative importance of pre-middle Carboniferous thrusting versus strike slip within the lower Paleozoic succession, it is apparent that the dominant sub-Carboniferous fabric strikes mostly between N55°E and N85°E, and that portions of both the central high and basinal-volcanic belt underlie the Carboniferous and younger succession within the Hvitland Peninsula region. It is equally apparent that either a major fault or fold belt re-entrant within the lower Paleozoic succession must underlie either western Hvitland Peninsula or Nansen Sound, or both, because lower Paleozoic strata on northern Axel Heiberg Island strike approximately N50°W.

Other tectonic events and features that have influenced the predominantly Tertiary (Eurekan) structural fabric within the report area include: extension-related structures associated with Carboniferous and Permian rifting of the Sverdrup Basin; the Tanquary High (Maurel, 1989) and related tectonic adjustments associated with the end of rifting in the mid- to late Permian; and gabbro dyke emplacement associated with Cretaceous igneous activity on the submerged and abandoned Alpha Ridge spreading centre (Embry and Osadetz, 1988).

Mapping during the present investigation concentrated on the distribution and deformation of the Carboniferous and Permian units. A simplified version of the results of the new mapping is given in Figure 4. The simplification consists of a combination of related map units and a selective depiction of dominant structural features. Some of the mapping is tentative and is awaiting confirmation from biostratigraphic collections. Details of stratigraphy and structure of the map area are contained elsewhere in this volume.

ACKNOWLEDGMENTS

Figure 4 was compiled and drafted by S. Levson.

REFERENCES

- Beauchamp, B., Mayr, U., and Harrison, J.C.**
1995a: Carboniferous and Permian stratigraphic sequences on Hvitland Peninsula and adjacent areas, northwestern Ellesmere Island, Arctic Canada; *in* Current Research 1995-B; Geological Survey of Canada, this volume.
- Beauchamp, B., Mayr, U., Harrison, J.C., and Desrochers, A.**
1995b: Uppermost Permian stratigraphy (Unit P6), Hvitland Peninsula and adjacent areas, northwestern Ellesmere Island, Arctic Canada; *in* Current Research 1995-B; Geological Survey of Canada, this volume.
- Beauchamp, B., Sherry, C.T., Mayr, U., Harrison, J.C., and Desrochers, A.**
1995c: Moscovian (Upper Carboniferous) to Sakmarian (Lower Permian) stratigraphy (Nansen and Hare Fiord formations; Unit C2), Hvitland Peninsula and adjacent areas, northwestern Ellesmere Island, Arctic Canada; *in* Current Research 1995-B; Geological Survey of Canada, this volume.
- Desrochers, A. and Beauchamp, B.**
1995: Ufimian-Kazanian (Lower and Upper Permian) stratigraphy (Van Hauen and Degerbøls formations), Hvitland Peninsula and adjacent areas, northwestern Ellesmere Island, Arctic Canada; *in* Current Research 1995-B; Geological Survey of Canada, this volume.
- Embry, A.F.**
1991: Mesozoic history of the Arctic Islands; Chapter 14 *in* Geology of the Inuitian Orogen and Arctic Platform of Canada and Greenland, (ed.) H.P. Trettin; Geological Survey of Canada, Geology of Canada, no. 3; (also Geological Society of America, The Geology of North America, v. E).
- Embry, A.F. and Osadetz, K.G.**
1988: Stratigraphic and tectonic significance of Cretaceous volcanism in the Queen Elizabeth Islands, Canadian Arctic Archipelago; Canadian Journal of Earth Sciences, v. 25, p. 1209-1219.
- Harrison, J.C., Mayr, U., and Beauchamp, B.**
1995: Preliminary observations on the structural geology of Hvitland Peninsula, northwestern Ellesmere Island, Arctic Canada; *in* Current Research 1995-B; Geological Survey of Canada, this volume.
- Kells, M.P., Beauchamp, B., and Desrochers, A.**
1995: Artinskian-Kungurian (Lower Permian) stratigraphy (Raanes, Great Bear Cape and Trappers Cove formations), Hvitland Peninsula and adjacent areas, northwestern Ellesmere Island, Arctic Canada; *in* Current Research 1995-B; Geological Survey of Canada, this volume.
- Maurel, L.E.**
1989: Geometry and evolution of the Tanquary structural high and its effects on the paleogeography of the Sverdrup Basin, northern Ellesmere Island, Canadian Arctic; *in* Current Research, Part G; Geological Survey of Canada, Paper 89-1G, p. 177-189.
- Okulitch, A.V. (compiler)**
1991: Geology of the Canadian Arctic Archipelago and North Greenland, Figure 2, scale 1:2 000 000; *in* Geology of the Inuitian Orogen and Arctic Platform of Canada and Greenland, (ed.) H.P. Trettin; Geological Survey of Canada, Geology of Canada, no. 3; (also Geological Society of America, The Geology of North America, v. E).
- Okulitch, A.V. and Trettin, H.P.**
1991: Late Cretaceous - Early Tertiary deformation, Arctic Islands; Chapter 17 *in* Geology of the Inuitian Orogen and Arctic Platform of Canada and Greenland, (ed.) H.P. Trettin; Geological Survey of Canada, Geology of Canada, no. 3; (also Geological Society of America, The Geology of North America, v. E).
- Thériault, P., Beauchamp, B., Harrison, J.C., Mayr, U., and Steel, R.**
1995: Serpukhovian and Bashkirian (Carboniferous) stratigraphy (Borup Fiord and Otto Fiord formations, Unit C1), Hvitland Peninsula and adjacent areas, northwestern Ellesmere Island, Arctic Canada; *in* Current Research 1995-B; Geological Survey of Canada, this volume.
- Thorsteinsson, R.**
1974: Carboniferous and Permian stratigraphy of Axel Heiberg Island and western Ellesmere Island, Canadian Arctic Archipelago; Geological Survey of Canada, Bulletin 224.
- Trettin, H.P.**
1994: Pre-Carboniferous geology of the northern part of the Arctic Islands: Hazen Fold Belt and adjacent parts of Central Ellesmere Fold Belt, Ellesmere Island; Geological Survey of Canada, Bulletin 430.
- Trettin, H.P. and Mayr, U.**
1981: Preliminary geological map and notes, parts of Otto Fiord and Cape Stallworthy areas, District of Franklin (NTS 340 C, 560 D); Geological Survey of Canada, Open File 757.

Geological Survey of Canada Project 850039

Preliminary observations on the structural geology of Hvitland Peninsula, northwestern Ellesmere Island, Arctic Canada

J.C. Harrison, U. Mayr, and B. Beauchamp

Institute of Sedimentary and Petroleum Geology, Calgary

Harrison, J.C., Mayr, U., and Beauchamp, B., 1995: Preliminary observations on the structural geology of Hvitland Peninsula, northwestern Ellesmere Island, Arctic Canada; in Current Research 1995-B; Geological Survey of Canada, p. 9-18.

Abstract: Tectonic elements of the Eurekan Orogen in the Hvitland Peninsula area are presented in three distinct structural regions. Mountain ranges north of the head of Otto Fiord feature thrust-imbricated panels of upper Paleozoic carbonates (30-55% shortening) arranged in Triangle Zone structures riding on a sub-Otto Fiord evaporite décollement. This belt is gradational with a coeval thrust belt to the north and east (30-35% shortening) that features folded and inverted outliers of Carboniferous to Triassic strata (including half-grabens), and thrusts rooted in anisotropic lower Paleozoic basement. Both thrust belts plunge southwest into a less deformed (10-15% shortening) area on southwestern Hvitland Peninsula featuring short sinuous thrusts, northward-striking strike-slip faults rooted in the basement, and transported evaporites in open folded Carboniferous to Triassic basin facies strata. Syntectonic conglomerates near Emma Fiord provide a probable early Eocene age for the first of two compressive deformation phases associated with the Eurekan Orogeny in this part of the Arctic Islands.

Résumé : Les éléments tectoniques de l'orogénèse eurékienne dans la région de la péninsule Hvitland sont présentés selon trois régions structurales distinctes. Les chaînes de montagnes au nord du fond du fjord Otto présentent des panneaux de roches carbonatées du Paléozoïque supérieur imbriqués par des chevauchements (30-55 % de raccourcissement) et disposés en structures dans la Zone triangulaire sur un décollement d'évaporites sous le fjord Otto. Cette ceinture passe progressivement à une zone de charriage contemporaine au nord et à l'est (30-35 % de raccourcissement) où l'on observe des lambeaux plissés et inversés de couches s'échelonnant du Carbonifère au Trias (y compris des demi-grabens), et des chevauchements enracinés dans le socle anisotrope du Paléozoïque inférieur. Les deux zones de charriage plongent vers le sud-ouest dans une région moins déformée (10-15 % de raccourcissement) dans le sud-ouest de la péninsule Hvitland, où l'on observe de courts chevauchements sinueux, des décrochements à direction nord qui sont enracinés dans le socle et des évaporites transportés dans des couches de faciès de bassin, allant du Carbonifère au Trias, lesquelles couches sont déformées en plis ouverts. Des conglomérats syntectoniques près du fjord Emma laissent entrevoir un âge remontant probablement à l'Éocène précoce pour la première des deux phases de déformation par compression associées à l'orogénèse eurékienne dans cette partie de l'archipel Arctique.

INTRODUCTION

The location, physiographic expression and geological setting of the Hvitland Peninsula region is presented elsewhere in this volume (Mayr et al., 1995). Formations and unnamed units are described in Mayr et al. (1995), Beauchamp et al. (1995), and other papers in this volume. The major compressive tectonic elements of the region are associated with the Eureka Orogeny, a prolonged polyphase mountain-building period related to the convergence of Greenland with the northern Canadian Arctic Islands and simultaneous plate spreading in the Labrador Sea and Baffin Bay (Trettin, 1991).

General geological features influencing deformation style on the Hvitland Peninsula are introduced by Mayr et al. (1995) and include: 1) a N55°E to N80°E bedding and cleavage-related anisotropy in Franklinian basement; 2) Permo-Carboniferous rift-related structures; 3) the distribution of ductile evaporites of the Otto Fiord Formation; 4) the facies change from mountain-forming upper Paleozoic carbonates in the east to more recessive shales in the west; 5) the Permo-Triassic Tanquary High of Yelverton Pass area (Maurel, 1989) which may extend into the eastern Hvitland area; and 6) northward-trending Cretaceous gabbro dykes.

STRUCTURAL SUBDIVISION OF THE HVITLAND PENINSULA REGION

A three-fold structural subdivision is evident within the Carboniferous and younger strata of the Hvitland Peninsula region (Fig. 1): a northeastern region of northeastward-trending and northeastward-striking, basement-rooted folds and thrusts; a central and southern thrust belt featuring a widespread décollement above evaporites of the Carboniferous Otto Fiord Formation; and a western belt with detached evaporites and northward-striking, basement-involved, strike-slip faults. Structural character of each of these three belts is discussed below.

The evaporite-based thrust belt

Base camp area

Parallel mountain ranges of inclined Carboniferous and Permian shelf-facies limestones, lying within the evaporite-detached thrust belt of the eastern Hvitland Peninsula (Fig. 3 in Mayr et al., 1995), dominate the landscape as one approaches the north shore of Otto Fiord by aircraft from the south. The area located immediately northwest of the Otto Fiord base camp (Fig. 2) is illustrative of the structural style of this region. The local undeformed section is 3500 m thick and includes: detached Otto Fiord evaporites (mostly gypsum and anhydrite); rigid carbonates of the Nansen, Raanes, Great Bear Cape and Degerbøls formations; and intervening and overlying shale-dominated units of the Hare Fiord, Trappers Cove, van Hauen and Blind Fiord formations, which serve as intermediate and upper decoupling levels within the thrust belt. Mappable faults include a southward- and southeastward-dipping set with four faults (informally labelled "Camp

thrusts A-D") lying within the Permian and Lower Triassic interval and one ("Front range thrust") lying low in the Hare Fiord Formation. A separate northwestward-dipping set ("Main range thrusts A-D") lies within the Hare Fiord Formation or below map unit C2 and the Otto Fiord evaporites.

The structure section (A-A') emphasizes the equal importance of oppositely and inwardly vergent thrusts to form a Triangle zone structure involving Triassic and older strata in the subsurface. The Otto Fiord evaporites serve as the main décollement level at and above about 3300 m below sea level. One remarkable early structure is Camp thrust C. This fault lies in the Raanes Formation along the eastern map boundary then rises in the section toward the south and west. In many areas, the Van Hauen Formation has been thrust to the south over the lowermost Blind Fiord Formation. In addition, Camp thrust C has been folded, along with the enveloping strata, into a tight anticline-syncline pair of chevrons located in the hanging wall of the younger evaporite-based Front range thrust. In contrast, Camp thrusts A and B feature eastward-trending hanging wall periclinal culminations in the Degerbøls Formation and appear to feature northward-directed slip over footwall Lower Triassic. The youngest fault in the area is the southeastward-transported Main range thrust D which truncates both the Front range thrust and Camp thrusts C and D. Estimated minimum compressive slip measured along the line of section A-A' is 11 km or about 55 per cent.

Otto Glacier area

The Triangle Zone structure near the Otto Fiord base camp extends and widens to the northeast into the mountainous region located north of Otto Glacier (Fig. 3; section B-B'). The footwall succession includes recessive Lower Triassic strata in the valley bottom between hanging wall Carboniferous mountain ranges to the northwest and southeast (Fig. 3 in Mayr et al., 1995). The hanging wall of the Front range thrust features prominently exposed facies changes between Nansen carbonates and slope facies Hare Fiord strata, which, in this area, exceed 1400 m in thickness. Depositional thickness variations are also evident in the Raanes to Degerbøls interval which collectively vary from less than 200 m to more than 800 m over distances of less than 10 km.

Northwest and southeast directions of transport on many of the thrusts within the Otto Glacier area are also indicated by numerous asymmetric shallow-plunging anticlines and synclines. Five of these lie in the hanging wall of the northwestward-transported Otto Glacier Thrust (Fig. 4). The depth to the subevaporite décollement is estimated to lie at or below 2800 m here and in the footwall of the Main range thrusts. However, it is clear that Main range thrust D, and probably others in this set, are rooted in the lower Paleozoic basement; the Otto Fiord Formation is absent in the hanging wall succession and the Borup Fiord Formation is folded along with conformable Nansen Formation in nunataks located at and above 800 m above sea level. This implies a differential compressive uplift of the basement amounting to at least 3600 m between the hanging wall of Main range thrust D and the footwall of Main range thrust E. Following from this observation is the implication that Main range thrust D

must ramp up from the basement to a subevaporite décollement somewhere between the Otto Glacier area and the base camp area. Regional mapping indicates that several other major faults on the Hvitland Peninsula also ramp up from the basement to the evaporites along strike toward the southwest. Included in this group is "Emma Fiord thrust A" and the "Triassic valley thrust" both of which carry basement strata, and the Otto Fiord Formation in the immediate hanging wall at different points along strike (Fig. 1).

Overall compressive slip measured along the line of section B-B' in the Otto Glacier area is at least 6 km and no less than 25 to 30 per cent.

The basement-rooted thrust belt

Thrusts and shallow plunging folds mapped throughout the basement-rooted thrust belt (Fig. 1) are expressed by the distribution of lower Paleozoic strata, the sub-Carboniferous angular unconformity and formations of the mid-Carboniferous through Triassic succession. In this area, basement-involved faults extend as high as the shales of the Lower Triassic and tend to bypass potential intermediate detachment levels such as the evaporites of the Otto Fiord Formation which are either thin and discontinuous, or absent due to nondeposition.

Southeast and northwest directions of tectonic transport in this belt are implied by shallow-plunging synclines with fold traces that parallel adjacent faults as observed in the footwall of "Hvitland thrust A", and Emma Fiord thrusts A, B, and C.

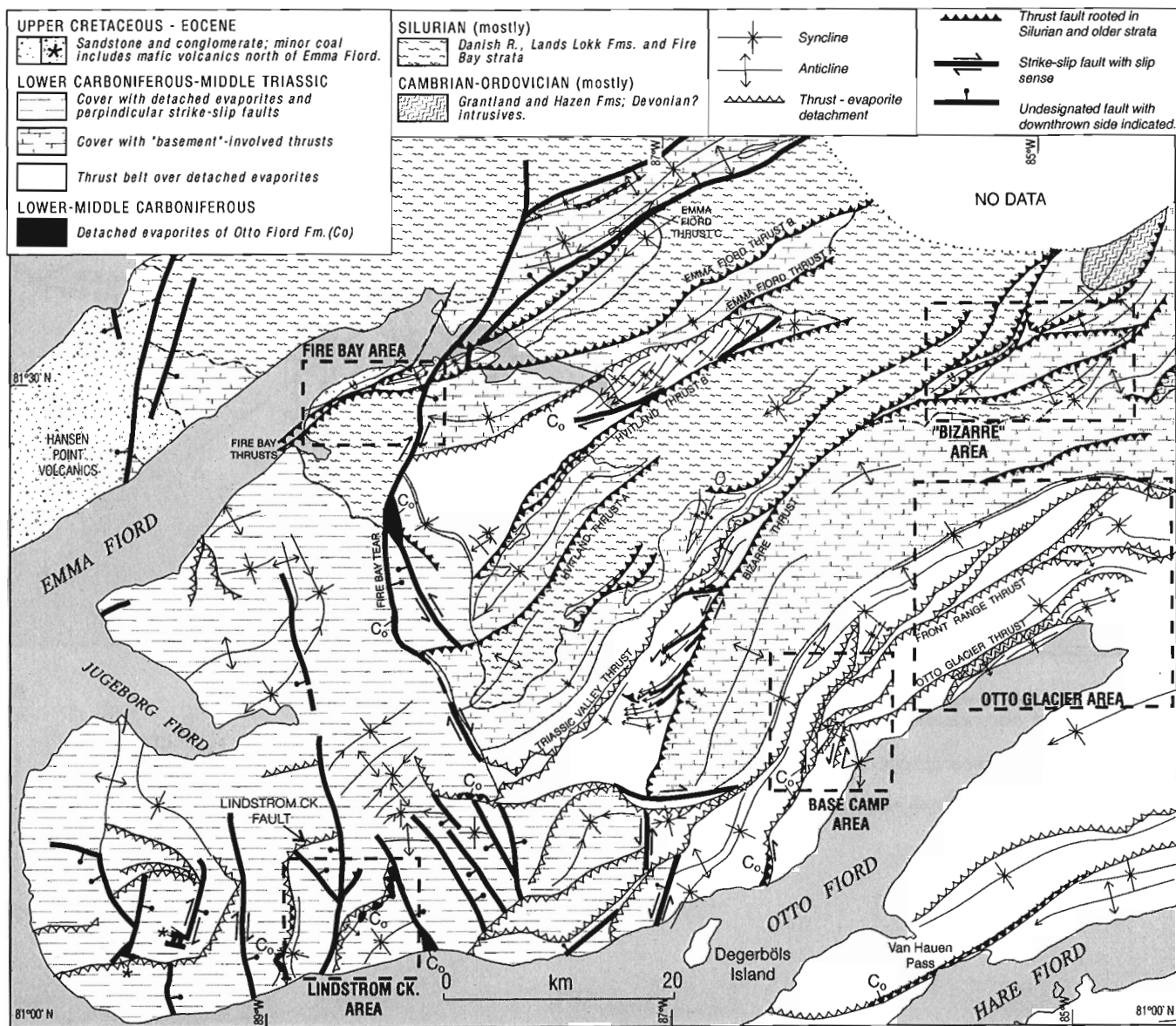
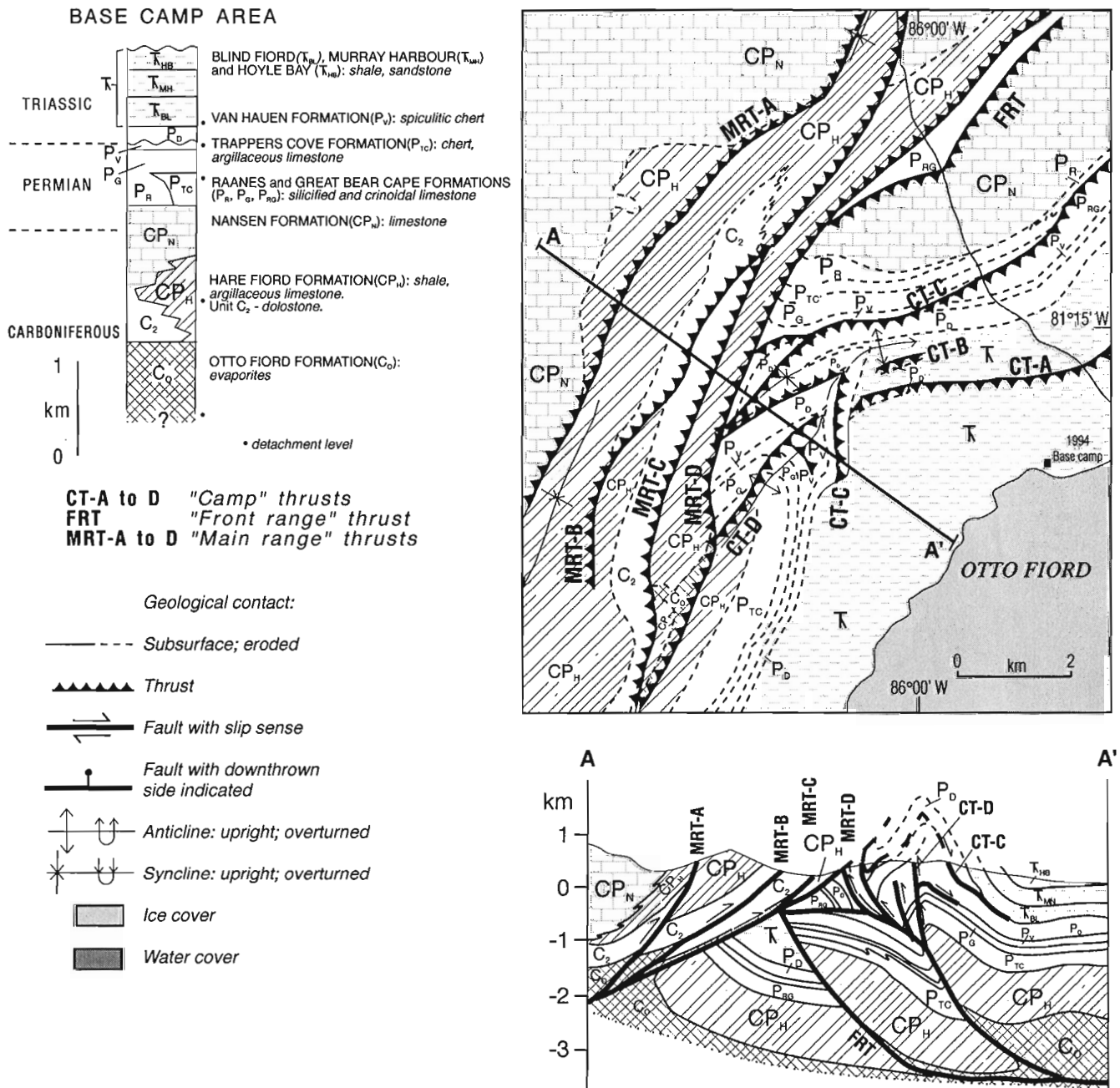
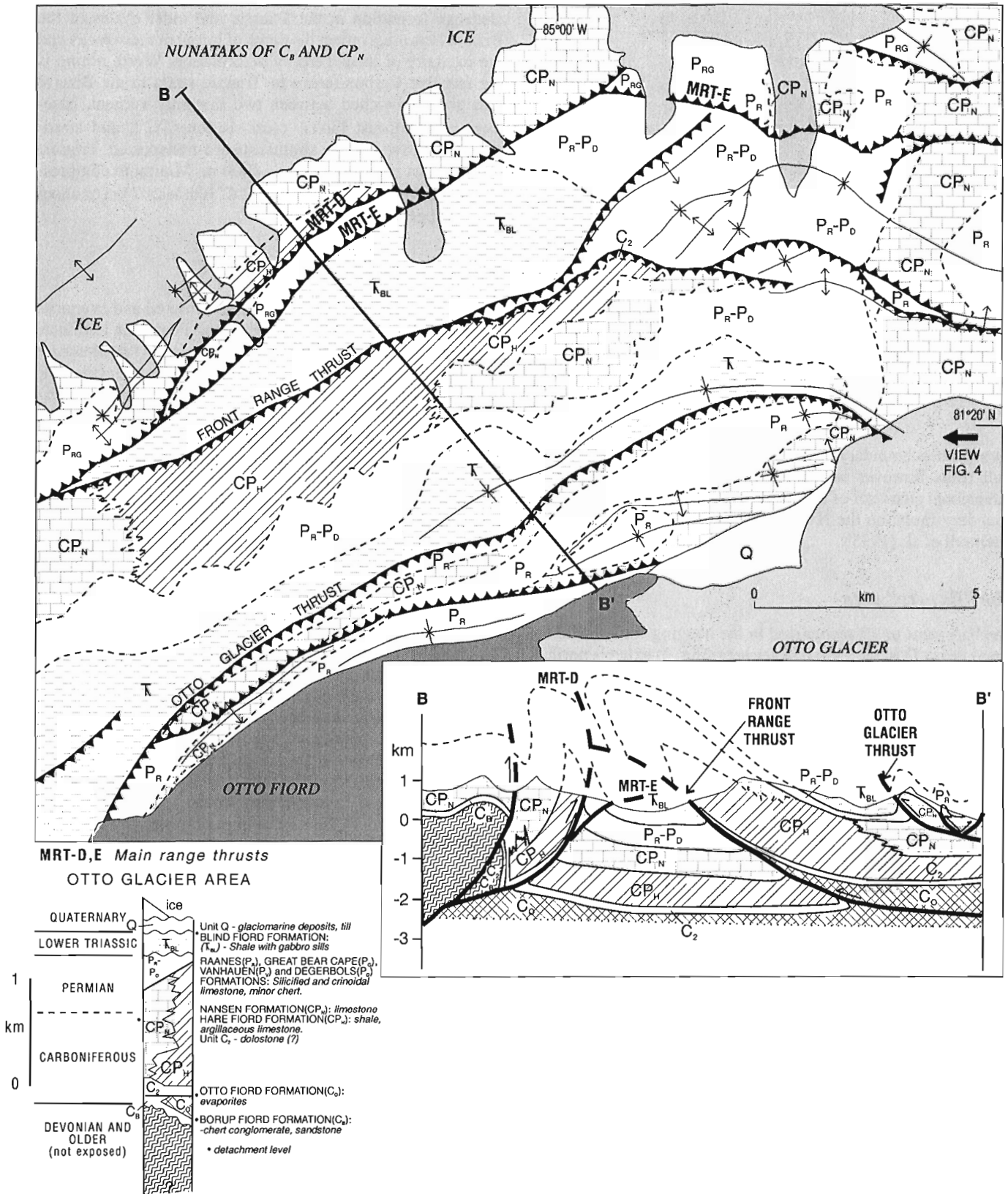


Figure 1. Structurally distinct regions and tectonic elements of the Hvitland Peninsula region. Mapped features have been locally projected through onland ice cover.

B and C. Similar conclusions can be reached for the "Bizarre thrust" and Hvitland thrust B, both of which possess shallow-plunging hanging wall anticlines. Additional support for northwest and southeast directions of transport are implied by a right-hand en echelon fold array that implies a component of dextral strike slip for the footwall succession beneath the eastward-striking portion of Hvitland thrust B. Similarly, sinistral strike slip is implied for en echelon folds in the footwall of the northward-striking portion of the Bizarre thrust.

In most areas, bedding and formational contacts in the lower Paleozoic are roughly parallel to the surface trace of the major northeastward-striking faults. Nevertheless, the sub-Carboniferous angular unconformity often ranges to 80 or 90°. This implies that the Tertiary tectonic fabric of the area is, to a large extent, inherited from a similar fabric of pre- to mid-Carboniferous age. Less certain is the extent to which basement-rooted Tertiary thrusts have exploited and inverted rift-related Permo-Carboniferous extension faults. One convincing inversion structure is presented by fault-bounded Carboniferous strata north of Emma Fiord thrust C (Fig. 1).





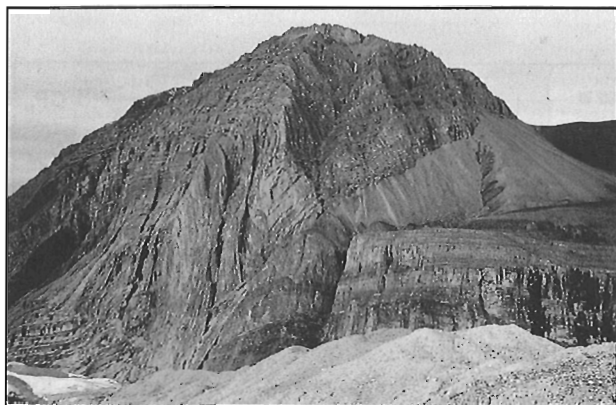


Figure 4. Mountain face exposure of the northwestward-vergent Otto Glacier thrust which places folded medial Nansen Formation over footwall cliffs of subhorizontal Raanes Formation, talus covered Great Bear Cape, van Hauen and Degerbøls formations and dark coloured Triassic (upper right). Vertical relief is up to 1000 m.

Two graben-boundary faults carry compressional hanging wall folds however inversion has not erased the original extensional character of this structure. Other potential graben boundary faults on the Hvitland Peninsula are illustrated in Thériault et al. (1995).

The "Bizarre" area

The basement uplift recognized in the hanging wall of Main range thrust D in the Otto Glacier area (Fig. 3) extends north for 15 km and terminates in a region that has been dubbed the "Bizarre" area (Fig. 5). This area is unlike any other on the Hvitland Peninsula for four reasons. First, the Nansen Formation and Unit C2 are dolomitized in most exposures observed north of the Bizarre thrust. Second, Permo-Carboniferous and Triassic shales of the Hare Fiord and Blind Fiord formations, respectively, as well as those in the Silurian, possess a strong penetrative cleavage (Fig. 6). Third, Permian formations from the Raanes to the Degerbøls are unrecognizable. Several of these formations would appear to have been cut out beneath a sub-Triassic disconformity. In the northwest corner of the "Bizarre" area, the entire mid to upper Permian is represented by about 35 m of sandstone and limestone resting with probable disconformity on typical reef-facies Nansen Formation. Finally, the Lower Triassic Blind Fiord Formation includes a substantial interval of turbiditic sandstone and conglomerate in beds up to 5 m thick. The clasts in some conglomerate beds range up to 20 cm and include variegated lower Paleozoic chert and clasts of Carboniferous coralline limestone. The energetic slope-facies character of these beds is indicated by sedimentary loads, tool marks and other sole markings.

The pervasive dolomitization in the Bizarre area is tentatively linked to coeval upper Paleozoic growth faulting in the area. It is also likely that a temporal and possible spatial association exists between the Permo-Triassic uplift in this area and the Tanquary High of the Yelverton Pass area

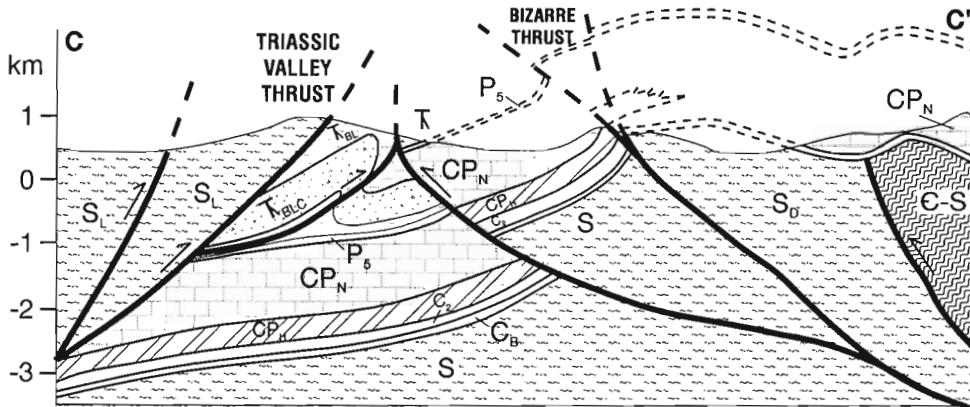
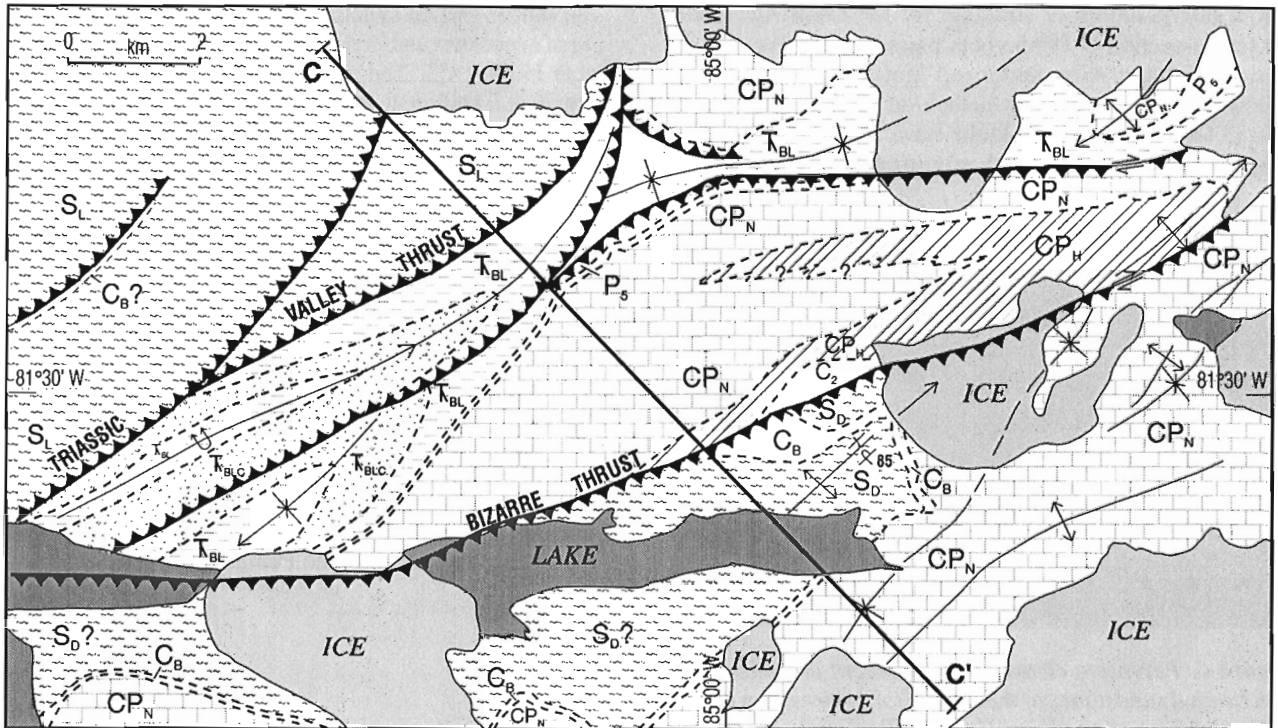
(Maurel, 1989), which is located beyond continuous ice covered highlands 105 km to the east-northeast. However, cleavage formation in the Triassic and older shales of the Bizarre area must reflect the depth of burial of these rocks and the intensity of local Tertiary deformation. Worth noting is the fact that Carboniferous to Triassic strata in the Bizarre area are sandwiched between two inwardly vergent, basement-rooted thrust faults (cross-section C-C'), and stratigraphic throw on the southeastward-transported Triassic valley thrust probably exceeds 4000 m. Minimum compressive slip measured along section C-C' is at least 7 km or about 30 to 35 per cent.

Western faulted belt

All of the southwest-striking basement-rooted and evaporite detached thrusts of the eastern Hvitland Peninsula terminate gradationally in a region of north-striking faults that dominate the geology throughout the western half of the peninsula. The disappearance of the thrusts is marked by a progressive loss of stratigraphic throw on individual fault strands and the along-trend termination of footwall and hanging wall folds. North of Degerbøls Island, the boundary between the thrust belt and the western faulted belt approximately follows along the line of facies change between Upper Carboniferous and Lower Permian limestones of the Nansen Formation to the east and age equivalent shales and basin facies carbonates of the Hare Fiord Formation to the west. This relationship does not follow in detail because embayments and tongues of Hare Fiord strata are known throughout the project area to the east, and tongues and reefal carbonate build-ups are also known to the west. Nevertheless, it is safe to conclude that the predominantly rigid beam of strata, typical of the Upper Paleozoic succession above the Otto Fiord evaporites in the mountain ranges of the east, has been replaced in the western hill country by a succession of less competent shale and chert formations. Contrary to the notion that one would expect to witness tight and repetitive chevron folding within these shales, the actual extent of shortening is estimated to be only about 10 to 15 per cent within the western half of the peninsula.

Lindstrom Creek area

Dominant structural elements of the western faulted belt are typified by features mapped in the Lindstrom Creek area. These include: doubly plunging, saucer-shaped synclines with limb dips not usually exceeding 30° or 40°; short, low amplitude, shallow-plunging anticlines; short sinuous thrusts, some carrying hanging wall evaporites; and steeply dipping northward-striking faults, most or all of which root into the lower Paleozoic basement. The sinuous thrusts display stratigraphic throws not normally exceeding 1000 m (although one thrust on the west end of the peninsula may have a local throw of up to 2200 m). Larger vertical separations, up to 3200 m or more, are indicated on several of the steep north-striking faults, including the Lindstrom Creek fault (Fig. 7) which carries elements of compressive slip as indicated by the associated array of short wavelength north-trending folds.



"BIZARRE" AREA

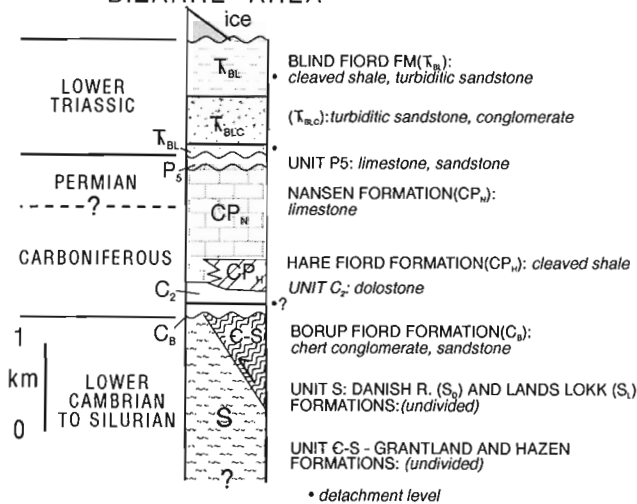


Figure 5. Simplified geology and structural cross-section C-C' of the "Bizarre" area located 22 to 27 km north of the head of Otto Fiord. The map area is outlined on Figure 1.

The interpretation of structure for the Lindstrom Creek area (cross-section D-D') favours basement-involvement on the steep north-striking faults and limited displacement on shallow-dipping thrusts that detach on the Otto Fiord evaporites. The north-striking faults have also acted as lateral ramp surfaces, facilitating forward slip on intervening thrusts.

The saucer-shaped synclines are associated with the pillow-ing of evaporites and/or differential growth of carbonate patch reefs in Unit C2. The patch reefs may in fact have grown directly on emergent evaporite pillows during deposition of Unit C2. The evaporites are carried upsection on the thrusts but are also exposed in anticlinal culminations and have been squeezed into available space where thrusts intersect the northward-striking system of faults. Although the evaporites have been moved and localized by faulting, there is nothing to indicate that these evaporites have evolved into classic piercement diapirs. Rather, these bodies are assumed to have originated as parautochthonous pillows during or soon after deposition of the overlying upper Paleozoic strata, and have been only modestly transported during the Tertiary compressive deformation.

Compressive slip measured along the line of section D-D' is 4 km or about 25 per cent. This magnitude of shortening is probably higher than the average for upper Paleozoic strata underlying western Hvitland Peninsula.



Figure 6. Pervasive cleavage development in shales and thin bedded sandstones of the Blind Fiord Formation in the "Bizarre" area of northeast Hvitland Peninsula.

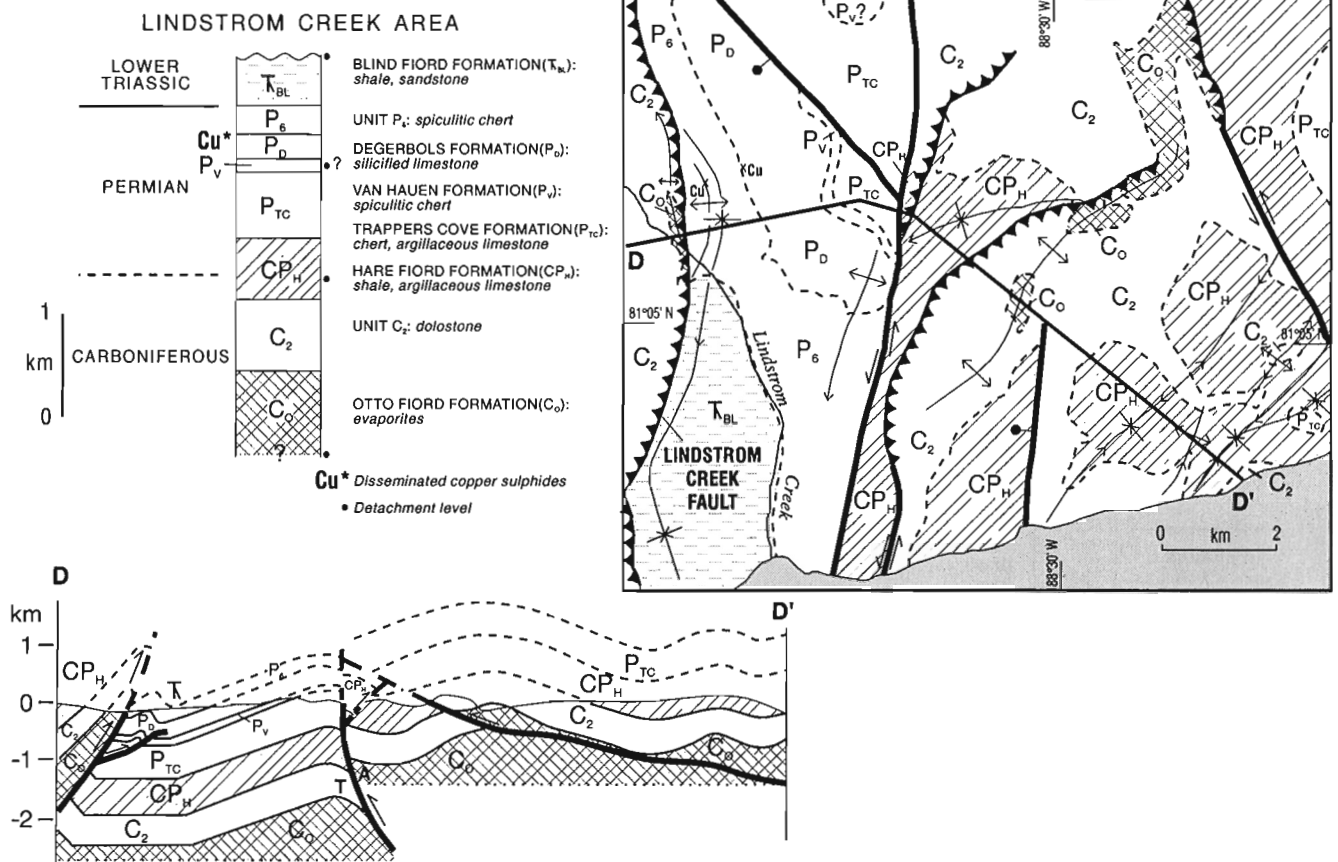


Figure 7. Simplified geology and structural cross-section D-D' of the Lindstrom Creek area on the southern coast of the Hvitland Peninsula. Occurrences of disseminated copper sulphides in the highest limestone beds of the Degerbøls Formation are also indicated. The map area is outlined on Figure 1.

Fire Bay area

The Fire Bay inlier and surrounding strata (Fig. 8) provide insight into the kinematic relationship between northward-striking faults of western Hvitland Peninsula and various northeast-striking thrusts typical of those mapped in the east. Lower Paleozoic strata (observed by JCH) within the inlier are similar to those described by Trettin and Nowlan (1990) and include: Hazen Formation chert and shale, Fire Bay assemblage shales, volcanic flows (including pillow basalts) and volcanoclastic rocks, and sandstones potentially assignable to the Danish River Formation. All of these strata have been intruded by numerous northward-striking Cretaceous(?) gabbro dykes. The lower Paleozoic strata possess steep to overturned dips along the northern and eastern margins of the inlier, strike northeastward and are roughly parallel to the surface trace of Fire Bay thrusts A and B which together define the northern limit of the inlier. In contrast, the northward-striking "Fire Bay tear", mapped along the east side of the inlier, displaces both previously folded Nansen and Raanes formations to the east and eastward-striking lower Paleozoic inlier strata to the west. While the Fire Bay tear appears to be unrelated to any form of pre-existing Paleozoic anisotropy,

Cretaceous dykes are exceedingly common in the inlier both near and parallel to the trace of the tear. Two of these dykes are indicated in Figure 8.

The Nansen Formation is also preserved in near flat-lying erosional remnants on the upthrown side of both the Fire Bay tear and in the hanging wall of Fire Bay thrust B. The sub-Carboniferous angular unconformity in these areas is close to 90°. In contrast, the Carboniferous succession in the hanging wall of Fire Bay thrust A features vertical to overturned strata and northwestward-vergent tight folds. These beds have been thrust over a distinctive succession of clastic rocks including syntectonic gravels that are assigned to two formations of the Eureka Sound Group (Mayr et al., 1995). The latter strata have been folded into a syncline with south limb strata overturned toward the northwest at 80° to 90° (Fig. 9).

The lower of the two formations in the Eureka Sound Group includes about 80 m of fine grained quartz sandstone, mudrock and coalified wood. Ricketts (1994) and McIntyre (in Ricketts, 1994) have assigned and dated these beds to the upper Paleocene to lower Eocene Iceberg Bay Formation. The base and full thickness of this unit is unknown, but it is assumed to overlie additional Eureka Sound beds and an

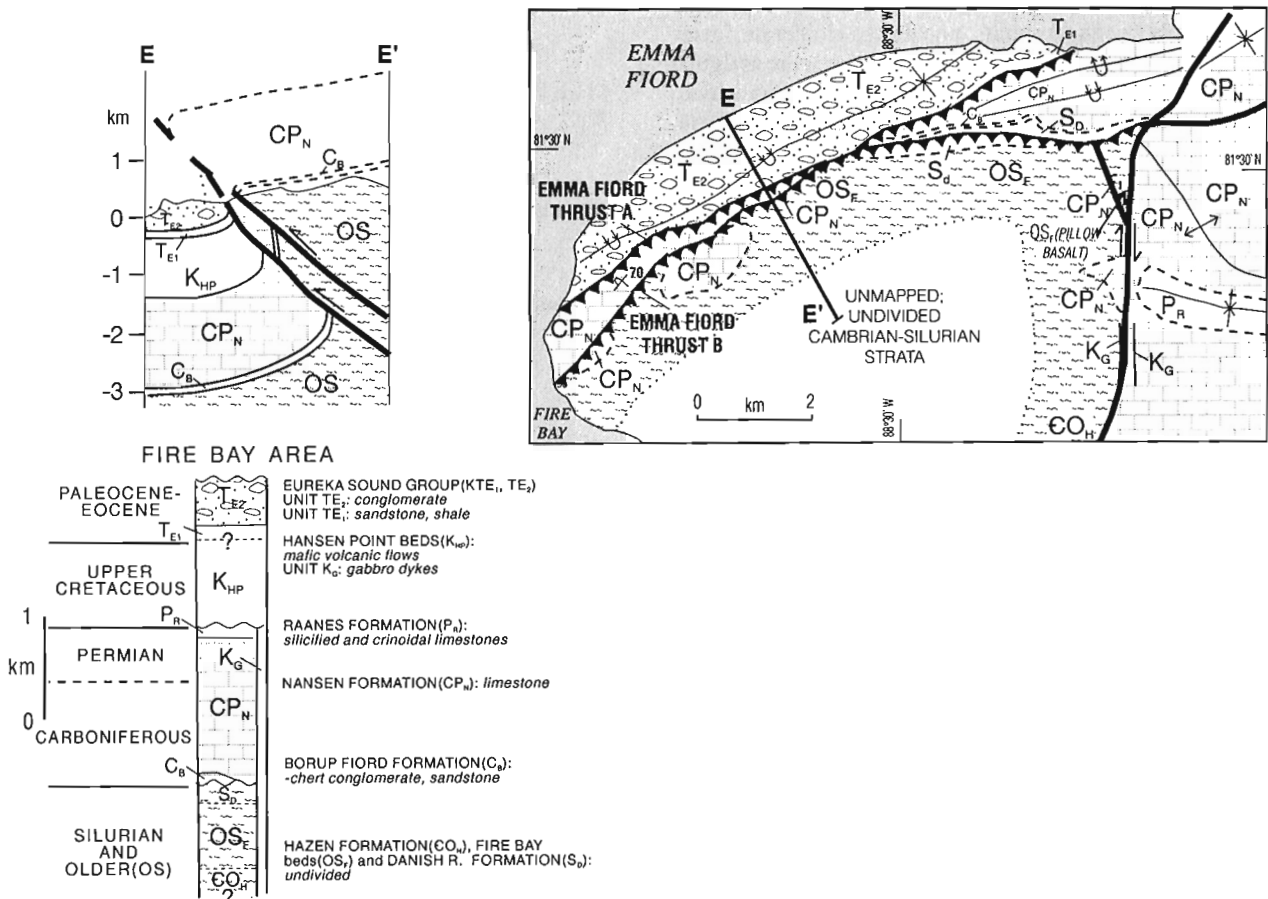


Figure 8. Simplified geology and structural cross-section E-E' of the Fire Bay area on the north coast of the Hvitland Peninsula. The map area is outlined on Figure 1.

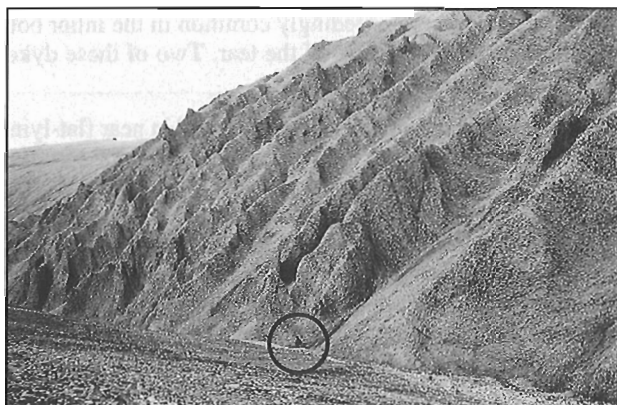


Figure 9. Vertically-dipping lower(?) Eocene syntectonic conglomerates of the Buchanan Lake Formation in the footwall of the northwestward-vergent Fire Bay thrust A. The person (circled) is for scale.

Upper Cretaceous succession that includes the Hansen Point volcanic rocks (Embry and Osadetz, 1988). The latter are extensively exposed north of Emma Fiord (Fig. 1). The upper formation of the Eureka Sound Group in this area lies in sharp, possibly disconformable, contact with the Iceberg Bay Formation and includes 600 to 800 m of clast-supported polymictic cobble conglomerate, pebble conglomerate, lesser sandstone and minor coalified wood. These beds are assigned by Ricketts (1994) to the Buchanan Lake Formation which, in this area, is probably lower Eocene (McIntyre, in Ricketts, 1994). Rounded clasts in the conglomerate range to several tens of centimetres and include lithologies clearly derived from both the Nansen Formation and the cherts, shales, volcanics and sandstones of the Fire Bay inlier. The weathering colour of the formation varies both vertically and laterally; from yellowish where dominated by limestone clasts to greenish grey where dominated by lower Paleozoic clasts. Although there is no indication of an unroofing sequence, this combination of clasts could only have come from a nearby source located either in the south or in the east.

The structural model favoured here is northwestward-directed compressive slip on the Fire Bay thrusts facilitated by a pre-existing lower Paleozoic anisotropy and by dextral strike slip on the Fire Bay tear fault; slip on the latter was facilitated by an anisotropy expressed by previously intruded Cretaceous gabbro dykes. The early Eocene deposition of proximal conglomerate in the footwall of Fire Bay thrust A dates a significant early phase of compressive unroofing of the hanging wall Paleozoic succession. A second phase of

post-early Eocene folding is responsible for the development of the footwall syncline in the same Tertiary section and some additional slip on the various inlier boundary faults.

ACKNOWLEDGMENTS

The authors would like to thank T. de Freitas and H. Trettin for their valued critical review comments, and P. Neelands and M. Deuling for the drafting of text figures. This study would not have been possible without the logistical and financial support of the Polar Continental Shelf Project and the Geological Survey of Canada.

REFERENCES

- Beauchamp, B., Mayr, U., and Harrison, J.C.**
1995: Carboniferous and Permian stratigraphic sequences on Hvitland Peninsula and adjacent areas, northwestern Ellesmere Island, Arctic Canada; in *Current Research 1995-B*; Geological Survey of Canada, this volume.
- Embry, A.F. and Osadetz, K.G.**
1988: Stratigraphy and tectonic significance of Cretaceous volcanism in the Queen Elizabeth Islands, Canadian Arctic Archipelago; *Canadian Journal of Earth Sciences*, v. 25, p. 1209-1219.
- Maurel, L.E.**
1989: Geometry and evolution of the Tanquary Structural High and its effects on the paleogeography of the Sverdrup Basin, northern Ellesmere Island, Canadian Arctic; in *Current Research, Part G*; Geological Survey of Canada, Paper 89-1G, p. 177-189.
- Mayr, U., Harrison, J.C., and Beauchamp, B.**
1995: Geological map of Carboniferous and Permian units on Hvitland Peninsula and adjacent areas, northwestern Ellesmere Island, Arctic Canada; in *Current Research 1995-B*; Geological Survey of Canada, this volume.
- Ricketts, B.D.**
1994: Basin analysis, Eureka Sound Group, Axel Heiberg and Ellesmere islands, Canadian Arctic Archipelago; Geological Survey of Canada, Memoir 439, 119 p.
- Thériault, P., Beauchamp, B., Harrison, J.C., Mayr, U., and Steel, R.**
1995: Serpukhovian and Bashkirian (Carboniferous) stratigraphy (Borup Fiord and Otto Fiord formations; Unit C1), Hvitland Peninsula and adjacent areas, northwestern Ellesmere Island, Arctic Canada; in *Current Research 1995-B*; Geological Survey of Canada, this volume.
- Trettin, H.P. (ed.)**
1991: Geology of the Innuitian Orogen and Arctic Platform of Canada and Greenland; Geological Survey of Canada, Geology of Canada, no. 3 (also Geological Society of America, *The Geology of North America*, v. E).
- Trettin, H.P. and Nowlan, G.S.**
1990: Middle Ordovician sedimentary and volcanic rocks at Fire Bay, Emma Fiord, northwestern Ellesmere Island; Geological Survey of Canada, Paper 90-1D, p. 147-151.

Carboniferous and Permian stratigraphic sequences on Hvitland Peninsula and adjacent areas, northwestern Ellesmere Island, Arctic Canada

B. Beauchamp, U. Mayr, and J.C. Harrison

Institute of Sedimentary and Petroleum Geology, Calgary

Beauchamp, B., Mayr, U., and Harrison, J.C., 1995: Carboniferous and Permian stratigraphic sequences on Hvitland Peninsula and adjacent areas, northwestern Ellesmere Island, Arctic Canada; in Current Research 1995-B; Geological Survey of Canada, p. 19-28.

Abstract: Six long-term transgressive-regressive sequences are recognized in the Carboniferous succession of Hvitland Peninsula, northwestern Ellesmere Island. The six sequences are unconformity-bounded packages that pass basinward into their correlative conformities. The six sequences are represented by the following lithostratigraphic units: 1) Serpukhovian Sequence: Borup Fiord Formation; 2) Bashkirian to Kasimovian Sequence: Otto Fiord, Nansen and Hare Fiord formations and units C1 and C2; 3) Gzhelian-Sakmarian Sequence: Nansen and Hare Fiord formations; 4) Artinskian Sequence: uppermost Nansen and Hare Fiord, Raanes, Trappers Cove and Great Bear Cape formations; 5) Kungurian-Kazanian Sequence: uppermost Great Bear Cape and Trappers Cove, Van Hauen and Degerbøls formations; and 6) post-Kazanian Sequence: uppermost Van Hauen and Degerbøls formations and Unit P6. In addition, the uppermost portion of Unit P6 forms the transgressive systems tract of a latest Permian-Early Triassic Sequence.

Résumé : On reconnaît six séquences transgressives-régressives de longue durée dans la succession du Carbonifère de la péninsule Hvitland, dans le nord-ouest de l'île d'Ellesmere. Les six séquences sont des ensembles limités par une discordance qui laissent place, en direction du bassin, à leurs concordances corrélatives. Les six séquences sont représentées par les unités lithostratigraphiques suivantes : 1) la Séquence serpukhovienne : Formation de Borup Fiord; 2) la Séquence bashkiriennne à kasimovienne : formations d'Otto Fiord, de Nansen et de Hare Fiord et unités C1 et C2; 3) la Séquence gzhélienne-sakmarienne : formations de Nansen et de Hare Fiord; 4) la Séquence artinskienne : partie sommitale des formations de Nansen et de Hare Fiord, formations de Raanes, de Trappers Cove et de Great Bear Cape; 5) la Séquence kungurienne-kazaniennne : partie sommitale des formations de Great Bear Cape et de Trappers Cove, formations de Van Hauen et de Degerbøls; et 6) la Séquence post-kazaniennne : partie sommitale des formations de Van Hauen et de Degerbøls et Unité P6. De plus, la partie sommitale de l'Unité P6 forme les systèmes transgressifs d'une séquence du Permien terminal-Trias précocce.

INTRODUCTION

This paper examines the Carboniferous and Permian stratigraphic record of Hvitland Peninsula, northwestern Ellesmere Island. It provides evidence that the numerous stratigraphic units mapped in the area (Mayr et al., 1995) together constitute six long-term transgressive-regressive (T-R) sequences. These sequences are bounded by unconformities in the eastern and northeastern areas and by correlative conformities in the southern and southwestern areas. The analysis of these sequences also provides evidence of significant paleogeographic, tectonic, and climatic shifts during the late Paleozoic. Generalities about the geological and structural setting of the area can be found in Mayr et al. (1995) and Harrison et al. (1995).

LITHOSTRATIGRAPHY AND SEQUENCE STRATIGRAPHY

The distribution of lithostratigraphic units on Hvitland Peninsula, northwestern Ellesmere Island (Fig. 1), is indicative that broad transgressions and regressions affected the area in Carboniferous and Permian time. This is best shown by a series of complex facies interfingerings between highly fossiliferous, light grey limestone (Nansen, Great Bear Cape and Degerbøls formations), interpreted as shallow water shelf deposits, and spiculitic to nonfossiliferous, dark grey mudrock (shale, chert, etc), interpreted as deeper-water slope to basinal deposits (Hare Fiord, Trappers Cove and Van Hauen formations) (Fig. 1). The lithostratigraphic framework (Fig. 2), strictly defined for mapping purposes, indirectly provides evidence for a dynamic spatio-temporal depositional history. This history, however, is better expressed in a sequence stratigraphic framework (Fig. 3).

Stratigraphic sequences, which are viewed as fundamental chronostratigraphic units, are genetic depositional packages bounded by unconformities and their correlative conformities. Each sequence comprises a series of systems tracts (genetically related packages of strata defined by their internal geometry and facies attributes). Systems tracts definition and terminology varies from author to author. For instance the Vail-Exxon group refers to lowstand, highstand and transgressive systems tracts based on their highly popularized model (e.g., Vail et al., 1977, 1991), whereas others refer simply to transgressive and regressive systems tracts, which is a simpler, more objective and less theoretical approach (e.g., Embry, 1993).

Eight Carboniferous and Permian T-R sequences have been documented in the Sverdrup Basin (Beauchamp et al., 1989a, b; Beauchamp, in press). Of those, six are recognized in the stratigraphic succession of Hvitland Peninsula, northwestern Ellesmere Island. The sequences are bounded by subaerial unconformities that pass basinward (in a general westward and southwestward direction) into their correlative conformities. In many instances, the transgressive portion of each sequence is subdivided into an early transgressive systems tract that accumulated in the deeper water areas, while the shelf received very little or no sediment, and a late

transgressive systems tract that accumulated on the shelf while the basinal and slope areas received very little or no sediment. The top of the transgressive systems tract is the maximum flooding surface which, in some instances, wraps around isolated offshore buildups that grew during the drowning event associated with the formation of that surface. The regressive systems tract lies above the maximum flooding surface and represents the progradation of shallow-water shelf deposits and the contemporaneous downlap of deeper water slope to basinal deposits on the maximum flooding surface (Fig. 3).

In some instances, sequence boundaries, flooding surfaces and maximum flooding surfaces coincide with lithostratigraphic boundaries, but in general, sequence-bounding unconformities and depositional surfaces carry across facies changes. As a rule of thumb, however, lithostratigraphic contacts generally lie at or slightly above sequence-bounding unconformities in basin marginal sections, and at or slightly below maximum flooding surfaces in basin axial sections (Fig. 2, 3).

CARBONIFEROUS AND PERMIAN SEQUENCES ON HVITLAND PENINSULA

The various Carboniferous and Permian lithostratigraphic units on Hvitland Peninsula are part of six T-R sequences interpreted as mostly representing the following time intervals: 1) Serpukhovian; 2) Bashkirian to Kasimovian; 3) Gzhelian to Sakmarian; 4) Artinskian; 5) Kungurian to Kazanian; and 6) post-Kazanian. In addition, uppermost Permian strata are part of the transgressive systems tract of a T-R sequence whose regressive portion is of Early Triassic age. Biostratigraphic data will be acquired to confirm these various ages, which are based on the known stratigraphic range of these sequences elsewhere in the basin (Beauchamp, in press; Beauchamp et al., 1989a, b). There is no published age for the Carboniferous and Permian succession of Hvitland Peninsula, but many biostratigraphic studies are currently in progress.

Serpukhovian Sequence

The Serpukhovian Sequence is represented by the Borup Fiord Formation and perhaps by strata assigned to Unit C1 of Mayr et al. (1995). The Serpukhovian Sequence lies with profound angular unconformity on deformed Silurian and older Franklinian basement. It thus represents the oldest stratigraphic unit of the Sverdrup Basin in the area. The Viséan Emma Fiord, which outcrops sparingly on northern Axel Heiberg and Ellesmere islands (Thorsteinsson, 1974), has not been recognized on Hvitland Peninsula. The upper sequence boundary is an unconformity that lies locally between or near the contact between red weathering clastic rocks of the Borup Fiord Formation and evaporite, dolostone or clastic rocks of the overlying Unit C1. An unconformity has also been observed between Borup Fiord and Nansen strata at a number of localities (Fig. 1).

In the Hare Fiord area southeast of Hvitland Peninsula, the Serpukhovian Sequence forms a broad, unconformity-bounded, retrogradational-progradational succession of non-marine fluvial strata that was deposited in a rift-related subbasin (Hare Fiord Subbasin; P. Thériault, pers. comm., 1994). The axial succession of the Hare Fiord Subbasin is represented by a sandstone assemblage and the correlative marginal succession by a conglomerate assemblage. A similar, albeit more complex situation occurs on Hvitland Peninsula, where four rift-related depocentres have been identified based

on the distribution of Borup Fiord, Unit C1 and Otto Fiord sediments in some areas, and the lack thereof in other areas (Fig. 4A). These subbasins were fault-bounded, rift-related structures that apparently formed through block rotation and half-graben development, the possible bounding faults of which are outlined in Figure 4A (see also Thériault et al., 1995).

In the Hvitland Subbasin, which is the best understood of the four subbasins, the Borup Fiord Formation comprises two major facies assemblages similar to those recognized in the

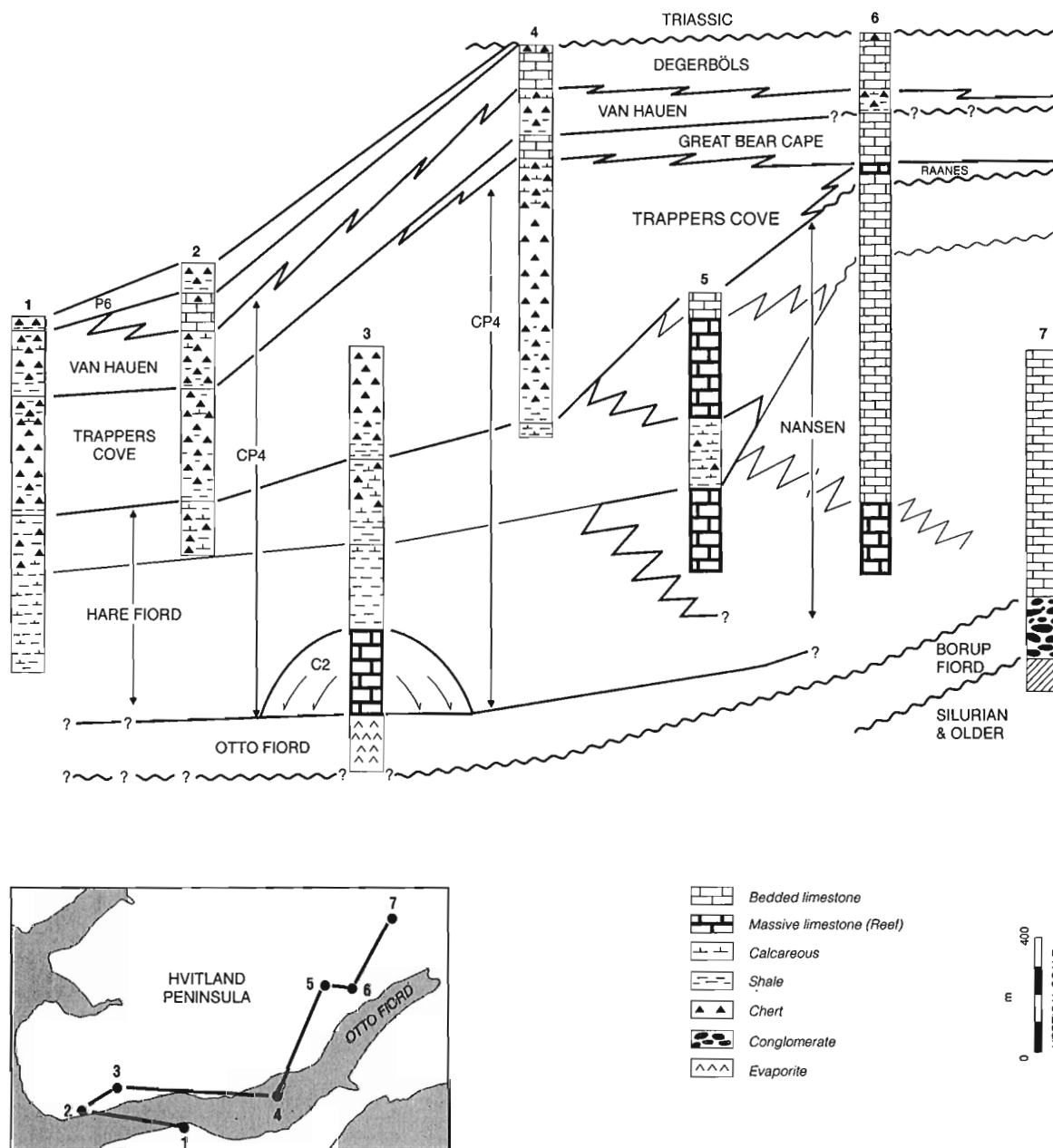


Figure 1. Cross-section showing distribution of Carboniferous and Permian main lithostratigraphic units along a general northeast-southwest profile on Hvitland Peninsula. The inset shows the location of the cross-section.

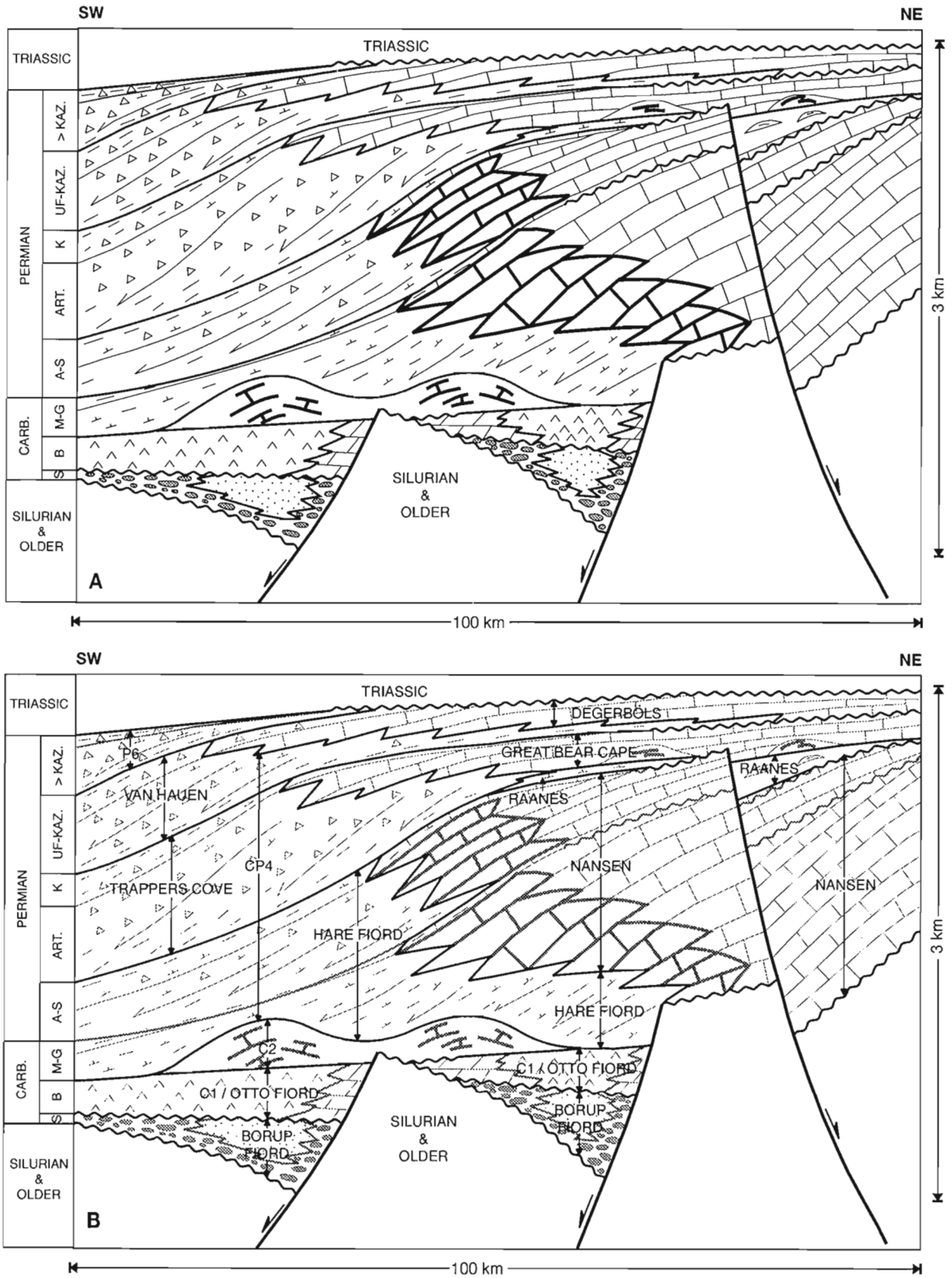


Figure 2. Carboniferous and Permian lithostratigraphic framework on Hvitland Peninsula along a schematic and composite northeast-southwest profile. **A)** Lithologies. **B)** Nomenclature. The key to the lithological symbols is the same as in Figure 1.

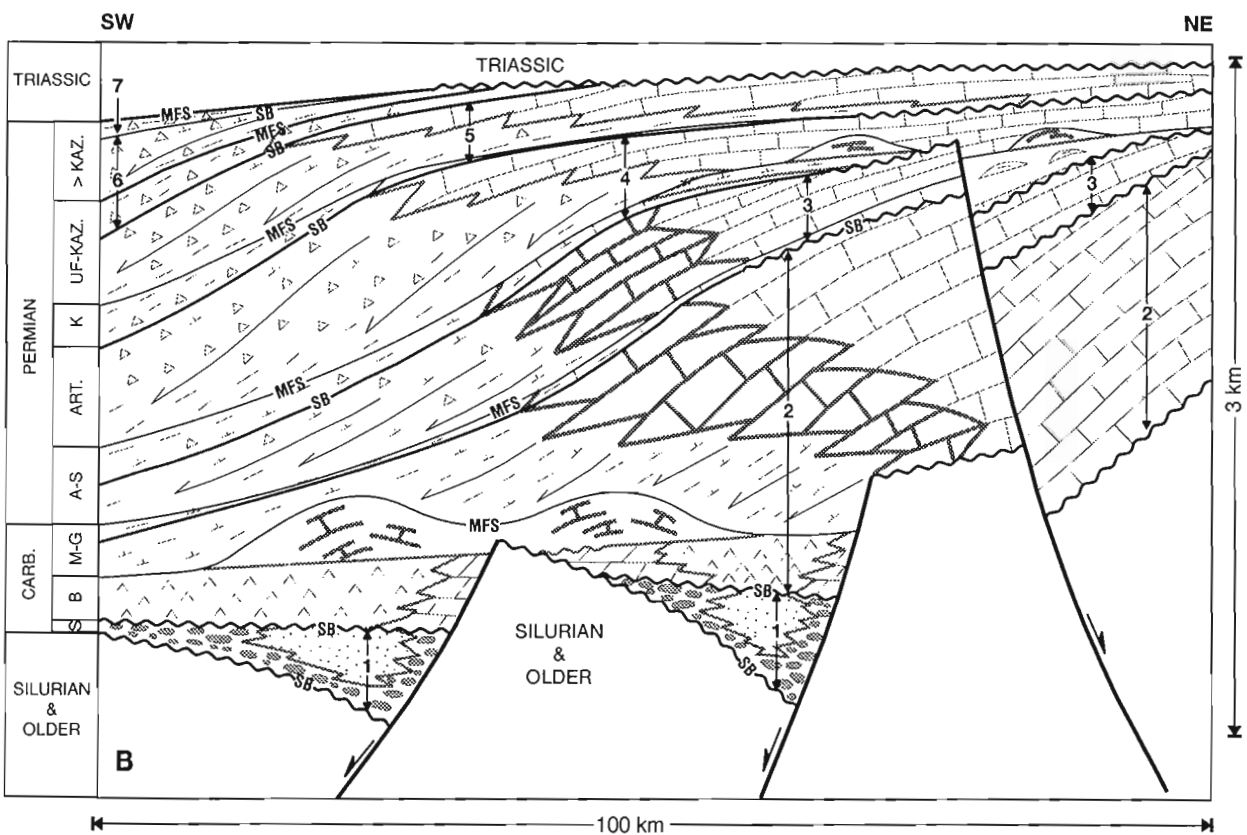
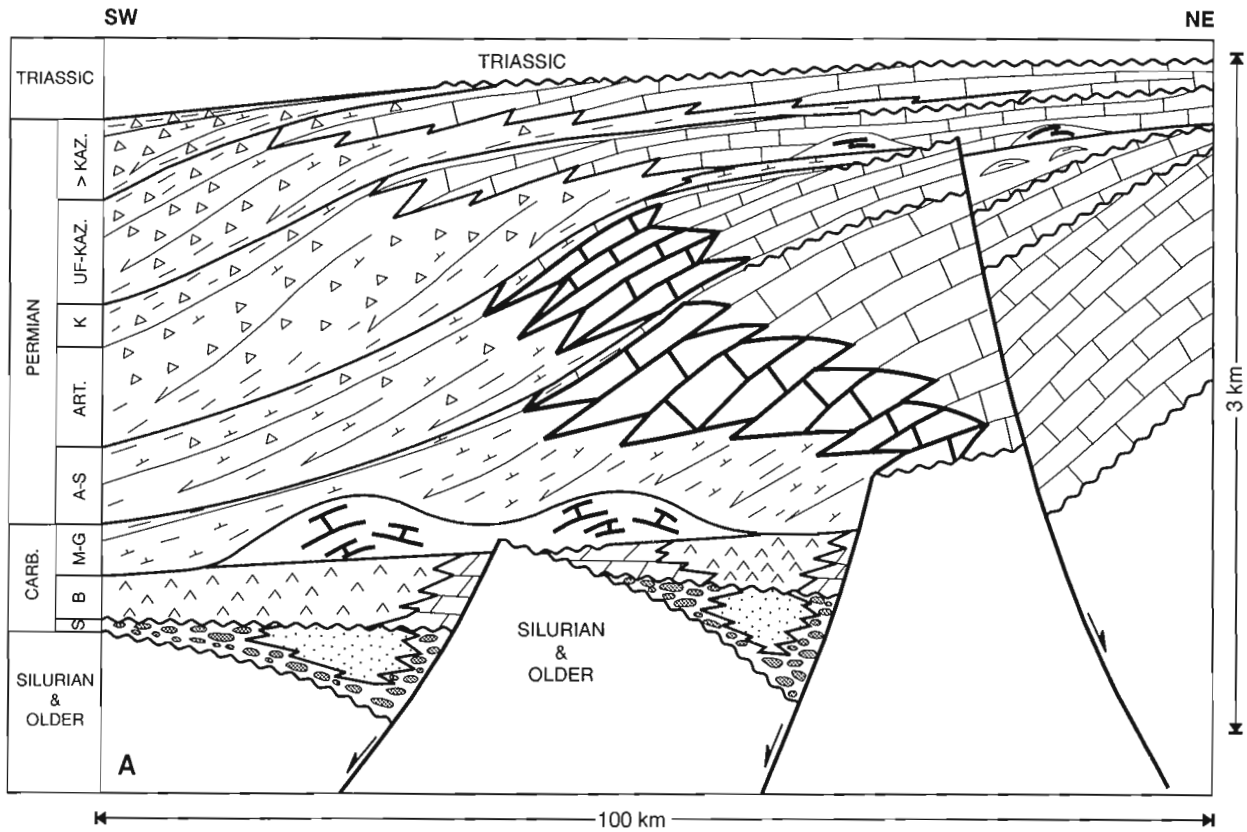


Figure 3. Carboniferous and Permian sequence stratigraphic framework on Hvitland Peninsula along a schematic and composite northeast-southwest profile. Note that the formation boundaries do not necessarily correspond to sequence boundaries or maximum flooding surfaces; compare with Figure 2. SB, sequence boundary. MFS, maximum flooding surfaces; long inclined arrows indicate the downlap of slope to basin sediments. Sequences are: 1, Serpukhovian; 2, Bashkirian-Kasimovian; 3, Gzhelian-Sakmarian; 4, Artinskian; 5, Kungurian-Kazanian; 6, Post-Kazanian; and 7, transgressive portion of Uppermost Permian-Early Triassic Sequence.

Hare Fiord Subbasin to the south: a conglomerate assemblage consisting of up to 50 m of pebble to cobble, red weathering conglomerate associated with minor sandstones and mudstones; and a sandstone assemblage comprising over 200 m of crossbedded, fine to coarse grained sandstones and minor conglomerates (Thériault et al., 1995). In the most distal areas, the sandstone assemblage interfingers with dolostone and evaporite units identical to the sediments contained in the younger Unit C1. A thin volcanic unit similar to that described by Trettin (1988) was also observed at one locality. The Serpukhovian Sequence of the Hvitland Subbasin is a broad retrogradational-progradational succession, bounded at the base and top by unconformities, and comprising locally derived basin marginal fluvial and fan conglomerates that pass basinward into fluvial sandstones and marginally marine sandstones, dolostones and evaporites, the deepest water facies in the succession (Fig. 3).

Bashkirian-Kasimovian Sequence

The Bashkirian-Kasimovian Sequence is represented by a series of units that includes the Nansen, Hare Fiord, and Otto Fiord formations (Thorsteinsson, 1974), and units C1, C2 and C3 of Mayr et al. (1995). The sequence is bounded at the base and top by subaerial unconformities. The basal unconformity lies at or close to the contact between the Borup Fiord Formation and overlying Otto Fiord Formation or Unit C1 (Fig. 2, 3). It locally lies between Borup Fiord and Nansen strata (Fig. 2), or between Nansen strata and the Franklinian basement.

The transgressive part of the sequence is represented by the Bashkirian Otto Fiord and presumably correlative Unit C1 and by the younger Bashkirian to earliest Moscovian Unit C2 (Fig. 2, 3). The Otto Fiord Formation and Unit C1 accumulated in the same rift-related subbasins that received mostly clastic sediments during deposition of the underlying Serpukhovian Sequence (Fig. 4A; Thériault et al., 1995). Similar clastic sediments also occur in Unit C1, but this lithology is subordinate to finely crystalline, variably silty dolostone which accumulated at the margins of the inferred rift basins. These strata pass basinward into evaporites and marine limestones representing deeper water, restricted marine sedimentation (Thériault et al., 1995; Nassichuk and Davies, 1980). These rocks are locally overlain by variably large carbonate buildups developed upon the surface formed by the top of Unit C1 or Otto Fiord Formation. These reefs (Unit C2 of Mayr et al., 1995; Beauchamp et al., 1995a) are keep-up reef mounds that grew while the surrounding areas were being drowned. Spectacular occurrences of such buildups occur south of Jugeborg Fiord, where one single bank, probably consisting of several coalesced reef bodies, grew over 200 km² (Fig. 4B). Less extensive buildups are also known from the area west of Lindstrom Creek, just north of Otto Fiord. Other buildups, lying at the same stratigraphic level, occur in the lower part of Unit C3 of Mayr et al. (1995). These buildups are similar to the large buildups lying at the base of the Hare Fiord Formation in the Blue Mountains, which are often referred to as "Televak" limestone (Davies et al., 1989).

The maximum flooding surface of the Bashkirian-Kasimovian Sequence lies close to the contact between the Otto Fiord and Hare Fiord formations, or wraps around the buildups of Unit C2 (Fig. 2, 3). The regressive portion of the sequence is contained in the lower two thirds of the Nansen Formation and laterally correlative lower Hare Fiord Formation (Fig. 2, 3). The regressive systems tract comprises prograding cyclic shelf and shelf-edge reefal carbonates and correlative slope to basinal deeper water mudrocks that prograded for several tens of kilometres in a general southwestward direction. The Nansen-lower Hare Fiord lateral transition, representing the Late Carboniferous shelf edge, formed a very irregular, sinuous feature, the position of which appears to have been influenced by the underlying Serpukhovian and Bashkirian rift structures (Fig. 4C). There is, however, no evidence of faulting during deposition of the regressive systems tract, suggesting that the basin underwent passive regional subsidence during that time interval. The upper sequence boundary is an unconformity that lies within the Nansen Formation (Fig. 2): it forms an erosion surface that is often overlain by red-weathering terra rosa-like paleosol material (Beauchamp et al., 1995b).

Gzhelian-Sakmarian Sequence

The Gzhelian-Sakmarian Sequence is represented by the upper Nansen and Hare Fiord formations (Thorsteinsson, 1974). It is bounded at the base and top by subaerial unconformities, both of which lay within the Nansen Formation,

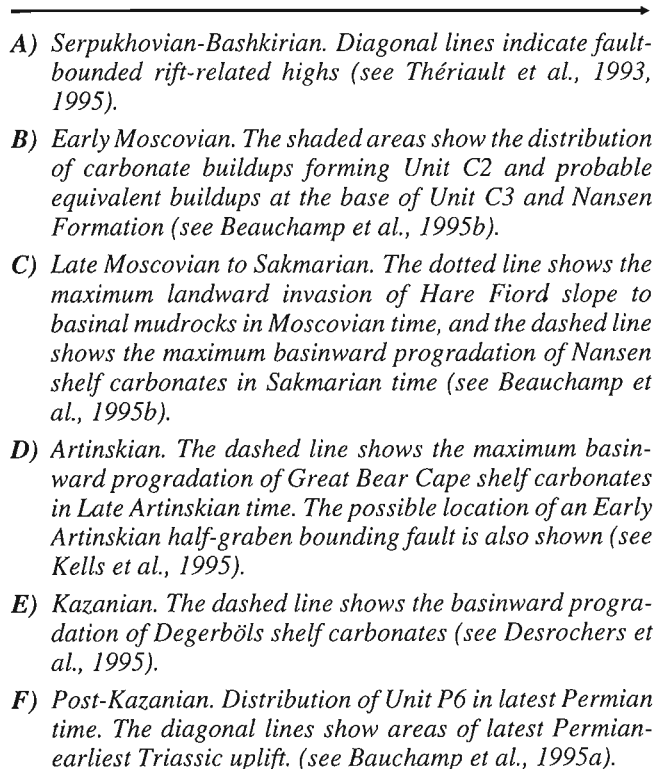
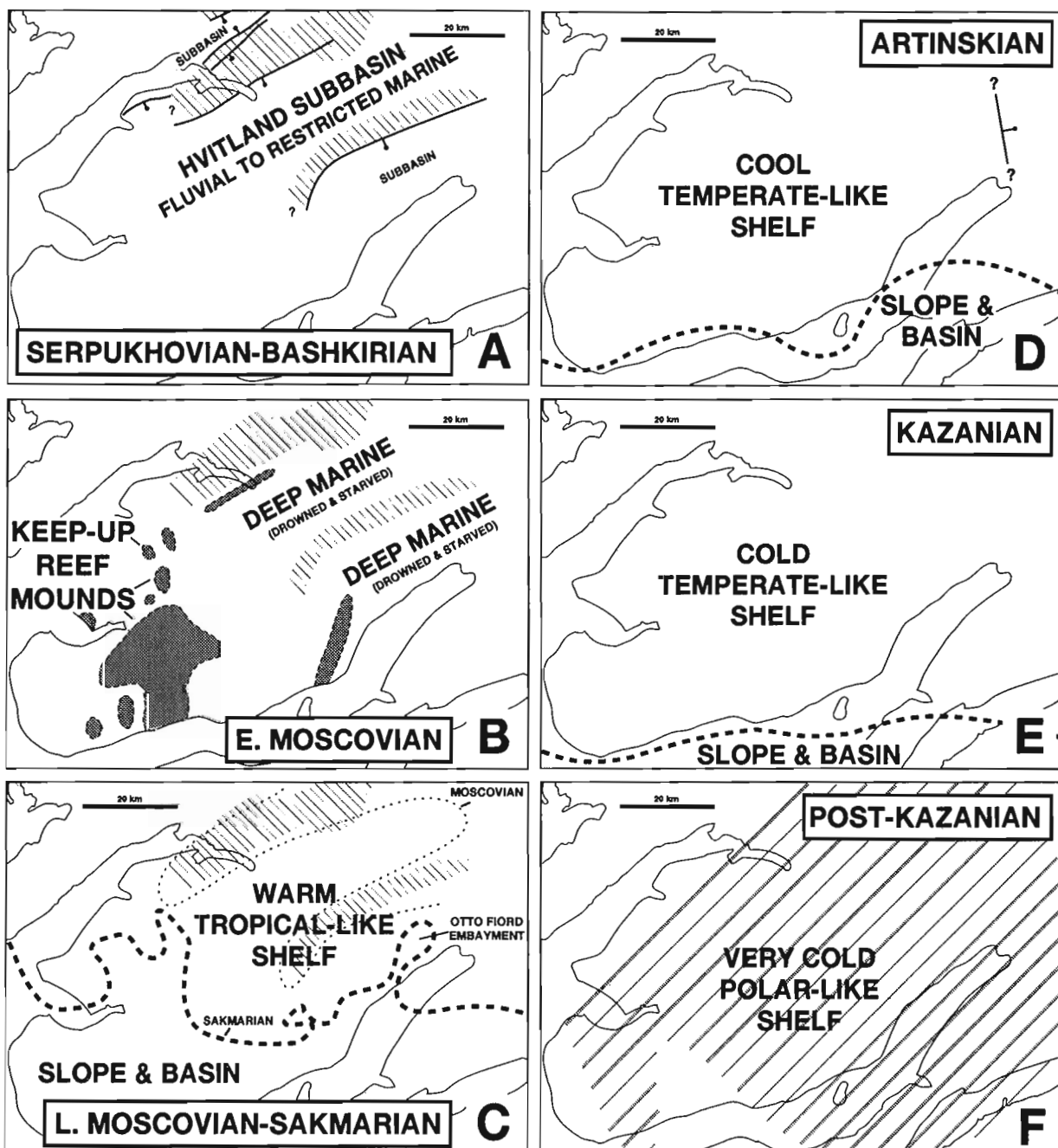
- 
- A) *Serpukhovian-Bashkirian.* Diagonal lines indicate fault-bounded rift-related highs (see Thériault et al., 1993, 1995).
 - B) *Early Moscovian.* The shaded areas show the distribution of carbonate buildups forming Unit C2 and probable equivalent buildups at the base of Unit C3 and Nansen Formation (see Beauchamp et al., 1995b).
 - C) *Late Moscovian to Sakmarian.* The dotted line shows the maximum landward invasion of Hare Fiord slope to basinal mudrocks in Moscovian time, and the dashed line shows the maximum basinward progradation of Nansen shelf carbonates in Sakmarian time (see Beauchamp et al., 1995b).
 - D) *Artinskian.* The dashed line shows the maximum basinward progradation of Great Bear Cape shelf carbonates in Late Artinskian time. The possible location of an Early Artinskian half-graben bounding fault is also shown (see Kells et al., 1995).
 - E) *Kazanian.* The dashed line shows the basinward progradation of Degerbøls shelf carbonates (see Desrochers et al., 1995).
 - F) *Post-Kazanian.* Distribution of Unit P6 in latest Permian time. The diagonal lines show areas of latest Permian-earliest Triassic uplift. (see Beauchamp et al., 1995a).

Figure 4. Carboniferous and Permian paleogeography of Hvitland Peninsula, northwestern Ellesmere Island.

and both characterized by sharp erosion surfaces associated with red weathering paleosol development (Fig. 3; Beauchamp et al., 1995b). The unconformities pass basinward into their correlative conformities which lie within the Hare Fiord Formation (Fig. 3). The transgressive systems tract is subdivided into an early and a late transgressive systems tract. The early transgressive systems tract, which lies within the Hare Fiord Formation, developed when the bulk of the Nansen shelf was subjected to erosion. It is composed of less than 50 m of calcareous shale and argillaceous limestone that rest between the shallowest facies in the underlying succession (variably fossiliferous limestone) and the overlying maximum flooding surface (base of black shale unit). The late transgressive systems formed when the

basinal area received little or no sediments. It comprises a 25 to 100 m thick deepening-upward succession of carbonate shelf cycles that onlap the unconformity in a landward direction.

The maximum flooding surface lies at the base of a prominent black shale unit within the Hare Fiord Formation. It is correlative with a surface that lies above the deepest water facies development in the carbonate shelf succession of the Nansen Formation. The overlying regressive systems tract comprises cyclic shelf and shelf edge reefal limestone that prograded basinward into argillaceous and cherty limestone, chert and shale of the upper Hare Fiord Formation (Fig. 3). The southwesternmost progradation of the Nansen Formation



represents the maximum basinward development of the Nansen shelf edge in Sakmarian time (Fig. 4C). The shelf-edge formed a very sinuous feature represented by a series of promontories separated by variably narrow embayments. Most of these features follow a very irregular northwest trend almost at a right angle to the old rift-related northeast trend (Fig. 4C).

Fossiliferous carbonate strata of the Nansen Formation comprise a series of highly diversified biotic associations, the shallowest of which is represented by abundant and highly diversified calcareous algae and foraminifers in addition to a great variety of other fossils. This assemblage, referred to as the Chloroform assemblage by Beauchamp (1994), is indicative of warm-water tropical conditions. This is further corroborated by the numerous reefs in the succession, abundant warm-water nonskeletal elements such as ooids and oncoids, pervasive aragonitic and high-magnesium calcite submarine cement, and common evaporites, paleosol calcretes and red weathering terra rosa material in the nonmarine to marginally marine equivalent succession. These features indicate that the Sverdup Basin climate remained relatively warm and semi-arid for more than 80 Ma (i.e., from the Serpukhovian to the Sakmarian) (Beauchamp, 1994; Thériault and Desrochers, 1993, 1994).

Artinskian Sequence

The Artinskian Sequence (Fig. 2, 3) is represented by the uppermost Hare Fiord and Nansen formations (Thorsteinsson, 1974), the Raanes Formation, and the bulk of the Great Bear Cape and Trappers Cove formations (Beauchamp and Henderson, 1994). The sequence is bounded at the base and top by subaerial unconformities. The lower unconformity lies within the uppermost portion of the Nansen Formation and the upper sequence boundary in the upper Great Bear Cape Formation. The transgressive systems tract is divided into an early and a late systems tract. The early transgressive systems tract lies in the uppermost portion of the Hare Fiord Formation and consists of calcareous shale and minor argillaceous limestone. These rocks lie between the conformable sequence boundary below (top of fossiliferous limestone and carbonate breccia) and the maximum flooding surface above (base of a prominent black shale unit in the overlying Trappers Cove Formation) (Fig. 3; see also Kells et al., 1995). Correlative strata in the Nansen Formation are composed of fossiliferous packstone and wackestone lying between the subaerial unconformity below and a significant flooding surface above: this surface marks the boundary with the Raanes Formation (Fig. 3).

The late transgressive systems tract is contained in the Raanes Formation. It comprises argillaceous limestone and minor shale, associated with variably large bryozoan-sponge mud mounds that accumulated during a renewed rifting phase in the area (Fig. 3; see also Kells et al., 1995). This is shown by dramatic thickness variations north and east of the mouth of Otto Fiord, where the Raanes Formation goes from a feather edge to more than 225 m over a few kilometres toward the east. The position of rift-related faults is at present uncertain, but the eastward thickening of the Raanes Formation suggests that the Artinskian rift structures formed at a high

angle relative to their Carboniferous counterparts (Thériault et al., 1995). Beauchamp and Henderson (1994) documented similar evidence of block faulting through dramatic thickness variations in the Raanes Formation on southwestern Ellesmere Island.

The maximum flooding surface closely corresponds to the contact between the Hare Fiord and Trappers Cove formations in the southwestern areas and to the contact between the Raanes and Great Bear Cape or Trappers Cove formations to the east and northeast (Fig. 3). The regressive portion is represented by the bulk of the Great Bear Cape and correlative Trappers Cove formations which together constitute a prograding and downlapping succession of shelf carbonates and slope to basinal cherty mudrocks. The Great Bear Cape Formation differs considerably from the Nansen Formation in that it comprises an impoverished biotic assemblage characterized by bryozoan, echinoderm, brachiopod and sponge, referred to as a Bryonoderm assemblage by Beauchamp (1994). This assemblage is indicative of a much cooler water temperate environment. In some basin marginal areas of the Sverdup Basin, these rocks are associated with large fusulinaceans and colonial rugose corals forming a somewhat more diversified assemblage referred to as the Bryonoderm-extended assemblage (Beauchamp, 1994). No such fossils were found in the Great Bear Cape Formation on Hvitland Peninsula.

The Great Bear Cape-Trappers Cove transition closely corresponds to the Artinskian shelf edge. This shelf edge, which prograded much farther south than its Nansen-Hare Fiord counterpart (Fig. 1-3), was almost parallel to Otto Fiord during its most basinward development (Fig. 4D).

Kungurian-Kazanian Sequence

The Kungurian-Kazanian sequence (Fig. 3) is represented by the uppermost Trappers Cove and Great Bear Cape formations (Beauchamp and Henderson, 1994) and by the overlying Van Hauen and correlative Degerbøls formations (Thorsteinsson, 1974). The transgressive portion of the sequence is contained in the uppermost Trappers Cove Formation and is represented by as much as 70 m of black shale and chert that lie stratigraphically between cliff-forming chert below and recessive black fissile shale above. These rocks pass landward into cherty carbonates that lay in the uppermost portion of the Great Bear Cape Formation (Fig. 3; Kells et al., 1995). The maximum flooding surface occurs near the Trappers Cove-Van Hauen contact in the distal areas, and in the lowest part of the Van Hauen Formation in the more proximal areas. In the latter areas, a variably thick, green glauconitic sandstone unit, representing the product of condensed transgressive sedimentation, lies between Great Bear Cape carbonates and typical Van Hauen black shales. This sandstone thickens eastward beyond Hvitland Peninsula, where it is included in the Assistance Formation forming the bulk of a late transgressive systems tract (Desrochers and Beauchamp, 1995).

The regressive portion of the sequence is represented by most of the Degerbøls Formation and correlative Van Hauen Formation. The Degerbøls Formation is lithologically similar to the Great Bear Cape Formation as it comprises an

impoverished Bryonoderm assemblage consisting of echinoderm, bryozoan, brachiopod and sponge (Beauchamp, 1994). Contrary to the Great Bear Cape Formation, the Degerbøls Formation contains no reefs, fusulinaceans, colonial rugose corals, ooids, or evidence of submarine cementation, suggesting an even colder climatic setting for the Kazanian time interval. The Degerbøls-Van Hauen transition, which represents the shelf-edge in Kazanian time, takes place through a series of well-developed, gently dipping clinofolds. The maximum progradation of the Degerbøls shelf edge lay south of Hvitland Peninsula (Fig. 4E; Desrochers and Beauchamp, 1995).

That the Kungurian-Kazanian succession of Hvitland Peninsula forms a single T-R sequence is somewhat at odds with some of the basin marginal areas of the Sverdrup Basin where this interval is represented by two broad sequences: one of mostly Kungurian age represented by the bulk of the Sabine Bay Formation and one Ufimian-Kazanian sequence represented by the Assistance and Troid Fiord formations (Beauchamp, 1994, in press). Strata equivalent to the elusive Kungurian Sequence are likely present in the transgressive systems tract in the uppermost portion of the Trappers Cove Formation. These strictly offshore strata by themselves form an asymmetrical T-R sequence, which is likely correlative with the Sabine Bay-bearing sequence at the basin margin. The Sabine Bay Formation, a succession of nonmarine to marginally marine deltaic sandstones, must have accumulated in some basin marginal subbasins at the same time as the uppermost Trappers Cove Formation. It should be emphasized that a 1 to 2 m thick sandstone bed was discovered in the eastern regions of Hvitland Peninsula. It lies at the base of a unit that is otherwise dominated by muddy carbonates. This Permian unit of uncertain age (Unit P5 of Mayr et al., 1995) lies unconformably on *Palaeoaplysina*-bearing reefal Sakmarian(?) carbonates of the Nansen Formation and is unconformably overlain by shale and conglomerate of the Triassic Blind Fiord Formation. Unit P5 could conceivably be equivalent to the Sabine Bay Formation.

Post-Kazanian Sequence

The youngest complete Permian sequence on Hvitland Peninsula is represented by a very irregularly distributed succession of dark to light grey chert and subordinate shale (Fig. 3). This post-Kazanian Sequence is contained in the uppermost Van Hauen and Degerbøls formations and in a new unnamed mappable unit referred to as Unit P6 by Mayr et al. (1995). Rocks assignable to that sequence occur only in the southwestern portion of Hvitland Peninsula. They are, however, well developed south and east of Hvitland Peninsula, as chert strata of Unit P6 attain considerable thickness in many areas, such as east of Girty Creek near the head of Hare Fiord, in the Blue Mountains, or around Mount Leith, west-central Ellesmere Island. The limited distribution of the post-Kazanian Sequence on Hvitland Peninsula is related to the broad uplift and buckling of large areas during the Permian-Triassic transition interval which led to the complete erosion of latest Permian strata (Fig. 4F; Beauchamp et al., 1995a).

The transgressive portion of the post-Kazanian sequence is represented by argillaceous, spiculitic chert in the uppermost Van Hauen Formation. This chert lay stratigraphically between shale-free, locally calcareous chert, forming the uppermost part of the underlying sequence, and black shale and chert at the base of Unit P6. These transgressive strata pass laterally into the uppermost part of the Degerbøls Formation which is represented by light grey, spiculitic chert and minor cherty limestone. The base of Unit P6 closely corresponds with the maximum flooding surface, above which the regressive systems tract is represented by over 125 m of spiculitic chert belonging to Unit P6.

The absence of fossils other than siliceous sponge spicules in the post-Kazanian Sequence has been interpreted by Beauchamp (1994) as indicative of very cold polar-like conditions, perhaps associated with a permanent or semipermanent ice cap over much of the Sverdrup Basin.

Latest Permian-Early Triassic sequence

The uppermost portion of Unit P6 is deepening-upward and therefore transgressive. It is overlain by the Triassic Blind Fiord shale, the base of which corresponds to the maximum flooding surface of a latest Permian-Early Triassic low order sequence. This surface, traditionally viewed as the basal Triassic in the Canadian Arctic, marks the eradication of siliceous sponge spicules and appears to coincide with the well-documented end-Permian mass extinction. It appears that, on Hvitland Peninsula, this event was associated with significant tectonism as shown by the buckling and erosion of most of the post-Kazanian Sequence (Fig. 4F). Similar evidence for Late Permian-Early Triassic tectonism was documented by Mayr (1992) from the Yelverton Pass area, Northern Ellesmere Island.

CONCLUSIONS

The Carboniferous and Permian succession of Hvitland Peninsula provides evidence for a complex tectonic, climatic and stratigraphic history that is recorded in six unconformity-bounded transgressive-regressive (T-R) sequences. The Serpukhovian Sequence accumulated in a series of northeastward-trending rift-related subbasins marking the earliest development of the Sverdrup Basin in the area. Rifting and fault-controlled subsidence remained active during the Bashkirian transgressive portion of the overlying Bashkirian to Kasimovian Sequence and resulted in the deposition of evaporite and dolostone in the tectonic depressions created earlier. Then followed the Moscovian to Kasimovian progradation of Nansen tropical shelf carbonates, first along the old rift structures, but later along a general northwest-southeast trend, almost at a right angle to the old rift structures. The following Gzhelian-Sakmarian Sequence led to further progradation of Nansen shelf carbonates.

The Artinskian Sequence was associated with a renewed rifting phase of the Sverdrup Basin, which led to thick accumulations of argillaceous limestone and bryozoan-sponge mud mounds of the Raanes Formation. The regressive portion of the sequence led to the progradation

of cool water temperate carbonates much beyond the position previously occupied by the Nansen shelf edge. The following Kungurian-Kazanian Sequence was also associated with the progradation of cool water carbonates (Degerbøls) and correlative chert-rich mudrocks (Van Hauen Formation) whereas the post-Kazanian Sequence was accompanied by the development of very cold water, polar-like spiculitic chert over much of the area, the bulk of which occurs within Unit P6. The youngest Permian sediments in the area are spiculitic chert that recorded a latest Permian transgression that culminated at the Permo-Triassic boundary. This event, which was associated with the eradication of siliceous sponge spicules, a return to warmer climate, and the creation of the maximum flooding surface, was also accompanied by major tectonism in the area as shown by significant erosion beneath the Triassic Blind Fiord shale.

ACKNOWLEDGMENTS

We are grateful to T. de Freitas for his review of the manuscript.

REFERENCES

- Beauchamp, B.**
1994: Permian climatic cooling in the Canadian Arctic; in *Pangea: Paleoclimate, Tectonics and Sedimentation during accretion, zenith and break-up of a super-continent*, (ed.) G.D. Klein; Geological Society of America, Special Paper 288, p. 229-246.
in press: Permian history of Arctic North America; in *The Permian of Northern Pangea*, volume 1, Paleogeography, Paleoclimates, and Stratigraphy, (ed.) P.A. Scholle, T.M. Peryt, and D.S. Ulmer-Scholle; Springer Verlag, New York.
- Beauchamp, B. and Henderson, C.M.**
1994: The Lower Permian Raanes, Great Bear Cape and Trappers Cove formations, Sverdrup Basin, Canadian Arctic: Stratigraphy and Conodont Zonation; *Bulletin of Canadian Petroleum Geology*, v. 42, p. 565-600.
- Beauchamp, B., Harrison, J.C., and Henderson, C.M.**
1989a: Upper Paleozoic stratigraphy and basin analysis of the Sverdrup Basin, Canadian Arctic Archipelago: Part 1 - time frame and tectonic evolution; in *Current Research, Part G*; Geological Survey of Canada, Paper 89-1G, p. 105-113.
1989b: Upper Paleozoic stratigraphy and basin analysis of the Sverdrup Basin, Canadian Arctic Archipelago: Part 2 - transgressive-regressive sequences; in *Current Research, Part G*; Geological Survey of Canada, Paper 89-1G, p. 115-124.
- Beauchamp, B., Mayr, U., Harrison, J.C., and Desrochers, A.**
1995a: Uppermost Permian stratigraphy (Unit P6), Hvitland Peninsula and adjacent areas, northwestern Ellesmere Island, Arctic Canada; in *Current Research 1995-B*; Geological Survey of Canada, this volume.
- Beauchamp, B., Sherry, C.T., Mayr, U., Harrison, J.C., and Desrochers, A.**
1995b: Moscovian (Upper Carboniferous) to Sakmarian (Lower Permian) stratigraphy (Nansen and Hare Fiord formations; Unit C2), Hvitland Peninsula and adjacent areas, northwestern Ellesmere Island, Arctic Canada; in *Current Research 1995-B*; Geological Survey of Canada, this volume.
- Davies, G.R., Nassichuk, W.W., and Beauchamp, B.**
1989: Upper Carboniferous Waulsortian reefs, Canadian Arctic Archipelago; in *Reefs, Canada and Adjacent Areas*, (ed.) H.H.J. Geldsetzer, N.P. James, and G.E. Tebbutt; Canadian Society of Petroleum Geologists, Memoir 13, p. 658-666.
- Desrochers, A. and Beauchamp, B.**
1995: Ufimian-Kazanian (Lower and Upper Permian) stratigraphy (Van Hauen and Degerbøls formations), Hvitland Peninsula and adjacent areas, northwestern Ellesmere Island, Arctic Canada; in *Current Research 1995-B*; Geological Survey of Canada, this volume.
- Embry, A.F.**
1993: Transgressive-regressive (T-R) sequence analysis of the Jurassic succession of the Sverdrup Basin, Canadian Arctic Archipelago; *Canadian Journal of Earth Sciences*, v. 30, p. 301-320.
- Harrison, J.C., Mayr, U., and Beauchamp, B.**
1995: Preliminary observations on the structural geology of Hvitland Peninsula, northwestern Ellesmere Island, Arctic Canada; in *Current Research 1995-B*; Geological Survey of Canada, this volume.
- Kells, M.P., Beauchamp, B., and Desrochers, A.**
1995: Artinskian-Kungurian (Lower Permian) stratigraphy (Raanes, Great Bear Cape and Trappers Cove formations), Hvitland Peninsula and adjacent areas, northwestern Ellesmere Island, Arctic Canada; in *Current Research 1995-B*; Geological Survey of Canada, this volume.
- Mayr, U.**
1992: Reconnaissance and preliminary interpretation of Upper Devonian to Permian stratigraphy of northeastern Ellesmere Island, Canadian Arctic Archipelago; Geological Survey of Canada, Paper 91-08, 117 p.
- Mayr, U., Harrison, J.C., and Beauchamp, B.**
1995: Geological map of Carboniferous and Permian units on Hvitland Peninsula and adjacent areas, northwestern Ellesmere Island, Arctic Canada; in *Current Research 1995-B*; Geological Survey of Canada, this volume.
- Nassichuk, W.W. and Davies, G.R.**
1980: Stratigraphy and sedimentation of the Otto Fiord Formation; Geological Survey of Canada, Bulletin 286.
- Thériault, P. and Desrochers, A.**
1993: Carboniferous calcrites in the Canadian Arctic; *Sedimentology*, v. 40, p. 449-465.
1994: Late Carboniferous calcrite development in the Canadian Arctic: evidence for a semi-arid climate in northwestern Pangea; in *Pangea: Global Environments and Resources*, (ed.) A.F. Embry, B. Beauchamp, and D. Glass; Canadian Society of petroleum Geologists, Memoir, v. 17, p. 319-332.
- Thériault, P., Beauchamp, B., Harrison, J.C., Mayr, U., and Steel, R.**
1995: Serpukhovian and Bashkirian (Carboniferous) stratigraphy (Borup Fiord and Otto Fiord formations; Unit C1), Hvitland Peninsula and adjacent areas, northwestern Ellesmere Island, Arctic Canada; in *Current Research 1995-B*; Geological Survey of Canada, this volume.
- Thériault, P., Beauchamp, B., and Steel, R.**
1993: Syntectonic deposition of the Carboniferous Borup Fiord Formation, northwestern Ellesmere Island, Northwest Territories; in *Current Research, Part E*; Geological Survey of Canada, Paper 93-1E, p. 105-112.
- Thorsteinsson, R.**
1974: Carboniferous and Permian stratigraphy of Axel Heiberg Island and western Ellesmere Island, Canadian Arctic Archipelago; Geological Survey of Canada, Bulletin 224, 210 p.
- Trettin, H.P.**
1988: Early Namurian (or older) alkali basalt in the Borup Fiord Formation, northern Axel Heiberg Island, Arctic Canada; in *Current Research, Part D*; Geological Survey of Canada, Paper 88-1D, p. 21-26.
- Vail, P.R., Audemard, F., Bowman, S.A., Eisner, P.N., and Perez-Cruz, G.**
1991: The stratigraphic signatures of tectonics, eustasy and sedimentology - an overview; Chapter 6 in *Cycles and Events in Stratigraphy*, (ed.) G. Einsele, W. Ricken, and A. Seilacher; Springer-Verlag, 1991, New York, p. 617-659.
- Vail, P.R., Mitchum, R.M., J.R., Todd, R.G., Widmier, J.M., Thompson, S., III, Sangree, J.B., Bubbs, J.N., and Hatelid, W.G.**
1977: Seismic stratigraphy and global changes of sea-level; in *Stratigraphic Stratigraphy - applications to hydrocarbon exploration*, (ed.) C.E. Payton; American Association of Petroleum Geologists, Memoir 26, p. 49-212.

Serpukhovian and Bashkirian (Carboniferous) stratigraphy (Borup Fiord and Otto Fiord formations; Unit C1), Hvitland Peninsula and adjacent areas, northwestern Ellesmere Island, Arctic Canada

P. Thériault¹, B. Beauchamp, J.C. Harrison, U. Mayr, and R. Steel¹
Institute of Sedimentary and Petroleum Geology, Calgary

Thériault, P., Beauchamp, B., Harrison, J.C., Mayr, U., and Steel, R., 1995: Serpukhovian and Bashkirian (Carboniferous) stratigraphy (Borup Fiord and Otto Fiord formations; Unit C1), Hvitland Peninsula and adjacent areas, northwestern Ellesmere Island, Arctic Canada; in Current Research 1995-B; Geological Survey of Canada, p. 29-36.

Abstract: The Borup Fiord Formation comprises red weathering, pebble to cobble conglomerates and sandstones that recorded fluvial sedimentation in a rift-related setting where tectonic highs shed coarse clastic material into adjacent lows. The Borup Fiord Formation is conformably overlain by Unit C1, which is represented by marine evaporites and minor limestones in the distal areas (Otto Fiord-like facies), and yellowish brown, fossiliferous dolostones and minor sandstones and conglomerates in the proximal areas. At the surface, the Otto Fiord Formation comprises marine evaporites (gypsum and anhydrite) interfingering with minor limestones. Unit C1, and likely correlative Otto Fiord Formation, recorded restricted marine sedimentation in a closed basin. The bulk of the Serpukhovian Borup Fiord Formation forms a broad, unconformity-bounded, progradational-retrogradational sequence, one that recorded nonmarine fluvial sedimentation in a series of fault-bounded, rift-related, northeastward-trending subbasins, the largest of which is here named the Hvitland Subbasin.

Résumé : La Formation de Borup Fiord comprend des conglomérats à cailloux et à galets et des grès à couleur d'altération rouge qui témoignent d'une sédimentation fluviale dans un milieu lié à un rift où les hauteurs tectoniques ont laissé tomber du matériel clastique grossier dans les zones basses adjacentes. La Formation de Borup Fiord repose en concordance sous l'Unité C1, qui est représentée par des évaporites marines et un peu de calcaire dans les zones distales (faciès semblable à celui de la Formation d'Otto Fiord), des dolomies fossilifères brun jaunâtre et, en faible quantité, des grès et des conglomérats dans les zones proximales. À la surface, la Formation d'Otto Fiord comprend des évaporites marines (gypse et anhydrite) interdigitées avec des calcaires peu abondants. L'Unité C1 et la Formation d'Otto Fiord, qui lui est vraisemblablement correlative, témoignent d'une sédimentation marine restreinte dans un bassin fermé. Le gros de la Formation de Borup Fiord du Serpukhovien forme une large séquence progradante-régressive limitée par une discordance, caractérisée par une sédimentation fluviale non marine dans une série de sous-bassins limités par des failles, liés à un rift et à direction nord-est, dont le plus vaste est appelé ici sous-bassin de Hvitland.

¹ Geological Institute Avd. A, University of Bergen, Allégaten 41, 5007 Bergen, Norway

INTRODUCTION

The oldest stratigraphic units of the Sverdrup Basin on Hvitland Peninsula, northwestern Ellesmere Island, are represented by the Carboniferous Borup Fiord and Otto Fiord formations and by a unit of uncertain stratigraphic affinity (Unit C1 of Mayr et al., 1995) that is partly identical to, and likely correlative with, the Otto Fiord Formation. These units, which outcrop sparingly, recorded the earliest rift development of the Sverdrup Basin in the area. Their distribution provides evidence for a series of northeastward-trending, fault-bounded subbasins on Hvitland Peninsula and adjacent areas, subbasins that received coarse clastic material from nearby highs and later became the locus of restricted marine sedimentation and evaporite accumulation.

HVITLAND SUBBASIN

The Borup Fiord Formation, overlying Otto Fiord Formation, and presumably correlative Unit C1 appear to have been deposited in a series of relatively narrow northeastward-trending subbasins on Hvitland Peninsula and adjacent areas (Fig. 1). The largest of these, here named the Hvitland Subbasin, was bounded to the north and south by linear highs that received little or no Borup Fiord sediments. In these areas, the Nansen Formation lies directly on Franklinian lower Paleozoic basement rocks with profound angular unconformity. Other depocentres lay north and south of the

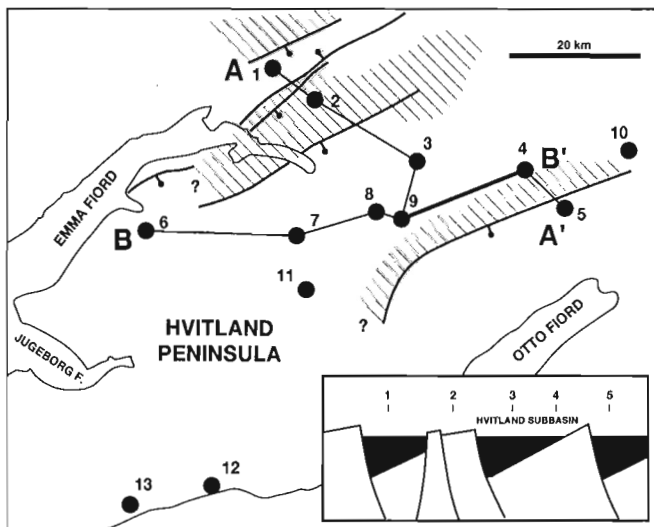


Figure 1. Map of Hvitland Peninsula showing measured sections and lines of cross-sections A-A' and B-B'. The faults shown are syn-rift structures that most likely played a role in subbasin formation in Carboniferous time. These normal faults, which probably originated as Ellesmerian (Devonian) thrust faults, were inverted back to thrust faults during the Tertiary Eurekan Orogeny. Diagonal lines outline the areas where Borup Fiord and Otto Fiord strata are absent between the lower Paleozoic basement and the Nansen Formation. The inset is one possible interpretation of the structural setting of the area in Carboniferous time. The geology is based on Mayr et al. (1995).

highs as shown by thick Borup Fiord accumulations in the vicinity of locality 1, north of Emma Fiord, and locality 5, north of Otto Fiord (Fig. 2). The internal structure of the various subbasins, including the Hvitland Subbasin, has been profoundly overprinted by Eurekan (Tertiary) folds and thrusts. These subbasins were probably part of a series of rotated blocks resulting in a half-graben geometry (Fig. 1). We assume that some of the Tertiary thrust faults adjacent to the Borup Fiord and Otto Fiord depocentres acted as graben-bounding normal faults in Carboniferous time. The same faults may have originated as Ellesmerian thrust faults in Devonian time, suggesting a very complex structural history for the area (Harrison et al., 1995).

BORUP FIORD FORMATION

Distribution and thickness

The Borup Fiord Formation is a unit of red weathering conglomerate, sandstone, and mudstone with subordinate limestone that outcrops locally on northern Ellesmere Island (Thorsteinsson, 1974; Mayr, 1992; Thériault et al., 1993). The type section of the formation is located in the vicinity of Stepanov Creek, north of Hare Fiord, where more than 120 m of strata lie unconformably upon the highly deformed lower Paleozoic Franklinian succession (Thorsteinsson, 1974). The age of the Borup Fiord Formation is generally assumed to be Serpukhovian, although foraminifers recovered from the upper part of the formation may range into the early Bashkirian (Groves et al., 1994). The Borup Fiord Formation lies unconformably either directly upon Franklinian basement rocks, or locally upon the Viséan Emma Fiord Formation. It is overlain either conformably or unconformably by marine carbonates of the Nansen Formation or evaporites of the Otto Fiord Formation. The maximum thickness of the Borup Fiord is 985 m as measured at Yelverton Inlet (Mayr, 1992).

On Hvitland Peninsula, the Borup Fiord Formation outcrops at various localities south of the head of Emma Fiord, where it rests mostly on Franklinian basement (Fig. 4A, B). Good exposures of the formation also occur immediately north of the head of Emma Fiord (Fig. 4C). Stratigraphic thicknesses range from a few metres to more than 190 m (Fig. 1, 2, locality 3; Fig. 4B). The Borup Fiord Formation is overlain unconformably by evaporites, dolostones or clastics of Unit C1, evaporites of the Otto Fiord Formation, or limestones and dolostones of the Nansen Formation. The Borup Fiord Formation is also known to be absent in some areas, such as in the vicinity of locality 2 (Fig. 1, 2), where Nansen strata lies directly upon Franklinian basement (Fig. 4D).

Lithologies and depositional environments

The Borup Fiord Formation of Hvitland Peninsula is composed of a variety of lithologies, including shale and siltstone (undifferentiated and herein called mudstone), sandstone, conglomerate, calcrete, dolostone, and evaporite. All clastic lithologies are red weathering, which imparts a bright reddish colour to the otherwise grey-brown weathering landscape.

The Borup Fiord lithologies can most suitably be grouped into two assemblages: a conglomerate assemblage and a sandstone assemblage.

The conglomerate assemblage has been examined in detail at locality 10, where it is 25 m thick and consists of cobble to boulder conglomerate and lesser interlayers of medium to pebbly sandstone and mudstone. The conglomerates occur as crude beds that are tabular in shape and vary from medium to thick bedded. Internally, the beds are for the most part matrix-supported, massive, unsorted and ungraded (Fig. 5A). Clasts are of various shapes, subrounded to subangular in outline, and composed of chert, sandstone, and limestone fragments. Maximum particle size values (average of the ten largest clasts in a bed) vary from 15 to 40 cm. The matrix is muddy and unsorted. The sandstones and mudstones are overall thin bedded, and massive to tabular crossbedded. One paleocurrent direction was obtained from a tabular crossbed in pebbly sandstone: it pointed to the west at 260°.

Based on these features, the conglomerate assemblage of the Borup Fiord Formation is interpreted as debris flow (conglomerate) and sheetflood (sandstones and mudstones)

deposits of alluvial fan origin (proximal reaches of large fans, or anywhere on small fans). Although the scattered nature of the exposure somewhat limits our interpretation, there is little doubt that the conglomerate assemblage is of proximal derivation and that it is associated with a series of marginal fans deposited adjacent to the Hvitland Subbasin. The exposure area of the conglomerate assemblage is situated near the southern margin of the subbasin, a margin that was either fault-bounded or characterized by a rotated and uplifted block crest (Fig. 1).

The sandstone assemblage occurs in several areas to the west of proximal sections 1 and 2. Two sections were described, one measuring 110 m (Fig. 3, 4A, locality 8) and the other 190 m (Fig. 3, 4B, locality 3). The thickness development at locality 3 represents a minimum value since the uppermost strata in this area forms a mountain summit and its top has been eroded (Fig. 4B). The sandstone assemblage comprises random interlayers of pebble to cobble conglomerate, very fine to coarse grained, pebbly sandstone, mudstone and nodular to massive calcarete. The conglomerates, which make up less than 5 per cent of the sandstone assemblage, occur as isolated units that are

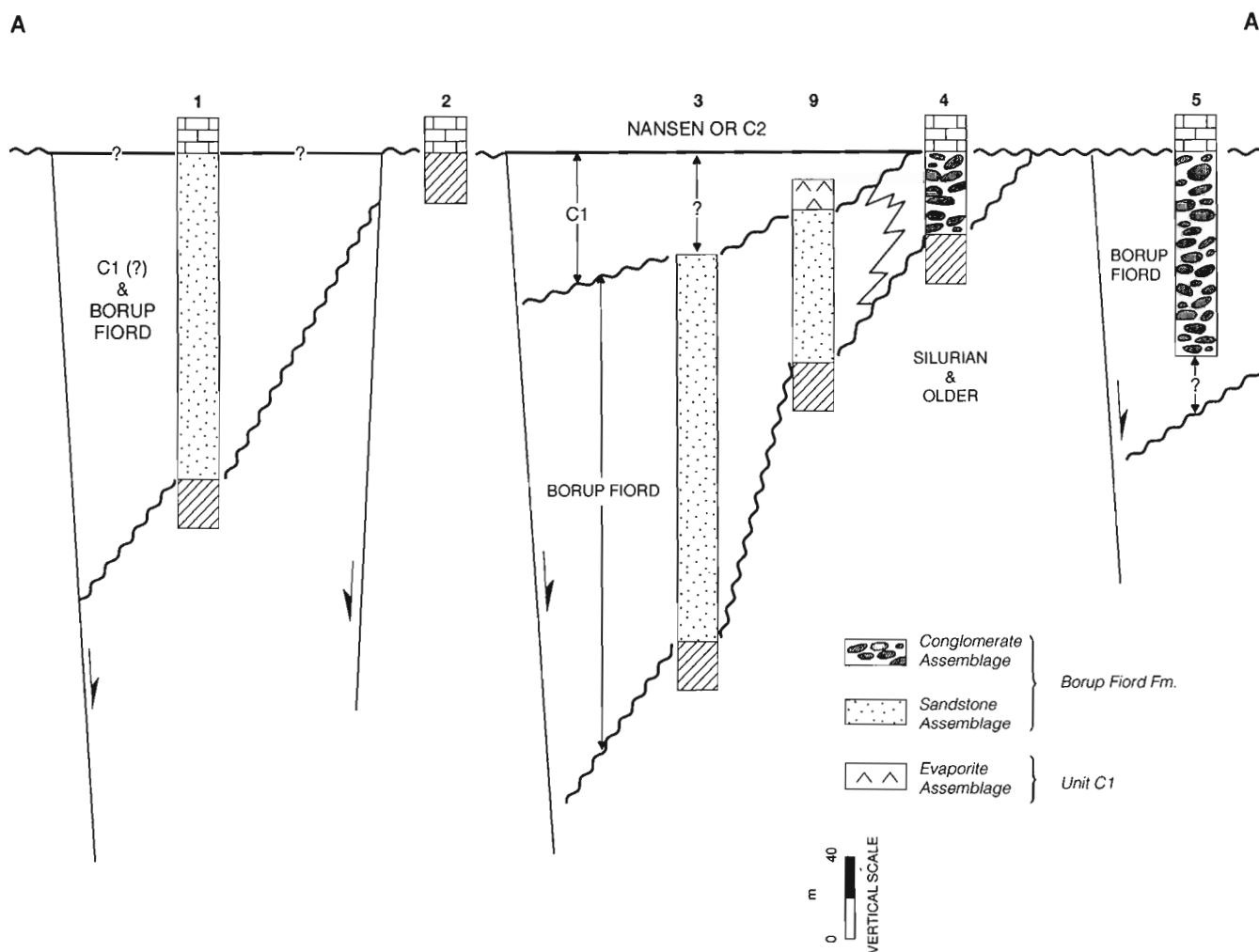


Figure 2. Cross-section A-A'. The cross-section is a northwest-southeast transect showing the various syntectonic highs and lows on Hvitland Peninsula and adjacent areas. See Figure 1 for the line of cross-section.

30 to 100 cm thick, erosively based, lenticular in shape, thin to medium bedded, and clast-supported. No internal stratification has been observed, partly because of mud coatings on the exposures. Clasts have maximum particle size values ranging from 2 to 6 cm, are mostly subrounded and are composed predominantly of chert and sandstone rock fragments. The matrix is relatively well sorted and sandy.

Fine to coarse grained sandstone is predominant in the sandstone assemblage, accounting for more than 80 per cent of the succession. Sandstone units are up to 10 m thick, have tabular to lenticular geometries and are thickly laminated to medium bedded (Fig. 5B). In general, very fine to fine grained sandstone beds are tabular in shape, massive to parallel laminated, and contain occasional granule-rich layers and calcrete-bearing horizons. Medium to coarse grained, pebbly sandstones, which are relatively uncommon in the succession, are typically lenticular in shape, erosively based, trough crossbedded and normal-graded. Rocks included in the sandstone assemblage include about 10 per cent of poorly exposed mudstones (not considering the covered intervals, which are recessive and believed to be represented by mudstone as well). The mudstone

is either parallel laminated or massive, the latter probably due to pedogenic destratification as suggested by associated calcrete nodules. Another common lithology of the sandstone assemblage consists of carbonates of calcrete paleosol origin. Both nodular and massive types are present, and their macro- and microfabric are reminiscent of those described from the Bashkirian lower clastic member of the Canyon Fiord Formation in southwestern Ellesmere Island (Thériault and Desrochers, 1993).

At locality 1, north of Emma Fiord, the sandstone assemblage is associated with a series of variably fossiliferous limestones and dolostones forming medium to thick, light grey to yellowish brown beds. These rocks are similar to those encountered in Unit C1 or in the Nansen Formation, suggesting a possible interfingering between these two units and the Borup Fiord Formation. Some evaporite beds occur in the upper part of the sandstone assemblage at locality 7, a few metres below the sharp unconformable contact with evaporites of Unit C1, providing evidence for marine incursion in the Hvitland Subbasin in probable Serpukhovian time.

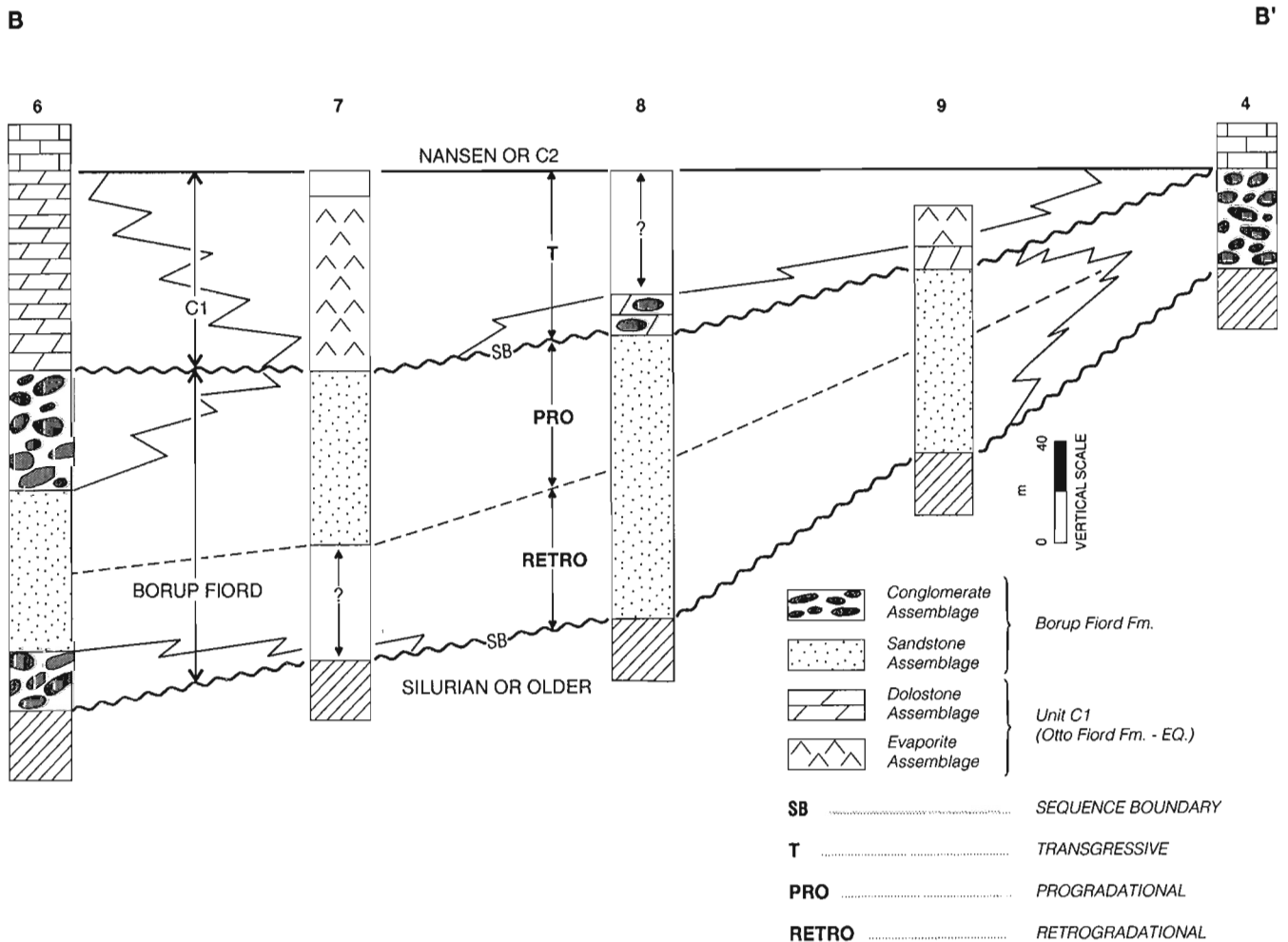


Figure 3. Cross-section B-B' oblique to the depositional axis of the Hvitland Subbasin. See Figure 1 for the line of cross-section.

The sandstone assemblage of the Borup Fiord Formation represents the deposits of distal alluvial fans and/or flood-basin. The bulk of sediments accumulated in overbank settings in the form of sheetflood and crevasse splay deposits (mudstone and very fine to fine grained sandstone), whereas the coarse to pebbly grained sandstone and the conglomerate have sedimentological features characteristic of stream-channel deposits. In terms of relative half-graben position, the sandstone assemblage would have characterized the lower part of the depositional slope and the axial area of the subbasin on Hvitland Peninsula. When considered together with the single north-south paleocurrent orientation, the lack of tabular cross-bedded sandstone or conglomerate beds suggests that the studied localities were crossed by single channel streams, which is characteristic of the distal, transverse alluvial drainage of modern rift settings such as the Basin and Range province (Leeder and Jackson, 1993).

Two additional sections of the Borup Fiord Formation require special consideration. The Borup Fiord succession at locality 6 is unique in that it represents an isolated occurrence on the northwestern part of the Hvitland Subbasin, and that it contains roughly equal proportions of coarse and fine grained clastic lithologies. The succession defines a broad retrogradational-progradational sequence about 135 m thick (Fig. 3), the lower and upper portions of which are dominated by clast-supported conglomerates with a maximum clast size of 2 to 10 cm. The middle portion is largely covered and recessive, and composed of isolated outcrop ledges of fine grained sandstone to mudstone hosting isolated calcrete nodules. The Borup Fiord Formation at Section 6 (Fig. 3) was deposited in relatively proximal alluvial settings, perhaps adjacent to a major subbasin-bounding fault. It is not entirely clear whether locality 6 was part of the Hvitland Subbasin, as shown in Figure 3, or separated from it by one or more faults.

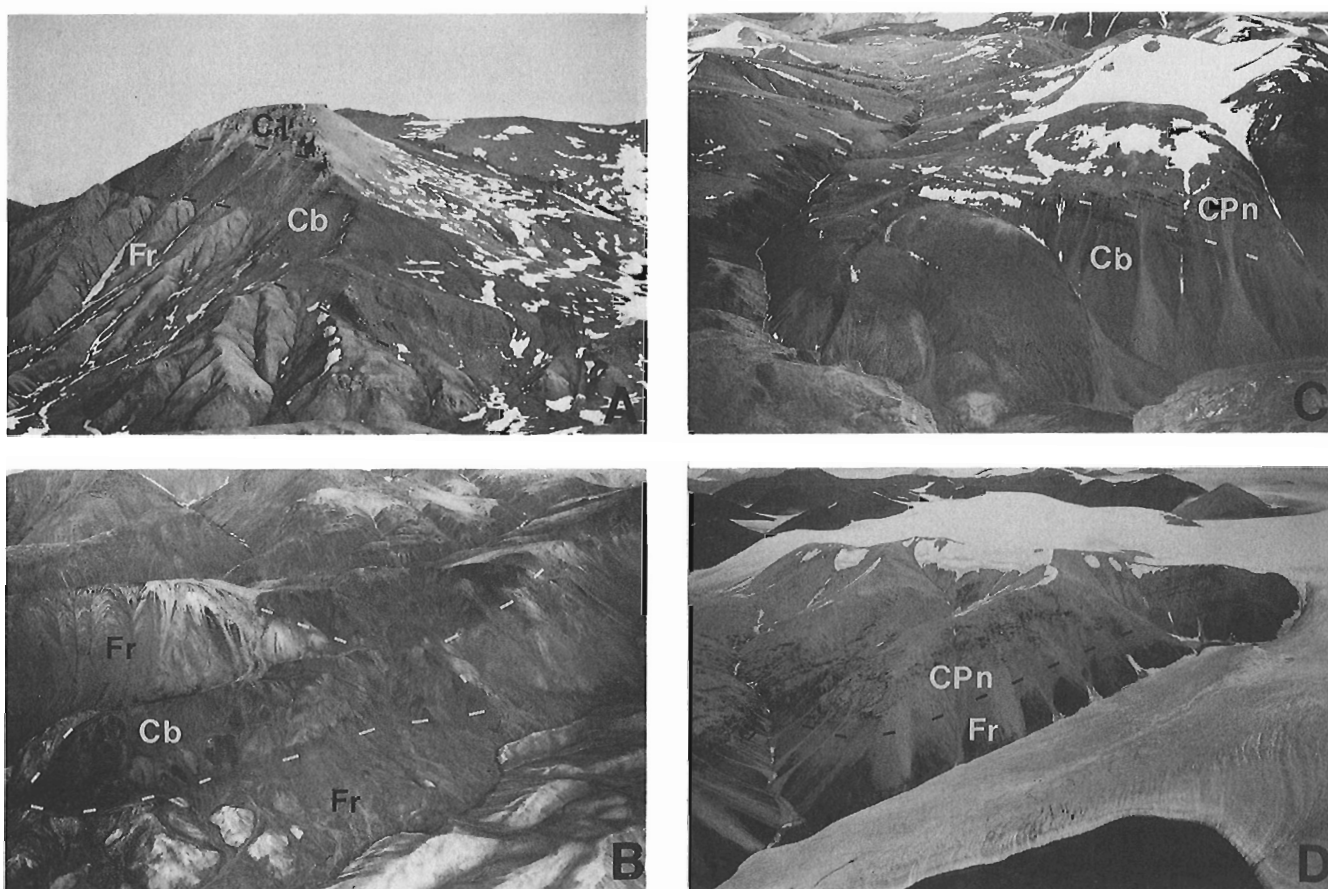


Figure 4. *A) Borup Fiord (Cb) Formation unconformably underlain by Franklinian basement (Fr) and unconformably overlain by conglomerates of Unit C1 at locality 8, Hvitland Peninsula, northwestern Ellesmere Island. B) Borup Fiord Formation (Cb) lying unconformably on Franklinian basement rocks (Fr) at locality 3, Hvitland Peninsula, northwestern Ellesmere Island. C) Borup Fiord Formation (Cb) overlain by Nansen Formation (CPn) at locality 1, north of Emma Fiord, northwestern Ellesmere Island. D) Nansen Formation (CPn) lying unconformably on Franklinian basement rocks (Fr) with no intervening Borup Fiord nor Unit C1 strata, locality 2, east of Emma Fiord, northwestern Ellesmere Island.*

Another unique occurrence is at locality 11, in the south-western part of the Hvitland Subbasin, where the Borup Fiord Formation is 75 m thick and bounded at the base by Franklinian basement rocks and at the top by Unit C1. It comprises fine grained, largely covered, red weathering clastics interspersed with three volcanic units measuring 12, 6, and 4 m. The volcanics are basaltic in composition and contain abundant amygdules and vesicles smaller than 5 mm. These volcanics represent the second evidence of volcanic activity contemporaneous with Serpukhovian rift sedimentation. In an area south of Rens Fiord on northern Axel Heiberg Island, two units of alkali basalts were found within redbeds of the Borup Fiord Formation (Trettin, 1988). The Borup Fiord volcanics near Rens Fiord and on Hvitland Peninsula are either correlative with the Audhild Formation of north-western Ellesmere Island, or they are slightly older.

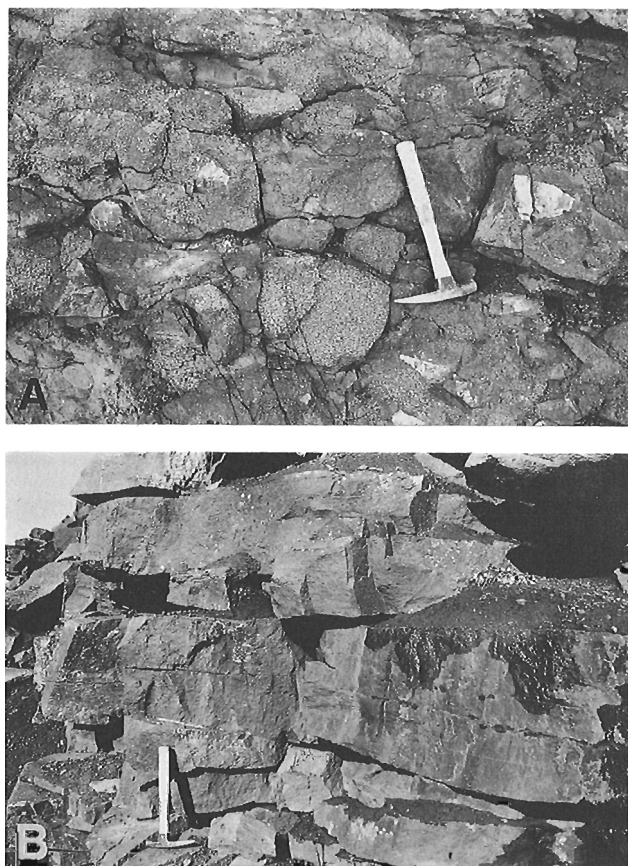


Figure 5. **A)** Conglomerate assemblage of Borup Fiord Formation: matrix-supported conglomerate, locality 4, Hvitland Peninsula, northwestern Ellesmere Island. Hammer for scale. **B)** Sandstone assemblage of Borup Fiord Formation: trough crossbedded fine grained sandstone, locality 3, Hvitland Peninsula, northwestern Ellesmere Island. Hammer for scale.

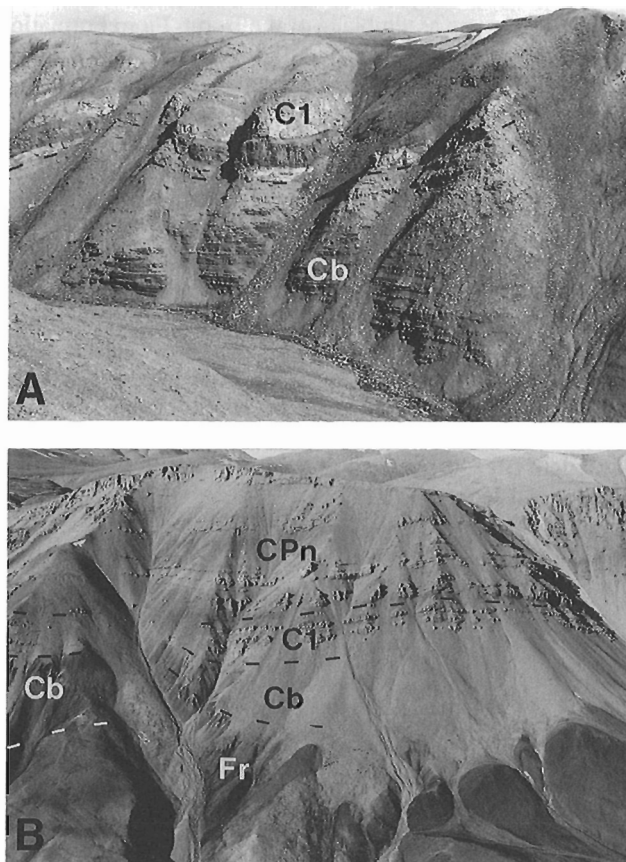


Figure 6. **A)** Unconformable contact between Unit C1 (C1; evaporite assemblage) and Borup Fiord Formation (Cb; sandstone assemblage) at locality 7, Hvitland Peninsula, northwestern Ellesmere Island. **B)** Contact between Borup Fiord Formation (Cb; sandstone and conglomerate assemblage), Unit C1 (C1; dolostone assemblage) and Nansen Formation (CPn) at locality 6, Hvitland Peninsula, northwestern Ellesmere Island. Fr, Franklinian basement rocks.

OTTO FIORD FORMATION AND UNIT C1

Distribution and thickness

The Otto Fiord Formation is a unit of marine evaporite and subordinate fossiliferous limestone that has a wide distribution in the axial regions of the Sverdrup Basin. The type section of the formation is at Van Hauen Pass, where the formation is over 400 m thick and exposed with little interruption along the north shore of Hare Fiord (Thorsteinsson, 1974; Nassichuk and Davies, 1980). Good exposures of the formation are also known from the Blue Mountains on west-central Ellesmere Island, and at various localities on northern Ellesmere Island. Diapiric exposures of Otto Fiord evaporites are also known from many areas of the Arctic Archipelago, especially on Axel Heiberg Island where they form various circular, oblong, and linear structures (Thorsteinsson, 1974).

On Hvitland Peninsula, evaporites assigned unequivocally to the Otto Fiord Formation occur in the southwestern regions where they lie in normal stratigraphic position (Fig. 1). Small, fault-bounded, tectonically transported masses enclosed by younger strata also occur in a few places (e.g., locality 12). The thickest development of the formation is around locality 13 where an estimated 250 m of evaporite and minor limestone occur; this value represents a minimum because the base of the formation is not exposed. The Otto Fiord Formation is overlain conformably by reefal limestone belonging to a Carboniferous unnamed unit (Unit C2 of Mayr et al., 1995) or by dark grey to black basinal mudrocks of the Hare Fiord Formation. The lateral extent of the Otto Fiord Formation appears to be controlled by the same rift-related faults that limit the distribution of the Borup Fiord Formation.

In many areas of Hvitland Peninsula, a unit mapped as Unit C1 by Mayr et al. (1995) lies stratigraphically above the Borup Fiord Formation. Unit C1 is represented by unfossiliferous, yellowish brown weathering dolostone and white evaporite, and subordinate dark grey limestone, red-brown to yellowish brown weathering conglomerate and sandstone. Dolostone and

evaporite facies of Unit C1 are probably correlative and most likely equivalent to the Otto Fiord Formation in the type area. If the inferred correlation between the evaporite assemblages and dolostone of Unit C1, and the Otto Fiord Formation is correct, then the dolostone is also correlative with the basal Nansen Formation. However, the unfossiliferous dolostones of Unit C1 form a distinct mappable unit that may better be included in the Otto Fiord Formation or given a separate formation name. Biostratigraphic data will hopefully help clarify the relationships between Unit C1 and the Borup Fiord, Otto Fiord and Nansen formations.

Strata assigned to Unit C1 have a distribution that is similar to the Borup Fiord Formation, except where red weathering Borup Fiord strata are unconformably overlain by light grey weathering carbonates of the Nansen Formation (e.g., locality 10), or in a band of outcrops centred around locality 14 where rocks mapped as belonging to Unit C1 lie directly upon Franklinian basement rocks. At locality 1, yellowish brown weathering, Unit C1-like dolostones and limestones are interbedded with red weathering Borup Fiord strata suggesting that both units may be partly correlative. The contact between Unit C1 and the Nansen Formation is locally unconformable as coarse grained pebble to cobble conglomerates and angular breccias of the former are sharply and erosively overlain by marine limestones of the latter (e.g., Fig. 3, locality 6). In other areas, however, the contact appears conformable.

Lithologies and depositional environments

On Hvitland Peninsula, the Otto Fiord Formation comprises anhydrite and gypsum units, 1 m to more than 10 m thick, alternating with much thinner units (less than 50 cm) of dark grey to black dolomitic limestone and dolostone, and greenish grey gypsiferous shale. Parallel laminations and irregular nodular mosaics are common in the evaporite facies. These lithologies are similar to those present in the type area at Van Hauen Pass to the south. In that area, the Otto Fiord Formation comprises variably thick evaporite units alternating with fossiliferous to nonfossiliferous limestone units, some forming small patch reefs. The Otto Fiord Formation has been interpreted as a subaqueous evaporite deposit based on such features as: its basin axial distribution, the presence of bottom growth gypsum fabrics, the presence of fossils in the interfingering carbonates, and its lateral transition into fossiliferous carbonates of the lower Nansen Formation (Nassichuk and Davies, 1980).

Strata of Unit C1 comprise two different, locally interfingering, facies assemblages. The first facies assemblage, referred to as the dolostone assemblage, consists of yellowish brown weathering, medium bedded, finely crystalline dolostone with subordinate red weathering pebble to cobble conglomerate, medium to coarse grained sandstone and unconsolidated red shale. The sandstone is parallel laminated in places, and commonly calcified. The second facies assemblage, referred to as the evaporite assemblage, is represented by variably "bedded" white evaporite (gypsum and anhydrite) and subordinate medium bedded, dark grey, finely crystalline dolostone and limestone. These strata are identical to the Otto Fiord Formation elsewhere on Hvitland

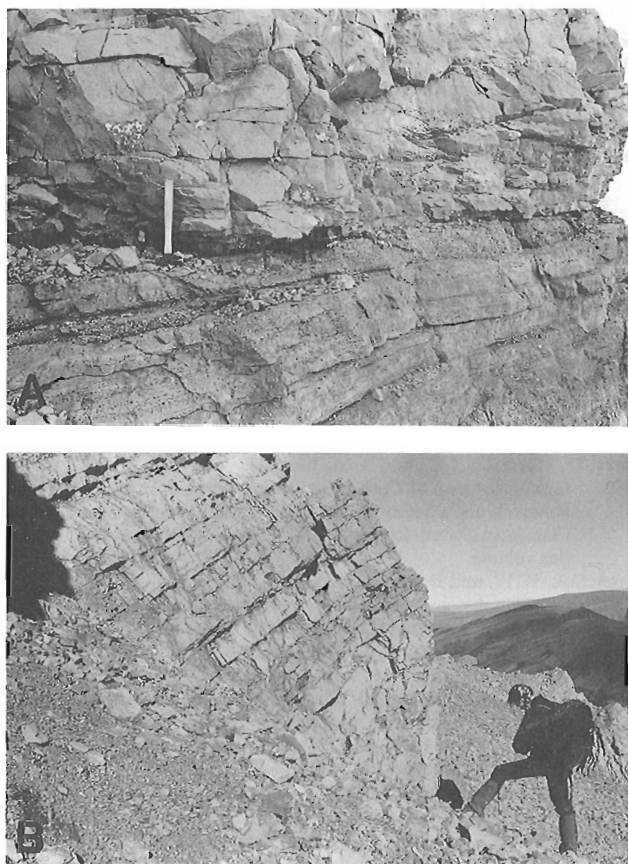


Figure 7. A) Dolostone assemblage of Unit C1: sharp contact between pebbly conglomerate and finely crystalline dolostone (above hammer), locality 4, Hvitland Peninsula, northwestern Ellesmere Island. B) Dolostone assemblage of Unit C1: medium bedded, finely crystalline dolostone, locality 6, Hvitland Peninsula, northwestern Ellesmere Island. Person (Melanie Kells) for scale.

Peninsula and farther south in the Hare Fiord area. Both facies assemblages of Unit C1 locally interfinger and are thus believed to be correlative. As discussed previously, they may also be partly correlative with the Borup Fiord Formation. The dolostone assemblage is believed to represent marginal marine to nonmarine sedimentation at the margin of a closed basin, the distal and deeper water portion of which is represented by the evaporite assemblage.

SEQUENCE STRATIGRAPHY

The Borup Fiord and Otto Fiord formations and Unit C1 recorded the earliest development of the Sverdrup Basin on Hvitland Peninsula. The bulk of the Borup Fiord Formation represents a broad, unconformity-bounded, retrogradational-progradational, mostly nonmarine (fluvial) sequence (Fig. 3; Beauchamp et al., 1995a). The retrogradational package is characterized by basal sandstones and conglomerates culminating in fine grained sandstones and mudstones containing well developed calcrete levels. The progradational package, which is poorly defined, is characterized by an upward reduction in calcrete and random presence of pebbly sandstone and conglomerate layers. The retrogradational-progradational character of the sequence is not discernible in the most proximal area (e.g., locality 9). Elsewhere in the Sverdrup Basin, the Borup Fiord Formation is more clearly retrogradational-progradational in nature (e.g., Yelverton Inlet; Hare Fiord area).

The contact between the Borup Fiord Formation and overlying Unit C1 is invariably sharp and corresponds to a low-order sequence boundary. The unconformity is marked by local fluvial incision (e.g., locality 8). The Otto Fiord Formation forms the basal transgressive portion of the overlying Bashkirian-Kasimovian transgressive-regressive sequence, a transgression that culminated in the development of large carbonate buildups at the maximum flooding surface (Beauchamp et al., 1995a, b). The regressive portion of the sequence is recorded in the Moscovian to Kasimovian parts of the Nansen and Hare Fiord formations (Beauchamp et al., 1995a, b).

CONCLUSIONS

The earliest development of the Sverdrup Basin on Hvitland Peninsula is recorded by the Borup Fiord Formation (fluvial red conglomerates and sandstones), Unit C1 (marine evaporites and limestones, minor marine sandstones in distal areas, nonfossiliferous, restricted marine dolostones, sandstones, siltstones and conglomerates in proximal areas), and the Otto Fiord Formation (subaqueous marine evaporites, minor marine limestones). The bulk of the Borup Fiord Formation appears to form a broad retrogradational-progradational unconformity-bounded sequence. The Otto Fiord Formation and, presumably, correlative Unit C1 are part of the transgressive systems tract of a probably Bashkirian and younger sequence. The Borup Fiord Formation and the overlying Otto Fiord Formation and Unit

C1 were deposited in a series of rift-related subbasins, the largest of which (Hvitland Subbasin) strikes in a northeastward direction and is separated from other subbasins by apparently linear and presumably fault-bounded highs.

ACKNOWLEDGMENTS

Many thanks to T. de Freitas who kindly reviewed this manuscript and suggested many improvements.

REFERENCES

- Beauchamp, B., Mayr, U., and Harrison, J.C.**
1995a: Carboniferous and Permian stratigraphic sequences on Hvitland Peninsula and adjacent areas, northwestern Ellesmere Island, Arctic Canada; in *Current Research 1995-B*, Geological Survey of Canada, this volume.
- Beauchamp, B., Sherry, C.T., Mayr, U., Harrison, J.C., and Desrochers, A.**
1995b: Moscovian (Upper Carboniferous) to Sakmarian (Lower Permian) stratigraphy (Nansen and Hare Fiord formations; Unit C2), Hvitland Peninsula and adjacent areas, northwestern Ellesmere Island, Arctic Canada; in *Current Research 1995-B*, Geological Survey of Canada, this volume.
- Groves, J.R., Nassichuk, W.W., Lin, R., and Pinard, S.**
1994: Middle Carboniferous fusulinacean biostratigraphy, northern Ellesmere Island (Sverdrup Basin, Canadian Arctic Archipelago); Geological Survey of Canada, Bulletin 469, 55 p.
- Harrison, J.C., Mayr, U., and Beauchamp, B.**
1995: Preliminary observations on the structural geology of Hvitland Peninsula and adjacent areas, northwestern Ellesmere Island, Arctic Canada; in *Current Research 1995-B*; Geological Survey of Canada, this volume.
- Leeder, M.R. and Jackson, J.A.**
1993: The interaction between normal faulting and drainage in active extensional basins, with examples from the western United States and central Greece; *Basin Research*, v. 5, p. 79-102.
- Mayr, U.**
1992: Reconnaissance and preliminary interpretation of Upper Devonian to Permian stratigraphy of northeastern Ellesmere Island, Canadian Arctic Archipelago; Geological Survey of Canada, Paper 91-8, 117 p.
- Mayr, U., Harrison, J.C., and Beauchamp, B.**
1995: Geological map of Carboniferous and Permian units on Hvitland Peninsula and adjacent areas, northwestern Ellesmere Island, Arctic Canada; in *Current Research 1995-B*; Geological Survey of Canada, this volume.
- Nassichuk, W.W. and Davies, G.R.**
1980: Stratigraphy and sedimentation of the Otto Fiord Formation; Geological Survey of Canada, Bulletin 286, 87 p.
- Thériault, P., Beauchamp, B., and Steel, R.**
1993: Syntectonic deposition of the Carboniferous Borup Fiord Formation, northwestern Ellesmere Island, Northwest Territories; in *Current Research, Part E*; Geological Survey of Canada, Paper 93-1E, p. 105-112.
- Thériault, P. and Desrochers, A.**
1993: Carboniferous calcretes in the Canadian Arctic; *Sedimentology*, v. 40, p. 449-465.
- Thorsteinsson, R.**
1974: Carboniferous and Permian stratigraphy of Axel Heiberg Island and western Ellesmere Island, Canadian Arctic Archipelago; Geological Survey of Canada, Bulletin 224, 210 p.
- Trettin, H.P.**
1988: Early Namurian (or older) alkali basalt in the Borup Fiord Formation, northern Axel Heiberg Island, Arctic Canada; in *Current Research, Part D*; Geological Survey of Canada, Paper 88-1D, p. 21-26.

Moscovian (Upper Carboniferous) to Sakmarian (Lower Permian) stratigraphy (Nansen and Hare Fiord formations; Unit C2), Hvitland Peninsula, northwestern Ellesmere Island, Arctic Canada

B. Beauchamp, C.T. Sherry¹, U. Mayr, J.C. Harrison, and A. Desrochers¹
Institute of Sedimentary and Petroleum Geology, Calgary

Beauchamp, B., Sherry, C.T., Mayr, U., Harrison, J.C., and Desrochers, A., 1995: Moscovian (Upper Carboniferous) to Sakmarian (Lower Permian) stratigraphy (Nansen and Hare Fiord formations; Unit C2), Hvitland Peninsula, northwestern Ellesmere Island, Arctic Canada; in Current Research 1995-B; Geological Survey of Canada, p. 37-46.

Abstract: The Nansen and Hare Fiord formations, together with Unit C2, contain two low-order, unconformity-bounded, transgressive-regressive sequences on Hvitland Peninsula: Bashkirian-Kasimovian and Gzhelian-Sakmarian. Unit C2 comprises large bryozoan keep-up reefs that grew during a late phase of a Bashkirian-Early Moscovian transgression. The overlying Upper Carboniferous Nansen (cyclic shelf carbonates and shelf edge reefs) and Hare Fiord formations (slope to basinal turbiditic mudrocks and debris flows) form a thick, regressive, southwestward progradational succession. The Gzhelian-Sakmarian Sequence, contained in the upper Nansen and Hare Fiord formations, was associated with the progradation of a second tongue of Nansen carbonates. The Nansen-Hare Fiord transition, which corresponds to the Late Carboniferous-Early Permian shelf edge, formed a sinuous northwestward-oriented feature associated with steep reef promontories and deeper water embayments.

Résumé : Les formations de Nansen et de Hare Fiord, de même que l'Unité C2, contiennent deux séquences transgressives-régressives limitées par une discordance, d'ordre inférieur, dans la péninsule Hvitland : bashkiriennne-kasimoviennne et gzhéliennne-sakmariennne. L'Unité C2 comprend de vastes récifs de bryozoaires conservés qui se sont édifiés durant une phase tardive d'une transgression du Bashkirien-Moscovien précoce. Les formations sus-jacentes du Carbonifère supérieur, soit les formations de Nansen (roches carbonatées de plate-forme et récifs de rebord de plate-forme cycliques) et de Hare Fiord (mudstones turbiditiques et coulées de débris de talus à bassin), forment une succession épaisse, régressive et progradante en direction du sud-ouest. La séquence gzhéliennne-sakmariennne, contenue dans la partie supérieure des formations de Nansen et de Hare Fiord, a été associée à la progradation d'une deuxième langue de roches carbonatées de Nansen. La transition Nansen-Hare Fiord, qui correspond au rebord de plate-forme du Carbonifère tardif-Permien précoce, a créé une sinuosité à orientation nord-ouest associée à des promontoires de récifs abrupts et à des baies d'eau plus profonde.

¹ Department of Geology, University of Ottawa, Ottawa, Ontario K1N 6N5

INTRODUCTION

The Upper Carboniferous to Lower Permian Nansen and Hare Fiord formations are the two most widely distributed stratigraphic units on Hvitland Peninsula, northwestern Ellesmere Island (Fig. 1). These units, together with an unnamed unit of reefal carbonates (Unit C2 of Mayr et al., 1995), form the bulk of two long-term transgressive-regressive sequences of the Sverdrup Basin.

Information about the geological setting of the area can be found in Mayr et al. (1995), Harrison et al. (1995), and Beauchamp et al. (1995).

UNIT C2

Distribution and thickness

Large carbonate buildups, lying stratigraphically above the Otto Fiord Formation and assigned to Unit C2 by Mayr et al. (1995) are widely exposed in the southwestern regions of Hvitland Peninsula. Unit C2 ranges in thickness from a few

metres to probably more than 300 m near Lindstroem Creek (locality 15 in Fig. 1; see also Fig. 4A). The smaller buildups are less than 1 km wide; the largest body is a huge buildup that can be traced over 200 km². Unit C2 lies conformably on evaporite strata of the Otto Fiord Formation and correlative Unit C1 (Thériault et al., 1995). The contact between the Hare Fiord and Unit C2 is complex in plan view because mudrocks of the former downlap and fill in topographic irregularities on top of the buildups. The distribution of the Hare Fiord Formation on top and in the vicinity of the large bank of Unit C2 on southwestern Hvitland Peninsula provides a glimpse at the topographic complexity of the reefal bank (e.g., Fig. 4B).

Correlative Unit C2-like buildups probably also occur at the base of the Nansen Formation, either immediately above Franklinian basement, or above the Otto Fiord Formation and probably correlative dolostones of Unit C1 (Thériault et al., 1995). Locally, where brecciation and extensive cementation has occurred, it is difficult to distinguish small developments of Unit C2 from the carbonates of Unit C1. In many localities north of Jugerborg Fiord and east of Emma Fiord, these buildups do not form mappable units and thus were included in Unit C3 or Nansen Formation (Mayr et al., 1995). Unit C2 buildups also appear to be smaller southwest of locality 7

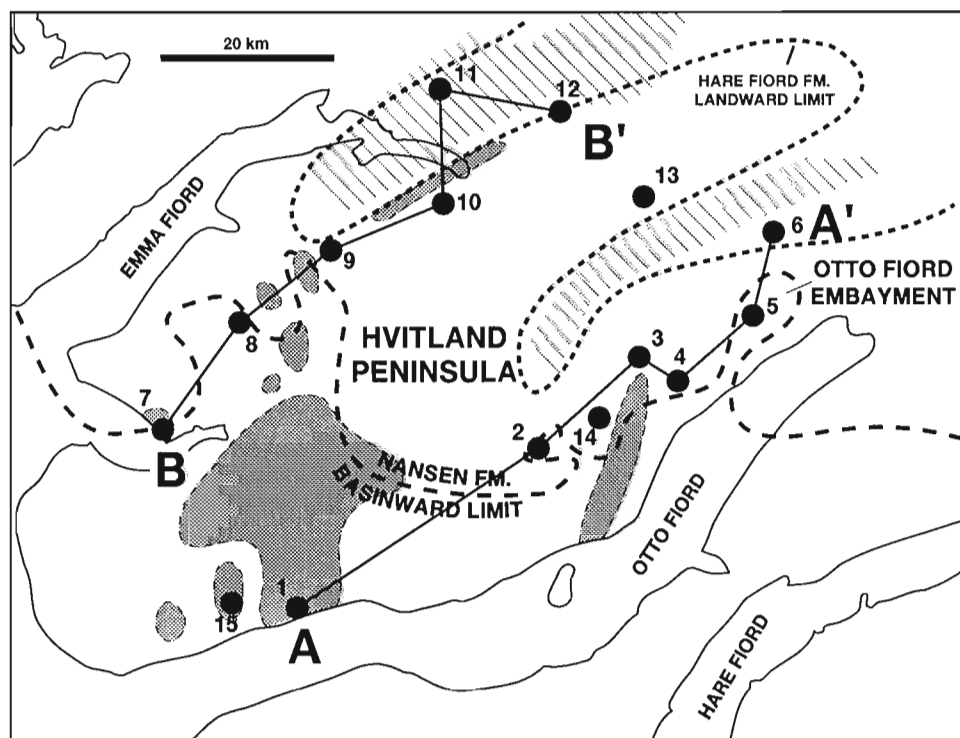


Figure 1. Map of Hvitland Peninsula, northwestern Ellesmere Island showing: measured sections; lines of cross-sections A-A' and B-B'; the approximate maximum landward extent of Hare Fiord mudrocks during Moscovian time (Late Carboniferous); the approximate position of maximum Nansen carbonate progradation during Sakmarian time (Early Permian); the location of large carbonate buildups of Unit C2 and other likely correlative buildups (shaded); and the position of Bashkirian-Serpukhovian rift-related highs (diagonal lines) that may have influenced the Late Carboniferous-Early Permian paleogeography. Geology from Mayr et al. (1995).

(Mayr et al., 1995). In between these more basinal occurrences, Hare Fiord mudrocks rest directly on evaporites of the Otto Fiord Formation; the same stratigraphic relationship is observed south of Otto Fiord, west and east of Van Hauen Pass (Thorsteinsson, 1974; Nassichuk and Davies, 1980).

Unit C2 is lithologically and stratigraphically identical to the large buildups that lie between the Otto Fiord and Hare Fiord formations at a number of localities south of Hvitland Peninsula (e.g., Stepanov Creek, Blue Mountains, etc.; see Davies et al., 1989). The most spectacular examples of these buildups are in the Blue Mountains of west-central Ellesmere Island, where reefs, locally exceeding 400 m in thickness, form a tract that extends over several tens of kilometres. Ammonoids recovered from the Blue Mountains reefs have indicated an Early Moscovian age (Nassichuk, 1975). These reefs, which are often referred to as the "Televak limestone" (Davies et al., 1989), are overlain by mudrocks of much younger age (Late Moscovian to Kasimovian) belonging to the Hare Fiord Formation.

Lithology and depositional environment

The reefs contained in Unit C2 are massive bodies of limestone with no internal structure associated with an apron of crudely bedded flank strata. Depositional slopes along the flanks are 25° to 45°. The massive reef core is mainly lime mudstone, wackestone and packstone that contain a biota dominated by fenestellid bryozoans, echinoderms, and sponge spicules. Accessory, but locally abundant organisms include brachiopods and various foraminiferal and algal encrusters. The lime mud matrix is commonly associated with variably large open space stromatactis which usually display a flat bottom and a digitate roof. Such cavities, often interpreted as the remnants of soft or semisoft bodied organisms (such as sponges), are common in Paleozoic mud mounds worldwide. The stromatactis mudstone facies is randomly associated with a cementstone facies in which the isopachous crust of submarine cement and later burial clear calcite cement form the bulk of the rock (Davies and Nassichuk, 1990). Fenestellid bryozoans are the most common organisms associated with this facies, forming the substrate upon which the marine cement grew. Both the muddy facies and the cement facies are locally dolomitized. The extent of dolomitization ranges from small isolated rhombs in the muddy matrix to coarsely crystalline pervasive dolomite that completely obliterated the depositional fabrics. The origin of the dolomite in these buildups still remains a mystery.

The flanks are crudely bedded, variably inclined units that contain graded to inversely graded, crinoidal grainstones and packstones interpreted as grain flow and turbidite current deposits. The flanks also comprise massive to crudely bedded carbonate breccia, with angular clasts ranging from a few millimetres to more than 10 cm in size. The clasts, which comprise typical lime mud-rich reef facies, and less commonly cementstone facies, are either self-supported or float in a lime mud matrix. Crinoids and other organisms that grew on the crest of the reef are commonly associated with the breccia.

The buildups contained in Unit C2 are isolated bodies that kept pace with a relative sea level rise that drowned the surrounding areas. Their voluminous lime mudstone together with content, as well as the lack of wave-reworked features, indicates that reefs grew below wave base. The reefs were eventually drowned as indicated by the lack of an interfingering relationship with the overlying mudrock facies of the Hare Fiord Formation. As will be discussed later, the reefs formed during a basin-wide episode of shelf drowning during the last stage of a Bashkirian-early Moscovian transgression. The drowned buildups were buried later under prograding and downlapping mudrocks of the Hare Fiord Formation during the next regressive phase.

In some areas, the upper surface of the buildups appears to form ring-like features, the central portion of which is filled by younger dark grey to black mudrocks. Such a ring is well exposed along the north shore of Otto Fiord (locality 1 in Fig. 1, 2; see also Fig. 4B), and similar structures also occur north of Otto Fiord, where they appear to have grown together forming beehive-like larger structures. Harrison et al. (1995) suggested that these features may have resulted from syn- to postdepositional lateral movement of Otto Fiord salt underneath the buildups. Alternately, they may be depositional features representing atoll-like differential buildup growth, perhaps initiated by salt movement beneath.

NANSEN FORMATION

Distribution and thickness

The Nansen Formation is a thick carbonate-dominated unit that outcrops widely on Ellesmere and Axel Heiberg islands (Thorsteinsson, 1974). The Nansen Formation attains a thickness of nearly 2 km, although complete sections from base to top are rare. The top of the type section, which is located at Girty Creek near the head of Hare Fiord, is faulted, but over 1800 km of highly fossiliferous carbonates and minor Hare Fiord-like dark grey mudrocks and Otto Fiord-like white to pale grey evaporites are exposed. Groves et al. (1994) documented some structural complications and possible repeats in the lower part of the type section. The Nansen Formation encompasses the Bashkirian to Sakmarian time interval. Beauchamp and Henderson (1994) recently emended the nomenclature of the Sverdrup Basin to exclude Artinskian strata (Raanes and Great Bear Cape formations) from the definition and usage of the Nansen Formation.

The Nansen Formation has a widespread distribution on Hvitland Peninsula where it forms spectacular mountain ranges, especially north of the head of Otto Fiord and east and north of Emma Fiord. Incomplete exposures of the formation range from 200 m to more than 1500 m. The Nansen Formation overlies and grades laterally over very short distances (sometimes less than 1 km) into dark grey mudrocks of the Hare Fiord Formation. Two major tongues, and probably numerous smaller tongues, of Hare Fiord facies interfinger with Nansen strata. The lower of the large tongues can be traced over several tens of kilometres beneath Nansen strata to the east; in contrast, the upper tongue extends for a few kilometres only beneath Nansen strata (Fig. 2, 3).

Abundant fusulinaceans, small foraminifers, conodonts, ammonoids, colonial rugose corals, and brachiopods, representative of the Bashkirian, Moscovian, Kasimovian, Gzhelian, Asselian and Sakmarian stages have been recovered from the Nansen Formation from various areas in the Sverdrup Basin (e.g., Groves et al., 1994; R. Lin et al., 1991). Preliminary biostratigraphic work on Hvitland Peninsula (fusulinaceans and small foraminifers; R. Lin and S. Pinard, pers. comm., 1994) have shown a Moscovian to Sakmarian stratigraphic range, indicating that the Upper Carboniferous part of the formation is much thicker than its Lower Permian counterpart.

Lithology and depositional environments

The Nansen Formation on Hvitland Peninsula comprises two distinct facies assemblages: a bedded carbonate assemblage and a massive carbonate assemblage. The bedded carbonate assemblage (Fig. 5A) is represented by a succession of resistant and recessive, 5 to 25 m thick, closely spaced units of thin to thick bedded, light to medium grey weathering, highly fossiliferous limestones and yellowish grey to pale grey weathering dolostones. Each recessive-resistant couplet is a generally thickening- and coarsening-upward package that is

interpreted as a single shallowing-upward high-order sequence or cycle. The transgressive portion of each cycle is either very thin or absent.

The composition of each couplet or cycle varies both in space and time, reflecting the long- and short-term relative sea level fluctuations that affected the area. Near the basin margin, typical cycles comprise wackestones and packstones at the base passing upward into coarse grained grainstones, rarely associated with crossbedding. Biota in the grainstones include calcareous algae, foraminifers, fusulinaceans, echinoderms, bryozoans, and brachiopods, commonly associated with ooids and oncoids. Sharp erosional surfaces, often associated with red terra rosa paleosol material, occur in the upper part of many cycles indicating maximum regression and subaerial exposure (Fig. 5B). Variably developed caliche features associated with *Microcodium* commonly occur beneath these surfaces. In the more distal areas, intraformational Nansen cycles culminate in fusulinacean- and foraminifer-rich packstones reflecting a deeper water environment. Some of the more distal cycles comprise wide tabular buildups in their upper part; these buildups are composed of lime mudstones, wackestones and packstones with phylloid algae and *Palaeoaplysina* as the dominant fossils.

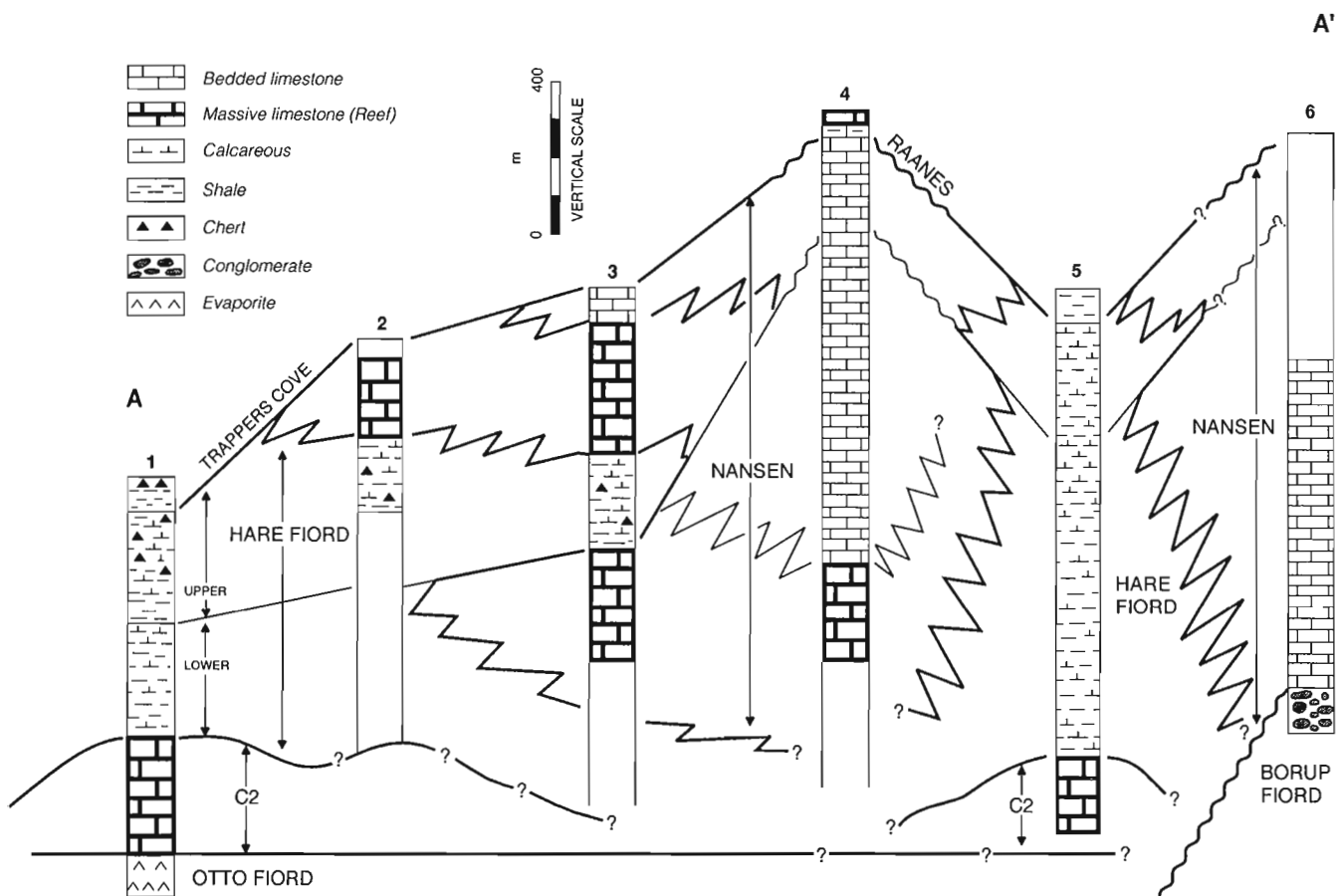


Figure 2. Cross-section A-A' across southern Hvitland Peninsula.

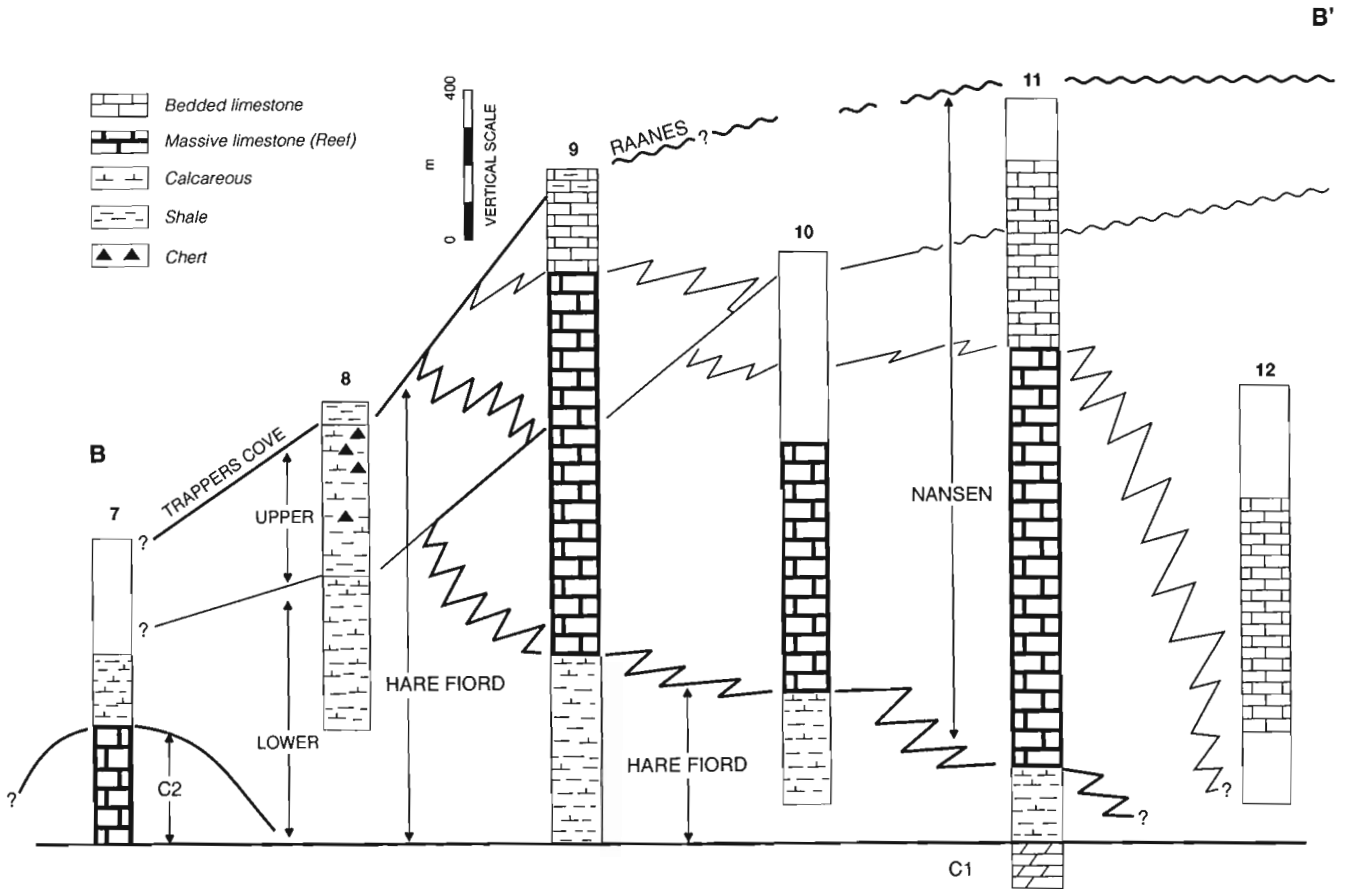


Figure 3. Cross-section B-B' across northern Hvitland Peninsula.

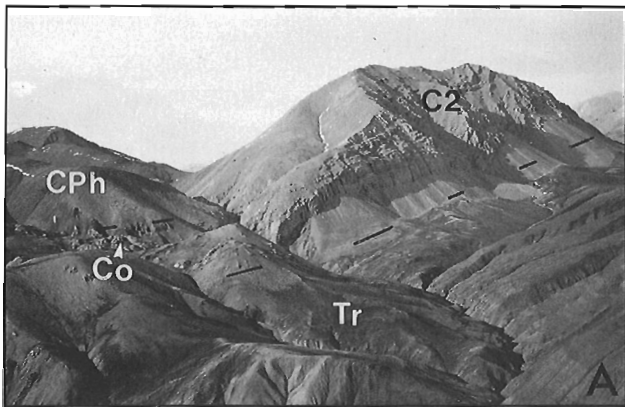


Figure 4. A) Large carbonate buildups forming Unit C2 lying conformably above evaporites of the Otto Fiord Formation (Co), and overlain by dark grey mudrocks of the Hare Fiord Formation (CPh), locality 15. Carboniferous strata are thrust over Triassic clastics (Tr). Reef is about 300 m thick.

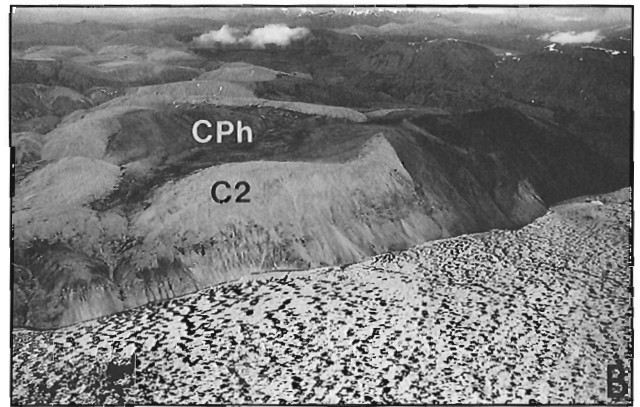


Figure 4. B) Large carbonate buildups of Unit C2 forming ring-like features interpreted as possible atoll-like reefal constructions, locality 1. The depositional relief on top of the reef is filled by younger dark grey to black mudrocks of Hare Fiord Formation (CPh). Light grey sea cliff is about 300 m high.

The bedded shelf carbonate assemblage of the Nansen Formation passes laterally into the massive shelf edge assemblage over a very short distance (Fig. 5C). The massive carbonate assemblage of the Nansen Formation comprises a very thick succession of massive to crudely "bedded" fossiliferous limestones (Fig. 5C, D). These rocks represent coalesced reef bodies that formed the bulk of the shelf edge in Late Carboniferous-Early Permian time. They are dominated by lime mudstone, wackestone, and packstone with abundant phylloid algae and *Palaeoaplysina*, and subordinate fenestellid and ramose bryozoans, *Tubiphytes*, brachiopods, echinoderms, and a plethora of small encrusting organisms such as fasciellid algae, apterrinellid and tuberetinid foraminifers. Small stromatolite cavities locally occur in the mudstone facies. Variably large areas in the massive reef facies are occupied by a cementstone facies in which *Palaeoaplysina* and phylloid algal plates form the substrate upon which several generations of isopachous cement grew (Davies and Nassichuk, 1990). The remainder of the pores are usually filled by late sparry calcite cements. In some areas, especially

north and east of Emma Fiord, the massive reef facies is pervasively dolomitized obliterating primary depositional fabrics.

The reefs that form the massive carbonate facies grew below wave base and formed the bulk of the shelf edge. The reef facies goes landward into cyclic shelf carbonates of the bedded limestone assemblage over a very short distance (Fig. 5C). An equally rapid transition occurs with the correlative mudrocks of the Hare Fiord Formation (Fig. 6A, B). This latter transition takes place through an interfingering of the massive reef facies and the bedded Hare Fiord facies over a distance ranging less than 1 km to rarely more than 3 km. The width of the massive reef facies extends from about 1 to 5 km. Nansen strata near the shelf-to-basin transition are generally more stratified than those of the reef facies. They comprise lime mud- and cement-rich reef facies associated with crinoidal debris and small angular limestone blocks (breccia). The Nansen-Hare Fiord transition displays variably-dipping (20-40°) clinofolds.

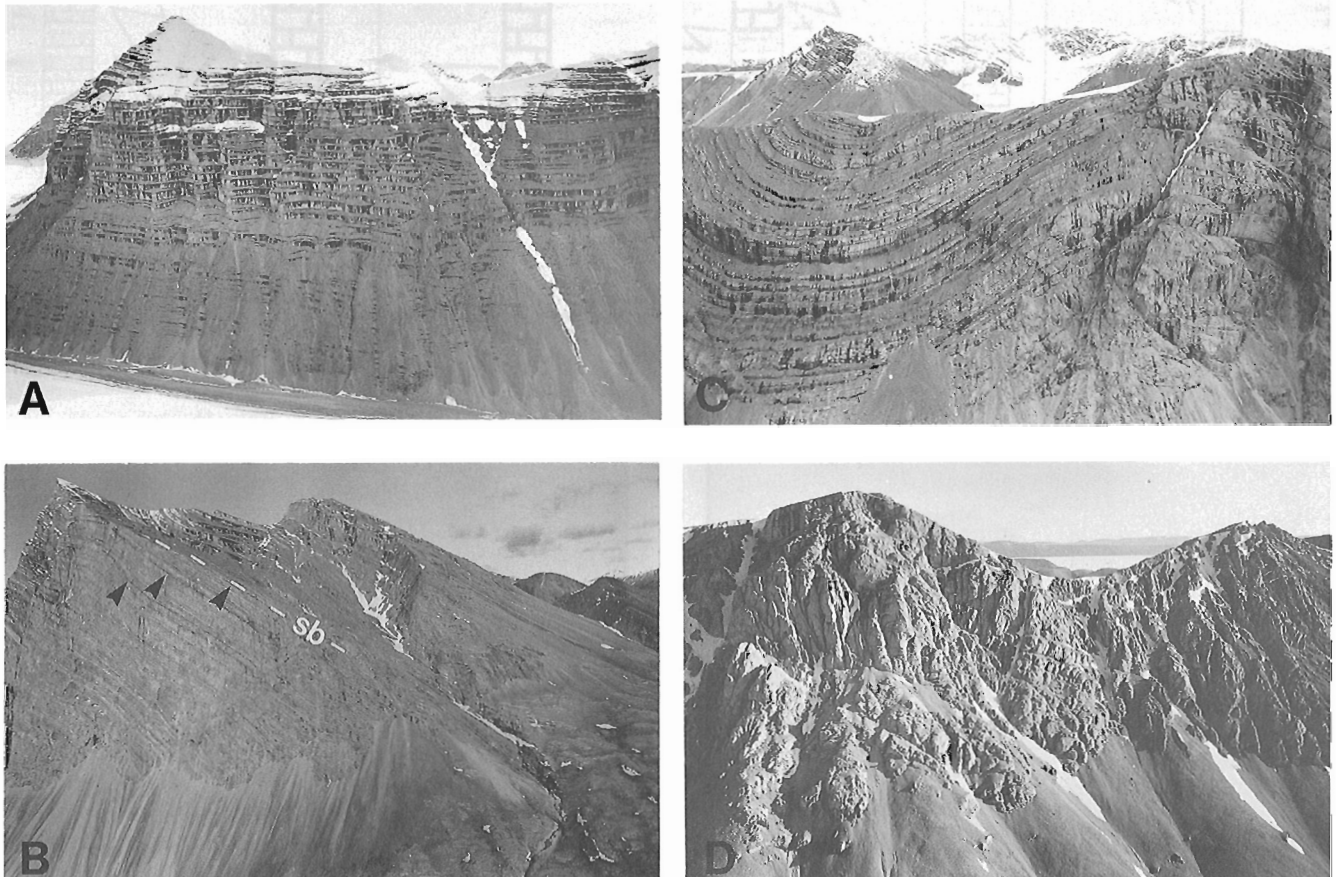


Figure 5. A) Well bedded cyclic shelf carbonates of Nansen Formation forming characteristic recessive-resistant couplets, locality 13. Cliff is about 600 m high. B) Thick section of cyclic shelf carbonates of Nansen Formation showing the entire Moscovian to Sakmarian succession (1.5 km thick), locality 4. Arrows point to unconformities in the upper regressive part of the Upper Carboniferous succession: sb, a low-order sequence boundary between presumably Kasimovian and Gzhelian strata. C) Lateral transition between well bedded cyclic shelf carbonates and massive shelf edge reefal carbonates of Nansen Formation, locality 3. About 250 m of strata are shown. D) Massive shelf edge reefal carbonates of Nansen Formation, locality 14. About 500 m of strata are shown.

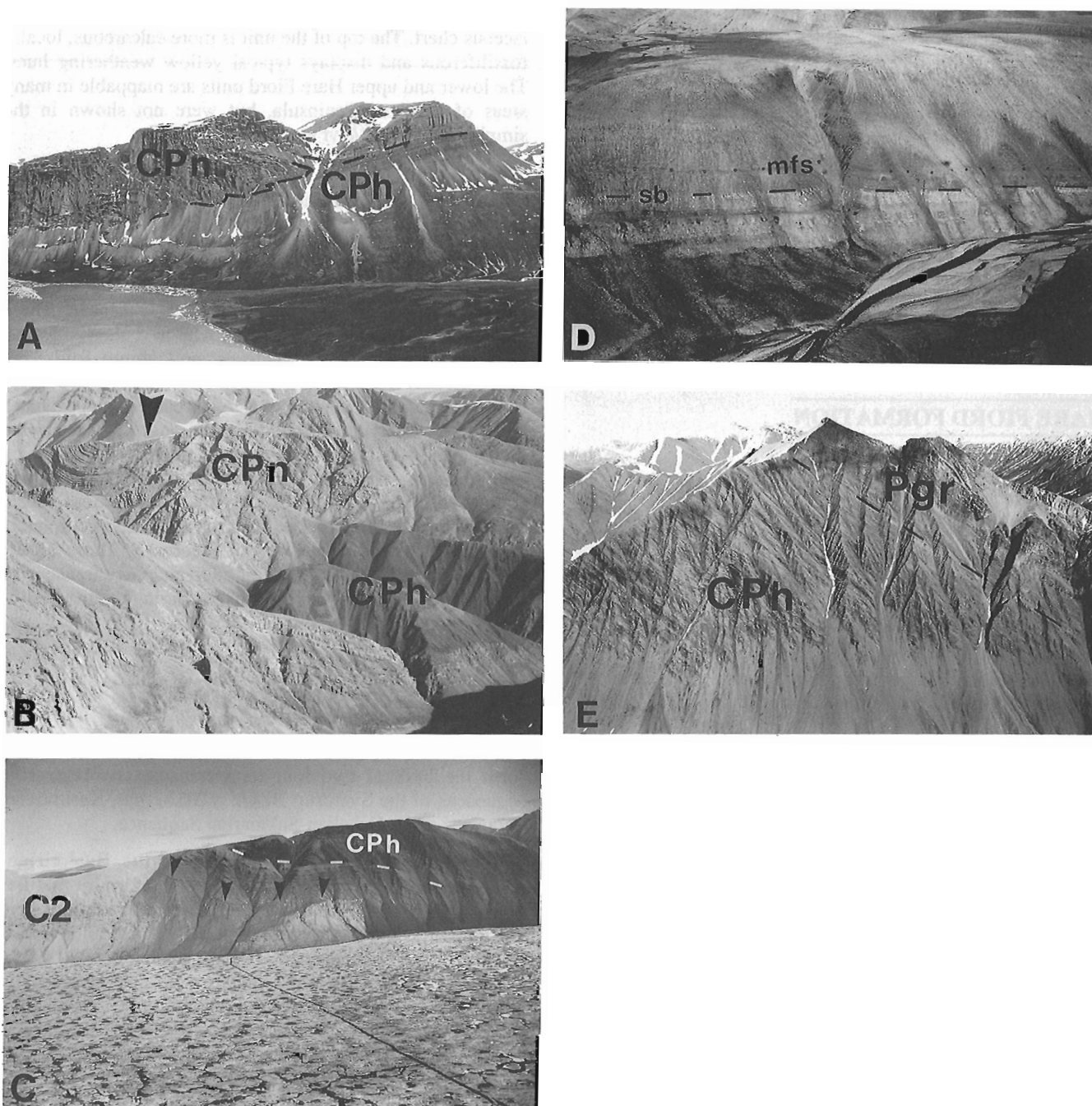


Figure 6. A) Upper Carboniferous shelf edge massive reefal carbonates of Nansen Formation (CPn) passing laterally into dark grey, medium to thin bedded mudrocks of Hare Fiord Formation (CPh), locality 10, south of Emma Fiord, Hvitland Peninsula, northwestern Ellesmere Island. Cliff is about 700 m high. B) Tongue of Lower Permian dark grey mudrocks of Hare Fiord Formation (CPh) pinching into massive shelf edge reefal carbonates of Nansen Formation (CPn), locality 3. Arrow shows area displayed in Figure 5C. C) Dark grey to black mudrocks of Hare Fiord Formation (CPh) onlapping (arrows) upper surface of Lower Moscovian carbonate buildup of Unit C2, locality 1. Dashed line is the contact between lower and upper Hare Fiord Formation. Sea cliff is about 300 m high. D) Contact (dashed line) between lower (argillaceous limestone) and upper Hare Fiord Formation (calcareous shale, siliceous shale, chert), locality 8: sb, Kasimovian-Gzhelian sequence boundary; mfs (dotted), maximum flooding surface. About 150 m of strata are shown. E) Thick (1.4 km) Moscovian to Sakmarian Hare Fiord (CPh) section that was deposited in a narrow embayment (Otto Fiord Embayment), locality 8: Pgr, Raanes and Great Bear Cape formations.

An algal- and foraminiferal-rich biota in the Nansen Formation (Chlorofoam assemblage of Beauchamp, 1994) – in association with abundant ooids, oncoids, aragonite and high-magnesium calcite submarine cements and numerous well-developed reefs; and in conjunction with the presence of contemporaneous evaporites, redbeds, and calcretes in the marginally marine to nonmarine environments – suggests a tropical-like, semiarid setting for the Late Carboniferous–Early Permian interval (Beauchamp, 1994).

A peculiar bivalve coquina, thoroughly cemented by submarine radiaxial calcite, was found south of Emma Fiord (vicinity of locality 10), where it is associated with copper sulphide occurrences. The depositional and economic significance of this association remains to be determined.

HARE FIORD FORMATION

Distribution and thickness

The Hare Fiord Formation is a Nansen-correlative unit of generally recessive, dark grey to black mudrock that has a broad distribution in the axial regions of the Sverdrup Basin (Thorsteinsson, 1974). The formation is well exposed on northern Ellesmere and eastern Axel Heiberg islands, where it is more than 1.5 km thick. In the type area at Van Hauen Pass, the Hare Fiord Formation lies conformably on the Otto Fiord Formation. Large carbonate buildups such as those assigned to Unit C2 on Hvitland Peninsula lie at the base of the formation in the Blue Mountains and in the Hare Fiord area. The Hare Fiord Formation is Moscovian–Sakmarian in age. Beauchamp and Henderson (1994) recently emended the stratigraphic nomenclature of the Sverdrup Basin to exclude Artinskian strata (Trappers Cove Formation) from the definition and type section of the formation.

The Hare Fiord Formation is widely exposed in the western regions of Hvitland Peninsula where it is the dominant unit forming a gently rolling landscape that contrasts sharply with the mountainous Nansen-dominated areas of eastern Hvitland Peninsula. The Hare Fiord Formation on Hvitland Peninsula is 200 m to more than 1000 m thick (Fig. 1, 2). The rapid thickness variations reflect the downlap of Hare Fiord mudrocks on the very irregular reefal surface formed by the top of Unit C2 (Fig. 2, 3, 6C). The thickest measured section of the Hare Fiord Formation is at locality 5 (Fig. 2, 6E), where it is part of a narrow deep-water embayment, the position of which may reflect the presence of an older Serpukhovian–Bashkirian tectonic depression in that area (Thériault et al., 1995).

On western Hvitland Peninsula, the Hare Fiord Formation can be subdivided into two broad units of more or less equal thickness, informally referred to as the lower and upper Hare Fiord units (Fig. 2, 3, 6D). The lower Hare Fiord unit comprises greenish grey weathering mudrock and argillaceous limestone that become thicker bedded, coarser grained and increasingly fossiliferous upward. The lower Hare Fiord unit thins dramatically over the top of Unit C2 and is locally absent. The upper Hare Fiord unit is very recessive at the base and comprises black fissile shale passing upward into thin to

medium bedded, argillaceous and cherty limestone and argillaceous chert. The top of the unit is more calcareous, locally fossiliferous and displays typical yellow weathering hues. The lower and upper Hare Fiord units are mappable in many areas of Hvitland Peninsula, but were not shown in the simplified map of Mayr et al. (1995).

Lithology and depositional environment

The Hare Fiord Formation comprises dark to greenish grey, brown and yellow shale, argillaceous limestone and chert rhythmically arranged in thin to medium beds that are often graded and display incomplete Bouma sequences. These rocks, which are often associated with large-scale clinofolds, slump-related truncation features, and slump folds, are interpreted as slope to basinal deposits. Massive to crudely bedded lenticular units of light grey weathering carbonates containing abundant echinoderms and angular Nansen-like carbonate blocks. These commonly channelized units, which often display a sharp erosive base, are interpreted as debris flow and turbidite deposits. Some of these units are associated with large carbonate blocks of Nansen reef facies completely enclosed in recessive Hare Fiord mudrocks. These blocks must have originated at the shelf edge and were transported downslope, either catastrophically or through some sort of slow creep.

SEQUENCE STRATIGRAPHY

The Nansen and Hare Fiord formations, along with Unit C2, form the bulk of two long-term transgressive-regressive sequences of the Sverdrup Basin: a Bashkirian–Kasimovian Sequence and a Gzhelian–Sakmarian Sequence.

The lower sequence boundary of the Bashkirian–Kasimovian Sequence is a subaerial unconformity that lies between the Borup Fiord and the Otto Fiord formations (and correlative Unit C1) in the eastern regions of Hvitland Peninsula (see Thériault et al., 1995; Beauchamp et al., 1995). As shown by Thériault et al. (1995), the Borup Fiord and Otto Fiord formations accumulated in a series of syndimentary tectonic depressions that were separated by uplifted highs. On such highs, the sequence boundary lies at the base of the Nansen Formation, which rests unconformably either on a thin Borup Fiord succession or directly on Franklinian basement.

The Otto Fiord Formation and Unit C2 represent the transgressive systems tract of the Bashkirian–Kasimovian Sequence (Beauchamp et al., 1995). Unit C2 lies conformably on the Otto Fiord Formation and comprises large buildups that maintained growth with a basin-wide relative sea level rise that drowned all coeval platforms; the reefs were later drowned too. Some of the reefs probably grew on top of the old rift-related linear highs as these structures were progressively flooded. Such Lower Moscovian buildups occur at the base of the Nansen Formation in the eastern regions of Hvitland Peninsula, or in Unit C3 of Mayr et al. (1995) which lies north of Jugeborg Fiord. The maximum flooding surface wraps around the buildups contained in Unit C2

(Beauchamp et al., 1995), and locally lies at the contact between the Hare Fiord and Otto Fiord formations where these two formations are vertically juxtaposed (e.g., south of locality 7 in Fig. 1).

The regressive systems tract of the Bashkirian-Kasimovian Sequence is represented by the progradation of the thick succession of shelf carbonates, shelf edge reefs and correlative slope to basinal mudrocks of the lower Nansen and correlative lower Hare Fiord formations. This is shown by the broad overall shallowing-upward nature of the succession and by the downlap of Hare Fiord mudrocks. The shelf-to-basin transition ranges from relatively steep, characterized by massive reefal promontories, to more gentle gradients interstratified with Nansen carbonates and Hare Fiord slope mudrocks with only minor isolated reef-mounds in an otherwise well-bedded succession. The Late Carboniferous shelf edge, represented by maximum progradation of the first Nansen tongue (Fig. 1, 3), runs in a general westward direction across Hvitland Peninsula. It forms a very sinuous feature characterized by shelf edge promontories surrounding deeper water embayments (Fig. 1). One such embayment developed at locality 5 (Fig. 2), where a 1.4 km section of Hare Fiord mudrocks occur (Fig. 6E; see also Harrison et al., 1995, Fig. 3). The Moscovian-Kasimovian part of the succession is nearly 1 km thick. The area of thick Hare Fiord accumulation is almost completely surrounded by Nansen carbonates (Mayr et al., 1995). The western edge of the embayment was characterized by massive shelf edge-type reefs, whereas the northern, eastern and southern edges were characterized by a more gentle transition as bedded Nansen carbonates interfinger with Hare Fiord mudrocks (Fig. 2). This embayment, here named the Otto Fiord Embayment, may reflect the position of a Bashkirian and Serpukhovian tectonic depression as suggested by the distribution of the Otto Fiord and Borup Fiord formations (Thériault et al., 1995; Beauchamp et al., 1995).

The top of the Bashkirian-Kasimovian Sequence is a subaerial unconformity that occurs in the upper two thirds of the Nansen Formation (Fig. 1, 5B). The unconformity forms an erosion surface above which thin layers of red terra rosa material occur. Reddish weathering clay is also incorporated in the overlying transgressive strata. This surface passes basinward into a conformity, that lies near the top of the lower Hare Fiord unit.

The unconformity and its correlative conformity form the lower sequence boundary of the Gzhelian-Sakmarian Sequence, which is represented by the upper Nansen and Hare Fiord formations on Hvitland Peninsula. This mostly Lower Permian sequence is thinner than its Upper Carboniferous counterpart. It comprises a relatively thin transgressive systems tract contained in the uppermost part of the lower Hare Fiord unit, and correlative shelf strata in the Nansen Formation. The maximum flooding surface closely corresponds with the boundary between the lower and upper Hare Fiord units in the axial areas, and to the deepest water facies development in the correlative Nansen Formation. A 200 to 300 m thick tongue of Hare Fiord-like facies lying in the middle of the Nansen Formation indicates the extent of the

transgression in latest Carboniferous-Early Permian time (e.g., locality 3 in Fig. 2, 6B). The regressive systems tract is represented by prograding shelf and shelf edge carbonates and correlative slope to basinal mudrocks included in the upper Hare Fiord unit. The Early Permian Nansen shelf edge prograded a few kilometres beyond its Late Carboniferous counterpart (Fig. 1). The upper sequence boundary is a major erosion surface in the upper part of the Nansen and correlative Hare Fiord formations. Transgressive strata contained in the uppermost portion of these formations belong to an overlying, mostly Artinskian Sequence (Kells et al., 1995; Beauchamp et al., 1995).

CONCLUSIONS

The Nansen and correlative Hare Fiord formations, and Unit C2 form the bulk of two long-term transgressive-regressive sequences of the Sverdrup Basin: a Bashkirian-Kasimovian Sequence (which also contains strata belonging to the Otto Fiord Formation) and a Gzhelian-Sakmarian Sequence. These two sequences recorded the progradation of two thick tongues of the Nansen Formation, which contain shelf and shelf edge carbonates that pass basinward into correlative turbiditic slope to basinal mudrocks of the Hare Fiord Formation. The Late Carboniferous and Early Permian shelf edges formed highly sinuous facies fronts characterized by massive reef promontories surrounding a number of deeper water embayments represented by a more gradational shelf-to-basin transition.

ACKNOWLEDGMENTS

Many thanks to T. de Freitas for reviewing the manuscript.

REFERENCES

- Beauchamp, B.**
1994: Permian climatic cooling in the Canadian Arctic; in *Pangea: Paleoclimate, Tectonics and Sedimentation during accretion, zenith and break-up of a super-continent*, (ed.) G.D. Klein; Geological Society of America, Special Paper 288, p. 229-246.
- Beauchamp, B. and Henderson, C.M.**
1994: The Lower Permian Raanes, Great Bear Cape and Trappers Cove formations, Sverdrup Basin, Canadian Arctic: Stratigraphy and Conodont Zonation; *Bulletin of Canadian Petroleum Geology*, v. 42, p. 565-600.
- Beauchamp, B., Mayr, U., and Harrison, J.C.**
1995: Carboniferous and Permian stratigraphic sequences on Hvitland Peninsula and adjacent areas, northwestern Ellesmere Island, Arctic Canada; in *Current Research 1995-B*; Geological Survey of Canada, this volume.
- Davies, G.R. and Nassichuk, W.W.**
1990: Submarine cements and fabrics in Carboniferous to Lower Permian, reefal, shelf margin and slope carbonates, northwestern Ellesmere Island, Canadian Arctic Archipelago; *Geological Survey of Canada, Bulletin 399*, 77 p.
- Davies, G.R., Nassichuk, W.W., and Beauchamp, B.**
1989: Upper Carboniferous Waulsortian reefs, Canadian Arctic Archipelago; in *Reefs, Canada and Adjacent Areas*, (ed.) H.H.J. Geldsetzer, N.P. James, and G.E. Tebbutt; Canadian Society of Petroleum Geologists, Memoir 13, p. 658-666.

Groves, J.R., Nassichuk, W.W., Lin, R., and Pinard, S.

1994: Middle Carboniferous fusulinacean biostratigraphy, northern Ellesmere Island (Sverdrup Basin, Canadian Arctic Archipelago); Geological Survey of Canada, Bulletin 469, 55 p.

Harrison, J.C., Mayr, U., and Beauchamp, B.

1995: Preliminary observations on the structural geology of Hvitland Peninsula, northwestern Ellesmere Island, Arctic Canada; in Current Research 1995-B; Geological Survey of Canada, this volume.

Kells, M.P., Beauchamp, B., and Desrochers, A.

1995: Artinskian-Kungurian (Lower Permian) stratigraphy (Raanes, Great Bear Cape and Trappers Cove formations), Hvitland Peninsula and adjacent areas, northwestern Ellesmere Island, Arctic Canada; in Current Research 1995-B; Geological Survey of Canada, this volume.

Mayr, U., Harrison, J.C., and Beauchamp, B.

1995: Geological map of Carboniferous and Permian units on Hvitland Peninsula and adjacent areas, northwestern Ellesmere Island, Arctic Canada; in Current Research 1995-B; Geological Survey of Canada, this volume.

Nassichuk, W.W.

1975: Carboniferous ammonoids and stratigraphy in the Canadian Arctic Archipelago; Geological Survey of Canada, Bulletin 237.

Nassichuk, W.W. and Davies, G.R.

1980: Stratigraphy and sedimentation of the Otto Fiord Formation; Geological Survey of Canada, Bulletin 286, 87 p.

Lin, R., Ross, C.A., and Nassichuk, W.W.

1991: Upper Moscovian (Desmoinesian) fusulinaceans from the type section of the Nansen Formation, Ellesmere Island, arctic Archipelago; Geological Survey of Canada, Bulletin 418, 121 p.

Thériault, P., Beauchamp, B., Harrison, J.C., Mayr, U., and Steel, R.

1995: Serpukhovian and Bashkirian (Carboniferous) stratigraphy (Borup Fiord and Otto Fiord formations; Unit C1), Hvitland Peninsula and adjacent areas, northwestern Ellesmere Island, Arctic Canada; in Current Research 1995-B; Geological Survey of Canada, this volume.

Thorsteinsson, R.

1974: Carboniferous and Permian stratigraphy of Axel Heiberg Island and western Ellesmere Island, Canadian Arctic Archipelago; Geological Survey of Canada, Bulletin 224, 210 p.

Geological Survey of Canada Project 870067

Artinskian-Kungurian (Lower Permian) stratigraphy (Raanes, Great Bear Cape, and Trappers Cove formations), Hvitland Peninsula and adjacent areas, northwestern Ellesmere Island, Arctic Canada

M.P. Kells¹, B. Beauchamp, and A. Desrochers¹

Institute of Sedimentary and Petroleum Geology, Calgary

Kells, M.P., Beauchamp, B., and Desrochers, A., 1995: Artinskian-Kungurian (Lower Permian) stratigraphy (Raanes, Great Bear Cape, and Trappers Cove formations), Hvitland Peninsula and adjacent areas, northwestern Ellesmere Island, Arctic Canada; in Current Research 1995-B; Geological Survey of Canada, p. 47-56.

Abstract: The Artinskian Raanes, Great Bear Cape and Trappers Cove formations are widely exposed on Hvitland Peninsula and adjacent areas, northwestern Ellesmere Island. The Raanes Formation consists of bryozoan- and echinoderm-rich argillaceous limestone and lesser bryozoan-rich muddy carbonates forming variably thick reef-mounds. The environments represented by these rocks include deep to shallow ramp and submarine fill of tectonic depressions. This unit is overlain by the Great Bear Cape Formation, which is composed of crinoidal packstone and grainstone deposited on a cool water temperate shelf. Both the Raanes and Great Bear Cape formations pass in a southwestward direction in black siliceous shale and spiculitic chert of the Trappers Cove Formation, which recorded slope to basin sedimentation. These three units form the bulk of a long-term, unconformity-bounded, transgressive-regressive sequence of the Sverdrup Basin, the early transgressive portion of which is contained in the upper Hare Fiord and correlative Nansen formations.

Résumé : Les formations de Raanes, de Great Bear Cape et de Trappers Cove de l'Artinskien sont abondamment exposées dans la péninsule Hvitland et les régions adjacentes, dans le nord-ouest de l'île d'Ellesmere. La Formation de Raanes comporte un calcaire argileux riche en bryozoaires et échinodermes et des quantités moindres de roches carbonatées boueuses riches en bryozoaires qui forment des monticules récifaux d'épaisseur variable. Les milieux représentés par ces roches comprennent une rampe profonde à peu profonde et le remplissage sous-marin de dépressions tectoniques. Cette unité, sur laquelle repose la Formation de Great Bear Cape, se compose de packstone et de grainstone à entroques déposés sur une plate-forme tempérée d'eau froide. Les deux formations de Raanes et de Great Bear Cape passent vers le sud-ouest à un schiste siliceux noir et un chert spiculitique de la Formation de Trappers Cove, qui présente une sédimentation de talus à bassin. Ces trois unités forment le gros d'une séquence transgressive-régressive, de longue durée, limitée par une discordance, dans le bassin de Sverdrup, dont la portion transgressive précoce est contenue dans la partie supérieure de la Formation de Hare Fiord et de la formation corrélatrice de Nansen.

¹ Department of Geology, University of Ottawa, Ottawa, Ontario K1N 6N5

INTRODUCTION

Artinskian units on Hvitland Peninsula and adjacent areas include the Raanes, Great Bear Cape and Trappers Cove formations, which have been defined recently on southwestern Ellesmere Island (Beauchamp and Henderson, 1994). These formations form the bulk of a long-term unconformity-bounded sequence of the Sverdrup Basin (Thorsteinsson, 1974), a sequence that also includes strata contained in the upper part of the Nansen and correlative Hare Fiord formations (Beauchamp et al., 1995a). The uppermost part of the Great Bear Cape and Trappers Cove formations comprise strata that belong to a younger Kungurian-Kazanian sequence (see Desrochers and Beauchamp, 1995; Beauchamp et al., 1995a). This paper provides generalities about the distribution and facies content of the Raanes, Great Bear Cape and Trappers Cove formations, the sequence stratigraphic significance of the strata they contain, and the Artinskian paleogeography of a study area that includes and extends south of the area mapped by Mayr et al. (1995). This study, which is based on the examination of 14 stratigraphic sections located north and south of Otto Fiord (Fig. 1-3), is part of a M.Sc. research project by M.P. Kells at the University of Ottawa.

Generalities about the geological setting of the area can be found in Mayr et al. (1995), Harrison et al. (1995), and Beauchamp et al. (1995a).

LITHOSTRATIGRAPHY

Raanes Formation

The Raanes Formation, introduced by Beauchamp and Henderson (1994), is a unit of variably recessive shale, siltstone, moderately fossiliferous, argillaceous and silty limestone, mixed clastic-carbonate, and fossiliferous limestone that overlies either the Canyon Fiord, Belcher Channel, Tanquary or Nansen formations and is overlain by either the Great Bear Cape or Trappers Cove formations. The type section of the formation is located on the east side of Blind Fiord, southwestern Ellesmere Island, where the formation is 167 m thick and lies on fossiliferous carbonates of the Belcher

Channel Formation. The age of the Raanes Formation is Early Artinskian based on conodonts (Beauchamp and Henderson, 1994). The Raanes Formation is widely distributed along the southern and eastern margins of the Sverdrup Basin where it ranges from a feather edge to more than 325 m measured at Mount Bridgman, west-central Ellesmere Island. Great thickness variations observed within the Raanes Formation reflect syndepositional block faulting associated with a renewed phase of rifting in the Sverdrup Basin (Beauchamp and Henderson, 1994). The Raanes Formation thins basinward as it grades into the partly correlative Trappers Cove Formation (Fig. 2, 3).

The Raanes Formation outcrops at various localities in the northern and eastern regions of Hvitland Peninsula (Fig. 1), and also south of the head of Otto Fiord. It ranges from less than 10 m to more than 225 m as measured at locality 7 north of the head of Otto Fiord. A dramatic thickness increase immediately east of locality 6 (Fig. 2) suggests the presence of at least one syndepositionary rift-related fault in the area. The Raanes Formation rests conformably on the Nansen Formation. A significant unconformity, interpreted as a sequence boundary, occurs in the upper part of the Nansen Formation, but not at its top, as will be discussed in a later section. The Raanes Formation is overlain conformably by either the Great Bear Cape or Trappers Cove formations, except at locality 6, where the Raanes-Great Bear Cape contact is a local unconformity.

The Raanes Formation of Hvitland Peninsula and adjacent areas comprises two main lithofacies: moderately recessive, medium bedded, yellowish to brownish grey, variably cherty, argillaceous and silty limestone with abundant bryozoans, echinoderms, brachiopods and sponges (Fig. 4, 5); and resistant, massive, bryozoan-containing lime mudstone, wackestone and packstone, with minor open space stromatolite cavities forming various buildups (Fig. 6). These mounds are patch reefs that are totally enclosed in the first facies type; they range from less than 10 m to more than 50 m in thickness. Crinoid-rich carbonate strata that surround the buildups often weather in various hues of red and pink, the origin of which is uncertain. Red coloration has a very irregular, patchy distribution suggesting a postdepositional origin. Raanes lithofacies on Hvitland Peninsula are much purer than their

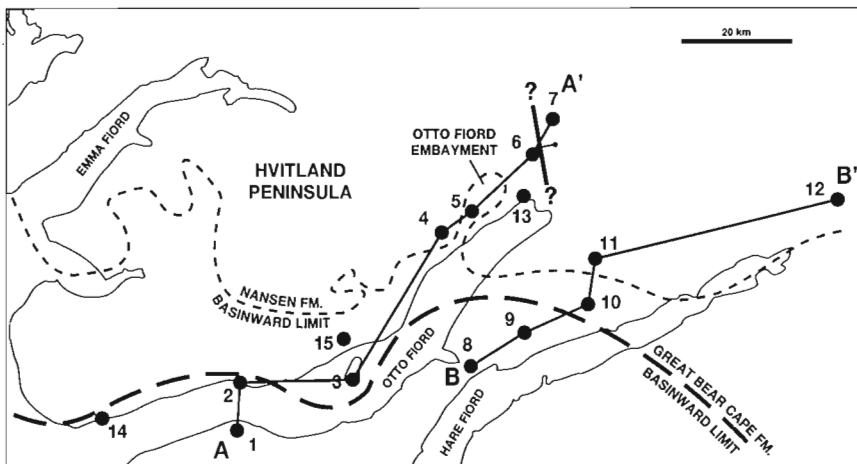


Figure 1.

Map showing locations of measured sections, lines of cross-sections A-A' and B-B', position of maximum Nansen (Late Sakmarian) and Great Bear Cape (Late Artinskian) shelf progradation, and hypothetical location of syntectonic graben-bounding fault.

southern Ellesmere Island counterparts, reflecting the close proximity of a terrigenous source in the latter areas. The Raanes Formation in the type area (Beauchamp and Henderson, 1994), for instance, comprises thick units of recessive shale and mixed shale-limestone that have no equivalents on northern Ellesmere Island. Likewise, carbonate facies on Hvitland Peninsula are only slightly argillaceous to silty.

Great Bear Cape Formation

The Great Bear Cape Formation is the name given to a unit of resistant, yellowish-grey weathering, pure to locally sandy, variably cherty, highly fossiliferous limestone that overlies either the Raanes or Trappers Cove formations and is overlain by the Van Hauen, Troid Fiord, Assistance, Sabine Bay or Esayoo formations (Beauchamp and Henderson, 1994). The type section of the Great Bear Cape Formation, located 7 km northeast of the head of Blind Fiord on Raanes Peninsula, lies above the type section of the Raanes Formation. The Great Bear Cape Formation is Early to Late Artinskian age, based on conodont age determinations (Beauchamp and Henderson,

1994). Uppermost strata in the formation include conodonts assignable to a latest Artinskian-Kungurian zone (Beauchamp and Henderson, 1994). The Great Bear Cape Formation, a unit interpreted as a cool water temperate carbonate based on its Bryonoderm assemblage (bryozoan, echinoderm, brachiopod and sponge; Beauchamp, 1994) passes laterally into spiculitic shale and cherty mudrock of the Trappers Cove Formation. The Great Bear Cape Formation is widely distributed around the Sverdrup Basin, where it ranges from 100 to 200 m thick on average.

The Great Bear Cape Formation outcrops widely on Hvitland Peninsula and adjacent areas (Fig. 1), where its thickness ranges from a feather edge to about 600 m (Fig. 2, Section 5, north of the head of Otto Fiord). The Great Bear Cape Formation overlies either the Raanes or Trappers Cove formations; it also passes laterally into the Trappers Cove Formation through a complex interfingering with dark grey to black cherty mudrocks characteristic of the latter formation. It is overlain by the Van Hauen Formation throughout Hvitland Peninsula or the Assistance Formation just south of the head of Otto Fiord.

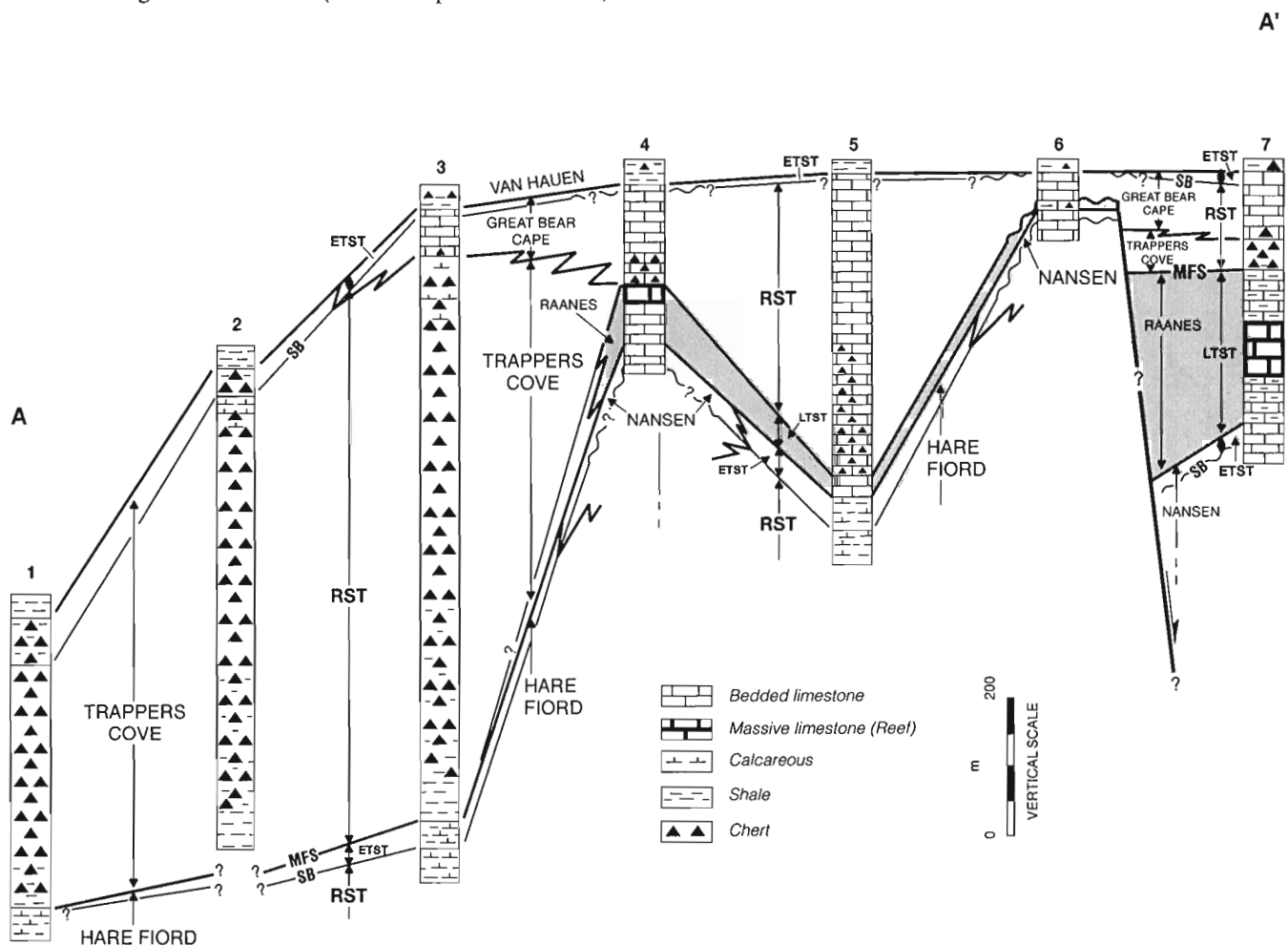


Figure 2. Cross-section A-A' showing the distribution of Raanes, Great Bear Cape and Trappers Cove formations on Hvitland Peninsula, northwestern Ellesmere Island: SB, sequence boundary; MFS, maximum flooding surface; ETST, early transgressive systems tract; LTST, late transgressive systems tract; RST, regressive systems tract.

The lithological spectrum displayed by the Great Bear Cape Formation of Hvitland Peninsula and adjacent areas is typical to that of the type area. Typically, the formation comprises medium to thick bedded, resistant, cliff-forming, yellowish to light grey weathering, fossiliferous packstone and grainstone with abundant echinoderms, bryozoans, brachiopods and sponges (Fig. 7A, B, 8). Subordinate lithologies include massive, light grey weathering, pure lime mudstone, wackestone and packstone with variably abundant fenestellid bryozoans, brachiopods and echinoderms. These massive bodies are patch reefs averaging 20 to 30 m in

thickness. Near the vertical and lateral transition with the Trappers Cove formation, the Great Bear Cap Formation contains greater quantities of spicule-bearing chert.

Trappers Cove Formation

The Trappers Cove Formation is a unit of dark grey to black siliceous shale and spiculitic chert and minor yellowish weathering, fossiliferous limestone that is correlative of the Great Bear Cape and Raanes formations (Beauchamp and Henderson, 1994). The type section is located on the west side

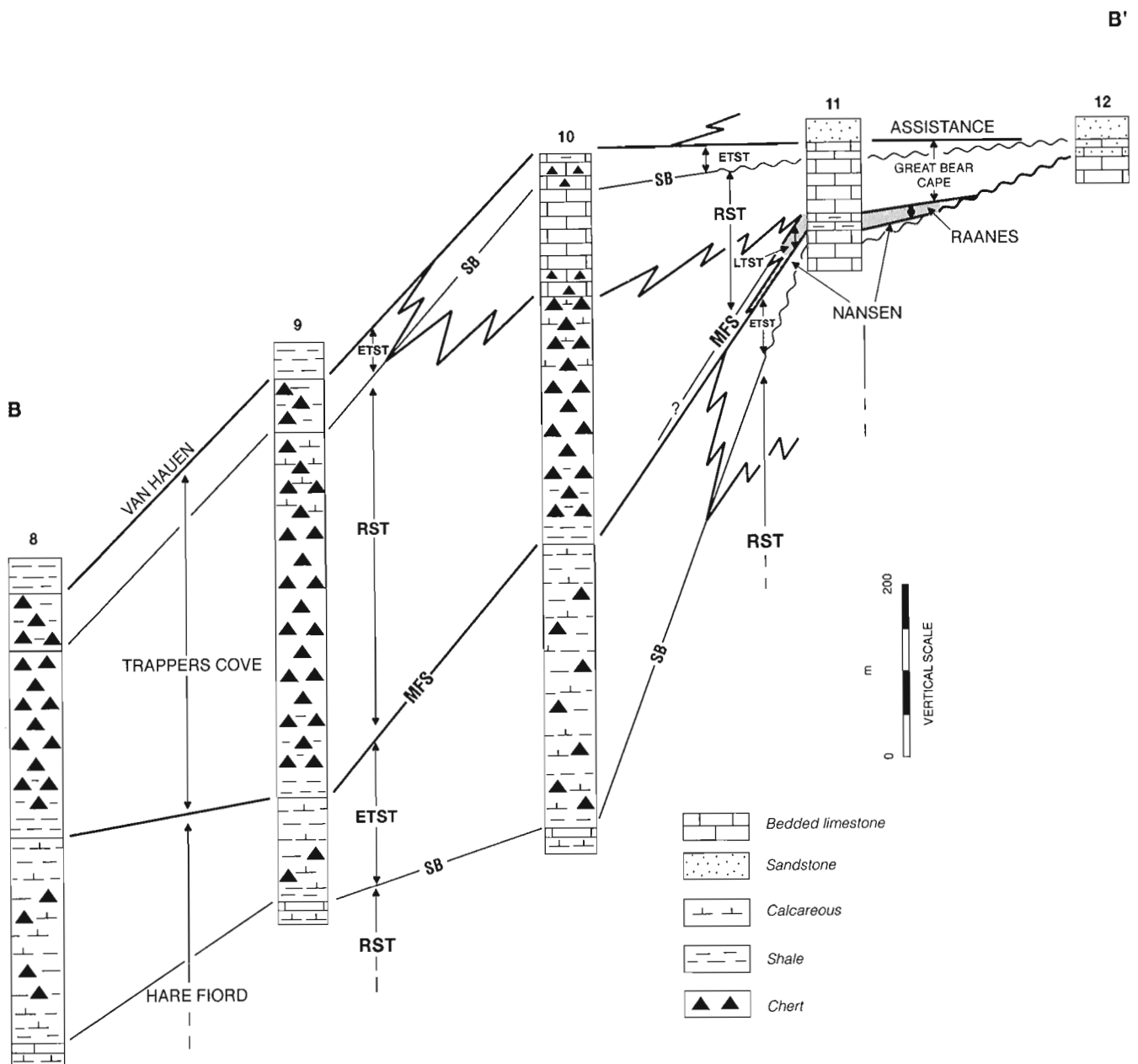


Figure 3. Cross-section B-B' showing the distribution of Raanes, Great Bear Cape and Trappers Cove formations south of Otto Fiord, northwestern Ellesmere Island: SB, sequence boundary; MFS, maximum flooding surface; ETST, early transgressive systems tract; LTST, late transgressive systems tract; RST, regressive systems tract.

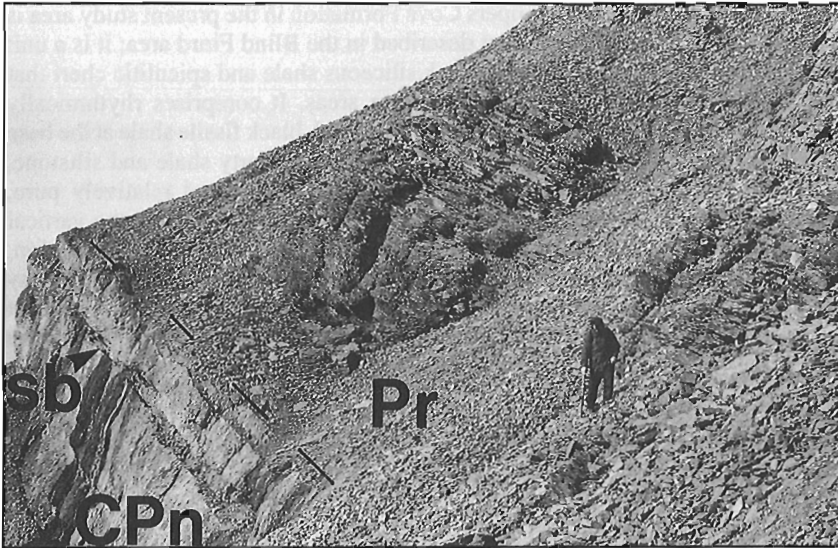


Figure 4.

Contact between Nansen (CPn) and Raanes (Pr) formations at locality 13, north of Otto Fiord: sb, sequence boundary in upper part of Nansen Formation. Person (Mike Powell) for scale.

Figure 5.

Uppermost Nansen (CPn), Raanes (Pr) and Great Bear Cape (Pg) and Van Hauen (Pv) formations at locality 6, north of Otto Fiord: sb, sequence boundaries in the upper part of the Nansen Formation, and the top of the Great Bear Cape Formation; fs, flooding surface marking the Nansen- Raanes contact; mfs, maximum flooding surface coinciding with the base of Great Bear Cape Formation. Note the erosional surface between Raanes and Great Bear Cape formations. Raanes Formation is 20 m thick.

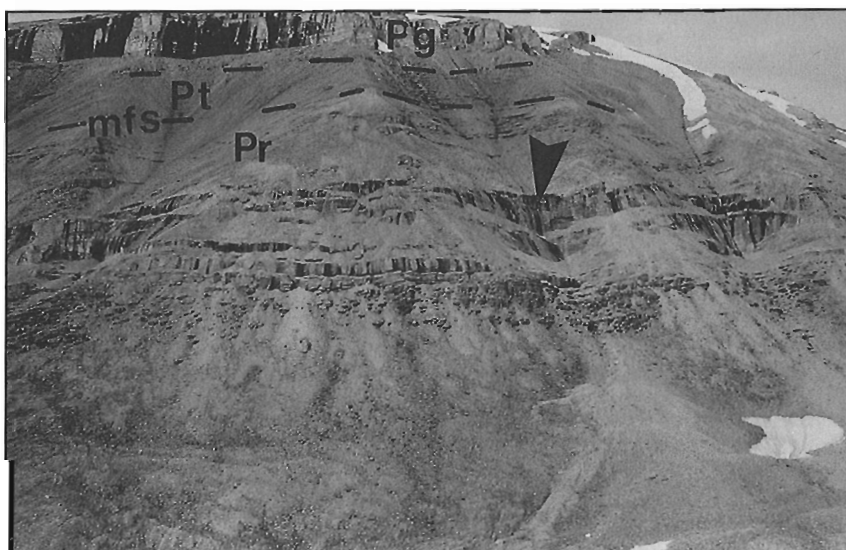
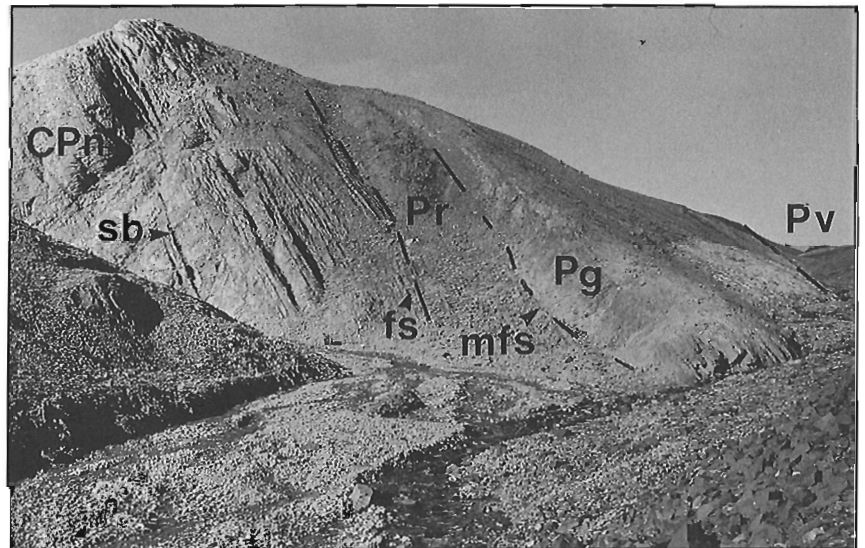
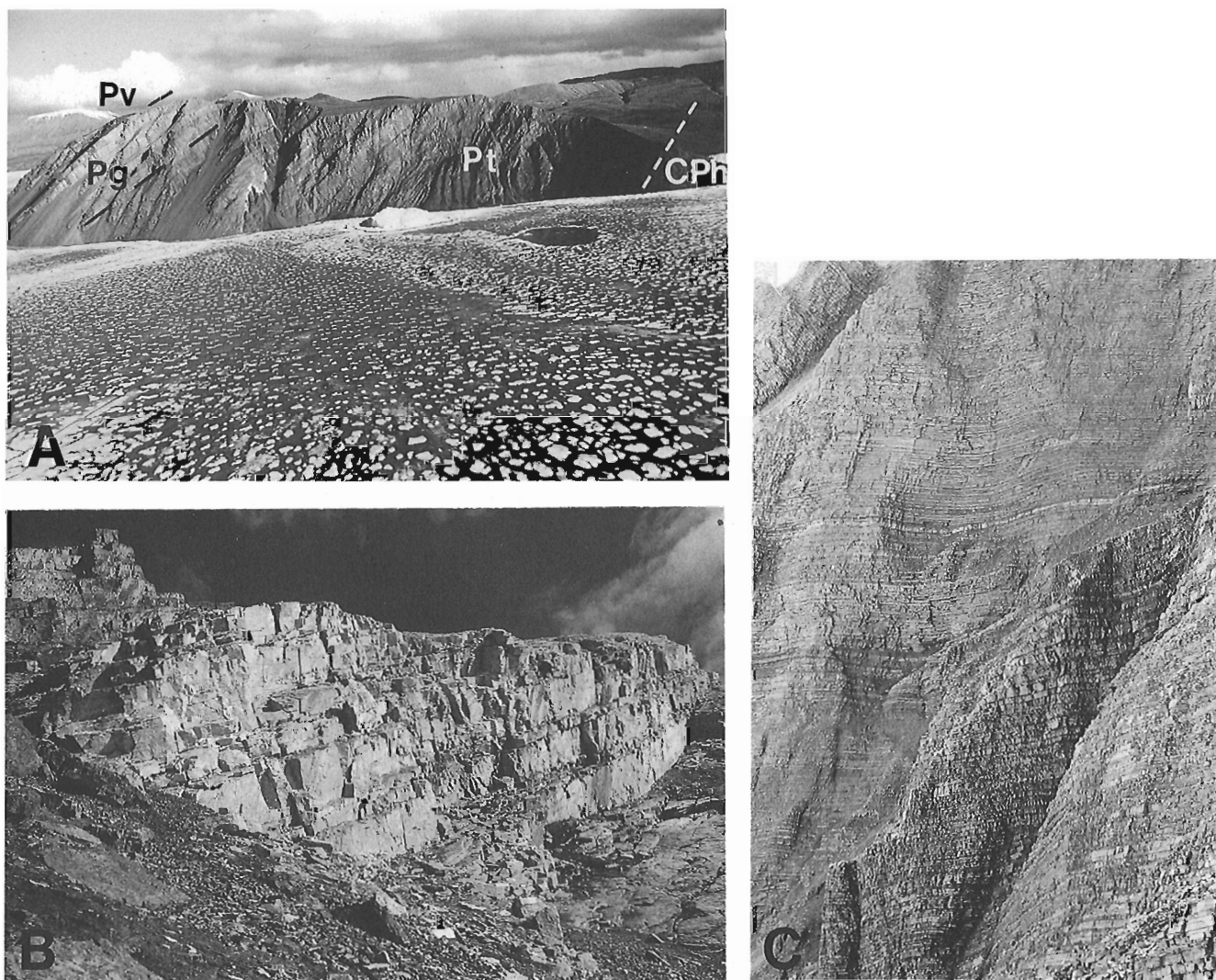


Figure 6.

Uppermost Raanes (Pr), Trappers Cove (Pt), and Great Bear Cape (Pg) formations at locality 7, north of Otto Fiord: mfs, maximum flooding surface coinciding with base of Trappers Cove Formation. Arrows indicate a large buildup in the Raanes Formation. Trappers Cove Formation is 45 m thick.

of Blind fiord, southwestern Ellesmere Island. The Trappers Cove Formation is overlain by the Van Hauen or Great Bear Cape formations, and overlies the Nansen, Hare Fiord or Raanes formations. It has a wide basin axial distribution in the Sverdrup Basin where its ranges from a few metres near its updip termination between the Raanes and Great Bear Cape Formation, to nearly 1 km at Degerbøls Island, northwestern Ellesmere Island (Fig. 2, locality 3; see also Fig. 7A). Physical and conodont biostratigraphic relationships indicate that the Trappers Cove Formation is of Artinskian age throughout the Sverdrup Basin.

The Trappers Cove Formation in the present study area is identical to that described in the Blind Fiord area: it is a unit of dark grey to black siliceous shale and spiculitic chert that weathers yellow in some areas. It comprises rhythmically bedded, thin to very thin bedded, black fissile shale at the base passing upward into increasingly cherty shale and siltstone, and ultimately into argillaceous chert and relatively pure, medium bedded spiculitic chert (Fig. 7C). Near the vertical and lateral transition with the Great Bear Cape Formation, Trappers Cove lithologies are more calcareous and display yellow weathering hues (Fig. 8). The contact with the Great Bear Cape Formation is gradational and is where limestone becomes the dominant lithology.



- A) Uppermost Hare Fiord (CPh), Trappers Cove (Pt), Great Bear Cape (Pg), and basal Van Hauen (Pv) formations;
- B) Medium to thick bedded bryozoan-rich packstone and grainstone in the Great Bear Cape Formation;
- C) Thin to medium bedded rhythmic alternations of shale and spiculitic chert in the Trappers Cove Formation. Trappers Cove Formation is 850 m thick;

Figure 7. Degerbøls Island, northwestern Ellesmere Island (locality 3).

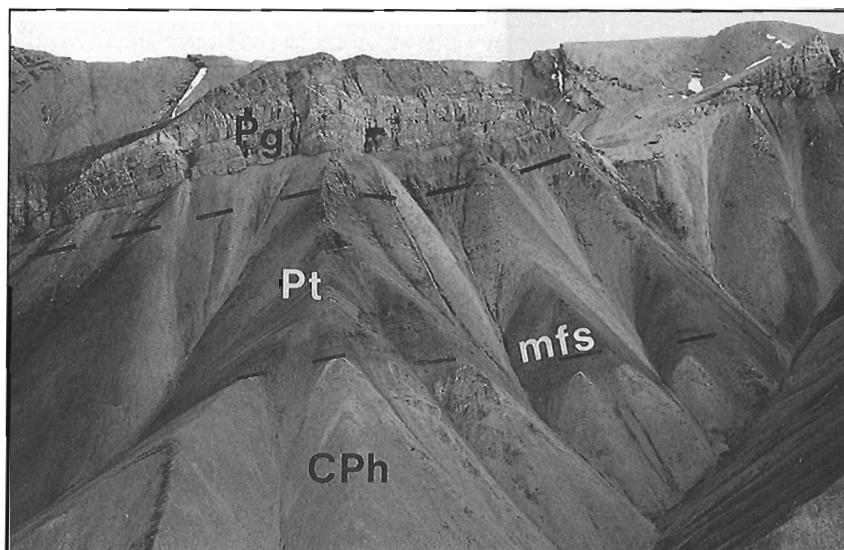


Figure 8.

Uppermost Hare Fiord (CPh), Trappers Cove (Pt), and Great Bear Cape (Pg) formations at locality 10, south of Otto Fiord: mfs, maximum flooding surface coinciding with the base of the Trappers Cove Formation. Trappers Cove Formation is nearly 300 m thick.

The rhythmic nature of the bedding and the basin axial position of the formation, in addition to the observation of large truncation features and variably dipping clinofolds, suggest that the bulk of the Trappers Cove Formation comprises sediments transported as turbidites in a slope to basinal setting.

SEQUENCE STRATIGRAPHY

On Hvitland Peninsula and adjacent areas, the uppermost Nansen and Hare Fiord formations, the entire Raanes Formation, and the bulk of the Great Bear Cape and Trappers Cove formations form a low-order transgressive-regressive (T-R) sequence of mostly Artinskian age (Beauchamp et al., 1995a; Beauchamp and Henderson, 1994). The uppermost Great Bear Cape and Trappers Cove formations belong to an overlying Kungurian-Kazanian Sequence (Desrochers and Beauchamp, 1995; Beauchamp et al., 1995a).

Lower sequence boundary

The basal sequence boundary is a subaerial unconformity within the uppermost Nansen Formation (Fig. 2, 3), where it lies between shallow-water high-energy grainstones below and slightly recessive, low-energy wackestones and packstones above (Fig. 4, 5). Field evidence of subaerial exposures includes thin layers of terra rosa paleosol clay immediately above the unconformity and incorporation of terra rosa material into the immediately overlying transgressive strata. Exceptionally, the sequence boundary coincides with the lithostratigraphic contact between the Great Bear Cape Formation and underlying Nansen Formation, east of Girty Creek, east of Hvitland Peninsula (Fig. 1, 3)

The unconformity representing the lower sequence boundary at the basin margin becomes a correlative conformity toward the basin centre (Fig. 2, 3). Here, the basal sequence boundary occurs within the uppermost Hare Fiord Formation

and is located at the top of a shallowing-upward progression comprising locally associated, very thick bedded crinoidal turbidite and debris flows (Fig. 9) with medium to thick bedded wackestone at its top. The overlying succession is deepening-upward and consists of nonfossiliferous mudrocks, mostly shale and argillaceous cherty limestone.

Upper sequence boundary

The upper sequence boundary is a regional subaerial unconformity that lies within the uppermost part of the Great Bear Cape Formation at a number of localities in the easternmost regions of the study area (Fig. 3). An unconformity of more local extent was also observed at locality 6 (Fig. 2, 5); this area is believed to represent a paleohigh, a possible origin of which is discussed below. The unconformable sequence boundary was best observed at locality 11 where the succession beneath the erosion surface is a shallowing-upward package of bryozoan-rich wackestone and packstone that pass upward into coarse grained crinoidal limestone. Above the surface lies a deepening-upward succession of finer grained, crinoidal packstone to wackestone.

The upper sequence boundary becomes a conformable surface basinward, and evidence for subaerial exposure disappears. In the more distal shelf setting, the upper sequence boundary is a conformable surface within the Great Bear Cape Formation (Fig. 2, 3). The succession below the sequence boundary is coarsening-, thickening- and shallowing-upward and culminates in crinoidal grainstones. The rocks above the sequence boundary are fining-, thinning-, and deepening-upward as grainstones give way to packstones and wackestones recording the initial stages of the next transgression.

In the distal areas, the upper sequence boundary can be traced from the Great Bear Cape Formation into the correlative basinal facies of the Trappers Cove Formation. In such settings, the sequence boundary is the surface that lies between resistant, shale-free spiculitic chert strata below and increasingly shalier, and thinner chert strata above (Fig. 2, 3).

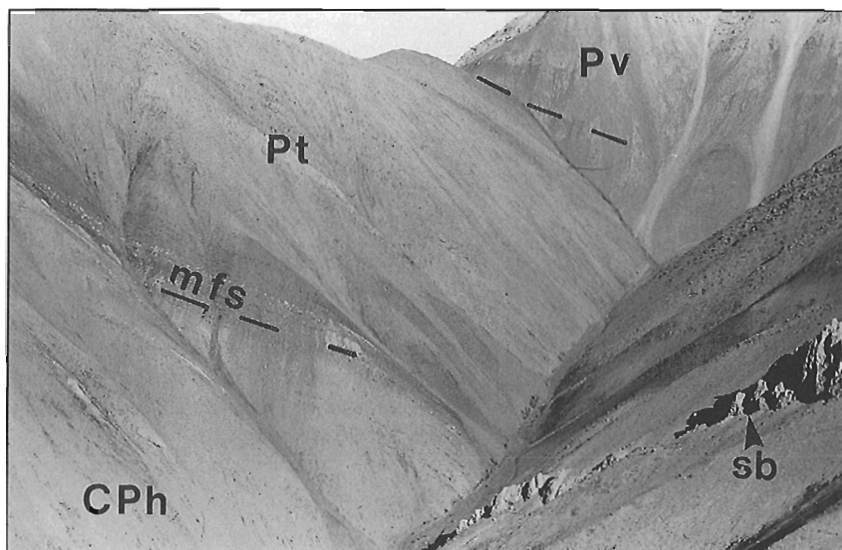


Figure 9.

Uppermost Hare Fiord (CPh), Trappers Cove (Pt), and Van Hauen (Pv) formations at locality 9, south of Otto Fiord: mfs, maximum flooding surface coinciding with the base of the Trappers Cove Formation; sb, sequence boundary in the Hare Fiord Formation associated with massive resistant debris flow units. Trappers Cove Formation is 420 m thick.

Maximum flooding surface

In proximal areas, the maximum flooding surface closely corresponds with the lithostratigraphic contact between the Raanes and Great Bear Cape formations (Fig. 4-6). At these localities the surface is associated with very silty carbonates, rich in pyrite and reduced iron giving a typical green appearance. In the more distal areas, the maximum flooding surface is close to the lithostratigraphic boundary between greenish grey shales of the Hare Fiord Formation and black shales of the Trappers Cove Formation (Fig. 7A, 8, 9). An unusual maximum flooding surface occurs at locality 6 (Fig. 5), where the surface is sharply erosive with evidence of subaerial exposure as suggested by the presence of soil-derived reddish clay in the rocks lying above the unconformity.

Transgressive systems tract

The transgressive systems tract is the stratigraphic succession between the lower sequence boundary and the maximum flooding surface. It is represented by the uppermost Nansen and correlative Hare Fiord formations, by the entire Raanes formation, and locally by reef mounds at the base of the Great Bear Cape Formation. On Hvitland Peninsula, the transgressive systems tract can be subdivided into an early transgressive systems tract (ETST in Fig. 2, 3) and a late transgressive systems tract (LTST in Fig. 2, 3). The early transgressive systems tract records the initial deepening phase and is represented by slope to basinal strata in the uppermost Hare Fiord Formation and correlative deep water shelf strata in the uppermost Nansen Formation (Fig. 4, 5, 8, 9). This early package lies between the lower sequence boundary and a marked flooding surface that is locally a shoreface unconformity, which corresponds to the sharp Nansen-Raanes contact at the basin margin (e.g., Fig. 5). The late transgressive systems tract coincides with a major deepening phase. It lies between the flooding surface that corresponds to the Nansen-Raanes contact and the maximum flooding

surface (Fig. 4-6). This subdivision is represented by the entire Raanes Formation and equivalent condensed basinal strata of Hare Fiord Formation. Sedimentation of the Raanes Formation took place on a variably inclined ramp, the steepest gradient of which occurred in a tectonically active, probably fault-bounded depression in the eastern regions of Hvitland Peninsula, as discussed later.

Regressive systems tract

The stratigraphic succession between the maximum flooding surface and the upper sequence boundary is the regressive systems tract. This systems tract is represented by shallowing-upward, progradational, temperate shelf carbonates of the Great Bear Cape Formation (Fig. 5, 6, 7A, 8), and laterally equivalent slope and basin deposits of shales and cherts of the Trappers Cove Formation (Fig. 6-9).

ARTINSKIAN PALEOGEOGRAPHY

Maximum progradation of Nansen carbonates in Sakmarian time formed a very sinuous reef-constructed shelf edge through Hvitland Peninsula in a general northwest direction (Fig. 1). The shelf edge was associated with various narrow embayments, some of which probably reflect the location of old Carboniferous rift-related tectonic depressions. One such deep-water embayment, the Otto Fiord Embayment of Beauchamp et al. (1995b), is located immediately north of the head of Otto Fiord (Fig. 2, locality 5). The embayment existed from the Moscovian to the Sakmarian, as shown by the more than 1.4 km thick section of Hare Fiord sediments in this area. Even the shallowest water facies beneath the sub-Artinskian sequence boundary are represented by relatively deep-water Hare Fiord mudrocks. Erosion associated with the creation of the sequence boundary did not affect these deeper water embayments, nor did it affect the distal areas lying west and south of the old Nansen shelf edge.

The early transgressive systems tract, which is contained in the upper Hare Fiord Formation, marked the initial stage of basinal and embayment sedimentation following the creation of the sequence boundary. This systems tract, which accumulated when the bulk of the Nansen shelf was exposed, progressively overlapped the unconformity in a landward direction. A significant and geologically rapid landward shift of facies (eastward in the study area) occurred later, coinciding with the base of the late transgressive systems tract. What followed was a setting whereby the deep basin and embayment received very little or no sediments at all, while the platform areas were rapidly overlapped and received the bulk of sediments (Raanes Formation).

That a renewed phase of rifting was associated with the late transgressive systems tract is suggested by the dramatic thickening (from less than 20 m to more than 225 m) of the Raanes Formation between sections 6 and 7 on eastern Hvitland Peninsula. A similar dramatic thickness increase in the Raanes Formation of the type area on southwestern Ellesmere Island was also interpreted as reflecting syntectonic rift-related block faulting (Beauchamp and Henderson, 1994). In addition to the great thickness of sediments, rapid tectonic subsidence of the area east of locality 6 is indicated by the development of numerous reef-mounds (more than 20 of them), as well as the presence of fairly deep-water spiculitic chert assignable to the Trappers Cove Formation above the maximum flooding surface at locality 7 (Fig. 2). It is interesting to note that the maximum flooding surface at locality 6 (i.e., on the upthrown side of the inferred tectonic depression) is a subaerial erosion surface indicating that the area was uplifted prior to Great Bear Cape sedimentation (Fig. 2). The uplift could conceivably represent syntectonic footwall uplift associated with half-graben formation and block rotation to the east. It should be emphasized that the inferred tectonic trend, based on thickness distribution of the Raanes Formation, is at high angle to the northeast-oriented rift depressions that formed in Early to Late Carboniferous time and were filled by the Borup Fiord and Otto Fiord formations (Thériault et al., 1995).

The development of the maximum flooding surface appears to mark the cessation of the Artinskian rifting pulse. Strata above this surface were deposited in a passively subsiding setting, one whereby cool temperate carbonates of the Great Bear Cape Formation prograded into slope to basinal spiculitic shale and chert of the Trappers Cove Formation. The Trappers Cove-Great Bear Cape couplet filled much of the space that was left following the Early Permian progradation of the Nansen shelf edge. This is shown by remarkably thick accumulations, such as Degerbøls Island (Fig. 2, locality 3) where over 1 km of Artinskian strata are present (Fig. 7A). Following the filling of the basin and the old shelf edge embayments, the Great Bear Cape shelf edge prograded much beyond the position occupied by its Nansen ancestor. Maximum progradation was attained in Late Artinskian time; the shelf edge then lay more or less parallel to Otto Fiord along the southern shore of Hvitland Peninsula (Fig. 1).

CONCLUSIONS

The Raanes, Great Bear Cape and Trappers Cove formations recorded the bulk of a long-term, mostly Artinskian transgressive-regressive sequence of the Sverdrup Basin. The early transgressive systems tract comprises mudrocks (Hare Fiord), and correlative limestones (Nansen Formation) that accumulated when the bulk of the shelf was exposed and subjected to erosion. The late transgressive systems tract comprises argillaceous limestones and mud mounds (Raanes Formation) that were accumulated when the deep basinal areas received little or no sediments and deposition was concentrated on the platform. Great thickness variations in the Raanes Formation suggest that rifting and fault-controlled subsidence played an active role during sedimentation of this unit. The regressive systems tract recorded the progradation of cool water temperate shelf carbonates of the Great Bear Cape Formation into dark shale and spiculitic mudrock of the Trappers Cove Formation. The uppermost part of these two formations also comprises transgressive strata that belong to an overlying Kungurian-Kazanian Sequence.

ACKNOWLEDGMENTS

Many thanks to T. de Freitas for reviewing the manuscript and providing useful comments.

REFERENCES

- Beauchamp, B.**
1994: Permian climatic cooling in the Canadian Arctic; in *Pangea: Paleoclimate, Tectonics and Sedimentation during accretion, zenith and break-up of a super-continent*, (ed.) G.D. Klein; Geological Society of America, Special Paper 288, p. 229-246.
- Beauchamp, B.**
in press: Permian history of Arctic North America; in *The Permian of Northern Pangea, volume 1, Paleogeography, Paleoclimates, and Stratigraphy*, (ed.) P.A. Scholte, T.M. Peryt, and D.S. Ulmer-Scholle; Springer-Verlag, New York.
- Beauchamp, B. and Henderson, C.M.**
1994: The Lower Permian Raanes, Great Bear Cape and Trappers Cove formations, Sverdrup Basin, Canadian Arctic: Stratigraphy and Conodont Zonation; *Bulletin of Canadian Petroleum Geology*, v. 42, p. 565-600.
- Beauchamp, B., Mayr, U., and Harrison, J.C.**
1995a: Carboniferous and Permian stratigraphic sequences on Hvitland Peninsula and adjacent areas, northwestern Ellesmere Island, Arctic Canada; in *Current Research 1995-B*; Geological Survey of Canada, this volume.
- Beauchamp, B., Sherry, C.T., Mayr, U., Harrison, J.C., and Desrochers, A.**
1995b: Moscovian (Upper Carboniferous) to Sakmarian (Lower Permian) stratigraphy (Nansen and Hare Fiord formations; Unit C2), Hvitland Peninsula and adjacent areas, northwestern Ellesmere Island, Arctic Canada; in *Current Research 1995-B*; Geological Survey of Canada, this volume.
- Desrochers, A. and Beauchamp, B.**
1995: Ufimian-Kazanian (Lower and Upper Permian) stratigraphy (Van Hauen and Degerbøls formations), Hvitland Peninsula and adjacent areas, northwestern Ellesmere Island, Arctic Canada; in *Current Research 1995-B*; Geological Survey of Canada, this volume.

Harrison, J.C., Mayr, U., and Beauchamp, B.

1995: Preliminary observations on the structural geology of Hvitland Peninsula, northwestern Ellesmere Island, Arctic Canada; in Current Research 1995-B; Geological Survey of Canada, this volume.

Mayr, U., Harrison, J.C., and Beauchamp, B.

1995: Geological map of Carboniferous and Permian units on Hvitland Peninsula and adjacent areas, northwestern Ellesmere Island, Arctic Canada; in Current Research 1995-B; Geological Survey of Canada, this volume.

Thériault, P., Beauchamp, B., Harrison, J.C., Mayr, U., and Steel, R.

1995: Serpukhovian and Bashkirian (Carboniferous) stratigraphy (Borup Fiord and Otto Fiord formations; Unit C1), Hvitland Peninsula and adjacent areas, northwestern Ellesmere Island, Arctic Canada; in Current Research 1995-B; Geological Survey of Canada, this volume.

Thorsteinsson, R.

1974: Carboniferous and Permian stratigraphy of Axel Heiberg Island and western Ellesmere Island, Canadian Arctic Archipelago; Geological Survey of Canada, Bulletin 224, 210 p.

Geological Survey of Canada Project 870067

Ufimian-Kazanian (Lower and Upper Permian) stratigraphy (Van Hauen and Degerbøls formations), Hvitland Peninsula and adjacent areas, northwestern Ellesmere Island, Arctic Canada

A. Desrochers¹ and B. Beauchamp

Institute of Sedimentary and Petroleum Geology, Calgary

Desrochers, A. and Beauchamp, B., 1995: Ufimian-Kazanian (Lower and Upper Permian) stratigraphy (Van Hauen and Degerbøls formations), Hvitland Peninsula and adjacent areas, northwestern Ellesmere Island, Arctic Canada; in Current Research 1995-B; Geological Survey of Canada, p. 57-63.

Abstract: The Van Hauen and Degerbøls formations are widely exposed on Hvitland Peninsula and adjacent areas. The Van Hauen Formation, a unit of dark grey to black, slope to basinal, spiculitic chert and shale, is overlain and grades laterally into the Degerbøls Formation, a unit of cool water bioclastic (Bryonoderm biota) shelf limestone and lesser chert. The Degerbøls Formation overlies, and passes landward into, green glauconitic, variably fossiliferous, shallow-water marine sandstones of the Troid Fiord Formation. These formations form the bulk of a low order, unconformity-bounded sequence of the Sverdrup Basin, a sequence that also includes strata contained in the upper part of the Great Bear Cape and correlative Trappers Cove formations. The uppermost part of the Van Hauen and Degerbøls formations comprises strata that belong to a younger post-Kazanian Sequence. Shelf to basin depositional facies are organized in decametre-scale, transgressive-regressive cycles with distinctive facies and stacking patterns.

Résumé : Les formations de Van Hauen et de Degerbøls sont largement exposées dans la péninsule Hvitland et dans les régions avoisinantes. La Formation de Van Hauen, unité de chert et de shale spiculitiques gris foncé à noirs, de talus à bassin, laisse place au-dessus et latéralement à la Formation de Degerbøls, unité de calcaire bioclastique (biote à bryonodermes) de plate-forme continentale d'eau froide et de chert en moindre quantité. La Formation de Degerbøls recouvre des grès épicontinentaux glauconieux verts plus ou moins fossilifères de la Formation de Troid Fiord, et passe à ces grès vers l'intérieur des terres. Ces formations constituent le gros d'une séquence d'ordre inférieur, limitée par une discordance, du bassin de Sverdrup; cette séquence comprend également des couches contenues dans la partie supérieure de la Formation de Great Bear Cape et la formation corrélatrice de Trappers Cove. La partie sommitale des formations de Van Hauen et de Degerbøls comprend des couches appartenant à une séquence post-kazanienne plus récente. Les faciès sédimentaires de plate-forme continentale à bassin sont organisés en cycles transgressifs-régressifs d'échelle décamétrique à faciès et modes de superposition distincts.

¹ Department of Geology, University of Ottawa, Ottawa, Ontario K1N 6N5

INTRODUCTION

The Van Hauen and Degerbøls formations are two units that are widely exposed on Hvitland Peninsula and adjacent areas. These formations form the bulk of a low-order unconformity-bounded sequence of the Sverdrup Basin, a sequence that also includes strata contained in the upper part of the Great Bear Cape and correlative Trappers Cove formations (Kells et al., 1995). The uppermost part of the Van Hauen and Degerbøls formations comprises strata that belong to a younger post-Kazanian Sequence (see Beauchamp et al., 1995a, b). This paper provides generalities about the distribution and facies content of the Van Hauen and Degerbøls formations, the sequence stratigraphic significance of these units, and the late Early to early Late Permian paleogeography of a study area that extends south and east of the area mapped by Mayr et al. (1995).

Generalities about the geological setting of the area can be found in Mayr et al. (1995), Harrison et al. (1995), and Beauchamp et al. (1995a). The age of the Van Hauen and Degerbøls formations has been substantiated by paleontological evidence (for a summary see Beauchamp et al., 1989a, b; Beauchamp, in press).

STRATIGRAPHY

Van Hauen Formation

The Van Hauen Formation (Thorsteinsson, 1974) is a unit of dark grey to black siliceous shale and chert, and lesser limestones that overlie the Great Bear Cape and the Trappers Cove formations. The type section of the formation is at Van Hauen

Pass, close to the north shore of Hare Fiord (Fig. 1), where the formation is over 385 m thick. The Van Hauen Formation is overlain by either the Degerbøls Formation or a younger Permian chert unit mapped as Unit P6 on Hvitland Peninsula (Mayr et al., 1995; see also Beauchamp et al., 1995b). The Van Hauen Formation, which passes in a proximal direction into the Degerbøls and Assistance formations, is widely distributed in the axial regions of the Sverdrup Basin where it locally reaches thicknesses exceeding 1 km (e.g., subsurface of northern Prince Patrick Island). Field exposures of the Van Hauen Formation around Ellesmere Island range from a few tens of metres in thickness (i.e., next to the updip termination) to 385 m at the type section. Much thinner sections of the formation were measured on Hvitland Peninsula, where the formation ranges from less than 10 m to a maximum of 160 m. Thicker sections, including the type section, occur south of Otto Fiord. In that area, the Van Hauen Formation passes laterally into cherty dark green siltstone assigned to the Assistance Formation (Fig. 2, locality 2). The Van Hauen Formation is less than 50 m thick at that locality.

On Hvitland Peninsula and adjacent areas (Fig. 3-6), the Van Hauen Formation comprises a basal recessive unit of black siliceous shale that grades upward into increasingly cherty shale, siltstone and ultimately into dark grey to black, variably shaly spiculitic chert. Yellowish to orange weathering, calcareous units, and minor limestones occur near the vertical and lateral transition with the Degerbøls Formation. One of the most spectacular features of the formation near this transition is the presence of large-scale, gently dipping clinoforms, which indicate a slope to basinal environment of deposition in conjunction with the rhythmic nature of the bedding, the deeper water aspect of the formation, and its basin axial distribution.

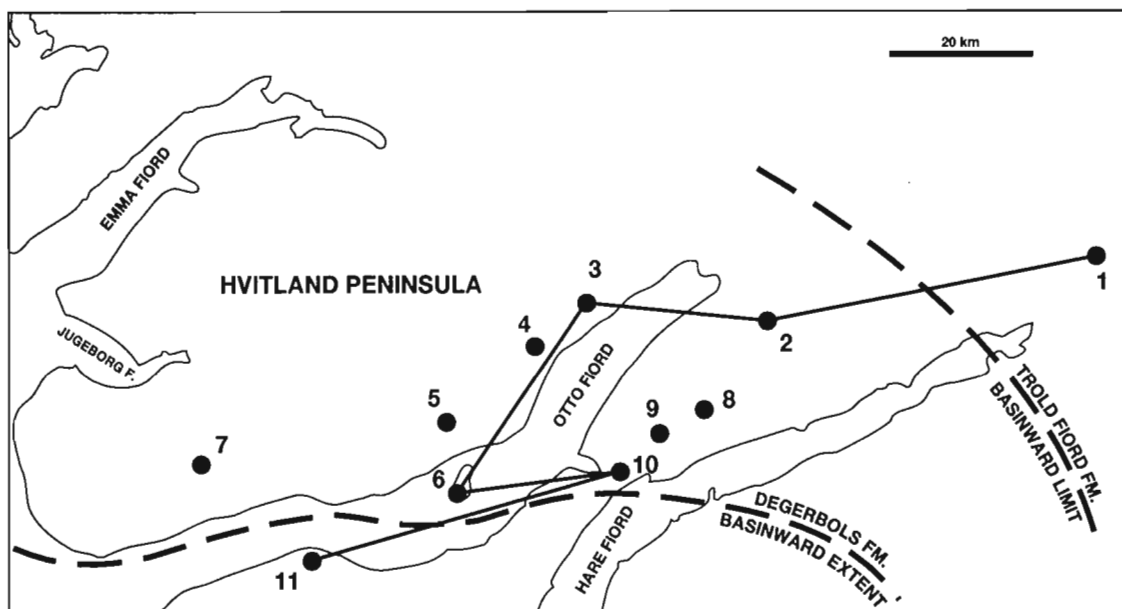


Figure 1. Map showing locations of measured sections, line of cross-section and basinward extent of Degerbøls carbonates and correlative Trolld Fiord sandstones in Kazanian time (Late Permian).

Degerbøls Formation

The Degerbøls Formation (Thorsteinsson, 1974) is a unit of bioclastic limestone that occurs at various localities along the northern, eastern and southern margins of the Sverdrup Basin. The type section of the formation is at Van Hauen Pass where it is about 165 m thick and unconformably overlain by the Triassic Blind Fiord Formation. The Degerbøls Formation, which overlies and grades laterally into the Van Hauen Formation, ranges from a few tens of metres in thickness to more than 165 m. The Degerbøls Formation passes landward into the Troid Fiord Formation, a variably thick succession of green glauconitic sandstone that contains locally abundant fossils. The Troid Fiord Formation is widely exposed near the

southern and eastern margins of the Sverdrup Basin, especially on Fosheim and Hamilton peninsulas where it reaches a thickness of over 600 m.

Several excellent exposures of the Degerbøls Formation were mapped on Hvitland Peninsula (Mayr et al., 1995), where it ranges from a few tens of metres to over 160 m at locality 3, near the Otto Fiord base camp. The Degerbøls Formation is overlain either conformably by an uppermost Permian chert unit (Unit P6 of Mayr et al., 1995; see also Beauchamp et al., 1995b), or unconformably by the Triassic Blind Fiord Formation (Fig. 2). The Degerbøls Formation grades in an eastward direction into the Troid Fiord Formation, which was examined at one locality only, east of Girty Creek (locality 1 in Fig. 1, 2).

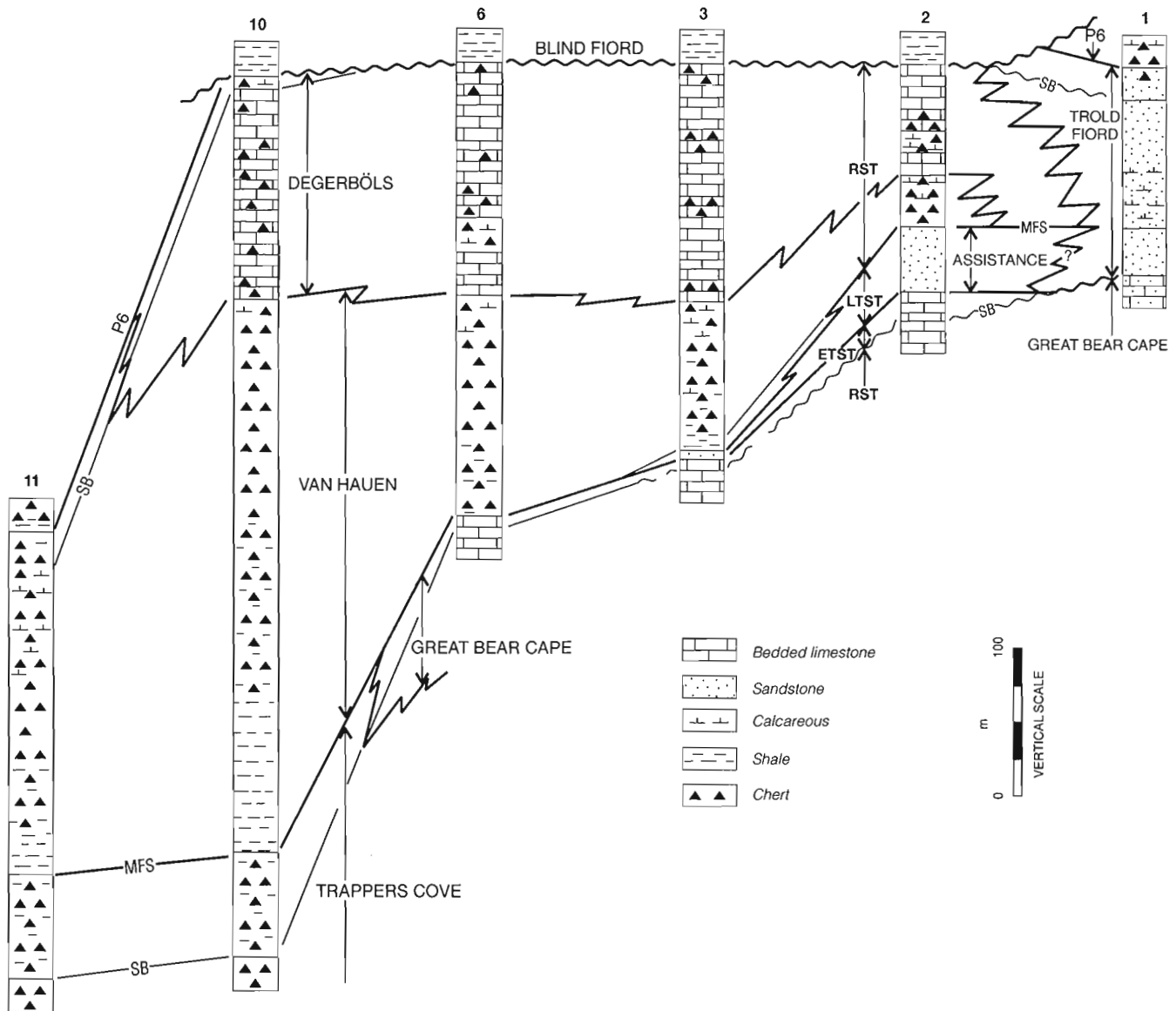


Figure 2. Cross-section showing the distribution of Van Hauen and Degerbøls formations, and correlative Assistance and Troid Fiord formations on Hvitland Peninsula and adjacent areas, northwestern Ellesmere Island: SB, sequence boundary; MFS, maximum flooding surface; ETST, early transgressive systems tract; LTST, late transgressive systems tract; RST, regressive systems tract.

On Hvitland Peninsula and adjacent areas, the Degerbøls Formation displays a characteristic alternation of broad recessive and resistant units. The resistant units comprise typical Degerbøls carbonates: medium to thick bedded, crinoidal grainstones associated with bryozoans, brachiopods and sponge. The recessive intervals display facies more typical of the Van Hauen Formation: thin to medium bedded, dark grey spiculitic cherts that become increasingly calcareous, thicker bedded, and increasingly fossiliferous upward as they grade into the resistant units. As many as five recessive-resistant couplets have been recognized, each of which is interpreted as one higher-order sequence or cycle, as will be discussed below. Carbonates of the Degerbøls Formation display a characteristic Bryonoderm assemblage (bryozoan, echinoderm, brachiopod, sponge), which has been interpreted as reflecting cold water, temperate deposition (Beauchamp, 1994). This interpretation is supported by the presence of dropstones in the Troid Fiord Formation in some areas, and by the complete absence of fusulinaceans, colonial rugose corals, reefs, ooids, oncoids, and submarine cements (Beauchamp, 1994). Spectacular clinofolds occur in the Degerbøls Formation near its lateral transition with the Van Hauen Formation (Fig. 5). The Degerbøls-Van Hauen lateral transition, which corresponds to the Kazanian shelf edge, prograded beyond the basinward extent of the previous Great Bear Cape shelf edge (Kells et al., 1995; see also Beauchamp et al., 1995a).

The Degerbøls-correlative Troid Fiord Formation of east Girty Creek comprises fossiliferous, glauconitic sandstone with abundant *Zoophycus* and other vertical and horizontal burrows. The sandstone units are commonly arranged in erosively soled, graded and inversely graded packages interpreted as tempestites. A 35 m thick unit of fining-upward sandstone at the base of the formation may be correlative with the Assistance Formation which is exposed to the west (Fig. 2).

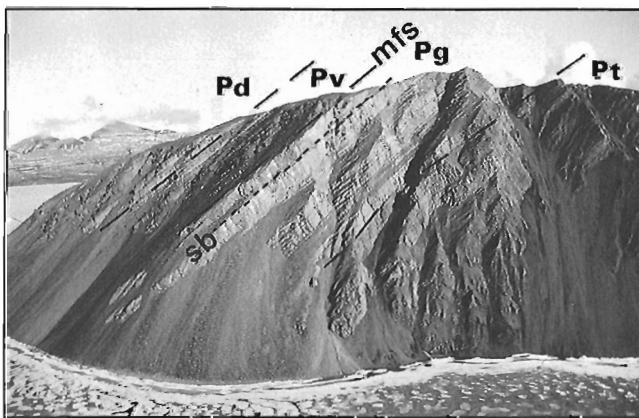


Figure 3. Contacts between upper Trappers Cove (Pt), Great Bear Cape (Pg), Van Hauen (Pv), and Degerbøls (Pd) formations at Degerbøls Island, northwestern Ellesmere Island (locality 6): sb, sequence boundary; mfs, maximum flooding surface. Van Hauen Formation is 150 m thick.

SEQUENCE STRATIGRAPHY AND DEPOSITIONAL ENVIRONMENTS

On Hvitland Peninsula and adjacent areas, the Van Hauen and Degerbøls formations, and correlative Assistance and Troid Fiord formations form the bulk of a low-order transgressive-regressive Kungurian-Kazanian sequence of the Sverdrup Basin, one that also includes strata contained in the upper part of the Trappers Cove and correlative Great Bear Cape formations (Kells et al., 1995). The uppermost Van Hauen and Degerbøls formations belong to an overlying post-Kazanian Sequence (Beauchamp et al., 1995a, b).

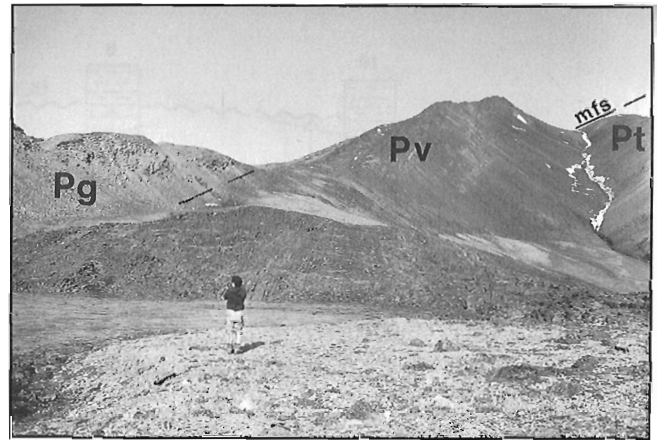


Figure 4. Uppermost Trappers Cove (Pt), Van Hauen (Pv) and Degerbøls (Pd) formations at Van Hauen Pass, northwestern Ellesmere Island (locality 10): MFS, maximum flooding surface. Exposure is about 500 m thick.

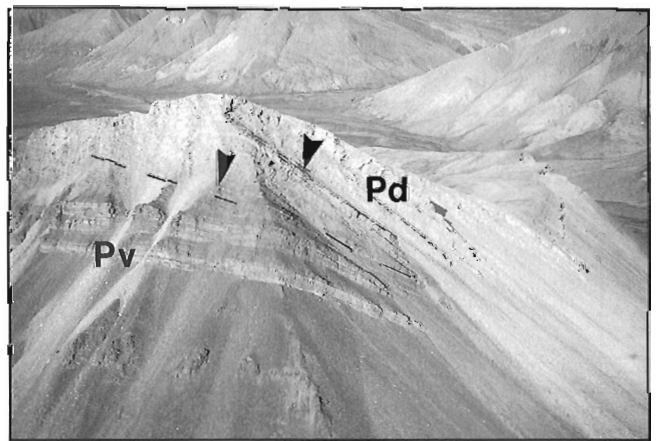


Figure 5. Upper Van Hauen (Pv) and Degerbøls (Pd) formations, north of Hare Fiord, east of Van Hauen Pass, northwestern Ellesmere Island (locality 8). Shelf edge carbonates (arrows) in Degerbøls Formation dip basinward. Strata exposed are about 200 m thick.

Sequence boundaries and maximum flooding surface

A subaerial unconformity present above shelf carbonates of the Great Bear Cape Formation marks the lower sequence boundary near the basin margin (Fig. 2, locality 1). This surface passes basinward into a correlative conformity that lies within the Great Bear Cape Formation (e.g., Fig. 3). The conformable sequence boundary lies between thickening-, coarsening- and shallowing-upward crinoidal grainstones and thinning-, fining- and deepening-upward muddy crinoidal limestones. Basinward of the Great Bear Cape paleoshelf margin, the conformable sequence boundary occurs within the Trappers Cove Formation separating a shallowing-upward package of cherty mudrocks from an overlying deepening-upward package of more argillaceous mudrocks (Fig. 6).

At the basin margin, the upper sequence boundary is an erosion surface that lay within the upper portion of the Troid Fiord Formation. This surface is truncated basinward by the sub-Triassic unconformity that resulted from uplift, buckling and erosion of large areas of Hvitland Peninsula in latest Permian-earliest Triassic time (Beauchamp et al., 1995b). In the more distal southwestern regions of Hvitland Peninsula, the upper sequence boundary is a conformable surface that lies in the upper Degerbøls Formation between bioclastic limestone below and variably calcareous spiculitic chert above. These uppermost Degerbøls strata belong to a post-Kazanian sequence, the regressive portion of which is contained in a chert unit mapped as Unit P6 by Mayr et al. (1995) (see also Beauchamp et al., 1995b).

In the more proximal areas, the maximum flooding surface separates glauconitic fine grained sandstone and siltstone of the Assistance Formation from deeper water, spiculitic chert of the Van Hauen Formation (Fig. 2, locality 2). At the basin margin, the maximum flooding surface lies within the Troid Fiord Formation between fining-upward sandstones and siltstones (Assistance correlative?) below and a thickening- and coarsening-upward succession of fossiliferous sandstone above. In the more distal areas, the maximum flooding surface

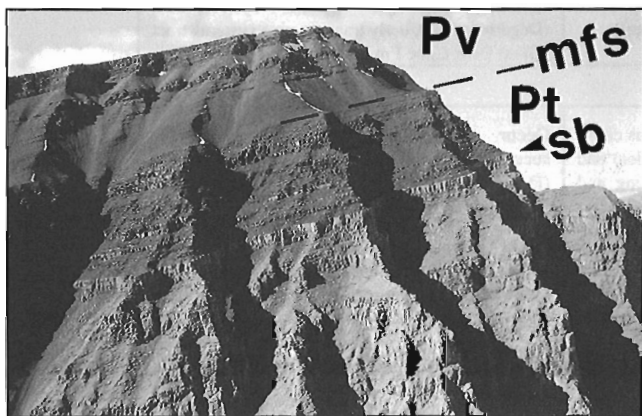


Figure 6. Uppermost Trappers Cove (Pt) and Van Hauen (Pv) formations, south of the mouth of Otto Fiord, northwestern Ellesmere Island (locality 11): sb, sequence boundary; mfs, maximum flooding surface. Total cliff exposure is about 900 m.

corresponds to a thin but distinctive unit within the lowest Van Hauen Formation (e.g., Fig. 6) composed of black fissile shale with abundant authigenic pyrite and phosphate minerals.

Transgressive and regressive systems tracts

The transgressive systems tract is the stratigraphic succession between the lower sequence boundary and the maximum flooding surface, represented by the uppermost Trappers Cove and correlative Great Bear Cape formations, the Assistance Formation, and locally by a thin succession at the base of the Troid Fiord Formation that is probably correlative to the Assistance Formation. On Hvitland Peninsula and adjacent areas, the transgressive systems tract can be subdivided into an early transgressive systems tract (ETST in Fig. 2) and a late transgressive systems tract (LTST in Fig. 2).

The early transgressive systems tract recorded the initial deepening phase and is represented by slope to basinal strata in the uppermost Trappers Cove Formation and correlative deep water shelf strata in the uppermost Great Bear Cape Formation (Fig. 2). This package lies between the lower sequence boundary and a marked flooding surface (locally a shoreface unconformity) that corresponds to the sharp Great Bear Cape-Assistance contact at locality 2 (Fig. 2). The early transgressive systems tract comprises shale, cherty mudrock, and chert organized into thickening-upward decameter-scale cycles. Individual cycles comprise a thin transgressive portion and a thicker regressive portion defined respectively by the thickening- and thinning-upward stacking patterns of smaller, metre-scale cycles.



Figure 7. Field photograph showing outer shelf subtidal decameter-thick cycles in a small cliff exposure, locality 3 near Otto Fiord Camp, Hvitland Peninsula, northwestern Ellesmere Island. Regressive echinoderm-rich grainstone (EG) is overlain by transgressive spiculitic chert and bryozoan-rich spiculitic chert (SP) of the next cycle. Note the massive, thick bedded nature of the grainstone capping the lower cycle. Jacob's staff is 1.5 m long.

The late transgressive systems tract coincides with a major deepening phase and a geologically rapid landward facies shift. This subdivision is represented by the entire Assistance Formation and equivalent condensed basinal strata at the base of the Van Hauen Formation, and by thin transgressive strata at the base of the Troid Fiord Formation. Together, these units recorded clastic deposition on a relatively steep ramp.

The strata between the maximum flooding surface and the upper sequence boundary represents the regressive system tract and forms a shallowing-upward succession. At the basin margin, the regressive systems tract is represented by a shallowing-upward, thickening- and coarsening-upward succession of variably fossiliferous sandstone forming the bulk of the Troid Fiord Formation. In distal shelf to slope areas, the succession forms a wedge of shale, cherty mudrock, and chert of the Van Hauen Formation, up to 500 m thick, passing gradually upward into cherty carbonate and bioclastic carbonate of the Degerbøls Formation (Fig. 4, 5). In the more distal

basinal areas, the succession is assigned to the Van Hauen Formation and composed of shale and cherty mudrock passing upward into pure cliff-forming chert (Fig. 6).

The regressive system tract comprises at least five basin-wide decameter-scale cycles. Facies distribution within these decameter-scale cycles varies both laterally and vertically, reflecting the overall regressive nature of the sequence. These cycles are best developed in outer shelf to shelf edge limestone of the Degerbøls Formation and slope to proximal basin shale and chert of the Van Hauen Formation, such as locality 3 close to the Otto Fiord base camp (Fig. 7). Decameter-scale cycles are present but they are more difficult to recognize and correlate in inner shelf sandstone of the Troid Fiord Formation and distal basinal shale and chert of the Van Hauen Formation.

In shelf areas, the decameter-scale cycles are composed of purely subtidal bioclastic chert and carbonate facies and are characterized by a thin or absent transgressive portion and a thick regressive portion. These asymmetric cycles have

Table 1. Lithological characteristics, occurrence, and interpretation of major depositional facies present in the Kungurian-Kazanian sequence of Hvitland Peninsula and adjacent areas.

Facies	Lithology	Occurrence
1. basal transgressive sandstones (<storm-influenced zone)		
Glaucinitic sandstone	Fined grained, highly bioturbated quartz-rich sands; mainly <i>Zoophycus</i> , locally abundant spicules	Occur as a thin basal transgressive siliciclastic deposit; restricted to the Assistance Formation
2. Inner shelf sandstones (wave-influenced zone)		
Poorly fossiliferous sandstone	Fine grained, bioturbated quartz-rich sandstone; variably fossiliferous, bryozoan, echinoderm and small benthic forams; local spicules and glauconite	Occur as decameter-scale cyclic successions of fossil-poor and fossil-rich glauconitic sandstone; regressive systems tract; restricted to the Troid Fiord Formation
3. Outer shelf to shelf edge carbonates (wave- to storm-influenced zone)		
Echinoderm-rich grainstone	Well-sorted, fine to coarse grained bioclastic in thick grainstone beds; echinoderm-dominated bryonoderm assemblage	Occur as part of decameter-scale cyclic successions; mainly in regressive systems tract (Degerbøls Fm.)
Bryozoan-rich packstone/grainstone	Well bedded, poorly sorted bioclastic packstone/grainstone in thin to medium beds; bryozoan-dominated (bryonoderm assemblage)	Occur as part of decameter-scale cyclic successions; mainly in regressive systems tract (Degerbøls Fm.); early transgressive systems tract (Great Bear Cape Fm.)
4. Proximal slope to distal slope chert (<storm-influenced zone)		
Bryozoan-rich spiculitic chert	Thinly bedded, dark to light grey fossiliferous chert; mixed hyalosponge (mainly monaxon spicules) and bryonoderm (mainly large delicate branching and fenestrate bryozoans) biotic assemblages	Occur as part of decameter-scale cyclic successions; mainly in regressive systems tract (Degerbøls Fm.), early transgressive systems tract (Great Bear Cape Fm.)
Spiculitic chert	Thinly bedded, dark to light grey chert; locally bioturbated; hyalosponge biotic assemblage with rare elements of the bryonoderm assemblage	Occur as part of decameter-scale cyclic successions; mainly in regressive systems tract (Van Hauen Fm.); early transgressive systems tract (Trappers Cove Fm.)
5. Proximal to distal basinal shale (<<storm-influenced zone)		
Spiculitic mudrock	Medium to dark grey, bioturbated fine grained mudrock; <i>Zoophycus</i> and/or <i>Nereitis</i> trace fossils; well-indurated; rare brachiopods, locally abundant spicules	Occur as part of decameter-scale cyclic successions; in both transgressive and regressive systems tracts; mainly in Van Hauen Formation
Fissile shale	Black to dark grey, fissile shale; weakly bioturbated; rare <i>Nereitis</i> trace fossils; locally abundant pyrite and phosphate	Occur as part of decameter-scale cyclic successions; in both transgressive and regressive systems tracts mainly in Van Hauen Formation

many characteristics of subtidal cycles described elsewhere in the geological record including: an upward increase in grain size, textural maturity, bed thickness, and crossbedding and other high-energy sedimentary features. The Degerböls cycles are not capped by peritidal facies, nor do any cycles exhibit subaerial features (karst, caliche, vadose cementation) or early sea floor cementation (hardground). The decameter-scale cycles form a continuum across the Degerböls shelf. Two idealized end-member cycles are recognized here: the outer shelf and the deeper shelf edge cycles. The outer shelf cycles comprise a thin basal unit of spiculitic chert grading upward into bryozoan-rich packstone/grainstone capped by a clean echinoderm-rich grainstone. The shelf edge cycles are composed of a relatively thick basal chert facies capped by a relatively thin bryonoderm packstone/grainstone facies. A possible control on these stacked decameter-scale cycles is eustasy acting in concert with intrinsic factors such as storm and wave reworking and sediment redistribution to inhibit shoaling to intertidal levels and limit aggradation within the zone of optimal carbonate production. Correlative strata in the Van Hauen Formation are also arranged in a series of decametre-scale cycles that may or may not be correlative with Degerböls cycles (e.g., Fig. 6).

Table 1 summarizes the lithological characteristics, occurrence, and depositional interpretation of the seven major depositional facies found in the transgressive and regressive systems tract of the Kungurian-Kazanian Sequence. These facies are: 1) glauconitic sandstone; 2) fossiliferous sandstone; 3) bryonoderm limestone (echinoderm-rich grainstone to bryozoan-rich packstone/grainstone); 4) bryozoan-rich spiculitic chert; 5) spiculitic chert; 6) spiculitic mudrock; and 7) fissile shale. Other minor facies include carbonate debrite and turbidite mixed locally with the slope facies of the Van Hauen Formation.

CONCLUSIONS

The bulk of the Van Hauen and correlative Degerböls and Trolld Fiord formations on Hvitland Peninsula and adjacent areas form the regressive systems tract of a Kungurian-Kazanian Sequence, the transgressive systems tract of which is contained in the uppermost Trappers Cove and correlative Great Bear Cape formations, and Assistance and correlative(?) basal Trolld Fiord formations. The uppermost part of the Van Hauen and Degerböls formations also comprise transgressive strata belonging to a younger post-Kazanian Sequence. The Degerböls Formation, which is arranged in a series of decametre-scale shallowing-upward cycles, contains cool water carbonate sediments that pass into slope to basinal cherty mudrocks of the Van Hauen Formation. The Degerböls-Van Hauen lateral transition, which corresponds to the Kazanian shelf edge, prograded beyond the basinward extent of the previous Great Bear Cape shelf edge.

ACKNOWLEDGMENTS

We are indebted to T. de Freitas who reviewed the original manuscript.

REFERENCES

- Beauchamp, B.**
1994: Permian climatic cooling in the Canadian Arctic; *in* Pangea: Paleoclimate, Tectonics and Sedimentation during accretion, zenith and break-up of a super-continent, (ed.) G.D. Klein; Geological Society of America, Special Paper 288, p. 229-246.
in press: Permian history of Arctic North America; *in* The Permian of Northern Pangea, volume 1, Paleogeography, Paleoclimates, and Stratigraphy, (ed.) P.A. Scholle, T.M. Peryt, and D.S. Ulmer-Scholle; Springer-Verlag, New York.
- Beauchamp, B., Harrison, J.C., and Henderson, C.M.**
1989a: Upper Paleozoic stratigraphy and basin analysis of the Sverdrup Basin, Canadian Arctic Archipelago: Part 1- time frame and tectonic evolution; *in* Current Research, Part G; Geological Survey of Canada, Paper 89-1G, p. 105-113.
1989b: Upper Paleozoic stratigraphy and basin analysis of the Sverdrup Basin, Canadian Arctic Archipelago: Part 2- transgressive-regressive sequences; *in* Current Research, Part G; Geological Survey of Canada, Paper 89-1G, p. 115-124.
- Beauchamp, B., Mayr, U., and Harrison, J.C.**
1995a: Carboniferous and Permian stratigraphic sequences on Hvitland Peninsula and adjacent areas, northwestern Ellesmere Island, Arctic Canada; *in* Current Research 1995-B; Geological Survey of Canada, this volume.
- Beauchamp, B., Mayr, U., Harrison, J.C., and Desrochers, A.**
1995b: Uppermost Permian stratigraphy (Unit P6), Hvitland Peninsula and adjacent areas, northwestern Ellesmere Island, Arctic Canada; *in* Current Research 1995-B; Geological Survey of Canada, this volume.
- Harrison, J.C., Mayr, U., and Beauchamp, B.**
1995: Preliminary observations on the structural geology of Hvitland Peninsula, northwestern Ellesmere Island, Arctic Canada; *in* Current Research 1995-B; Geological Survey of Canada, this volume.
- Kells, M.P., Beauchamp, B., and Desrochers, A.**
1995: Artinskian-Kungurian (Lower Permian) stratigraphy (Raanes, Great Bear Cape and Trappers Cove formations), Hvitland Peninsula and adjacent areas, northwestern Ellesmere Island, Arctic Canada; *in* Current Research 1995-B; Geological Survey of Canada, this volume.
- Mayr, U., Harrison, J.C., and Beauchamp, B.**
1995: Geological map of Carboniferous and Permian units on Hvitland Peninsula and adjacent areas, northwestern Ellesmere Island, Arctic Canada; *in* Current Research 1995-B; Geological Survey of Canada, this volume.
- Thorsteinsson, R.**
1974: Carboniferous and Permian stratigraphy of Axel Heiberg Island and western Ellesmere Island, Canadian Arctic Archipelago; Geological Survey of Canada, Bulletin 224, 210 p.

Uppermost Permian stratigraphy (Unit P6), Hvitland Peninsula and adjacent areas, northwestern Ellesmere Island, Arctic Canada

B. Beauchamp, U. Mayr, J.C. Harrison, and A. Desrochers¹
Institute of Sedimentary and Petroleum Geology, Calgary

Beauchamp, B., Mayr, U., Harrison, J.C., and Desrochers, A., 1995: Uppermost Permian stratigraphy (Unit P6), Hvitland Peninsula and adjacent areas, northwestern Ellesmere Island, Arctic Canada; in Current Research 1995-B; Geological Survey of Canada, p. 65-70.

Abstract: An uppermost Permian unit of chert (Unit P6), mapped in the southwestern areas of Hvitland Peninsula, comprises dark grey to black chert and lesser siliceous shale passing upward into thick bedded, light grey chert. Sponge spicules are the only fossil remains in the chert. Deposition of Unit P6 probably occurred in a very cold environment, forming a spiculitic blanket that probably extended throughout the area. Unit P6 forms the regressive portion of a transgressive-regressive sequence, the transgressive systems tract of which is contained in the underlying uppermost Van Hauen and Degerbøls formations. The uppermost part of Unit P6 comprises shalier chert sediments that form the transgressive systems tract of a latest Permian-Early Triassic sequence, the maximum flooding surface of which lies at the base of the Triassic Blind Fiord shale. The absence of Unit P6 throughout most of Hvitland Peninsula is indicative of broad uplift and erosion in latest Permian-earliest Triassic time.

Résumé : Une unité de chert du Permien sommital (Unité P6), cartographiée dans les secteurs sud-ouest de la péninsule Hvitland, comprend un chert gris foncé à noir et un shale siliceux moins abondant se transformant vers le haut en un chert gris pâle à lits épais. Les spicules d'éponges sont les seuls vestiges de fossiles présents dans le chert. L'Unité P6 s'est probablement déposée dans un milieu très froid, formant une couverture spiculitique qui s'est probablement étendue à toute la région. L'Unité P6 forme la portion régressive d'une séquence transgressive-régressive, dont les systèmes transgressifs sont contenus dans les parties sommitales des formations sous-jacentes de Van Hauen et de Degerbøls. La partie sommitale de l'Unité P6 comprend des sédiments de chert plus shaleux qui forment les systèmes transgressifs d'une séquence du Permien terminal-Trias précoce, dont la surface maximale d'inondation repose à la base du shale triasique de Blind Fiord. L'absence de l'Unité P6 dans presque toute la péninsule Hvitland est le signe d'un soulèvement et d'une érosion considérables au Permien terminal-Trias initial.

¹ Department of Geology, University of Ottawa, Ottawa, Ontario K1N 6N5

INTRODUCTION

A spiculitic chert unit that lies beneath the Triassic Blind Fiord Formation has been mapped in the southwestern region of Hvitland Peninsula, northwestern Ellesmere Island. The bulk of this unit (Unit P6 of Mayr et al., 1995) is part of a post-Kazanian (latest Permian; Tatarian?) transgressive-regressive sequence. The uppermost part of Unit P6 also includes transgressive strata belonging to a sequence that straddles the Permian-Triassic boundary. This paper provides information about the distribution and facies composition of Unit P6, and the Late Permian paleogeography of the area. Details concerning the geological setting of the area can be found in Mayr et al. (1995), Harrison et al. (1995) and Beauchamp et al. (1995)

UNIT P6

Distribution and thickness

Strata mapped as Unit P6 comprise relatively resistant dark greenish grey to pale yellow weathering spiculitic chert and minor shale that conformably overlie the Degerbøls Formation on southwestern Hvitland Peninsula and the Van Hauen Formation just south of Otto Fiord (Fig. 1, 2). Unit P6 is overlain by very recessive shale of the Triassic Blind Fiord Formation. The contact with the Blind Fiord Formation ranges from conformable in the southwesternmost areas to unconformable in the east where significant sub-Triassic

erosion has partly to completely removed Unit P6 (Fig. 1, 2). Unit P6 ranges from 0 m to more than 125 m at locality 2 (Fig. 1, 2). Elsewhere in the Sverdrup Basin, Unit P6-equivalent strata form variably thick mappable units in the uppermost portion of the upper Paleozoic column. Good examples of this chert, previously mapped in a variety of units, are numerous: the uppermost part of the Trolld Fiord Formation on Melville Island; the uppermost Van Hauen and Degerbøls formations in the Blind Fiord (southwestern Ellesmere Island), Blue Mountain-Van Royen Ridge (west-central Ellesmere Island), and Confederation Point areas (northwestern Ellesmere Island); the upper Trolld Fiord Formation in the Mount Leith (west-central Ellesmere Island), Girty Creek (northwestern Ellesmere Island), and Svartevaeg Cliffs areas (northern Axel Heiberg Island). The uppermost chert unit in these areas is 100 m thick on average.

The age of the unit has not been substantiated by biostratigraphic evidence, because sponge spicules are often the only fossils present. The unit is referred to as post-Kazanian (or post-Wordian; see Beauchamp, 1994, in press; Beauchamp et al., 1989) based on its stratigraphic position between dated Kazanian (Wordian) Degerbøls carbonates and dated Lower Triassic (Griesbachian) Blind Fiord shales. The view that Unit P6 is of latest Permian age is at odds with the traditional position defended by Thorsteinsson (1974) and Nassichuk et al. (1973) whereby a major hiatus encompassing the entire post-Kazanian time interval separates the youngest Paleozoic rocks from the oldest Triassic strata everywhere in the Sverdrup Basin. It should be emphasized, however, that the proponents of this view were unaware of the existence of a

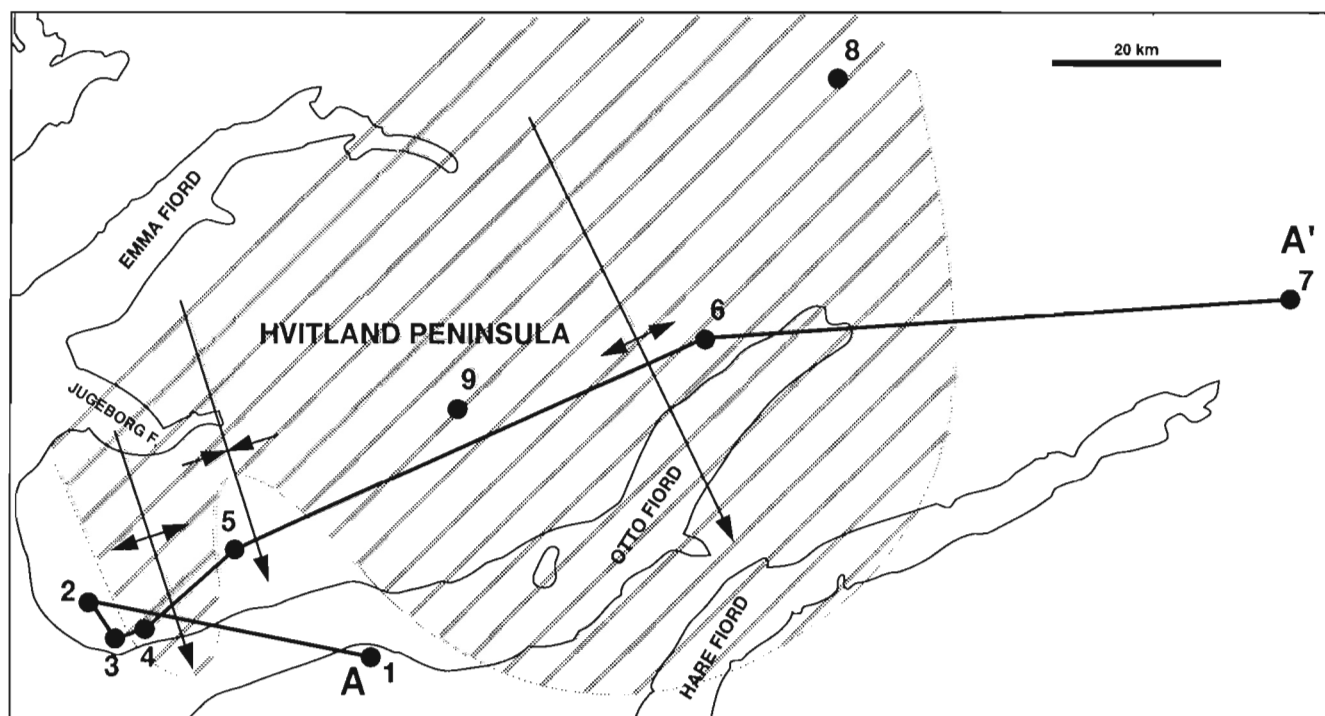


Figure 1. Map showing studied localities, line of cross-section A-A', areas of latest Permian-earliest Triassic uplifts (diagonal lines), and hypothetical sub-Triassic broad anticlines and syncline. Geology based on Mayr et al., 1995.

post-Degerbøls chert in the Sverdrup Basin, nor were they aware of the lateral basinward transition between Degerbøls and Van Hauen strata (as described in Desrochers and Beauchamp, 1995). In the stratigraphic scheme of Thorsteinsson (1974), the Van Hauen Formation was seen as a basinal unit equivalent to the Assistance Formation, while the Degerbøls Formation had no basinal equivalents. The Blind Fiord-Van Hauen contact in the axial regions of the Sverdrup Basin was hence interpreted as a major erosional unconformity between Lower Permian and Lower Triassic strata.

Lithology

Unit P6 comprises medium- to thick-bedded, dark to greenish grey weathering argillaceous chert and minor shale at the base (Fig. 3, 5) passing upward into a purer succession of pale yellow- and green-weathering, medium- to thick-bedded spiculitic chert associated with locally abundant glauconite and rusty pyrite-rich layers (Fig. 4B). Pervasive bioturbation has eradicated any primary depositional fabric that may have developed. Ghosts of fine subparallel laminations are visible locally. Other than sponge spicules, silicified ramose and fenestellid bryozoans and brachiopods occur in the middle to

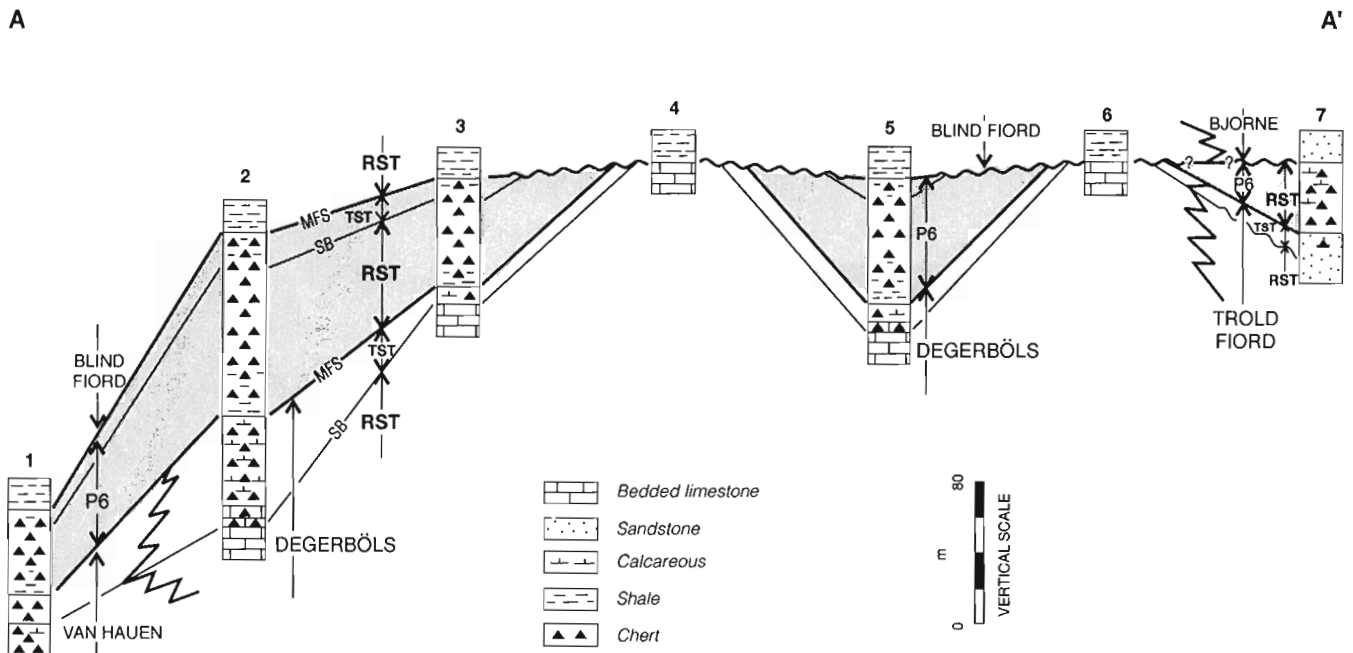


Figure 2. Cross-section showing the distribution of Unit P6 on Hvitland Peninsula and adjacent areas, northwestern Ellesmere Island: SB, sequence boundary; MFS, maximum flooding surface; TST, transgressive systems tract; RST, regressive systems tract.

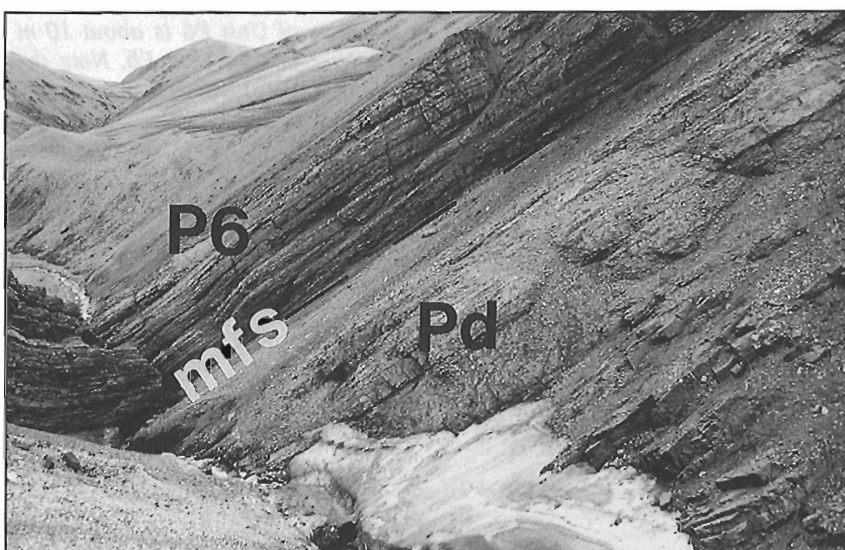


Figure 3.

Uppermost Degerbøls Formation (Pd) and Unit P6 (P6) at locality 3, Hvitland Peninsula: mfs, maximum flooding surface. About 40 m of strata are shown.

upper part of Unit P6 east of Girty Creek (locality 7 in Fig. 1, 2). Thin section examination of uppermost Permian chert from the Blind Fiord area has revealed remarkably well preserved monaxons and rarer tetraxons, many of which have their internal canal still preserved (Beauchamp, 1994). These rocks are pervasively cemented by microcrystalline chert in the form of chalcedony, a diagenetic replacement product.

Depositional environment

The depositional environment represented by Unit P6 is an enigma. The absence of carbonates and the extreme scarcity of fossils other than sponge spicules, even in the most proximal areas, calls for a unique explanation. Beauchamp (1994) interpreted this environment as a very cold, polar-like one. This suggestion is based on a number of facts and previously documented conclusions, the most important of which are: 1) the already cold climatic Kazanian setting (see Desrochers and Beauchamp, 1995); 2) the Permian cooling trend in the northern Hemisphere from an Asselian-Sakmarian tropical

setting, to an Artinskian temperate warm setting, to a Kazanian temperate cold setting, the next logical step is an even colder climatic setting; 3) the presence of dropstones in some areas of southern Ellesmere Island as preserved in the Kazanian Trold Fiord Formation; and 4) the knowledge that relatively shallow-water, modern accumulations of siliceous sponge spicules are known only from very cold Arctic and Antarctic shelves with permanent or seasonal ice packs. Good examples of such spiculitic blankets were recently documented from the Canadian polar continental shelf and the Vesterisbanken Seamount of east Greenland (Van Wagoner et al., 1989; Henrich et al., 1992).

Beauchamp (1994) has therefore evoked the possibility that a permanent or semipermanent marine ice pack lay over much of the Sverdrup Basin at the end of the Permian, but admittedly dropstones or other direct evidence of ice have yet to be found in the uppermost Permian chert. Regardless, some dramatic environmental cooling must have eliminated most carbonate-secreting organisms in latest Permian time, not only in the Sverdrup Basin but also in other circum-Arctic

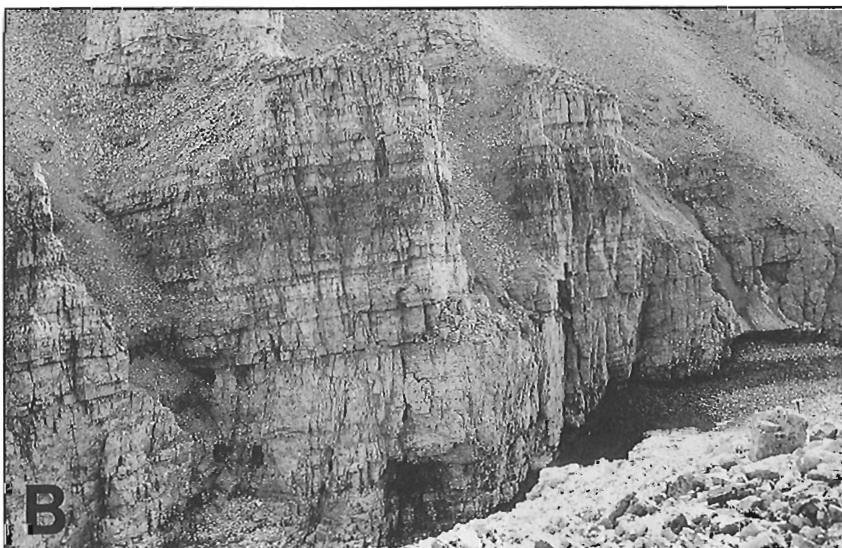
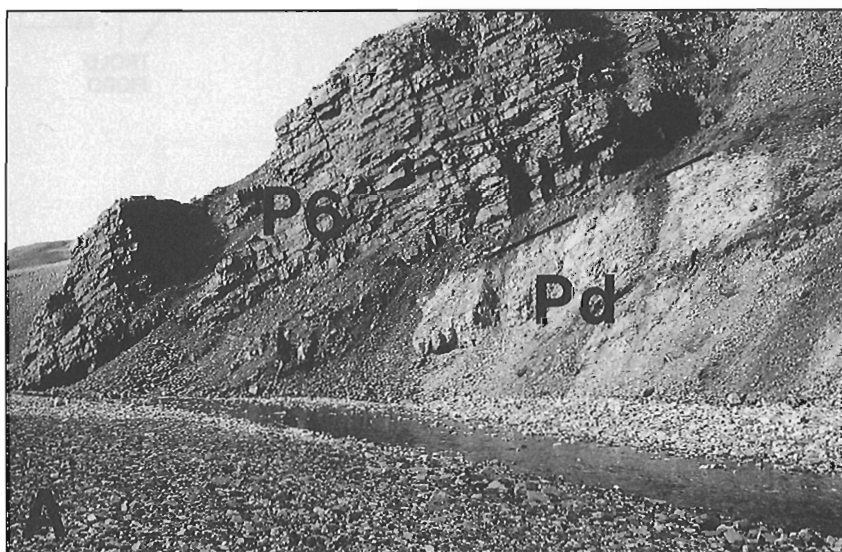


Figure 4.

Locality 2, Hvitland Peninsula, north-western Ellesmere Island. A) Uppermost Degerbøls Formation (Pd) and Unit P6 (P6): MFS, maximum flooding surface. Dark cliff at the base of Unit P6 is about 10 m thick. B) Upper part of Unit P6. Note the darker coloured rusty layer in the upper part of the outcrop. About 8 m of strata are shown.

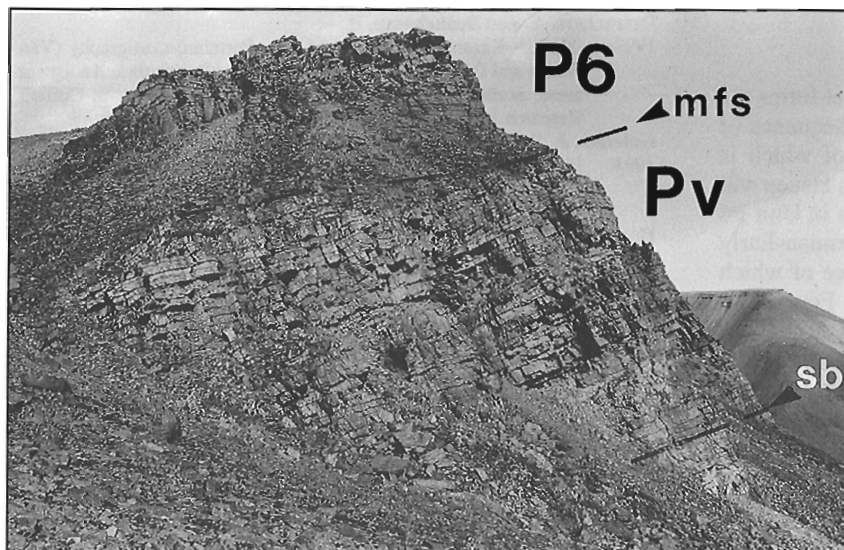


Figure 5.

Uppermost Van Hauen Formation (Pv) and Unit P6 (P6) at locality 1, south of Otto Fiord; mfs, maximum flooding surface; sb, sequence boundary. Note light grey calcareous chert beneath sequence boundary in upper Van Hauen Formation. About 30 m of strata are shown.

regions such as Svalbard, Barents Sea, and Bjørnøya (Stemmerik and Worsley, 1989). The onset of Triassic sedimentation in the Sverdrup Basin marked a return to much warmer conditions, as shown by the presence of redbeds and calcretes in nonmarine overbank strata, and by a lack of siliceous sponge spicules (Beauchamp, 1994). The Sverdrup Basin lay at a latitude of about 40°N around the Permian-Triassic boundary (Golonka et al., 1994).

SEQUENCE STRATIGRAPHY

The bulk of Unit P6 is the regressive part of a post-Kazanian transgressive-regressive sequence of the Sverdrup Basin, the transgressive portion of which is contained in the uppermost Van Hauen and Degerbøls formations (Fig. 2). The conformable lower sequence boundary lies on top of the last prograding fossiliferous carbonates of the Degerbøls Formation (see Desrochers and Beauchamp, 1995), which correlates with the top of a light grey, calcareous chert unit in the upper part of the Van Hauen Formation on the south side of Otto Fiord (Fig. 5). The transgressive systems tract is represented by increasingly shaly, dark grey, spiculitic chert in the upper Van Hauen Formation (Fig. 5) and correlative pale yellow, medium- to thick-bedded, calcareous chert in the upper Degerbøls Formation (Fig. 3, 4A). In the more proximal areas, such as east of Girty Creek (locality 7 in Fig. 1, 2), the sequence boundary is an unconformity represented by an erosional surface within the upper part of the Trolld Fiord Formation. At that locality the transgressive systems tract is represented by increasingly cherty green glauconitic sandstone of the Trolld Fiord Formation.

The maximum flooding surface lies at the base of Unit P6 in both the proximal and distal areas (Fig. 3-5). Most of Unit P6 forms the regressive systems tract as it passes upward from interfingering dark grey shale and medium bedded, dark grey chert (Fig. 3-5) into thick bedded, light grey, cleaner chert (Fig. 4B). At the basin margin (locality 7), the lithostratigraphic contact with the overlying Triassic Bjorne Formation is the sequence-bounding unconformity. In the more distal

areas (localities 1-3), thinning- and fining-upward chert interfingering with shaly strata occur in the uppermost part of Unit P6. These rocks represent the transgressive systems tract of a latest Permian-Early Triassic sequence, the maximum flooding surface of which lies in the lowest part of the Blind Fiord Formation (Fig. 2), a very recessive succession of non-siliceous, spicule-free shale. The base of the Triassic has been traditionally placed at the base of the Blind Fiord Formation.

PALEOGEOGRAPHY

Unit P6 is restricted to the southwestern portion of Hvitland Peninsula. It is, however, known to outcrop widely south of Otto Fiord. Unit P6 was eroded beneath a sub-Triassic unconformity throughout most of Hvitland Peninsula, extending as far south as Van Hauen Pass (Fig. 1). In these areas, fossiliferous carbonates of the Degerbøls Formation are overlain unconformably by Blind Fiord shales (Fig. 2). Post-Kazanian cherts most likely formed a relatively uniform blanket of spiculitic sediments that extended from the mouth of Otto Fiord to the area east of Girty Creek. Latest Permian-earliest Triassic uplift and buckling of Hvitland Peninsula resulted in the widespread erosion of most of Unit P6 (Fig. 1). Tectonism may have been partly contemporaneous with the deposition of Unit P6.

Evidence of tectonic activity around the Permian-Triassic boundary is suggested by the presence of a thick Lower Triassic conglomerate-bearing succession that lies unconformably on much older Permian (probably pre-Kazanian) sandstone and dolomitic carbonates of a unit of uncertain affinity in the eastern regions of Hvitland Peninsula (Fig. 1, locality 8; Unit P5 of Mayr et al., 1995; see also Harrison et al., 1995). Additional possible evidence of latest Permian-Early Triassic uplift occurs about 17 km northwest of Degerbøls Island (Fig. 1, locality 9) where Triassic Blind Fiord shales appear to rest directly upon Artinskian Great Bear Cape carbonates. Triassic or older faulting from the Yelverton Pass area, on northern Ellesmere Island, is described by Mayr (1992).

CONCLUSIONS

The bulk of Unit P6 comprises spiculitic chert that forms the regressive portion of a transgressive-regressive sequence of the Sverdrup Basin, the transgressive portion of which is contained in the upper part of the underlying Van Hauen and Degerbøls formations. The uppermost sediments in Unit P6 form the transgressive systems tract of a latest Permian-Early Triassic sequence, the maximum flooding surface of which lies near the base of the Triassic Blind Fiord Formation. Spiculitic chert of Unit P6 probably accumulated throughout Hvitland Peninsula in a very cold setting. The irregular distribution of Unit P6 is believed to have resulted from broad uplifts of Hvitland Peninsula in latest Permian-earliest Triassic time, and partial to complete erosion of these strata beneath a widespread sub-Triassic unconformity.

ACKNOWLEDGMENTS

We are indebted to T. de Freitas for reviewing this manuscript and providing useful comments.

REFERENCES

- Beauchamp, B.**
1994: Permian climatic cooling in the Canadian Arctic; in *Pangea: Paleoclimate, Tectonics and Sedimentation during accretion, zenith and break-up of a super-continent*, (ed.) G.D. Klein; Geological Society of America, Special Paper 288, p. 229-246.
- Beauchamp, B.**
in press: Permian history of Arctic North America; in *The Permian of Northern Pangea*, v. 1, Paleogeography, Paleoclimates, and Stratigraphy, (ed.) P.A. Scholle, T.M. Peryt, and D.S. Ulmer-Scholle; Springer-Verlag, New York.
- Beauchamp, B., Harrison, J.C., and Henderson, C.M.**
1989: Upper Paleozoic stratigraphy and basin analysis of the Sverdrup Basin, Canadian Arctic Archipelago: Part 2 – transgressive-regressive sequences; in *Current Research, Part G*; Geological Survey of Canada, Paper 89-1G, p. 115-124.
- Beauchamp, B., Mayr, U., and Harrison, J.C.**
1995: Carboniferous and Permian stratigraphic sequences on Hvitland Peninsula and adjacent areas, northwestern Ellesmere Island, Arctic Canada; in *Current Research 1995-B*; Geological Survey of Canada, this volume.
- Desrochers, A. and Beauchamp, B.**
1995: Ufimian-Kazanian (Lower and Upper Permian) stratigraphy (Van Hauen and Degerbøls formations), Hvitland Peninsula and adjacent areas, northwestern Ellesmere Island, Arctic Canada; in *Current Research 1995-B*; Geological Survey of Canada, this volume.
- Golonka, J., Ross, M.I., and Scotese, C.R.**
1994: Phanerozoic paleogeographic and paleoclimatic modeling maps; in *Pangea: Global Environments and Resources – An Introduction*, (ed.) A.F. Embry, B. Beauchamp, and D. Glass; p. 1-48.
- Harrison, J.C., Mayr, U., and Beauchamp, B.**
1995: Preliminary observations on the structural geology of Hvitland Peninsula, northwestern Ellesmere Island, Arctic Canada; in *Current Research 1995-B*; Geological Survey of Canada, this volume.
- Henrich, R., Hartmann, M., Reitner, J., Schäfer, P., Freiwald, A., Steinmetz, S., Dietrich, P., and Thiede, J.**
1992: Facies belts and communities of Arctic Vesterisbanken Seamount (Central Greenland Sea); *Facies*, v. 27, p. 71-104.
- Mayr, U.**
1992: Reconnaissance and preliminary interpretation of Upper Devonian to Permian stratigraphy of northeastern Ellesmere Island, Canadian Arctic Archipelago; Geological Survey of Canada, Paper 91-08, 117 p.
- Mayr, U., Harrison, J.C., and Beauchamp, B.**
1995: Geological map of Carboniferous and Permian units on Hvitland Peninsula and adjacent areas, northwestern Ellesmere Island, Arctic Canada; in *Current Research 1995-B*; Geological Survey of Canada, this volume.
- Nassichuk, W.W., Thorsteinsson, R., and Tozer, E.T.**
1973: Permian-Triassic boundary in the Canadian Arctic Archipelago; in *The Permian and Triassic systems and their mutual boundary*, (ed.) A. Logan and L.V. Hills; Canadian Society of Petroleum Geologists, Memoir 2, p. 286-293.
- Stemmerik, L. and Worsley, D.**
1989: Late Palaeozoic sequence correlations, North Greenland, Svalbard and the Barents Shelf; in *Correlation in Hydrocarbon Exploration*, (ed.) J.D. Collinson; Norwegian Petroleum Society, Graham and Trotamn, London, p. 99-111.
- Thorsteinsson, R.**
1974: Carboniferous and Permian stratigraphy of Axel Heiberg Island and western Ellesmere Island, Canadian Arctic Archipelago; Geological Survey of Canada, Bulletin 224, 210 p.
- Van Wagoner, N.A., Mudie, P.J., Cole, F.E., and Daborn, G.**
1989: Siliceous sponge communities, biological zonation, and Recent sea-level change on the Arctic margin: Ice Island results; *Canadian Journal of Earth Sciences*, v. 26, p. 2341-2355.

Geological Survey of Canada Project 870067

Establishing the chronology of snow and pollen deposition events on Agassiz Ice Cap (Ellesmere Island, Northwest Territories) from autostation records

B.T. Alt and J.C. Bourgeois
Terrain Sciences Division

Alt, B.T. and Bourgeois, J.C., 1995: Establishing the chronology of snow and pollen deposition events on Agassiz Ice Cap (Ellesmere Island, Northwest Territories) from autostation records; in Current Research 1995-B; Geological Survey of Canada, p. 71-79.

Abstract: Regional pollen concentrations in seasonal snow layers of Agassiz Ice Cap for the years 1981-89 and preliminary results for 1991 are compared with the first quality controlled records from the experimental autostation established at the 1977 borehole site. Emphasis is placed on the distinctive, coarse grained (a) layer which is deposited by the first snow storm of each new mass balance year. These storms are sufficiently well developed to pick up, transport, and precipitate the tundra pollen, and to wash out pollen stored in the atmosphere. The extremes of (a) layer pollen concentrations reflect the climate conditions of the inland areas of the intermontane region to the southeast of the Agassiz Ice Cap station. Accurate dating using the autostation records allows the atmospheric circulation conditions to be examined resulting in valuable information on the source and pathways of the pollen, moisture, contaminants and paleoenvironmental indicators deposited with the snow of the (a) layer.

Résumé : Les concentrations régionales de pollen dans les couches de neige saisonnières de la calotte glaciaire Agassiz pendant les années 1981-1989 et les résultats préliminaires de 1991 font l'objet de comparaisons avec les premières données qui ont été soumises à un contrôle de la qualité et qui ont été enregistrées à la station automatique expérimentale mise en place à l'emplacement du sondage de 1977. L'accent est mis sur la couche (a) distinctive, à grain grossier, qui est déposée par la première tempête de neige de chaque nouvelle année du bilan massique. Ces tempêtes sont suffisamment fortes pour recueillir, transporter et précipiter le pollen de la toundra et pour entraîner le pollen en suspension dans l'atmosphère. Les concentrations extrêmes de pollen de la couche (a) reflètent les conditions climatiques régnant dans les zones intérieures de la région intermontagneuse, au sud-est de la station de la calotte glaciaire Agassiz. Une datation précise, basée sur les données enregistrées par la station automatique, permet d'étudier les conditions de circulation atmosphérique. Il en résulte des informations utiles sur la source et la trajectoire du pollen, l'humidité, les polluants et les indicateurs paléo-environnementaux qui se déposent avec la neige de la couche (a).

INTRODUCTION

The distribution of pollen with time has been recorded in deep ice cores (Fredskild and Wagner, 1974; McAndrews, 1984; Bourgeois, 1986; Koerner et al., 1988) and in snow pits and shallow cores on high arctic ice caps (Bourgeois et al., 1985; Short and Holdsworth, 1985; Bourgeois, 1990a, b). In order to interpret the pollen deposition results from the deep and shallow ice core work and from the seasonal snow over the Arctic Ocean, it is necessary to understand the mechanisms of transport and deposition of pollen in the High Arctic region. The effect of extreme deposition events on the long-term records and their quantitative importance relative to prevailing conditions must also be addressed. To this end, seasonal and annual pollen deposition in snow layers of the Agassiz Ice Cap (Fig. 1) were investigated by Bourgeois (1990a). These studies have been continued and expanded. In 1988 an autostation was established at the drill site on Agassiz Ice Cap (Fig. 2). The autostation records combined with seasonal pollen deposition investigations provide the first opportunity to study the specific atmospheric conditions under which pollen deposition takes place on the ice cap.

The present report makes use of these autostation records for an initial examination of the very distinctive coarse grained late summer/autumn seasonal layer. This layer, which has been labelled the (a) layer because it is the first layer following the end of summer melt, has been found in the annual snow for each of the 13 years sampled to date on

Agassiz Ice Cap (Bourgeois, 1990a; Bourgeois, unpublished field reports 1986 to 1994). We have also found this coarse grained layer on Penny Ice Cap (Baffin Island), Devon Island Ice Cap, and on Academii Nauk Ice Cap (Severnaya Zemlya, Russia). On Agassiz Ice Cap, the highest regional pollen (i.e., from the high arctic tundra) deposition was observed in this layer. Bourgeois (1990a) found there appeared to be a good relationship between extremes of these regional pollen values and July mean monthly temperature from the permanent weather station at Eureka. As this (a) layer was found to be only 5 to 15 cm thick, it thus represents a relatively short time period in the seasonal record.

The detailed meteorological records will be used to address the following questions regarding the (a) layer. 1) What is responsible for the distinct nature of this layer and why is it so widespread? 2) Why does this late summer/fall layer rather than the melt layer contain the highest deposition of regional pollen? 3) To what extent does it represent the

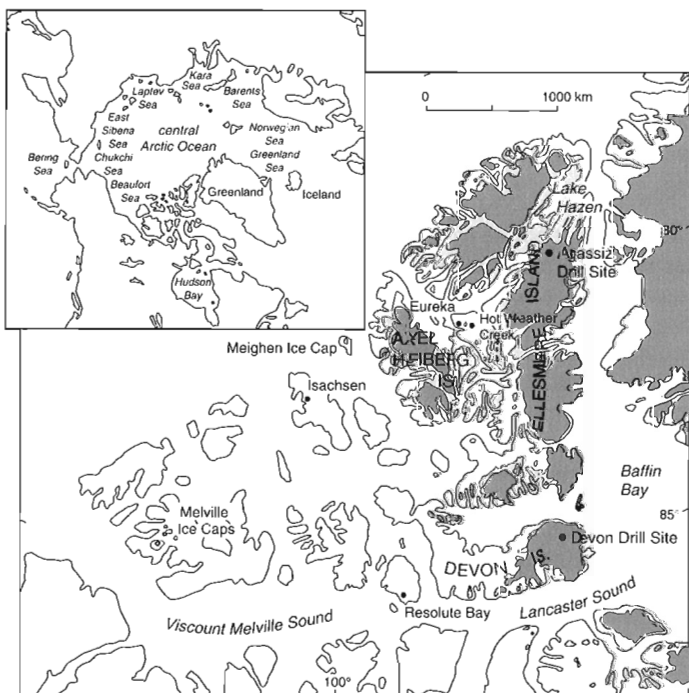


Figure 1. Map of the high arctic islands showing the Agassiz drill site and some other locations mentioned in the text. The dark shaded areas are glacier ice and the light shaded areas represents land above 610 m. a.s.l. The insert shows the circumpolar region.

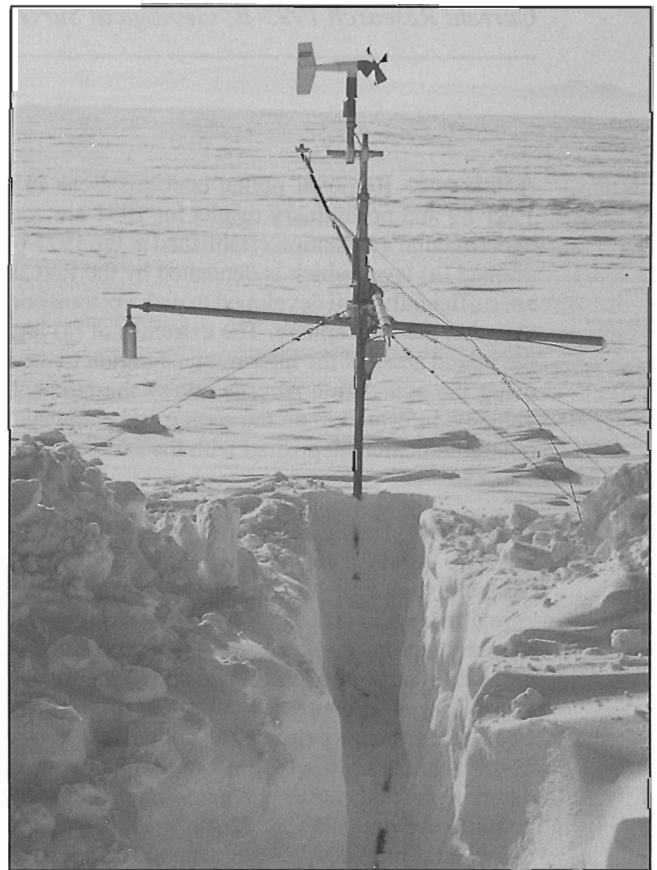


Figure 2. Agassiz Ice Cap 1977 borehole site autostation mast with two snow depth sensors (one hidden behind mast), Gill radiation shield, and wind sensor. The data logger enclosure is buried under the snow. The instrumentation has been provided and maintained in the past few years by Campbell Scientific Canada Corporation as part of a Industrial Partners Program, testing autostation technology in the severe climatic conditions experienced on high arctic ice caps. (photo: M. Waszkiewicz)

climate of the source region and how important are extreme seasons and events in determining the annual and long-term pollen deposition values? 4) How accurately can this layer be dated? Based on this dating, what weather patterns were responsible for this deposition and what were the circumpolar atmospheric circulation conditions producing these local weather patterns?

BACKGROUND AND METHODS

Geographical location

The northern part of the Agassiz Ice Cap, on Ellesmere Island, has been the site of glaciological investigations since 1974. The pollen sampling site (80.7 N - 73.1 W, 1700 m a.s.l.) is located near the location of a deep borehole, drilled in 1977 (A77), approximately 1 km from a local ice divide. The closest unglaciated terrain from the Agassiz Ice Cap sampling site is about 35 km to the north but the most likely pollen sources for the ice cap site are more than 75 km away in the intermontane region of central and northern Ellesmere Island and on Axel Heiberg Island. Some parts of this region, such as the Fosheim Peninsula, support a relatively dense and diverse vegetation cover with more than 100 species of vascular plants (Edlund and Alt, 1989).

Pollen

In 1986, samples were collected from one wall of a 2.5m deep pit located near the A77 bore hole. In each of the following springs the previous year's snow accumulation (as discussed below) was sampled in the vicinity of that pit. The results of the 1987, 1988, and 1989 sampling and some initial results from the 1992 sampling are used in the study. The samples cover the time period from late summer 1981 to late summer 1991.

In order to obtain an adequate pollen sum, from 13 to 35 kg of snow were sampled for each layer. The sampling method and laboratory procedures are discussed in Bourgeois (1990a). The results of the seasonal pollen analysis used in the present paper are expressed as pollen concentration rather than as percentages. Detailed results for the 1981-89 period are also presented in Bourgeois (1990a). Approximately 50 per cent of the pollen grains deposited on the ice cap are tree and shrub pollen from the boreal forest and low arctic region. The other half are from plants that can be found in the high arctic tundra. In the following discussion, only the total regional pollen influx values will be considered.

Stratigraphy

The annual and seasonal layers were determined from the snow stratigraphy in the snow pit (Fig. 3). The glaciological term "balance year" is used to label the annual layers. A glacier mass balance year starts when the snow begins to accumulate at the end of the melt season and ends when melting stops the following summer. The dates of these events vary from year to year and from site to site.

On high arctic ice caps, in most years, the summer melt produces a layer of hard granular snow. These summer surfaces are usually clearly visible in the snow stratigraphy. On Agassiz Ice Cap, they can be recognized on a regular basis to a depth of approximately 10 m, equivalent to about thirty years of accumulation (R.M. Koerner, pers. comm.). This is the final layer of the mass balance year and in this study we label it the (d) layer.

Immediately above this melt layer, in each season sampled to date, a well-defined coarse grained layer has been observed. As the snow in this layer is the first accumulation of the new mass balance year it is labelled the (a) layer. This layer is relatively thin (Fig. 3 and Bourgeois, 1990a). Detailed stratigraphic studies on Devon Ice Cap (Koerner, 1966) showed that the condition of this (a) layer is the result of intense metamorphism of the snow after it is deposited. The coarse grained, loosely packed layer is overlain by a thick layer of high density, fine grained snow. Unless some stratigraphic boundary was evident this winter layer was divided into two equal parts (b) and (c).

Koerner (1966) pointed out that although all snow accumulation undergoes metamorphism, the degree to which this occurs is dependent on a number of variables. The process is dependent on the transport of water vapour, which takes place from warm to cold snow and from surfaces of high curvature (ie., points) to surfaces of lower curvature. The steep reversal of temperature gradient experienced in the surface snow layer in autumn results in strong upward vapour transport and growth of large snow grains. The vapour gradient is twice as great at temperatures between 0°C and -10°C as between -10°C and -20°. Vapour transport is suppressed in the dry, fine grained winter snow which is not resistant to drifting and packing. Autumn snow which falls as wet, complex flakes is more resistant to packing therefore remains more porous (and provides many pointed surfaces), thus promoting strong vapour transport.

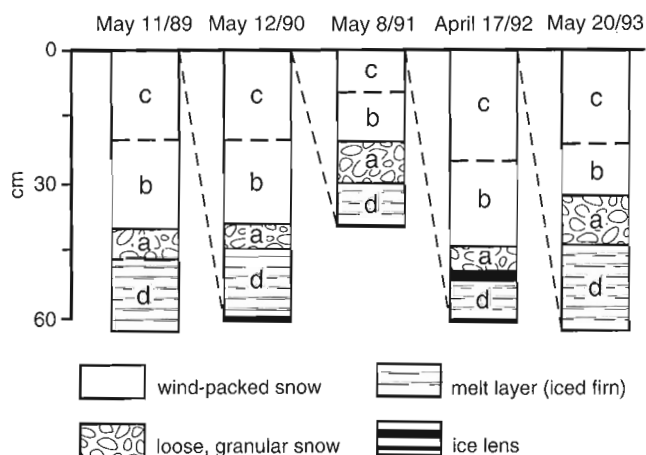


Figure 3. Annual snow stratigraphy and sample increments for the summer of 1988 to the spring 1993. The (a) to (d) layers represent a glacier balance year.

Climate and weather

Long-term climate records are available from two coastal stations each 260 km distant from the ice cap sampling site. Alert, to the northeast, lies on the coast of the Arctic Ocean and is affected by the broad expanse of the polar pack and the proximity of Greenland. Eureka lies on Slidre Fiord to the southwest of the ice cap in the protected intermontane region (Edlund and Alt, 1989; Alt and Maxwell, 1990). Autostation records were begun at Hot Weather Creek in 1988. These data represent the climate of the inland areas of the intermontane region. This inland region is a possible source for pollen reaching the ice cap sampling site. Smaller inland areas and so called "arctic oases" in northwestern Ellesmere Island would experience similar climatic conditions to that recorded by the Hot Weather Creek autostation.

The record from the Agassiz 1977 borehole site (AGA(A77)) autostation (Fig. 2), established and maintained in co-operation with Campbell Scientific Canada Corporation (a GSC Industrial Partner), began in May 1988. These data

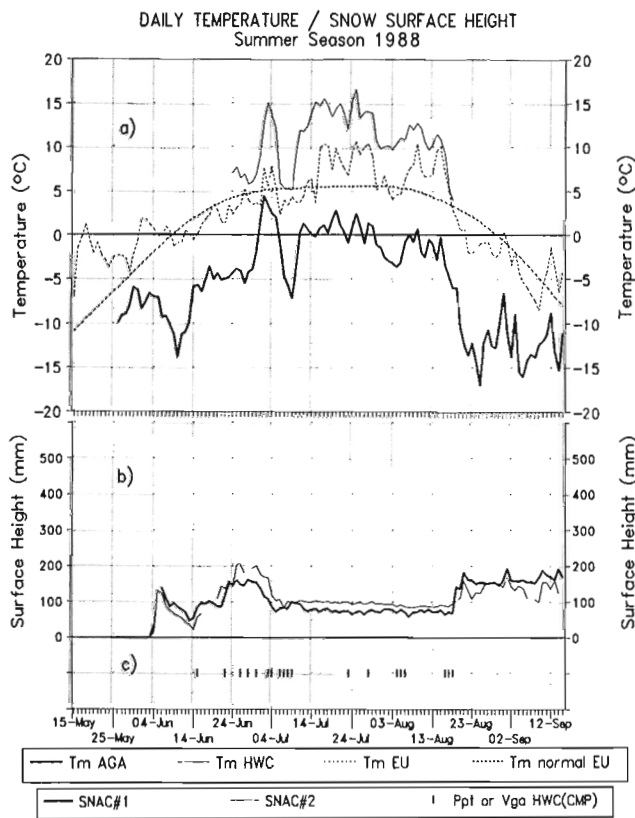


Figure 4. a) Mean daily temperature ($^{\circ}\text{C}$) Agassiz Ice Cap 1977 borehole site autostation AGA(A77), Hot Weather Creek HWC(AWS) autostation and Eureka (EU) weather station for summer 1988 and 30 year normal daily temperature for Eureka for 1988. b) Snow surface height recorded daily by two CSMALL01 sensors mounted on the same instrument mast at AGA(A77). c) Vertical lines represent days when some form of precipitation or virga was recorded on the aviation weather forms from the Hot Weather Creek field camp.

provide the first opportunity to study actual climatic parameter values associated with the deposition of snow which is being sampled for pollen, atmospheric contaminants and paleo-indicators such as oxygen isotope values. Two summer seasons, 1988 and 1991, were chosen for the present analysis based on the availability of snow depth records, snow stratigraphy, and (initial) regional pollen data. The snow surface heights were measured once daily in 1988 with two CSMALL01 snow sensors (Fig. 4b) and at six-hour intervals in 1991 with two improved UDG01 sensors (Fig. 6b). Daily maximum, minimum, and mean temperatures were obtained from values sampled at one minute intervals (Fig. 4a, 5a, 6a, 7a). The daily wind speed means, available in 1991, are calculated from two minute vector means taken every six hours (Fig. 6b). Daily temperature means from the Hot Weather Creek autostation (HWC(AWS)) are the mean of the daily maximum and minimum temperatures which are obtained from values sampled at one minute intervals

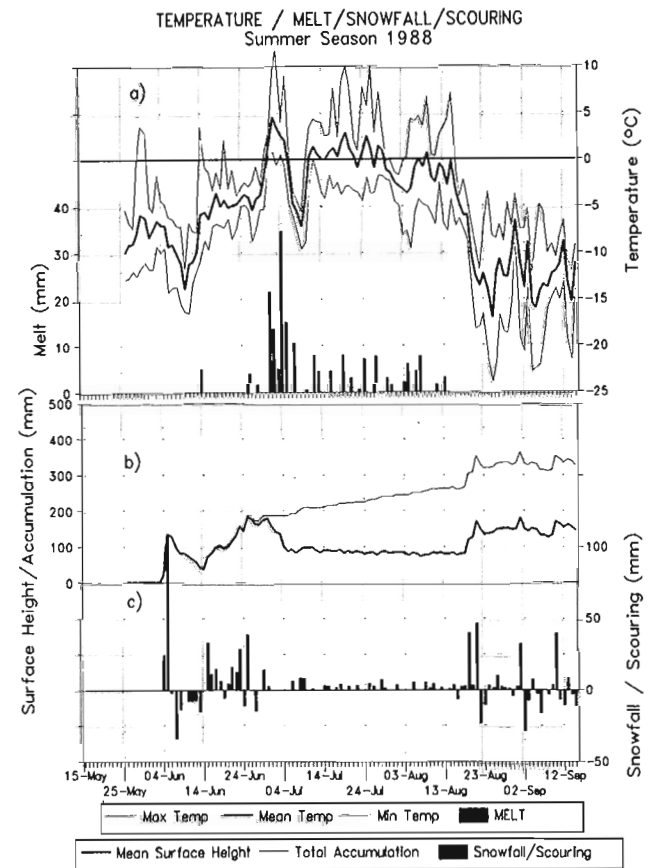


Figure 5. a) Maximum, mean and minimum temperature and melt calculated from surface lowering events and expressed as millimetres of new snow for AGA(A77) autostation from 1988. b) Mean snow surface height from two CSMALL01 sensors and calculated total accumulation assuming melt is retained and all scoured snow is lost to the snow pack, expressed as millimetres of new snow. c) Snowfall (positive) and snow wind scour (negative) calculated from mean surface height expressed as millimetres of new snow.

(Fig. 4a, 6a). Detailed site descriptions, instrumentation and quality control procedures are given in Labine et al. (1994) for AGA(A77) and HWC(AWS). The Eureka daily mean values (AES archive) are calculated from the maximum and minimum temperatures (Fig. 4). The remarks section of the Hot Weather Creek field camp aviation weather records were used to obtain the precipitation occurrence information included in Figure 4b. The synoptic weather patterns associated with the deposition events seen in the AGA(A77) autostation records were studied using microfilm records of surface and upper air charts from the AES Central Meteorological Centre in Dorval. Due to the lack of data over most of the Arctic Ocean and the sparse surface data network in the Canadian high arctic, charts often need to be reanalyzed for the regions influencing the study area. The summer atmospheric circulation patterns for the study area are discussed in detail elsewhere (Alt and Maxwell, 1990; Alt, 1987a, b; Bourgeois et al., 1985).

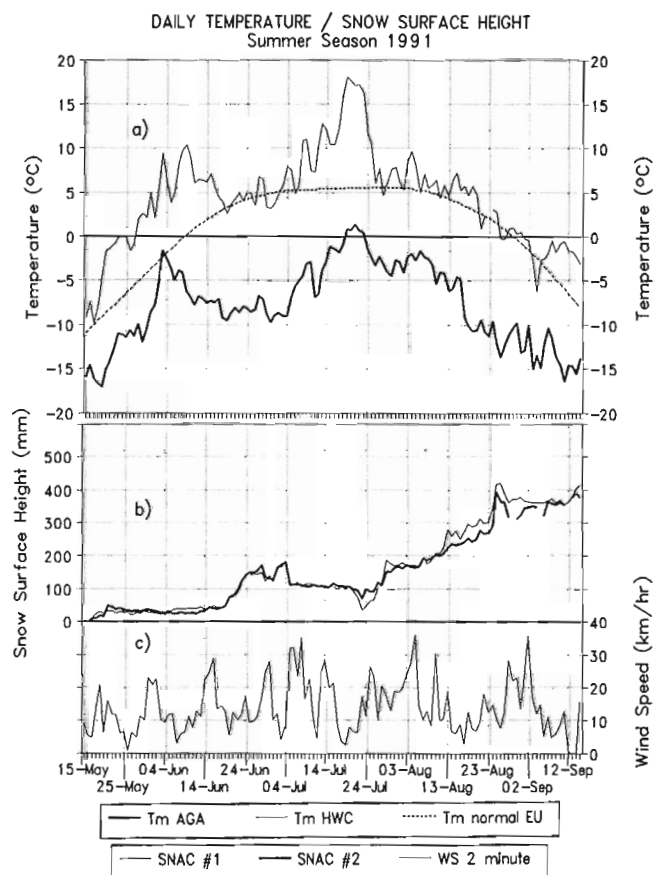


Figure 6. a) Mean daily temperature (°C) Agassiz Ice Cap 1977 borehole site automatic weather station (AGA(A77)), Hot Weather Creek HWC(AWS) autostation for summer 1991 and 30 year normal daily temperature for Eureka. b) Snow surface height recorded daily by two UDG01 sensors mounted on the same instrument mast at AGA(A77). c) Mean daily wind speed from six-hour 2 minute vector means for AGA(A77) autostation.

Snow accumulation

The sensors measure the height of the snow surface relative to the position of the sensor. The mean value of the two snow surface height measurements (Fig. 5b, 7b) have been translated into snowfall, melt, and snow scour. The daily snowfall values (Fig. 5c, 7c) are calculated assuming that any rise in the surface height is the result of deposition of snow. Each surface lowering event for the summers of 1988 and 1991 was examined along with the temperature, wind speed and other weather records. It was found that if the mean temperature was above -4°C or the maximum temperature was above freezing (0°C) the event was likely to be a melt event. The exceptions were isolated surface lowering events occurring late in the season when solar radiation is low. In these cases the maximum air temperature must reach 1°C , regardless of the mean temperature, for melt to take place. Surface lowering due to melt was usually gradual while surface lowering due to wind scour was abrupt and normally followed a new

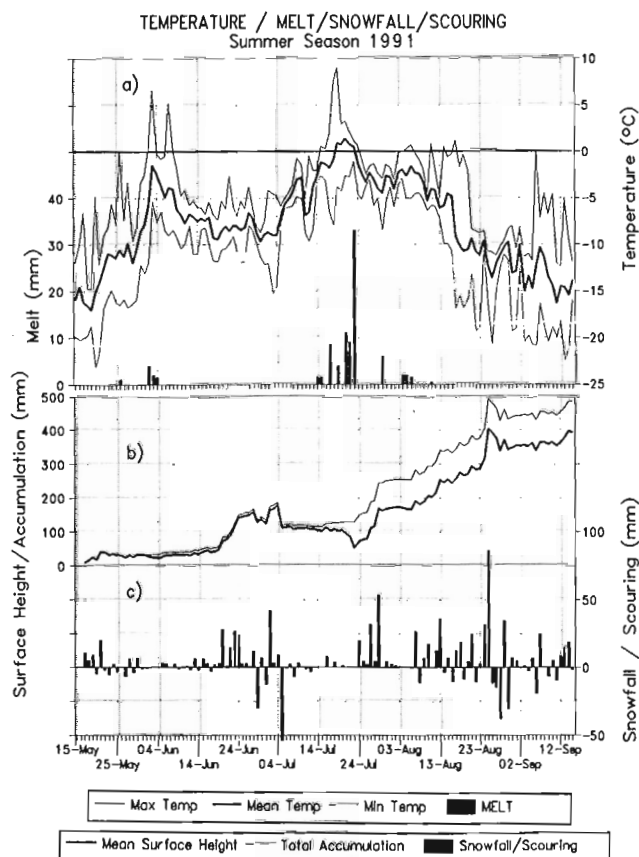


Figure 7. a) Maximum, mean and minimum temperature and melt calculated from surface lowering events and expressed as millimetres of new snow for AGA(A77) autostation for 1991. b) Mean snow surface height from two UDG01 sensors and calculated total accumulation assuming melt is retained and all scoured snow is lost to the snow pack, expressed as millimetres of new snow. c) Snowfall (positive) and snow wind scour (negative) calculated from mean surface height expressed as millimetres of new snow.

snowfall. Based on these assumptions daily melt (Fig. 5a, 7a) and snow scour (Fig. 5c, 7c) values have been calculated for the two summers. The total daily accumulation in the snow pack is calculated assuming that all melt is retained by the snow pack and all scouring lost (Fig. 5b, 7b).

RESULTS

Relationship of pollen in (d) and (a) layers to July temperature on the tundra

The relationship noted by Bourgeois (1990a) between maxima and minima of regional pollen influx values for the (a) layer and maxima and minima in the mean July temperatures at Eureka can be seen in Figure 8. The very high concentration for the (a) layer of 1988 is better reflected in the mean temperature record for Hot Weather Creek as this station is truly representative of conditions on the inland tundra areas. To date there is only a brief overlap between the Hot Weather Creek record and the pollen record. The preliminary results from 1991 show far less pollen than would be expected based on the temperatures at Eureka and Hot Weather Creek.

This may reflect poor pollen production due to the deleterious effect of the short early warm period which was followed by three weeks of well below normal conditions in late June-early July. This may have depressed pollen production despite the warm July mean temperatures.

Chronology of the (d) layer in 1988

The 100 mm of gradual surface lowering, in the seven days following 1 July, represents melting of all the snow that fell on the ice cap during the period 20-30 June. Melt ended abruptly on 8 July when the maximum temperature dropped to -4.4°C during a brief cold spell.

Between 10 July and 13 August a net surface lowering of 20 mm took place which would have melted the snow deposited between 16-19 June. In addition, during July and early August, 53 mm of new snow fell and melted. The (d) layer as seen in the pollen pit was 160 mm thick. Assuming a density for this melt layer snow of 0.37 g/cm³ and for new-fallen snow of 0.15 g/cm³ (Koerner, pers. comm.), the (d) layer contains the refrozen melt water of 120 mm of spring snow plus 53 mm of summer snow and another 220 mm of spring snow deposited before 16 June into which the melt water percolated. Thus of the 400 mm of (d) layer deposition only 53 mm (or 14%) fell during the pollen production season in the tundra.

The last significant melt probably occurred on 13 August although the surface lowering of 6 mm on 16 August may have been due to melting. The melt season came to a definite close with the deposition of 40 mm of new snow on 19 August.

Chronology of the (a) layer in 1988

The (a) layer in the pollen sampling pit was only 70 mm thick. Given a density for new-fallen snow of 0.15 g/cm³ (Koerner, pers. comm.) and for the (a) layer of 0.23 g/cm³ (Koerner, 1966), the (a) layer required 107 mm of new snow accumulation. Assuming that melt ceased and the (a) layer deposition began on 14 August this amount of accumulation was reached by 31 August but much of it was scoured the following day. The required accumulation was definitely received by 19 September. Well over half of this snow, however, was deposited between 14 and 22 August.

The first 51 mm of (a) layer snow was deposited directly on top of the melting snow surface over a six day period 14 to 20 August. Mean air temperatures at this time are in the -5°C range. These conditions would produce a very steep negative 5°C temperature gradient in the first 51 mm of new snow. This same precipitation fell as rain at Hot Weather

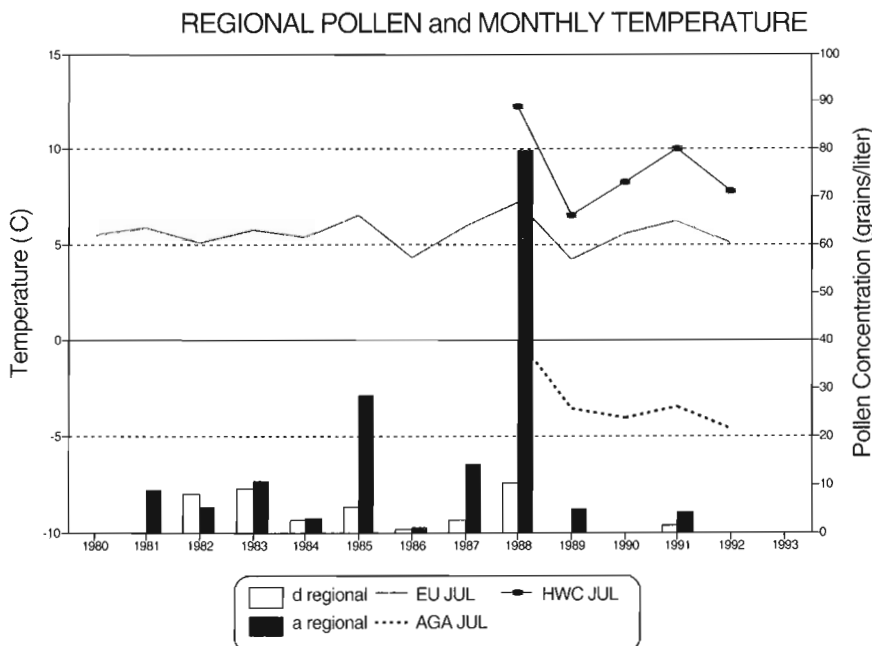


Figure 8.

Pollen concentrations in the (d) melt layer and (a) metamorphosed layer with mean July daily temperatures from Agassiz Ice Cap (AGA), Hot Weather Creek (HWC), and Eureka (EU).

Creek. There is no evidence of scouring of this snow. All these factors suggest that this 51 mm of new snow meet all the criteria suggested by Koerner (1966) for very rapid metamorphism. The synoptic charts for this period show passage of two surface lows over the northern Ellesmere area. Both these systems travel along the strongly baroclinic zone north of Alaska. At this time of year a band of open water bordered by warm land to the south and cold sea ice to the north provides the necessary temperature gradient and moisture source to provide support for typical mid-latitude low pressure systems with well defined frontal systems.

The first of these systems dissipates as it reaches the high arctic islands and moves south around the blocking high pressure system which dominated the preceding month. Deposition associated with this system is in the 2 mm/day range similar to that experienced during the melt season when weak troughs passed over the area depositing a dusting of snow. The second of these systems (Fig. 9) tracks from northern Siberia into the Bering Sea reaching the Beaufort Sea by 15 August. Here it is regenerated and moves northwest along the edge of the high arctic islands with strong upper air support from the 50 kPa circumpolar vortex which moves into the Beaufort Sea sector of the central Arctic Ocean. The surface frontal system occludes and the trowal (trough of warm air aloft) is over Eureka early on the morning of 19 August and is responsible for the 40 mm of snow deposited on Agassiz Ice Cap later that day. This upper trough contains relatively warm air and considerable moisture. The moisture falls in the form of wet snow which melts before reaching the ground over the tundra but is deposited as snow on the ice cap. Upward vertical motion associated with the trough would provide a mechanism for entrainment of the pollen from the tundra regions it passes over.

On reaching the eastern side of Ellesmere Island the surface feature appears to split, the southern portion moving into Baffin Bay while the northern portion moves north to sit under the upper polar vortex in the central Arctic Ocean north of the islands. Subsequent systems move into the islands from the Arctic Ocean. This is reflected by the rapid drop in temperatures at the ice cap station between the 19 and 22 August.

The snow deposited on 22 August and scoured (or packed) the following two days would be colder and drier than that which fell on 19 August. However a strong temperature gradient would still exist in the upper layer of snow as air temperatures are in the -10°C range while the top of the melt surface would not have cooled below -5°C in such a short time. Thus metamorphism would still take place although probably at a reduced rate. Air temperatures remain in the -10°C range for over a month. During this time the warm melt surface layer now buried under some 70 mm of new snow would be cooled from above and below and the negative temperature gradient in the snow which is conducive to rapid metamorphism would slowly disappear. Snow deposited in late September would not undergo rapid change and thus would appear as winter snow in the stratigraphy the next spring.

Chronology of the (d) layer in 1991

At the very top of the melt layer (d) of summer 1991 the stratigraphy shows a thick ice layer. The only melt event strong enough to create such an ice layer was that which ended abruptly with the seasons maximum melt of 33 mm on 23 July. The 110 mm depth of the (d) layer represents 270 mm of new fallen snow (using density of 0.37 g/cm^3 for the melt layer and 0.15 g/cm^3 for the new fallen snow). As most of the new snow deposited in late June - early July was scoured, the 70 mm of melt occurring between 15 and 23 July was snow deposited in mid June well before pollen production would have begun on the tundra. This and the early June melt percolated 190 mm into the snow pack deposited prior to mid June.

Deposition occurred on only one day during the melt period when a low moved into northern Ellesmere Island from the central Arctic Ocean. This weak Arctic Ocean low would be responsible for the only precipitation deposition of regional pollen to the ice cap during the main melt period of 1991.

Chronology of the (a) layer in 1991

When the first snow of the (a) layer was deposited, the melt water produced the previous day was in the process of refreezing at the surface. The melt was responsible for lowering the

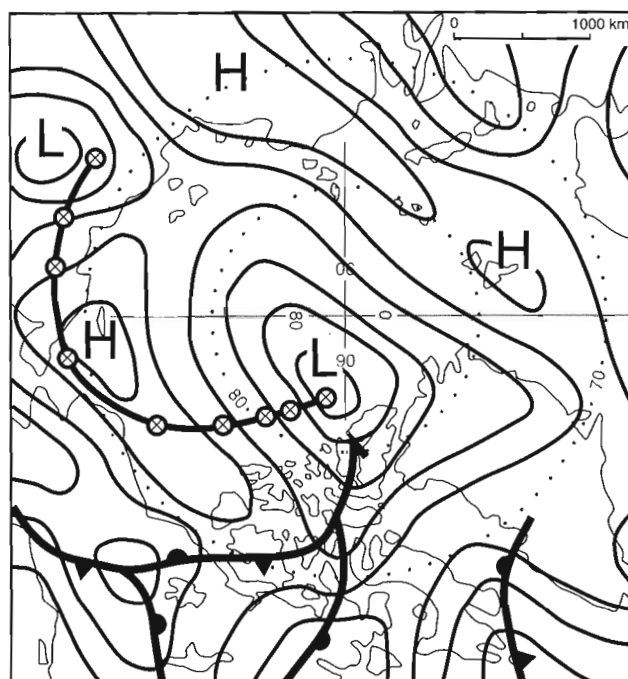


Figure 9. Surface atmospheric pressure contours (in millibars) for 12h00 UCT on 19 August 1988 showing passage of trowal (trough of warm air aloft) over Eureka. Track of low pressure system is shown by joined circles denoting the centre position for consecutive 24 hour intervals.

surface by 33 mm. The snow fell with air temperatures in the -2°C to -5°C range and winds between 10 and 20 km/h. Most of the 63 mm of new snow, required to make up the 50 mm of observed (a) layer, fell during the 4 days following the maximum melt event of the 1991 summer. A total accumulation of 116 mm was reached by the 6th day after the melt event. No scouring was observed in the daily surface lowering record during this time although there is possible evidence in the six-hour record of some scouring or packing on 28 July. A three to four degree temperature gradient would have existed in this relatively new snow to support rapid metamorphism of this layer. There is the possibility of several very minor melting events after the deposition of this layer but the mean air temperature remains below -2°C . These minor melt events, in fact, may have contributed to the formation of large snow grains of the (a) layer.

The first 58 mm of new snow accompanied the passage of a well developed surface low pressure system. This system moved into the islands from north of the Beaufort Sea having stalled there for several days (Fig. 10). Prior to stalling north of the Beaufort Sea this system can be traced back to the East Siberian Sea but the lack of data in the ocean makes its exact history uncertain. Satellite imagery might provide more information. The system appears to have had a frontal system associated with it but the surface fronts passed south of northern Ellesmere Island. There is evidence, in the 85 kPa chart (which is the approximate altitude of the ice cap

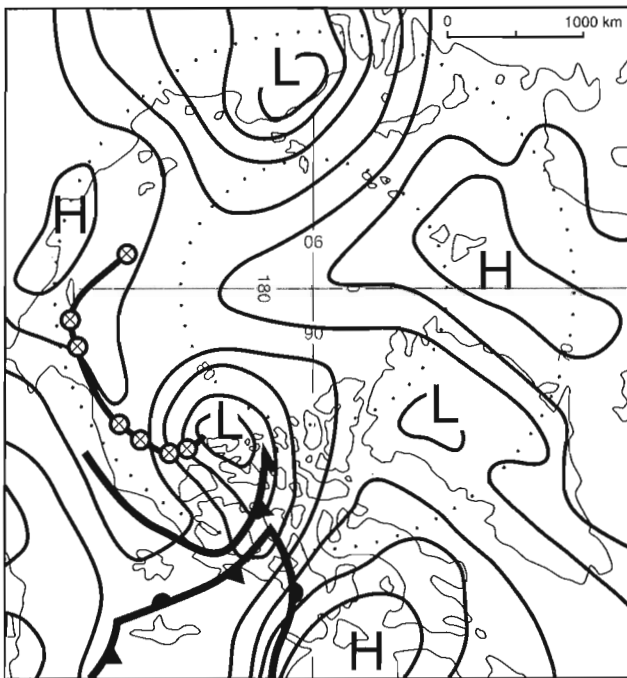


Figure 10. Surface atmospheric pressure contours (in millibars) for 12h00 UCT on 25 July 1991 showing approach of system with fronts to Ellesmere Island. Track of low pressure system is shown by joined circles denoting the centre position for consecutive 24 hour intervals.

sampling site), of the upper warm trough reaching as far north as Alert. Winds at the ice cap station become southerly on 26 July during the major period of deposition.

By contrast the 53 mm deposition on 29 July was accompanied by northerly winds at the ice cap station. These are consistent with the northerly flow on the surface and upper air charts at this time. It is not clear what produced this high accumulation value. It may have been orographic lift of the moist Arctic Ocean air mass or there may be a small trough or low pressure system which, due to the lack of data over the central Arctic Ocean, cannot be located. One further possibility is that much of the surface change on that day was due to drifting of snow to the autostation site from elsewhere on the ice cap. In this latter case the (a) layer would consist entirely of snow from the low pressure system discussed above.

Air temperatures at the ice cap station remained in the -2°C to -5°C range for another 20 days after the deposition of the (a) layer. Temperatures on the tundra were still above freezing and the ground was not yet snow covered. Snow deposited during this period would not be significantly colder than the snow surface which would now be in equilibrium with the ice cap air temperature. This isothermal gradient in the top layer of snow would not promote rapid metamorphism in the new snow. The (b) layer accumulation for this year (1991-92) can be taken as having begun with the deposition event of 7 August.

CONCLUSIONS

The results of this initial study of autostation records and the (a) layer in the pollen seasonal record provide the following answers to the questions posed in the introduction.

1. The loosely packed, coarse grained (a) layer is a result of the deposition in a short period of time of a significant amount of snow on to the melting or recently melting summer snow surface. Only the first significant snowfall deposited over the melting snow surface develops a sufficient temperature gradient to undergo rapid metamorphism. This accounts for the relatively thin depth of this layer. The widespread distribution of this distinctive layer suggests that on arctic ice caps the melt season is usually culminated by an accumulation event.
2. Only a small portion of the (d) layer deposition occurs during or after the pollen production season on the tundra. The first storm of the accumulation season, which is responsible for the (a) layer deposition, has two sources of pollen to draw on. The first is the pollen that has accumulated in the atmosphere during the pollen production (melt) season but which has not been washed out. Some dry deposition doubtless takes place and some instances of light precipitation occur but these are often local events as shown by comparison of the Agassiz and Hot Weather Creek records in 1988 (Fig. 4b, c). The second is the pollen deposited during the pollen season on the dry, snow free ground of the tundra. In both summers studied, the first storm of the accumulation season was a

well developed system with good upper atmosphere support. Both passed over the tundra areas to south and west of the ice cap. These systems had the necessary upward vertical motion to pick the pollen up from the ground and carry it to the altitude of the ice cap. They also contained sufficient moisture to cause significant precipitation when the upper trowal passed over the mountains.

3. Pollen deposition in the (a) layer on the ice cap appears to better represent the continental climate of the inland tundra regions than that of either of the coastally located permanent weather stations. There appears to be an almost exponential increase of pollen reaching the ice cap with increasing temperature. Extreme situations are better represented than are the more normal seasons. It is particularly interesting to note that proximity of the date of deposition of the (a) layer to the date(s) of pollen production does not seem to influence pollen concentration in the layer. The extremely pollen rich (a) layer of 1988 was deposited almost a month later than the pollen poor (a) layer of 1991. The pollen production in the source region may itself not always accurately represent the climate of the source region as suggested by the preliminary 1991 results. The overlapping record, presently available, is too short to make a quantitative assessment of the various relationships or of the impact of extreme events on the paleo record.
4. Using the autostation records, it was definitely possible to date the two (a) layers studied. In both years, the well developed surface systems, responsible for most of the snow in the layer, originated in the Siberian sector and tracked around the central Arctic Ocean, entering the high arctic islands from the west or southwest. The 1991 system followed a more northerly track than the 1988 system which travelled along southern boundary of the permanent sea ice. In both cases the regional pollen source(s) was probably west or southwest of the ice cap. The exotic pollen source for the layers might differ somewhat between the two years, as might the moisture and contaminant source. The preliminary results indicate that all would, however, have come from Siberia and Alaska rather than eastern North America.

These results show the importance of continuing the simultaneous collection of seasonal pollen and autostation records from Agassiz Ice Cap and the Hot Weather Creek tundra site. Detailed analysis of the (a) layer of each year in the overlapping record is necessary to verify the results of this preliminary study. Study of the other seasonal layers and of other constituents of the snow pack are also warranted.

ACKNOWLEDGMENTS

We would like to thank all those who took part in the autostation and pollen sampling work in the field on Agassiz Ice Cap and at Hot Weather Creek. In addition to members of

Terrain Sciences Division, this includes personnel from Campbell Scientific Canada Corporation and Atmospheric Environment Services, Arctic Division. Polar Continental Shelf Project has provided flying time and logistic support to the Agassiz Ice Cap and Hot Weather Creek programs since their inception. R.M. Koerner provided valuable discussion regarding the snow stratigraphy. Ana Djuric helped in the pollen analysis and diagram preparation and Tracy Barry prepared the maps.

REFERENCES

- Alt, B.T.**
 1987a: Arctic Climates; in *Encyclopedia of Climatology*, (ed.) J.E. Oliver and R.W. Fairbridge; Van Nostrand-Reinhold, p. 82-91.
 1987b: Developing synoptic analogs for extreme mass balance conditions on Queen Elizabeth Islands Ice Caps; *Journal of Climate and Applied Meteorology*, v. 26, p. 1605-1623.
- Alt, B.T. and Maxwell, J.B.**
 1990: The Queen Elizabeth Islands: a case study for Arctic climate data availability and regional climate analysis; in *Canada's Missing Dimension, Volume 1*, (ed.) C.R. Harrington; Canadian Museum of Nature, p.294-326.
- Bourgeois, J.C.**
 1986: A pollen record from the Agassiz Ice Cap, northern Ellesmere Island, Canada; *Boreas*, v. 15, p. 345-354.
 1990a: Seasonal and annual variation of pollen content in the snow of a Canadian high Arctic ice cap; *Boreas*, v. 19, p. 313-322.
 1990b: A modern pollen spectrum from Dye 3, south Greenland Ice Sheet; *Journal of Glaciology*, v. 36, p. 340-342.
- Bourgeois, J.C., Koerner, R.M., and Alt, B.T.**
 1985: Airborne pollen: a unique air mass tracer, its influx to the Canadian high Arctic; *Annals of Glaciology*, v. 7, p. 109-116.
- Edlund, S.A. and Alt, B.T.**
 1989: Regional congruence of vegetation and summer climate patterns in the Queen Elizabeth Islands, Northwest Territories, Canada; *Arctic*, v. 42, p. 3-23.
- Fredskild, B. and Wagner, P.**
 1974: Pollen and fragments of plant tissue in core samples from the Greenland Ice Cap; *Boreas*, v. 3, p. 105-108.
- Koerner, R.M.**
 1966: A mass balance study: the Devon Island Ice Cap, Canada; PhD. thesis, Department of Geography, University of London, London, 340 p.
- Koerner, R.M., Bourgeois, J.C., and Fisher, D.A.**
 1988: Pollen analysis and discussion of time-scales in Canadian ice cores; *Annals of Glaciology*, v. 10, p. 85-91.
- Labine, C.L., Alt, B.A., Atkinson, D., Headley, A., Koerner, R.M., Edlund, S.A., and Waszkiewicz, M.**
 1994: High Arctic IRMA Automatic Weather Station Field Data 1991-92. Part 1: Documentation, Part 2: Plots; Geological Survey of Canada, Open File 2898.
- McAndrews, J.H.**
 1984: Pollen analysis of the 1973 ice core from Devon Island Ice Cap, Canada; *Quaternary Research*, v. 22, p. 68-76.
- Short, S.K. and Holdsworth, G.**
 1985: Pollen, oxygen isotope content and seasonality in an ice core from the Penny Ice Cap, Baffin Island; *Arctic*, v. 38, p. 214-218.

Estimates of methane hydrate volumes in the Beaufort-Mackenzie region, Northwest Territories

S.L. Smith and A.S. Judge
Terrain Sciences Division

Smith, S.L. and Judge, A.S., 1995: Estimates of methane hydrate volumes in the Beaufort-Mackenzie region, Northwest Territories; in Current Research 1995-B; Geological Survey of Canada, p. 81-88.

Abstract: An extensive hydrate-prone zone has been determined to exist in the Beaufort-Mackenzie region. Geophysical evidence interpreted from 201 wells suggests that a significant volume of natural gas may be stored as hydrate within the sediments of this region. It is difficult to determine the total volume of hydrate within the region because the point information from a nonuniform distribution of wells must be generalized to the region as a whole. A Geographic Information System (GIS) approach has been used to determine the area represented by each well and to incorporate factors such as hydrate stability and uncertainty into estimates of hydrate volume. Maps have also been produced which outline probable areas of hydrate accumulation. The results of this analysis suggest that the volume of hydrate in this region is in the order of 10^{11} m³.

Résumé : Une vaste zone à forte teneur en hydrates a été identifiée dans la région de Beaufort-Mackenzie. Des indices géophysiques tirés de 201 puits laissent supposer qu'un volume important de gaz naturel pourrait être emmagasiné sous forme d'hydrates dans les sédiments de cette région. Il est difficile de déterminer le volume total des hydrates au sein de la région parce que l'information ponctuelle tirée de puits répartis de façon non uniforme doit être généralisée à l'ensemble de la région. Une approche basée sur un système d'information géographique (SIG) a été utilisée pour déterminer le secteur représenté par chaque puits et pour incorporer des facteurs tels que la stabilité des hydrates et un facteur d'incertitude dans les estimations du volume des hydrates. Des cartes, qui délimitent les régions probables où se sont accumulés des hydrates, ont aussi été produites. Les résultats de cette analyse suggèrent que le volume des hydrates dans cette région est de l'ordre de 10^{11} m³.

INTRODUCTION

Large areas of the Canadian Arctic have conditions suitable for natural gas hydrates. Analysis of thermal data indicates that hydrate is stable in sediments beneath the Beaufort Shelf and the Mackenzie Delta. Evidence from geophysical well logs shows that hydrate exists in this area and a large amount of methane gas may be stored as hydrate (Majorowicz et al., 1990; Judge and Majorowicz, 1992).

Recently, attention has been focused on natural gas hydrates as a contributor to future energy supplies and to atmospheric greenhouse gas content (eg. Kvenvolden, 1991). The overall importance of gas hydrates however cannot be evaluated until reliable estimates of hydrate volumes have been made. Present global estimates of the amount of methane stored as hydrate are speculative and range over three orders of magnitude from

2.5×10^3 to 5×10^6 Gt of methane (Kvenvolden, 1991). These estimates, however, are based on analyses of pressure and temperature conditions and very limited geophysical data, and the results were extrapolated over large areas.

Although hydrate may be stable over a considerable thickness of sediment, its actual distribution will depend on the geological history and stratigraphic environment because these will influence the availability of gas and water and the location of hydrocarbon reservoirs and traps. Geophysical well logs can be used to determine the intervals in which hydrate occurs. High quality geophysical data from 201 wells in the Beaufort-Mackenzie Basin have been examined to determine the intervals in which hydrate is likely to occur (D&S Petrophysical Consultants, 1983; Thurber Consultants, 1986, 1988). These data can be used to determine the total volume of hydrate in the basin, but the point information must be extrapolated to the basin

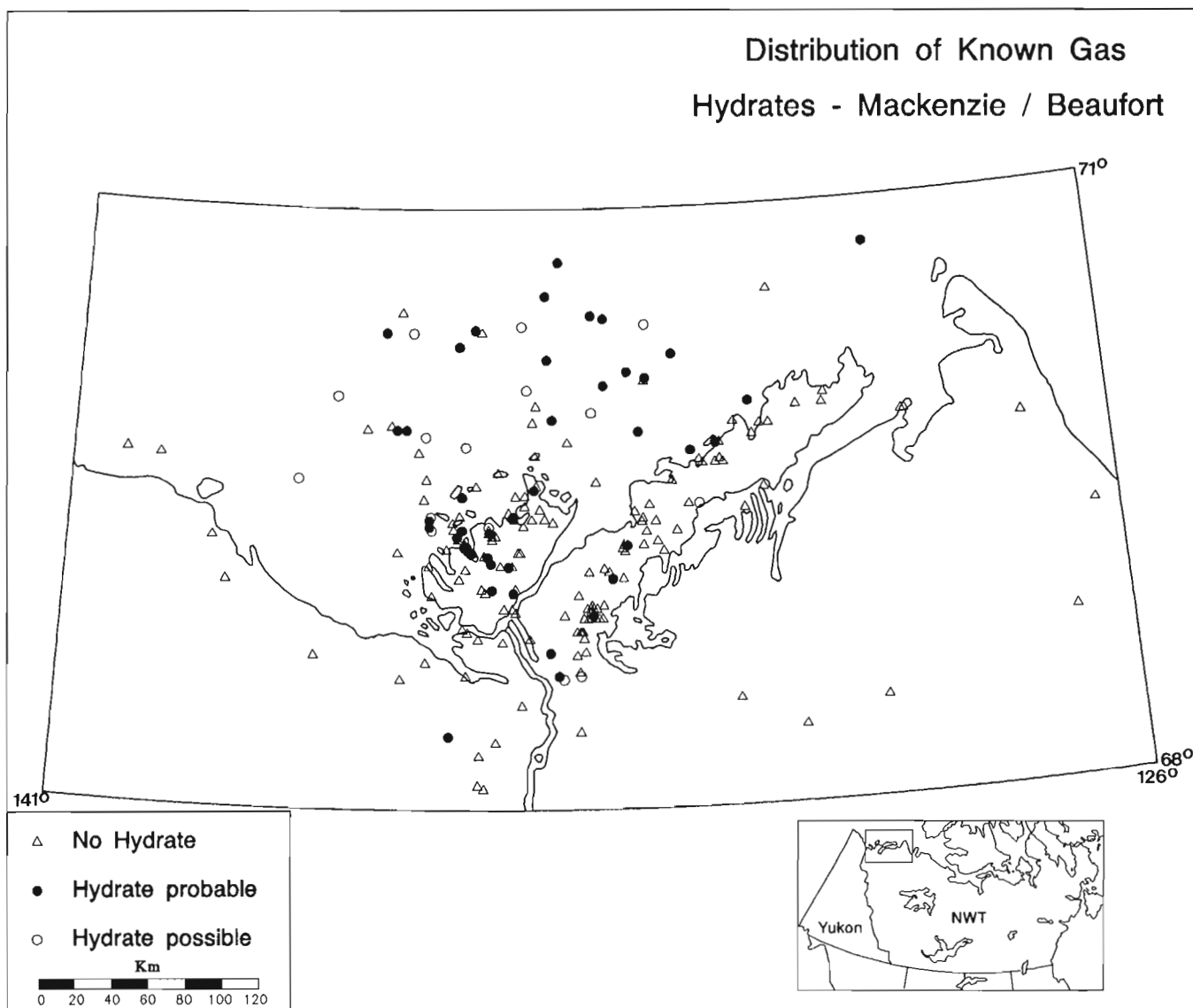


Figure 1. Location of wells and known hydrate occurrences in the Beaufort-Mackenzie region.

as a whole. Each well must be weighted according to the proportion of the regional area it represents recognizing that, in addition, uncertainty in the estimate of hydrate volume increases with distance from a well.

Statistical methods and GIS (Geographic Information System) have been used in an attempt to apply information from well logs to map the spatial distribution of hydrate in the entire region and to estimate the total volume of hydrate, the range of values, and the amount of methane gas in the Beaufort-Mackenzie region. This is, to our knowledge, the first time that such an approach has been applied to gas hydrate mapping. The United States Geological Survey is in the process of developing a resource assessment approach with which to include methane stored in gas hydrate in hydrocarbon reserve estimates (T.S. Collett, pers. comm.)

DATA AVAILABLE

Petrophysical methods have been used to outline the occurrence of gas hydrates in 201 wells between 126°W and 141°W and between 68°N and 71°N (Fig. 1) in the Beaufort-Mackenzie region (D&S Petrophysical Consultants, 1983; Thurber Consultants, 1986 and 1988). Petrophysical characteristics of hydrate intervals include high resistivity, very low sonic velocity with cycle skipping, low density, high neutron porosity, and an enlarged borehole diameter on the caliper log (Collett et al., 1988), but are highly dependent on the drilling history of the well. Peaks on mud gas logs (if available) were used to confirm hydrate picks. Intervals likely to contain hydrate have been identified and a reliability factor has been assigned to each pick. From this information hydrate occurrence at each site is described as possible, probable, or not likely. The total thickness of hydrate-bearing sediment has been determined for each well.

Deep temperature data for 181 wells located between 129°W and 141°W and between 68°N and 71°N have been used by Judge and Majorowicz (1992) to analyze stability conditions for methane hydrate. Information provided by the National Energy Board on significant hydrocarbon discoveries has also been used to determine areas which may have sufficient gas for hydrate formation.

Thermal data were not available for the area between 126°W and 129°W, therefore all analyses will be done for a region that is located between 129°W and 141°W and 68°N and 71°N. This region covers approximately 155 219 km².

GAS HYDRATE OCCURRENCE

Suitable conditions for methane hydrate stability were found in 65 per cent of the wells analyzed leading to an extensive methane-hydrate-prone layer extending to as deep as 1400 ± 200 m (Judge and Majorowicz, 1992). Hydrate was interpreted as present in 29 per cent of the wells (Fig. 1) and may be present to depths as great as 1500 m (Smith and Judge, 1993). Most hydrate appears to be concentrated beneath the Beaufort Shelf and the northern Mackenzie Delta.

Information from individual well logs can be used to make very preliminary estimates of hydrate volume. The average thickness of hydrate-bearing sediment in the wells is 260 m. If it is assumed that hydrate occurring in 29 per cent of wells also occurs over 29 per cent of the area, 1.17 × 10¹³ m³ of hydrate-bearing sediment exists in the region. The porosity of reservoir rocks averages between 10 and 20 per cent (Hitchon et al., 1989). The volume of hydrate within the region is therefore estimated to be between 1.17 × 10¹² m³ and 2.38 × 10¹² m³. Assuming that cavities in the hydrate contain only methane, and 1 m³ of hydrate releases approximately 160 m³ of methane (Lewin and Associates, 1983), the amount of methane stored as hydrate is between 129 and 262 Gt. This value represents an upper limit because an assumption is made of saturation of pore space by hydrate.

ESTIMATES OF HYDRATE VOLUME

Area represented by wells

In the above determination of total hydrate volume, all wells were assigned equal weight (i.e. an average thickness of 260 m was used) in the calculation. In fact well density is higher in the central part of the region (Fig. 1). A weighted average for the thickness of hydrate-bearing sediment was therefore determined. The area represented by each well was determined by constructing polygons around each well using the THIESSEN polygon module in the Idrisi (Version 4.0) GIS software package (Eastman, 1992). This module produces a raster image of the region consisting of a grid with 25 rows and 25 columns (625 cells), with each grid cell assigned a value according to the well (and polygon) with which it is associated. Grid size is chosen by the user.

The total area of polygons within the methane-hydrate-prone zone represented 63 per cent of the region. The total volume of the hydrate stability zone was determined using a weighted average for the thickness of the stability zone, assuming the depth of the top of the stability zone is 250 m. Hence, the total volume of sediment within this zone is estimated to be 5.4 × 10¹³ m³. Assuming hydrate exists throughout the stability zone and a porosity of 10 to 20 per cent, the maximum amount of hydrate in this area is 5.4 × 10¹² to 1.08 × 10¹³ m³. Assuming all hydrate cavities are filled with methane, the maximum amount of methane in this region would be between 594 and 1190 Gt.

The total area of the polygons for wells in which hydrate was interpreted represents 24 per cent of the region, which is similar to the proportion of wells (29%) in which hydrate has been interpreted from geophysical logs. Similar estimates of hydrate volume were obtained using a weighted mean for the thickness of hydrate-bearing sediment as the estimate in which all wells were given equal weight. A hydrate volume between 1.26 × 10¹² and 2.53 × 10¹² m³ and a methane amount of 139 to 278 Gt were determined using the weighted mean method. If only probable hydrate (the most confident interpretations) occurrences are considered, a volume of 8.06 × 10¹¹ to 1.61 × 10¹² m³ is estimated containing 89 to 177 Gt of methane.

Probability factors

In the above analysis, the probability of hydrate occurrence was not considered. The reliability of hydrate picks was available, however, but lower reliability picks were given the same weight as those of high reliability in one estimate and eliminated from the second estimate. Hydrate is interpreted as possible in intervals where there is disagreement between different logs, possibly where hydrate saturation is lower than those in which hydrate occurrence is described as probable. Hydrate detection can be ambiguous at times due to the complex drilling conditions of many wells, and geological materials other than hydrate may exhibit similar responses on resistivity, acoustic, and other logs. Thus, hydrate stability is another factor that should be considered to eliminate areas in which hydrate may have been interpreted but would not be stable under equilibrium conditions. An example of this is electrically resistive freshwater sand aquifers, which are found at depth in the area.

To incorporate these factors into the calculation of hydrate volume, two images were produced which described respectively hydrate stability and reliability of interpretation. Polygons were constructed around wells for which thermal data were available and a binary image was constructed which described hydrate stability. A value of 0 was assigned to polygons associated with wells outside the stability zone and a value of 1 was assigned to areas within the zone. The second image described the reliability of hydrate interpretation. A value of 0 was assigned to polygons associated with wells in which hydrate was not found. Values of 1 and 0.5 were assigned to sites where hydrate occurrence was interpreted as probable and possible respectively.

The stability and reliability images and the image describing the thickness of hydrate-bearing sediment were multiplied together and the volume of hydrate-bearing sediment was determined from the resulting image (OVERLAY1). The hydrate volume estimated (assuming porosity of 10 to 20%) from OVERLAY1 is between 1.1×10^{12} and 2.2×10^{12} m³.

In producing the image describing the thickness of hydrate-bearing sediment, the entire area of each polygon was given the same value as the representative well. We can be fairly confident in our estimates of the thickness of hydrate-bearing sediment at the well site but, as distance from a well increases, there is an increase in the degree of uncertainty of our estimates. This is more important where well density is fairly low. The degree of uncertainty was incorporated into estimates of hydrate volume by overlaying an image based on distances from each cell to the nearest well. Hydrate volume was determined using the three different "factors of uncertainty" described below; the results are compared in Table 1.

A linear increase in the degree of uncertainty with distance from a well was considered first. Distances between each grid cell and the nearest well were determined using the DISTANCE module in the Idrisi GIS (Eastman, 1992). These distances were adjusted so that cells containing a well were given a value of 1 and those without a well were given a value of less than 1 with the cells located farthest from a well having a value of 0. This image was multiplied by OVERLAY1 and the volume of hydrate-bearing sediment determined from the resulting image (OVERLAY2). The volume of hydrate estimated from OVERLAY2 is between 8.5×10^{11} and 1.7×10^{12} m³.

An exponential change in the degree of uncertainty with distance was also considered. One image was produced which resulted from a transformation of the distances between cells and wells where the "factor of uncertainty" (referred to as EXP1) equals $\exp(-\text{distance})$. Another image was produced representing a greater increase in the degree of uncertainty with distance in which the "factor of uncertainty" (referred to as EXP10) equals $\exp(-10 \times \text{distance})$.

Hydrate volume determined from the image (OVERLAY3) using the EXP1 "factor of uncertainty" is similar to that determined from OVERLAY2 (Table 1). When the EXP10 "factor of uncertainty" is considered (OVERLAY4), hydrate volume is estimated to be between 2.4×10^{11} and 4.8×10^{11} m³.

Table 1. Hydrate volumes and amount of methane gas determined for the Beaufort-Mackenzie region using the different methods outlined in the text

Overlay	Overlay images	Hydrate volume ($\times 10^{11}$ m ³)	Gt Methane gas
OVERLAY1	Thickness x Stability x Reliability	11.2 - 22.4	123 - 246
Models considering distance factor			
OVERLAY2	OVERLAY1 x Linear distance factor	8.51 - 17.0	93 - 187
OVERLAY3	OVERLAY1 x EXP1	7.85 - 15.7	86 - 173
OVERLAY4	OVERLAY1 x EXP10	2.42 - 4.84	27 - 53
Models considering hydrocarbon discoveries			
OVERLAY5	OVERLAY2 x Significant hydrocarbon discoveries	1.61 - 3.22	18 - 35
OVERLAY6	OVERLAY3 x Significant hydrocarbon discoveries	1.45 - 2.90	16 - 32
OVERLAY7	OVERLAY4 x Significant hydrocarbon discoveries	0.319 - 0.638	3.5 - 7

The area (determined from OVERLAY 1-4) over which hydrate occurs is approximately 30 771 km² (20%) of the 155 219 km² considered. Using the range of values for total hydrate volume presented in Table 1, hydrate-bearing sediments in the Beaufort-Mackenzie region are estimated to contain on average between 7.9×10^6 and 7.3×10^7 m³ of hydrate/km². Collett et al. (1988) determined from well logs that a 380 km² area of the North Slope of Alaska contains approximately 2.0×10^9 m³ of hydrate. This is equivalent to 5.3×10^6 m³ of hydrate/km². They suggest that this value represents a minimum value because of the low well density in most of their study region. The values presented in this paper are within an order of magnitude of those suggested for the North Slope. The present estimates of hydrate volume for the Beaufort-Mackenzie region therefore appear to be comparable with the only other area having a significant density of well data.

Hydrate distribution

The maps (Fig. 2, 3, 4) produced from the four overlay images described above show the spatial distribution of hydrate volume. A porosity of 10 per cent was assumed for all calculations. Figure 2 (OVERLAY1) does not include the "factor of uncertainty", while Figures 3 (OVERLAY2) and 4 (OVERLAY4) consider linear and exponential (EXP10) increase in the degree of uncertainty with distance from the nearest well, respectively. The three maps show that hydrate occurs over an extensive area in the offshore Beaufort area. Hydrate occurrence is limited in the onshore areas and major accumulations are restricted to the northern Mackenzie Delta and southwestern Tuktoyaktuk Peninsula.

The addition of the "factor of uncertainty" results in a map which introduces greater spatial variation in the hydrate distribution, especially in areas where well density is low. The addition of a "factor of uncertainty" varying linearly with

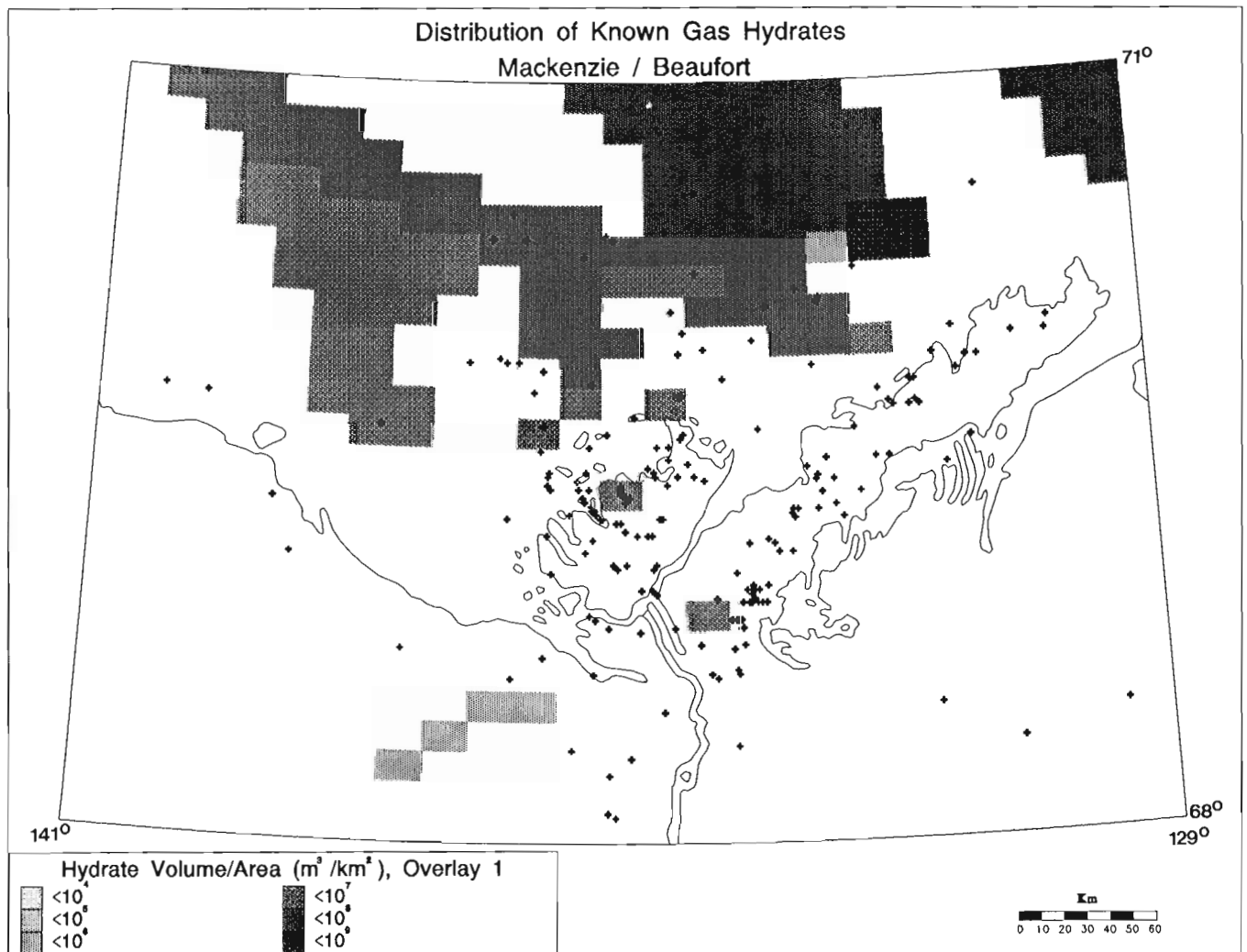


Figure 2. Hydrate distribution as determined from OVERLAY1. The crosses represent wells at which geophysical data were analyzed.

distance (Fig. 3) does not have much of an effect on estimates of hydrate volume compared to those estimates from OVERLAY1 (Fig. 2) from which the factor is omitted. In most areas, hydrate volume estimated from OVERLAY2 is within an order of magnitude of that estimated from OVERLAY1, especially in the central part of the region where well density is high. Results similar to those in Figure 3 were obtained using the EXP1 "factor of uncertainty".

When the EXP10 "factor of uncertainty" is incorporated into estimates of hydrate volume, the map (Fig. 4) shows a much greater spatial variation in hydrate volume than those in Figures 2 and 3. Addition of a large exponential change in the degree of uncertainty with distance results in estimates of hydrate volume that may decrease by several orders of magnitude as distance from the well increases. Essentially the model assumes that all wells encountering hydrate were drilled through the greatest concentration of hydrate.

Underlying geological features have not been taken into account in the estimation of hydrate volume. It is unlikely that hydrate volume decreases as rapidly within a short distance from a well as suggested by Figure 4. There may however be a sudden drop in hydrate volume at the edge of the reservoir which in some cases would be at a fault. If hydrate is formed from gas migrating from below, fault structure may be an important delimiting factor. Further study on the relationship between hydrate occurrence and factors such as fault distribution and hydrocarbon migration can be added to further refine the estimates. An analysis of high resolution seismic data may give some idea of the lateral extent of the hydrate "reservoirs".

Relationship between hydrocarbon and hydrate occurrences

Hydrate distribution as determined from geophysical evidence appears to be associated with the location of underlying oil and gas reservoirs (Judge and Majorowicz, 1992). Sufficient gas for hydrate formation is most likely to

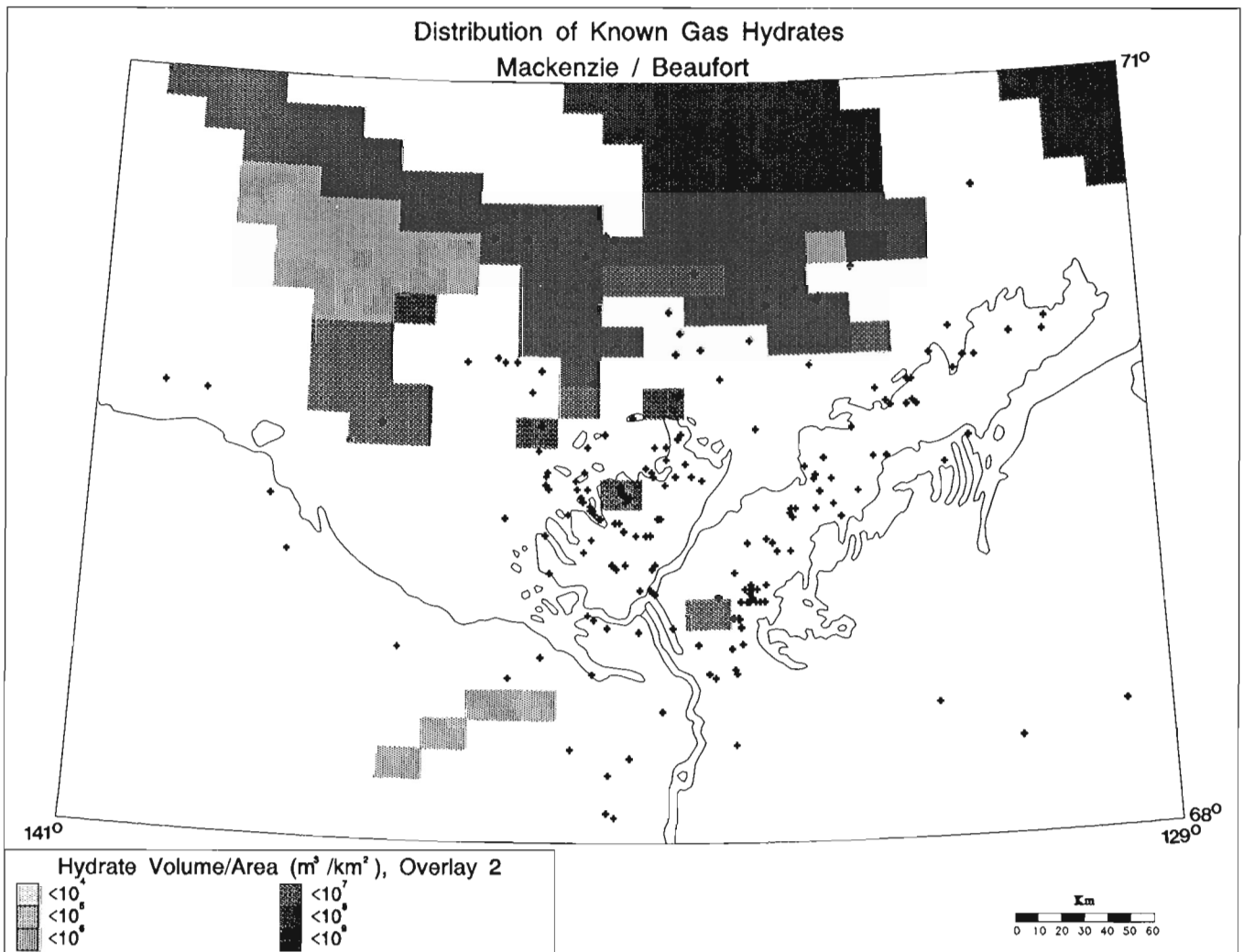


Figure 3. Hydrate distribution as determined from OVERLAY2, which considers a linear increase in the degree of uncertainty with distance from a well.

be present in these areas. Significant hydrate accumulations would be expected in areas where significant hydrocarbon discoveries have been made, provided temperature and pressure stability conditions are satisfied. An estimate of hydrate volume was made by combining an image of the location of discovery wells with those produced above (OVERLAY2-4). Depending on the "factor of uncertainty" used, hydrate volume is estimated to be between 3.9×10^{10} and $3.22 \times 10^{11} \text{ m}^3$ (OVERLAY5-7 in Table 1). These values probably reflect the minimum amount of hydrate contained in the region, since it is assumed that little dispersion or diffusion of methane occurs and in situ biogenic production of methane from organics in the sediments has not been considered.

CONCLUSIONS

Geophysical evidence suggests that major accumulations of natural gas hydrates exist in the Beaufort-Mackenzie region. Estimates suggest that hydrate underlies approximately

$30\,771 \text{ km}^2$ (20%) of the $155\,219 \text{ km}^2$ region with most of the hydrate concentrated in the offshore Beaufort area. A GIS approach has been used to refine estimates of hydrate volume. The results indicate that hydrate volume in this region is on the order of 10^{11} m^3 and that local volumes range to a maximum of $10^8 \text{ m}^3/\text{km}^2$.

Maps have been produced which describe the spatial distribution of hydrate. Although geological features such as fault boundaries have not been considered in determining the variation in hydrate volume with distance from a well, the maps do outline areas where hydrate is likely to occur. This information is also useful in identifying areas where hydrate may present a hazard during drilling. The maps outline areas where hydrate accumulation is likely to be greatest, and this information is useful in determining the potential of natural gas hydrates as an unconventional gas resource.

The present estimates of hydrate can be refined. Factors influencing hydrate distribution need to be incorporated into the estimates of hydrate volume as information becomes

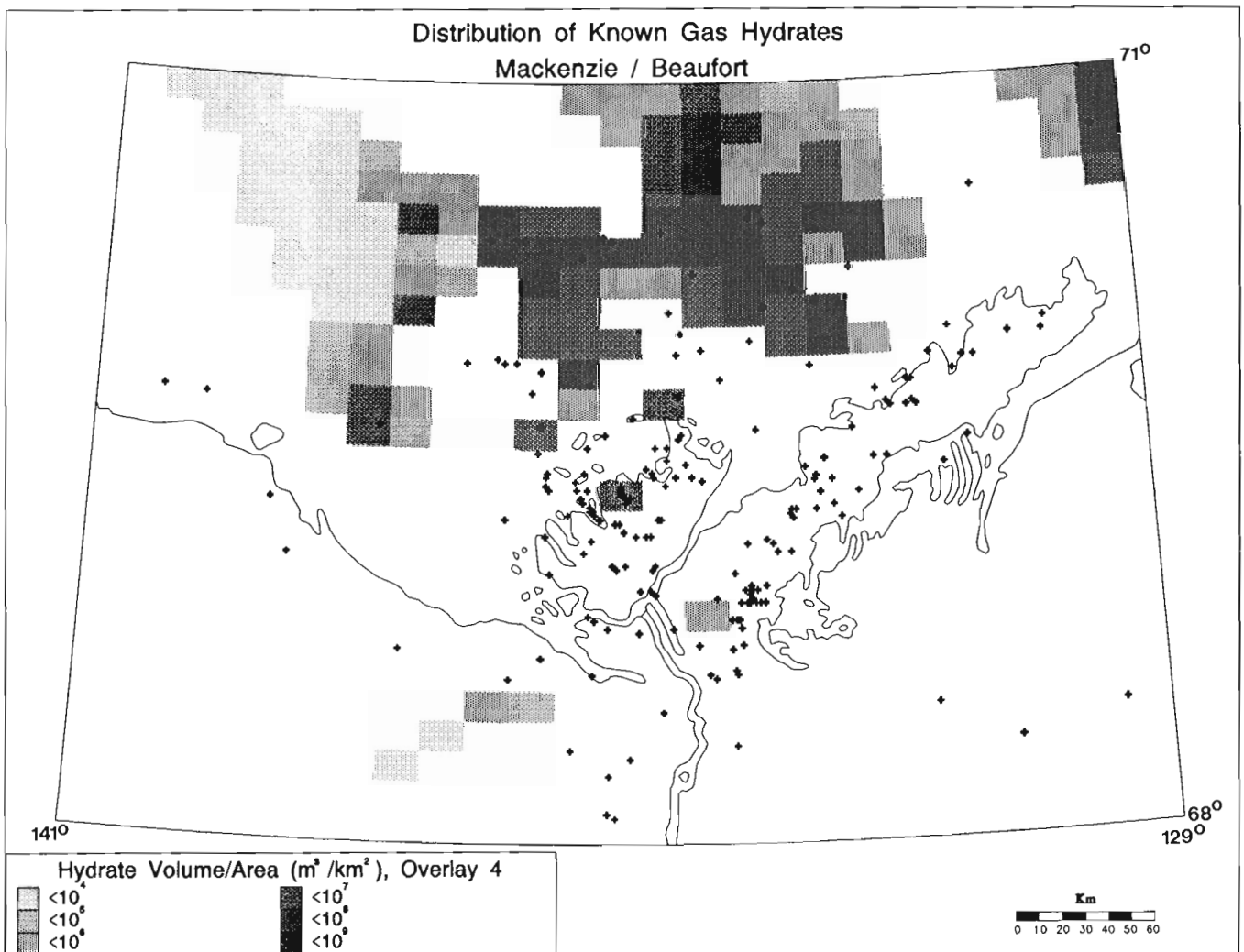


Figure 4. Hydrate distribution as determined from OVERLAY4, which considers an exponential increase in the degree of uncertainty with distance from a well.

available. The boundaries of potential reservoirs, fault distribution, and migration patterns of hydrocarbons could also be included in the estimation of hydrate volume.

ACKNOWLEDGMENTS

This project was funded by the Panel on Energy Research and Development (Energy, Mines, and Resources). This analysis depended heavily on high-quality measurements made during exploratory drilling in northern Canada. The authors wish to acknowledge the great dedication of numerous oil industry, logging company, and government regulatory personnel. We also wish to thank A.J. Desbarats of the Mineral Resources Division for his useful suggestions and A. Prigent of Informatics and Scientific Services for producing the maps.

REFERENCES

Collett, T.S., Bird, K.J., Kvenvolden, K.A., and Magoon, L.B.

1988: Geologic interrelations relative to gas hydrates within the North Slope of Alaska; U.S. Geological Survey, Open File Report 88-389, 150 p.

D&S Petrophysical Consultants

1983: A study of well logs in the Mackenzie Delta/Beaufort Sea to outline permafrost and gas hydrate occurrence; Energy, Mines, and Resources Canada, Earth Physics Branch, Open File 83-10.

Eastman, J.R.

1992: Idrisi Version 4.0 Technical Reference; Clark University Graduate School of Geography, 213 p.

Hitchon, B., Sauveplane, C.M., Underschultz, J.R., and Bachu, S.

1989: Hydrogeology, geopressures, and hydrocarbon occurrences, Beaufort-Mackenzie Basin; Geological Survey of Canada, Open File 2046, 216 p.

Judge, A.S. and Majorowicz, J.A.

1992: Geothermal conditions for gas hydrate stability in the Beaufort-Mackenzie Area: The global change aspect; *Global and Planetary Change*, v. 6, p. 251-263.

Kvenvolden, K.A.

1991: A review of Arctic gas hydrates as a source of methane in global change; in *International Conference on the Role of the Polar Regions in Global Change*, Vol II, (ed.) G. Weller, C.L. Wilson, and B.A.B. Severin; University of Alaska at Fairbanks, p. 696-701.

Lewin and Associates

1983: Handbook of gas hydrate properties and occurrence; Report for United States Department of Energy, Office of Fossil Energy, contract No. DE-AC21-82-MC19239, Morgantown, West Virginia.

Majorowicz, J.A., Jones, F.W., and Judge, A.S.

1990: Deep subpermafrost thermal regime in the Mackenzie Delta Basin, northern Canada – Analysis from petroleum bottom-hole temperature data; *Geophysics*, v. 55, p. 362-371.

Smith, S.L. and Judge, A.S.

1993: Gas hydrate database for Canadian Arctic and selected East Coast wells; Geological Survey of Canada, Open File Report 2746, 120 p.

Thurber Consultants Ltd.

1986: Study of well logs in the Mackenzie Delta/Beaufort Sea area and Arctic Islands to outline permafrost thickness and/or gas hydrate occurrence: an update of wells; Prepared for Supply and Services Canada, DSS File No. 15SQ.23235-5-1145, 19 p.

1988: Update of well log studies Mackenzie Delta/Beaufort Sea area, Arctic Islands and offshore East Coast, v. 1, Arctic Canada; Prepared for Supply and Services Canada, DSS File No. 69SZ.23233-7-0925, 19 p.

Geological Survey of Canada Project 870023

Field measurements of n-factors for natural forest areas, Mackenzie Valley, Northwest Territories

Alan E. Taylor

Terrain Sciences Division

Taylor, A.E., 1995: Field measurements of n-factors for natural forest areas, Mackenzie Valley, Northwest Territories; in Current Research 1995-B; Geological Survey of Canada, p. 89-98.

Abstract: The n-factor is defined as the ratio of the ground surface index of seasonal thawing (or freezing) to the air index of seasonal thawing (or freezing). Equivalently, the n-factor relates mean seasonal ground surface temperatures to the more readily available mean air temperatures. In geotechnical engineering calculations, the n-factor for a phase change season is a single parameter that represents the complex process of heat transfer through vegetation and snowcover. In 1993-94, the GSC established a latitudinal transect along the Mackenzie River valley using inexpensive miniature data loggers to record air and ground temperatures. N-factors calculated from the first year of data reflect the diverse forest, vegetation, and snowcover. Freezing season n-factors are lower because of the attenuation effect of snow, in addition to that of vegetation. N-factors may be used in quantitative permafrost mapping and climate change-permafrost impact prediction.

Résumé : Le facteur-n se définit comme étant le rapport entre l'indice de dégel (ou d'engel) saisonnier à la surface du sol et l'indice de dégel (ou d'engel) saisonnier dans l'air. De manière équivalente, le facteur-n lie les températures saisonnières moyennes de la surface du sol aux températures moyennes de l'air, qui s'obtiennent plus facilement. Dans les calculs de génie géotechnique, le facteur-n pour une saison de changement de phase est un paramètre unique qui représente le processus complexe de transfert de chaleur par la végétation et le manteau nival. En 1993-1994, la CGC a établi un transect latitudinal le long de la vallée du fleuve Mackenzie au moyen de capteurs miniatures et peu chers pour recueillir des données sur les températures de l'air et du sol. Les facteurs-n calculés à partir des données de la première année reflètent la diversité de la forêt, de la végétation et du manteau nival. Les facteurs-n de la saison de gel sont plus bas en raison de l'effet tampon de la neige, en plus de celui de la végétation. Les facteurs-n peuvent servir à la cartographie quantitative du pergélisol et à la prévision des effets des changements climatiques sur le pergélisol.

INTRODUCTION

The prediction of ground temperatures and the response of the ground to seasonally changing air temperatures are major problems in geotechnical engineering. The design of building foundations and road bases, for instance, depends on an accurate prediction of ground temperatures and the depth of seasonal freezing and thawing. This is particularly true in permafrost regions, where the depth of the soil that seasonally freezes and thaws (the active layer) and the possibility of increased heat transfer into the underlying permafrost through engineered structures must be considered (e.g. Lunardini, 1978, 1981). A recent concern is the possible effect of climate warming on permafrost and the ensuing geomorphic consequences, such as changes in active layer, slope stability, erosion, and hydrogeological processes (e.g. Jorgenson and Kreig, 1988; Kane et al., 1991; Wright et al., 1994).

A problem common to both these applications is the ready availability of data with which to undertake thermal calculations. The modified Berggren equation, commonly cited in engineering handbooks, relates the phase change depth Z_B to the thermal conductivity k and latent heat density L of the soil, and the surface index ("degree-days") of freezing or thawing, I_s .

$$Z_B = \lambda \sqrt{\frac{2k}{L} I_s} \quad (1)$$

λ is a constant. I_s varies due to local parameters such as snowcover, vegetation, and other factors and is not available unless specifically measured. However, the air index of freezing or thawing, I_a , is readily available from meteorological data on a regional basis or can be measured more easily at the local scale. Hence, a factor has been invoked to enable an estimation of the surface index from the more readily obtainable air index of thawing or freezing (e.g. Lunardini, 1981, chap. 10):

$$I_s = n I_a \quad (2)$$

where n is known as the "n-factor". The practical definition of the n-factor (Lunardini, 1981) is:

$$n = \frac{I_s}{I_a} = \frac{\int_0^{\theta_s} (T_f - T_s) dt}{\int_0^{\theta_a} (T_f - T_a) dt} \quad (3)$$

where T_a , T_s , and T_f are the air temperature, ground surface temperature, and freezing point of the soil, respectively, and θ_s , θ_a are the lengths (in time t) of the surface and air phase change seasons. Freezing n-factors (n_{fr}) are defined by freezing indices $I_{s,fr}$ and $I_{a,fr}$ in equation 3, and thawing n-factors (n_{th}) are defined by using the thawing indices $I_{s,th}$ and $I_{a,th}$ (Fig. 1).

This equation is equivalent to

$$T_s = T_f - n [T_f - T_a] \frac{\theta_a}{\theta_s} \quad (4)$$

which shows that the n-factor provides a way of expressing the mean seasonal ground surface temperature in terms of air temperature. At any site, a one-year time series of air temperatures and ground surface temperatures is sufficient to calculate estimates of n_{th} and n_{fr} , either by integrating the area under the curves and forming the ratio (equation 3, Fig. 1) or by calculating the seasonal means (equation 4).

A compilation of nearly a hundred values published by many workers is given in Lunardini (1978, 1981); however, most are for pavements, fewer than 20 are for natural surfaces, and only half are for permafrost areas with only one for undisturbed arctic forest. A few additional values for the latter category have appeared recently (e.g. Jorgenson and Kreig, 1988). Yet any active layer calculations in natural areas and quantitative calculation of regional permafrost distribution require this parameter when more detailed energy transfer parameters are unavailable.

To facilitate compilation of a database of n-factors for common and typical arctic forested areas, one component of the GSC's Mackenzie Valley active layer monitoring transect was the installation, in 1993 and 1994, of 36 air and surface temperature data recording stations (Nixon and Taylor, 1994; Nixon et al., 1995). The first year of data from the sites in the upper Mackenzie Valley (Fig. 2) was obtained in 1994; the present paper uses this data to calculate preliminary n-factors for a number of typical forested areas in this region.

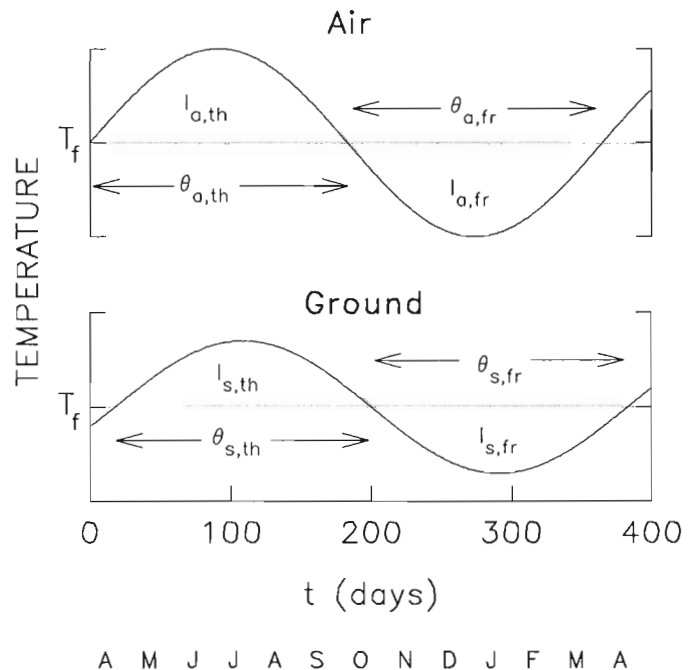


Figure 1. Schematic of air and ground temperatures for just over one year, showing phase change seasons and thawing and freezing indices. $I_{a,th}$ for instance, is the area between air temperatures greater than the freezing point and the freezing point.

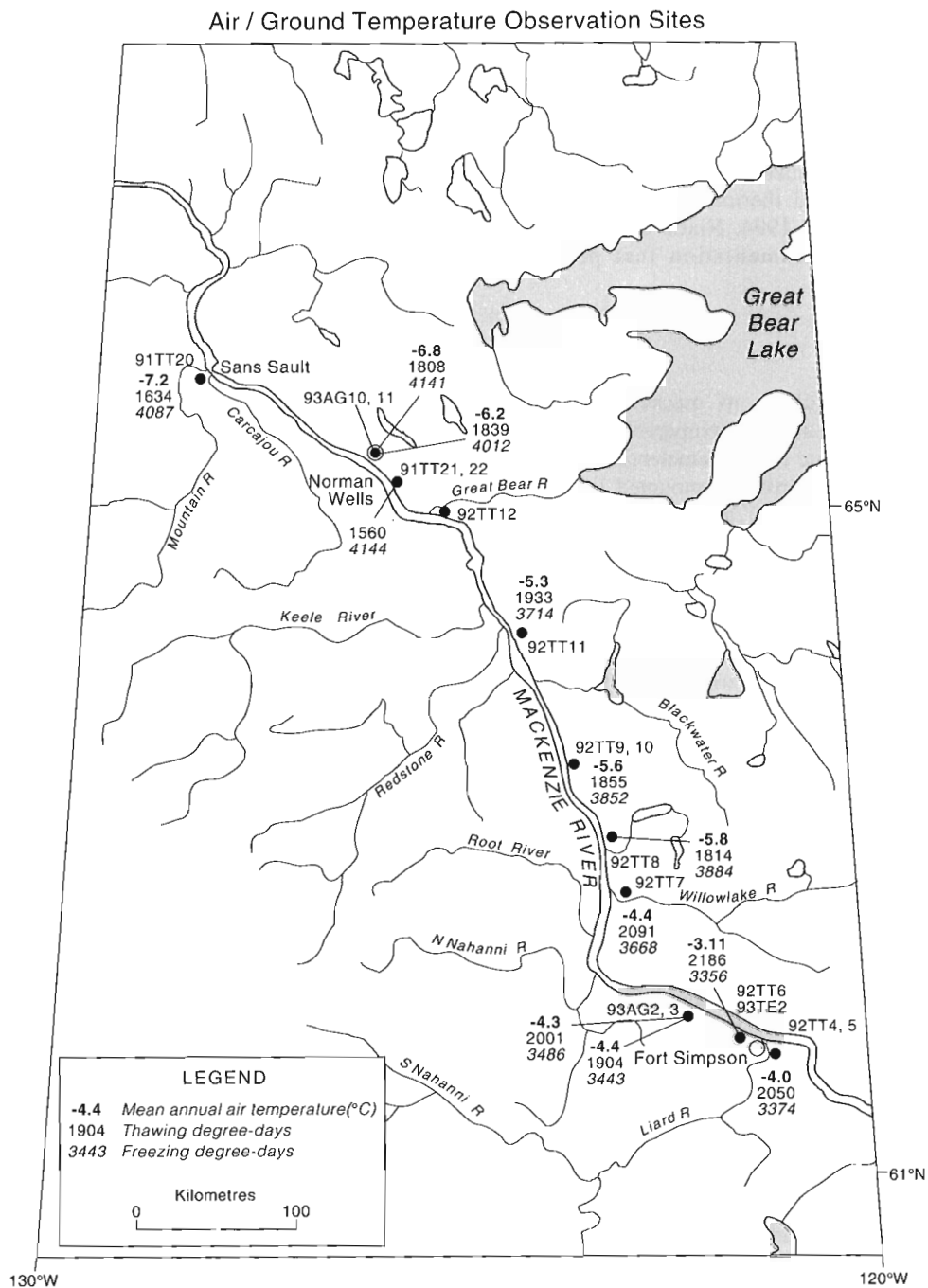


Figure 2. Location of sites with air and ground temperature data loggers, upper Mackenzie Valley, Northwest Territories. Site names are keyed to Table 1 and Nixon and Taylor (1994). Mean annual temperatures ($^{\circ}\text{C}$), air thawing index $I_{a,th}$ (units K-d), and freezing index $I_{a,fr}$ for the 1993-94 year are calculated from the data at each site.

DATA

The Mackenzie Valley active layer monitoring transect

As part of Global Change research being undertaken by GSC, a transect has been established along the Mackenzie Valley, from the discontinuous permafrost at Fort Simpson to the thick, continuous permafrost of the Beaufort Sea coast. Fifty-nine sites have been established in natural, undisturbed areas with a variety of instruments to monitor changes in the active layer and the ground thermal regime over several decades (Nixon and Taylor, 1994; Nixon et al., 1995). Of these, 36 sites have instrumentation that permit the calculation of n-factors.

Air temperatures

At these latter sites, simultaneous measurements of air temperatures and ground surface temperatures are being made every 5 hours. A 6-plate 12 cm diameter radiation shield built to meteorological standards was mounted 1.5 m above the ground at each site. Air temperatures are measured by a thermistor in the screen that is connected to an inexpensive miniature data logger enclosed within the mast near its base. This logger has a range of -37° to 46°C and a resolution of 0.025 K. While the air screen and data logger were purchased commercially, the mast and logger enclosure were made in-house (Fig. 3; for details, see Nixon et al., 1995).

Ground temperatures

Two styles of instrumentation are used to measure near-surface ground temperatures. At most sites, a similar miniature data logger with built-in thermistor was fitted inside a "35-mm" film canister (53 mm x 32 mm), sealed with silicone rubber and buried near the base of the air screen at a nominal depth of 3-7 cm; this depth is generally within a dense peat layer for most of the installations. A second ground temperature logger is buried several tens to a hundred metres away in a distinctly different vegetation or forest environment. For calculations of n-factors, air temperature is also assumed to approximate that of this remote site.

A more elaborate near-surface temperature instrumentation is employed at five sites in the upper Mackenzie Valley: temperature profiles are being measured with seven thermistor probes inserted horizontally at uniform intervals in the sidewall of a carefully dug and backfilled pit. Each pit was dug in July to the frost table, about 40-70 cm below the surface; the top probe is inserted about 7 cm from the ground surface (a depth similar to that of the single channel logger, above) and the others are spaced uniformly to the base of the pit. An eighth temperature sensor is used to record temperatures in a radiation shield, as above, and all sensors are connected to an 8-channel data logger that records temperatures every six hours. This instrumentation was designed for other applications, but it permits the calculation of the ground index (and n-factors) at various depths. For further details on the instrumentation, see Nixon and Taylor (1994).

RESULTS

Figure 4 shows a typical set of air and ground temperatures. Wide variations in air temperatures appear to be attenuated by vegetation and the few centimetres of burial during the thawing season, and further attenuated by snow during the freezing season. Note the decrease in high-frequency variations in ground temperatures during the winter. The "zero curtain", a maintenance of ground temperatures at the freezing point during fall freezing and spring thaw, is apparent but somewhat different on each ground temperature record.

Figure 2 shows the site locations, each annotated with mean annual air temperature, and the air thawing and freezing indices $I_{a,th}$ and $I_{a,fr}$, respectively; the latter are in K-d, i.e. Kelvin-days in SI units, or " $^{\circ}\text{C}$ -days". These values are for 1993-94. Table 1 summarizes these values and the resulting thawing and freezing n-factor values. In Table 1, site descriptions represent the local environment of each installation (Nixon and Taylor, 1994), while the ESP-NP class is the

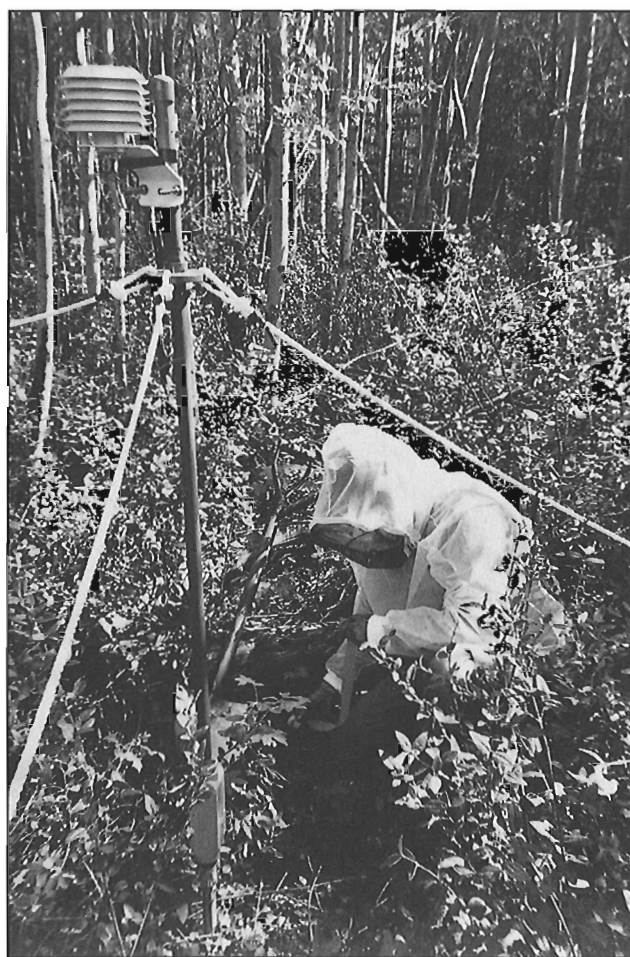


Figure 3. View of site 92 TT 5, Manners Creek, showing the air temperature screen and mast; the air temperature logger is housed in the elongated box near the base of the mast. The miniature ground temperature logger is being "planted" near the base of the mast.

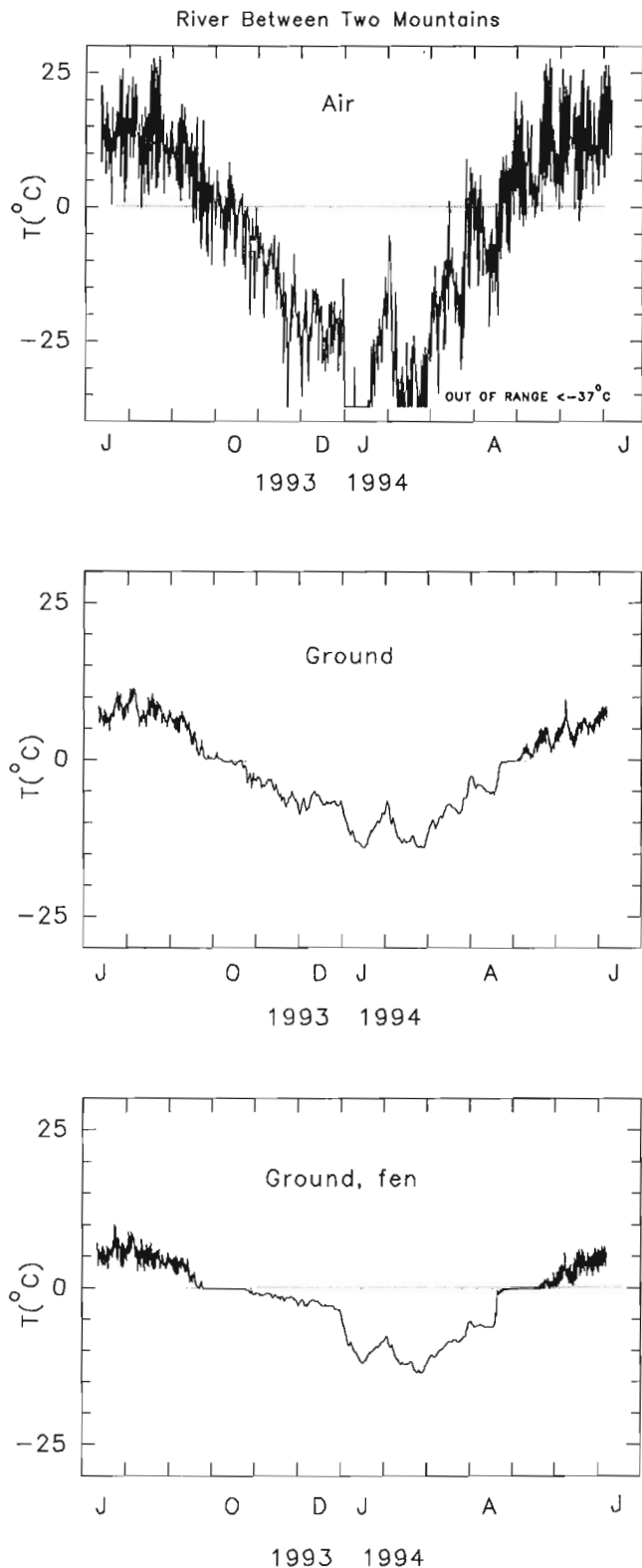


Figure 4. Typical record of air temperatures and ground temperatures, site 92 TT 8, River Between Two Mountains.

forest/vegetation type at the 1:125 000 scale (Environment Canada, 1974). The second line at most sites represents values for the ground logger remote from the air screen. Results labelled "8-ch" are calculated from the shallowest sensor in the pit sidewall temperature profiles.

DISCUSSION

N-factors for the thaw season appear to be highest in more open areas having good sun exposure (Table 1). The site 93 AG 2, Wrigley Hwy. km 507.6 (Fig. 2; $n_{th}=0.66$) is some 100 m south of a road in a small bog between a fen and upland mixed forest (Fig. 5); the bog was wet and the ground logger was submerged at time of installation in July 1993 but dry in July 1994. In contrast, site 93 AG 3, Wrigley Hwy. km 504.7 ($n_{th}=0.30$) is in a shady upland hardwood and spruce forest with 10 cm or more moss (Fig. 6); at the remote logger some 30 m away, $n_{th}=0.79$ in mineral soil on an overgrown but more exposed cut line through similar forest. At 92 TT 11, Saline River on a steep ($\sim 30^\circ$) south-facing slope in open aspens, $n_{th}=0.72$; a low cranberry cover may keep the n-factor from being higher. At 93 AG 10, Norman Wells AES, $n_{th}=0.72$ in the short grass of the cleared area of the AES compound, while about 100 m further north in bush and moss, $n_{th}=0.34$. At 92 TT 8, River Between Two Mountains, both freezing and thawing n-factors are higher in the hardwood/spruce forest than in the open fen some 30 m distant. This is partially a result of a longer "zero curtain" at the wetter fen site (Fig. 4).

N-factors for the freezing season are lower than corresponding thaw season values (Table 1), reflecting attenuation by snow of the impact of air temperatures on the ground surface. N_{fr} values also exhibit less variability and are higher on exposed ridges (e.g. km 507.6 and Mountain River) where snow depths may be less.

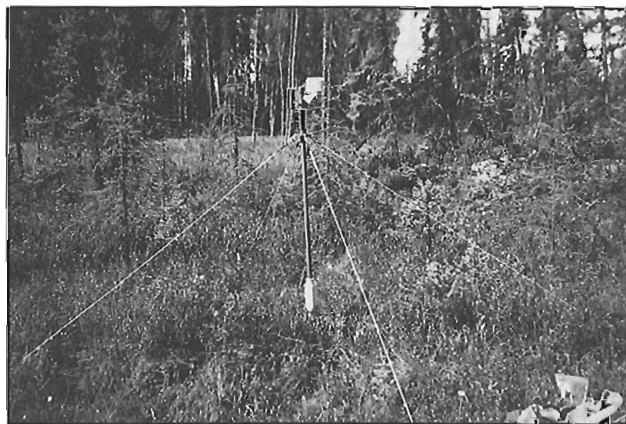


Figure 5. View of site 93 AG 2, Wrigley Hwy. km 507.6. Air and one ground temperature installation in a small bog, remote ground sensor on ridge to right, with fen in background.

Table 1. Location and description of active layer monitoring sites

Site	Air		Gnd		n_{th}	n_r	Description	ESP-NP Class ⁷
	$I_{a,th}$ (K-d)	$I_{a,fr}$ (K-d)	$I_{s,th}$ (K-d)	$I_{s,fr}$ (K-d)				
Manners Creek 61°45'58" 121°11'6" (92 TT 5)	2050	3374	1244	1379	0.61	0.41	silt of lacustrine plain ¹ ; site in aspen thicket with spruce, feather moss, hardwoods	-3SH3 E
Manners Creek 61°46'13" 121°11'33" (92 TT 4)	a/a	a/a	1220	1240	0.59	0.37	confluence of Manners Creek and Liard River; organic silt on alluvial terrace ¹ ; open upland hardwood forest	-5HS5 D
Martin R. 8-ch. (7 cm) 61°53'13" 121°35'59" (92 TT 6)	2186	3356	1442	1430	0.66	0.43	broad thermokarst depression in sand of lacustrine-eolian complex ¹ ; spruce, feather moss	-5PS5 D
Wrigley Hwy. km 504.7 61°58' 121°49' (93 AG 3)	1904	3443	576	695	0.30	0.20	on silt of lacustrine plain ¹ ; upland hardwood, spruce forest	-3bSH3 F(7) I(3)
Wrigley Hwy. km 507.6 61°58' 121°52' (93 AG 2)	a/a	a/a	1513	599	0.79	0.17	a/a, on overgrown bush road	-a/a
Wrigley Hwy. km 507.6 61°58' 121°52' (93 AG 2)	2001	3486	1331	402	0.66	0.12	lacustrine plain ¹ ; small bog between fen and open upland mixed forest	-3bSH3 F(7) I(3)
Willowlake River 62°41'48" 123°3'46" (92 TT 7) 8 ch. (7 cm)	a/a	a/a	750	912	0.36	0.25	a/a	-a/a
Willowlake River 62°41'48" 123°3'46" (92 TT 7) 8 ch. (7 cm)	2091	3668	1000	1319	0.48	0.36	silt on low terrace bar ² site in open succession vegetation of burn	-7HS3
River Between Two Mountains 62°57'40" 123°12'32" (92 TT 8)	1814	3884	790	1402	0.44	0.36	silt on alluvial terrace above Mackenzie ² ; tall open hardwood, spruce upland forest	-5HS3 D
	a/a	a/a	480	1136	0.26	0.29	a/a, site in fen	-a/a

Ochre River 63°27'59" 123°41'35" (92 TT 10)	1855	3852	1091	1211	0.59	0.31	stony alluvial terrace ² ; tall spruce, birch, and hardwoods	-5H5 D(6)
8 ch.	a/a a/a 1985	a/a a/a 3767	1280 1475 1263	1005 467 1134	0.69 0.80 0.64	0.26 0.12 0.30	a/a, overgrown bush road a/a, middle of small fen organics and silt on low alluvial terrace open upland spruce with hardwoods	-a/a -5SH5 L -a/a
Saline River 64°17'20" 124°31'28" (92 TT 11)	1933	3714	1385	1043	0.72	0.28	spur cut in high stony alluvial terrace ⁴ steep south-facing slope in open aspen grove	-3bS1 F
8 ch. (10 cm)	a/a a/a	a/a a/a	1518 803	948 844	0.78 0.42	0.26 0.23	a/a, top of slope on level ground silt veneer over stony colluvium open upland spruce with hardwoods	-a/a -5SH3 L
Francis Creek 65°11'52" 126°27'56" (91 TT 22)	1560	4144	602	1275	0.38	0.32	alluvial terrace in stony silt till ⁵ open mixed forest, birch willow thicket	-3SH3 E
(91 TT 21)	a/a	a/a	915	1708	0.59	0.41	a/a, closer to Mackenzie River	-a/a
Norman Wells AES 65°17'35" 126°45'40" (93 AG 10)	1839	4012	630	510	0.34	0.13	till plain ⁵ low, open black spruce and hardwoods over moss	-3S3 E
Norman Wells IPL 65°17'35" 126°53'08" (93 AG 11)	1808	4141	624	1168	0.34	0.28	a/a in uncut grassy area of AES compound	-a/a
Mountain River 65°40'29" 128°49'37" (91 TT 20)	1634	4087	577	857	0.35	0.21	alluvial terrace above Mackenzie ⁵ open black spruce and hardwoods over moss	-3bS3 F(6) 1bS3 F(4) -a/a
	a/a	a/a	594	1832	0.33	0.44	a/a, open larch site	-?S1 C
							low terrace in stony sand on alluvial plain ⁶	-a/a
							on ridge above terrace open, exposed spruce, hardwoods	
Mean values					0.59	0.20		
Standard deviation					0.20	0.11		
¹ (after Hawes, 1980a)	⁵ (after Duk-Rodkin and Hughes, in prep.) ⁶ (after Duk-Rodkin and Hughes, 1993) ⁷ (after Environment Canada, 1974)							
² (after Hawes, 1980b)								
³ (after Hawes, 1980c)								
⁴ (after Hanley and Hughes, 1973)								

Approximations in the calculation of the n-factor

These n-factors were derived from the first year of data obtained at these sites. While the 12-month period embraced a full continuous freezing cycle, it included the end of one thawing season and the beginning of the following thawing season (Fig. 4). For these preliminary estimates, it was assumed that the two thawing segments could be added together to approximate a single segment in the application of equation 3.

Several excursions across the freezing point occur in the spring and fall, before consistent thawing or freezing conditions set in, particularly in air temperature data (Fig. 4). This creates uncertainty in the determination of θ_s and θ_a (equation 3 and Fig. 1). Hence, for purposes of calculation, $I_{a,th}$ (and $I_{s,th}$) was taken as the total area throughout the year above the soil freezing point (identified by the temperature of the "zero curtain" in most soil temperatures (Fig. 4)) and $I_{a,fr}$ (and $I_{s,fr}$) was taken as the area below the soil freezing point.

The major limitation of the miniature single-channel data loggers for this application is the lower limit of their temperature range: -37°C . While shallow ground temperatures in this region were rarely less than -20° , winter air temperatures were less than -37°C for several weeks at all sites, leading to an underestimate in I_a for the freezing case. The 8-channel loggers installed at the four pit sites did not have this limitation, enabling the contribution to $I_{a,fr}$ below -37°C to be calculated; these values varied from 50-100 K-d and $I_{a,fr}$ at the single-channel sites were augmented by these amounts. This correction was small, of the order of 2-5 per cent. A similar adjustment was made to correct mean temperatures for this effect (Fig. 2).

Dependence of n on depth of ground temperature sensor

To calculate the n-factor, temperatures are required at the ground surface, yet practically, to avoid the influence of air circulation, the sensor is buried at some small depth.



Figure 6. View of site 93 AG 3, Wrigley Hwy. km 504.7. Ground sensor is buried at arrow; remote sensor is on nearby cut line.

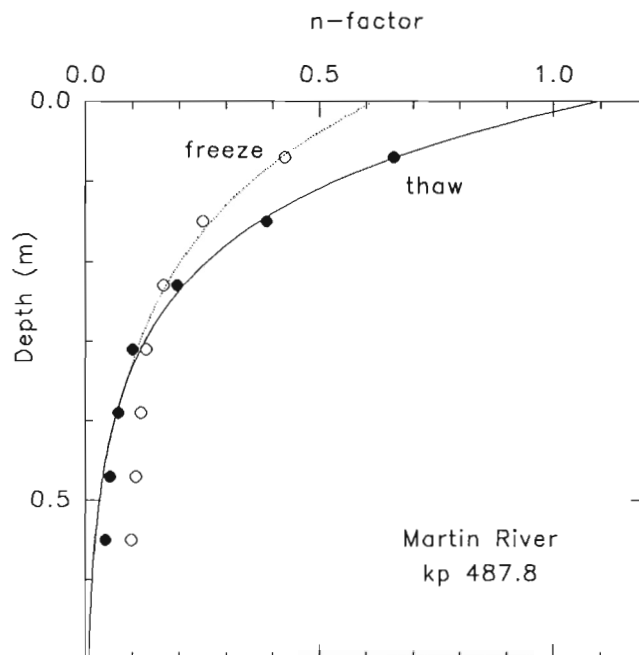


Figure 7. N-factors versus depth at site 92 TT 6, Martin River.

However, ground temperature amplitude decreases exponentially with depth and latent heat of phase change in the soil may introduce non-linearities: the choice of this burial depth may significantly effect the calculated magnitude of the n-factor. Ideally, a vertical profile of sensors positioned at several depths (as from the pit sites) would permit an extrapolation to the ground surface. N-factors were calculated from the time series of temperatures for seven depths at one of the pit sites (Fig. 7): extrapolation to the ground surface indicates that the n-factor for "depth 0 cm" might be 50 per cent or more higher than the value at the upper data point, as taken here. Also, in the field, the position of the ground surface is difficult to identify in many of these environments; the transition from the vegetation mat (moss, grasses, small plants) to the denser "ground surface" can be identified only within 1-2 cm.

Miniature data loggers with internal temperature sensors have been buried consistently at depths 3-7 cm. N-factors calculated from these will underestimate the surface value but will be consistent in portraying trends between thawing and freezing factors at a site, and among sites.

Comparison of n-factors to pre-existing data

Lunardini (1981) tabulated I_a and n-factors from the literature; Arctic data in his collection are summarized and compared to data from the present paper in a plot of I_s is versus I_a (Fig. 8). Data from the literature comprise mostly disturbed or prepared surfaces, and data from natural forest areas of the upper Mackenzie Valley appear to have lower values. Shur and Slavin-Borovski (1993) have produced contour maps of summer n-factors for sandy surfaces without plant cover in the Russian permafrost region.

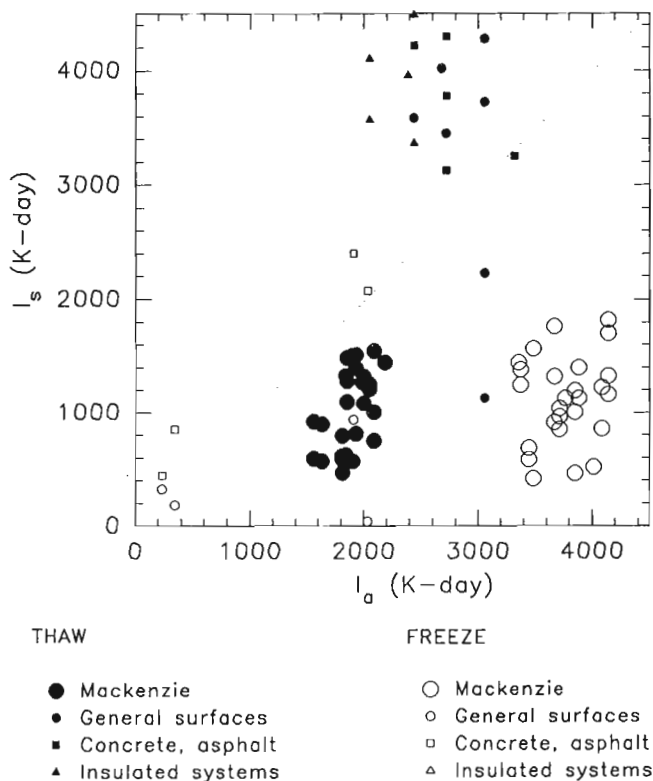


Figure 8. Surface indices versus air indices. Large symbols, Mackenzie Valley, this work; small symbols, other Arctic areas, from Lunardini, 1981. The 1:1 relation is dotted.

N-factors reported here are all less than 1.0, reflecting attenuation of air temperatures at the ground surface by intervening vegetation and snowcover. Thaw season n-factors greater than 1.0 have been reported for ground surfaces such as sand, gravel, and pavements (Lunardini, 1981), suggesting that mean temperatures of such surfaces are higher (equation 4) than mean air temperatures (e.g. due to direct sun exposure).

Application of n-factors

The present tabulation of n-factors is preliminary, primarily because they have been calculated from only one year's data. Several years may be required to assess the natural interannual variability (e.g. Lunardini, 1981, chap. 10.4). Otherwise, these values may be used for thermal calculations and characterization of these sites, for instance to reconcile the maximum depth of the active layer recorded by thaw tubes (Nixon and Taylor, 1994). The response of the ground thermal regime to hypothesized higher (or lower) air temperatures might also be calculated as part of a climate change study.

Application only to these sites is restrictive, and the intent is that these n-factors might be representative of similar sites within the region. "Equivalent sites" might be those having a similar site description or the same forest classification (Table 1). Figures 3, 5, and 6 are photos of three sites studied

here; in a future publication, a more detailed description and photo will be given for each site to facilitate the identification of similar sites in the region.

Jorgenson and Kreig (1988) provide an example of the use of n-factors in an area where forestry, vegetation, and surficial geology have been mapped. They predicted the distribution of discontinuous permafrost in a small area of some 10 km² in Alaska by assigning n-factors to mapped units of forest and vegetation cover. Wright et al. (1994) undertake a similar climate change-permafrost impact prediction at a regional scale in the Mackenzie Valley, using the ESP-NP classification for assigning n-factors.

CONCLUSIONS

1. Preliminary values of 27 n-factors for the thawing and freezing seasons have been calculated at 13 sites in diverse, natural forest areas along the upper Mackenzie River valley between Fort Simpson and Norman Wells, Northwest Territories. N-factors are known to vary from year to year, and confidence in these values will increase when data for subsequent years are analyzed. Preliminary average values are $n_{th} = 0.6 \pm 0.2$, $n_{fr} = 0.2 \pm 0.1$.
2. All n-factors, including those on a steep, south-facing slope, are less than 1.0, indicating that vegetation and snowcover attenuate the effect of air temperatures on the ground surface. At any site, n-factors for the freezing season are much less than for the thawing season because of the additional thermal effect of snowcover.
3. These n-factors may be typical of similarly described forest sites in the region.

ACKNOWLEDGMENTS

Funding was provided by the Geological Survey of Canada under the Green Plan. Logistic support (particularly a boat and motor) was provided in the field by Mr. Pat Wood and staff, Water Resources Branch, Environment Canada, Fort Simpson. V. Allen designed the air temperature masts, M. Nixon provided detailed site descriptions, and F. Wright assisted in the field.

REFERENCES

- Duk-Rodkin, A. and Hughes, O.L.**
1993: Surficial geology, Sans Sault Rapids, District of Mackenzie, Northwest Territories; Geological Survey of Canada, Map 1784A, scale 1:250 000.
- Environment Canada**
1974: Vegetation types of the Mackenzie corridor; Environmental-Social Program, Northern Pipelines, Report no. 73-46, Canadian Forestry Service, Environment Canada, 85 p., appendices, maps.
- Hanley, P.T. and Hughes, O.L.**
1973: Surficial geology and geomorphology of Fort Norman, Carcajou Canyon, Norman Wells and Sans Sault Rapids map areas, District of Mackenzie, Northwest Territories; Geological Survey of Canada, Open File 155, scale 1:125 000.

Hawes, R.J. (comp.)

- 1980a: Surficial geology and geomorphology of Fort Simpson, District of Mackenzie; Geological Survey of Canada, Map 3-1978, scale 1:125 000.
- 1980b: Surficial geology and geomorphology of Camsell Bend, District of Mackenzie; Geological Survey of Canada, Map 9-1978, scale 1:125 000.
- 1980c: Surficial geology and geomorphology of Wrigley Lake, District of Mackenzie; Geological Survey of Canada, Map 13-1978, scale 1:125 000.

Jorgenson, M.T. and Kreig, R.A.

- 1988: A model for mapping permafrost distribution based on landscape component maps and climatic variables; in Proceedings of the Fifth International Conference on Permafrost, v.1, p. 176-182.

Kane, Douglas L., Hinzman, Larry D. and Zarling, John P.

- 1991: Thermal response of the active layer to climatic warming in a permafrost environment; Cold Regions Science and Technology, v. 19, p.111-122.

Lunardini, V.J.

- 1978: Theory of n-factors and correlation of data; in Proceedings, Third International Conference on Permafrost, Natural Research Council of Canada, v. 1, p. 40-46.

Lunardini, V.J. (cont.)

- 1981: Heat transfer in cold climates; Van Nostrand Reinhold, New York, 704 pages.

Nixon, F.M. and Taylor, A.E.

- 1994: Active layer monitoring in natural environments, Mackenzie Valley, Northwest Territories; in Current Research 1994-B; Geological Survey of Canada, p. 27-34.

Nixon, F.M., Taylor, A.E., Allen, V.S. and Wright, J.F.

- 1995: Active layer monitoring in natural environments, lower Mackenzie Valley, Northwest Territories; in Current Research 1995-B; Geological Survey of Canada, this volume.

Shur, Y.L. and Slavin-Borovskiy, V.B.

- 1993: N-factor maps of Russian permafrost region. Sixth International Conference on Permafrost, Beijing, China; South China University of Technology Press, vol. 1, p. 564-568.

Wright, J.F., Smith, M.W. and Taylor, A.E.

- 1994: A hybrid model for predicting permafrost occurrence and thickness; EOS v. 75, no. 44, p. 77 (American Geophysical Union, Fall Meeting, San Francisco, CA).

Geological Survey of Canada Project 920046AT

Active layer monitoring in natural environments, lower Mackenzie Valley, Northwest Territories

F.M. Nixon, A.E. Taylor, V.S. Allen, and F. Wright
Terrain Sciences Division

Nixon, F.M., Taylor, A.E., Allen, V.S., and Wright, F., 1995: Active layer monitoring in natural environments, lower Mackenzie Valley, Northwest Territories; in Current Research 1995-B; Geological Survey of Canada, p. 99-108.

Abstract: Relict active layers in permafrost regions have been interpreted as indicators of past changes in climate (Mackay, 1976). The present active layer above the permafrost should respond to enhanced warming in Arctic areas (Mackay, 1975) as predicted by global circulation models for the next several decades. A transect has been established along the Mackenzie Valley in diverse natural environments to monitor changes in the active layer over this period; 17 multi-instrumented sites between Fort Simpson and Norman Wells have been described previously (Nixon and Taylor, 1994). This past field season, the addition of 14 ground surface and air temperature sensing automatic data loggers were added to 14 of the 46 thaw tube sites installed several years ago to complete instrumentation of the transect between Norman Wells and the Beaufort Sea coast.

Résumé : Les mollisols résiduels dans les régions de pergélisol ont été interprétés comme des indicateurs de changements climatiques antérieurs. Le mollisol actuel, au-dessus du pergélisol, devrait réagir au réchauffement dans les régions arctiques, tel que prédit par les modèles de circulation globale des prochaines décennies. Un transect a été établi le long de la vallée du Mackenzie dans divers milieux naturels pour suivre les changements du mollisol au cours de cette période; 17 emplacements munis de plusieurs instruments entre Fort Simpson et Norman Wells ont été décrits antérieurement. Au cours de la dernière campagne sur le terrain, 14 instruments automatisés de collecte de données sur la température de l'air et de la surface du sol ont été ajoutés à 14 des 46 emplacements dotés depuis plusieurs années de tubes de dégel, pour compléter l'instrumentation du transect entre Norman Wells et la côte de la mer de Beaufort.

INTRODUCTION

Nixon and Taylor (1994) describe a transect along the Mackenzie Valley for long-term monitoring of the thermal character of permafrost and the thickness of the active layer in the context of climate change. In the first phase of implementation described in that paper, multi-instrumented sites were established at 17 locations in discontinuous permafrost of the upper Mackenzie Valley between Fort Simpson and Norman Wells, Northwest Territories; see Taylor (1995) for preliminary analysis of the first year of part of the data. This past field season, instrumentation installed several years ago at 46 sites in the discontinuous to continuous permafrost zone of the lower Mackenzie Valley, between Norman Wells (latitude 65°N) and the Beaufort Sea coast (70°N), was enhanced by the addition of 14 air and ground surface temperature sensing automatic data loggers. This paper describes the completion of this northern section of the transect.

Global circulation models (GCMs) indicate that the predicted increase in air temperatures over the next several decades due to increasing CO₂ concentrations may be greatest in Arctic regions, particularly in winter; predictions are less certain for other climate parameters such as precipitation and snow cover (e.g. Mitchell et al., 1990). These predictions raise concern for the impact on permafrost in Canada's Arctic.

One scenario for environmental change is a deeper penetration of seasonal thaw resulting from global warming of several degrees during the next few decades. Kane et al. (1991) have shown that an increase of 3.5°C over 50 years may double the thickness of the active layer. Under such conditions, a likely impact will be on slope stability, resulting in more active layer detachment slides and retrogressive thaw flows. This in turn will change sediment loads in hydrological systems. Active layer thickening and melting of ground ice will affect active layer hydrology and discharge, potentially altering channel stability, and sediment load conditions (Kane et al., 1991). Where slopes are gentle or absent, penetration

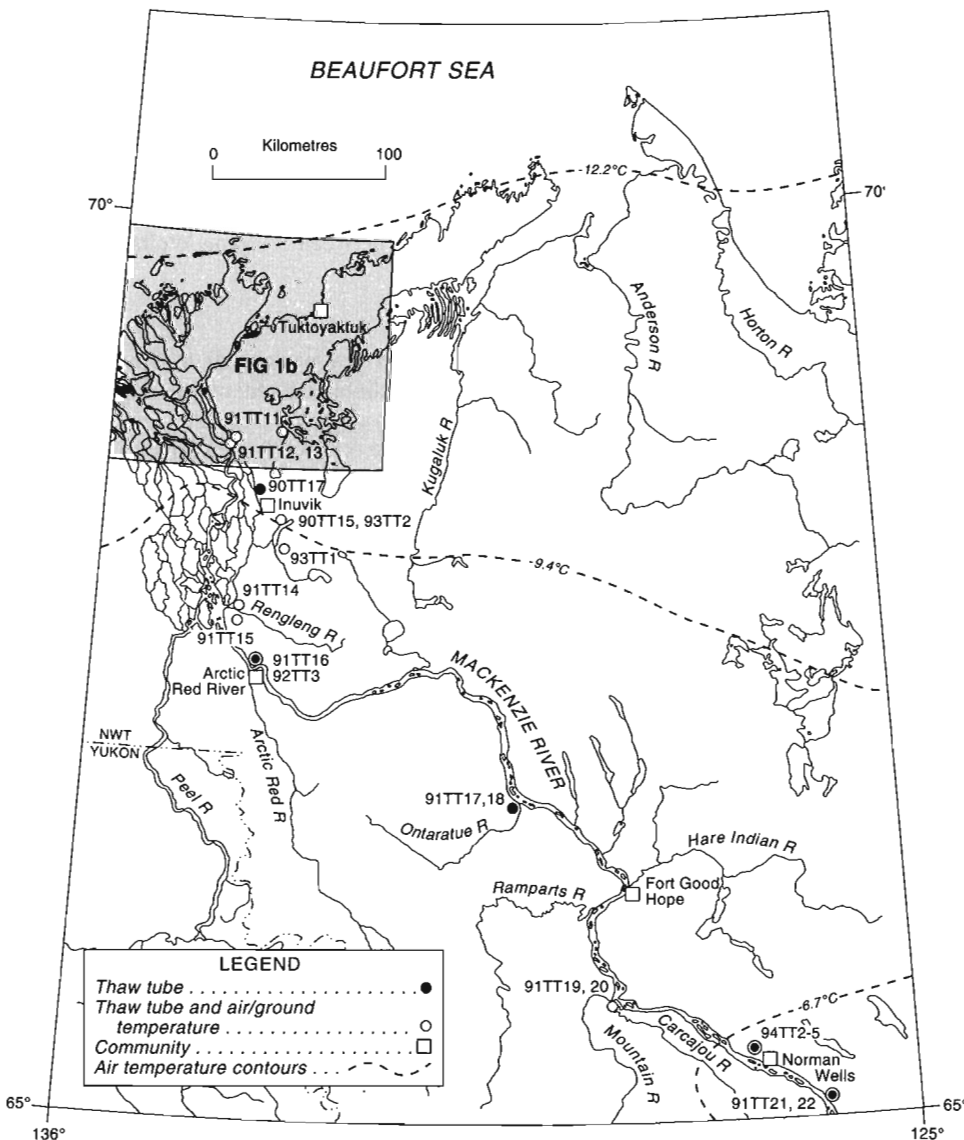


Figure 1a.

Location of instrumented sites, lower Mackenzie Valley, Northwest Territories. Sites are named according to year and first type of principal instrumentation installed, e.g. 90 TT 4, and keyed to Table 1. Annual mean air temperature contours (°C) are from Burns, 1973, Fig. 4.18.

of thaw into ice-rich permafrost may change the capacity to support traffic. Knowledge of how the active layer responds in many situations and how the response is related to widely available or easily measured parameters, may enable a more reliable estimation of impacts for the proposed changes.

Regional setting

The lower Mackenzie River flows northwestward from Norman Wells (Fig. 1a) through mountainous terrain as far as Sans Sault Rapids, below which it winds across broad plains to the Mackenzie Delta (Fig. 1b) north of Arctic Red River. The entire region was glaciated during various advances of Laurentide ice (Hughes, 1986), leaving glacial and proglacial deposits over underlying Paleozoic to Cenozoic rocks (Norris, 1984, and Walter, 1981). Since the last deglaciation, various processes have added to this sedimentary cover, the most spectacular example being the Holocene Mackenzie Delta. All installations for the present study are in these glacial and postglacial sediments and terrains. Materials comprise alluvial and lacustrine silt and sand, deltaic silt and sands, fluvio-glacial sand and gravel, and diamictons of colluvial and glacial origin. Significantly, sites may be covered by varying thicknesses of organic material and are generally forested as far north as Inuvik (Environment Canada, 1974), traversing the boreal forest and the boreal-tundra transition with the Mackenzie Delta-Tuktoyaktuk coastlands lying in the tundra zone (Edlund, 1992).

The lower Mackenzie Valley lies within the zone of extensive to intermediate discontinuous permafrost (south of Arctic Red River and in the Holocene Mackenzie Delta) and within deep, continuous permafrost north to the Beaufort coast (Heginbottom and Radburn, 1992). The -6.7°C annual

mean daily air temperature isotherm crosses the valley just north of Norman Wells and the -9.4° and -12.2°C isotherm passes just south and north, respectively, of the Mackenzie Delta (Fig. 1a; Burns, 1973, Fig. 4.18). Mean surface temperatures are, however, some 2° to 8° higher than mean air temperatures in the area, a reflection of the influence of winter snow cover and vegetation in moderating the ground thermal regime (Judge, 1973, 1975). Permafrost thicknesses reach 52-143 m at Norman Wells, 65-95 m in the Holocene Mackenzie Delta, and up to 660 m in the Tuktoyaktuk coastlands along the Beaufort coast (Judge, 1975; Judge et al., 1987; Taylor et al., 1982). The abundance of ground ice in this thermal environment is variable (Heginbottom and Radburn, 1992) but can be both high and near the surface, particularly in the Tuktoyaktuk coastlands area (Pollard and French, 1980).

SITE SELECTION CRITERIA

In the zone of discontinuous permafrost, sites were chosen in areas underlain by permafrost, as determined by probing. As the development of the active layer is affected by meteorological, biological, and geological factors, sites have been chosen to reflect the diversity of these environments, by reference to available surficial geology (Hanley and Hughes, 1973; Duk-Rodkin and Hughes, 1992a, b, c, 1993; Rampton, 1987) and forestry and tundra vegetation maps (Environment Canada, 1974). Emphasis was placed on finding representative natural areas remote from recent disturbance. Logistic considerations required ease of foot access from the Mackenzie River, the sea coast, or roads, and availability of a small quantity of water for jet-drilling thaw tube installations.

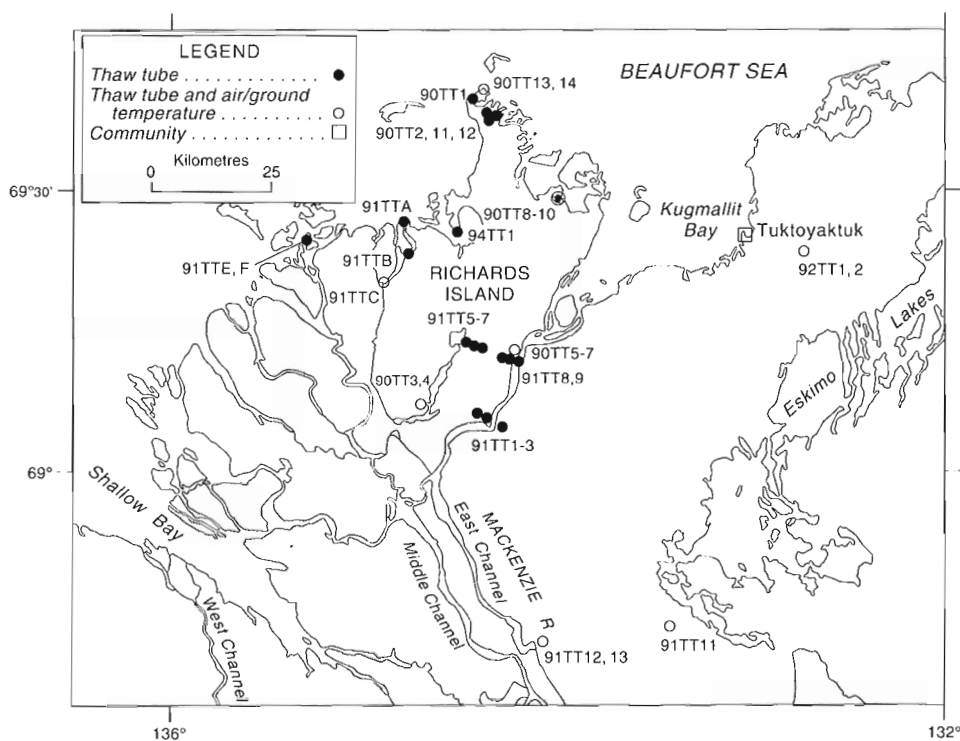


Figure 1b.

Location of instrumented sites, Mackenzie Delta area. Site names as for Figure 1a.

Every effort was made to minimize surficial disturbance to the vegetation and soils during the installations, because of the effect of terrain disturbance on the thermal regime. Holes for thaw tubes were jet drilled with a light, back-packable water pump, using 2.5 cm diameter pipe and a maximum flow rate of 70 litres per minute. Figures 2 and 3 show sites in the Mackenzie Delta several years after jet-drilling. Figures 1a, and b show site locations, and Table 1 includes a site description and list of instrumentation.

DESCRIPTION OF SITE INSTRUMENTATION

General site description

Permafrost temperatures and the thickness of the active layer depend on the integrated effects of air temperature, snow cover, vegetation, soil properties, and drainage (e.g. Judge, 1973, 1975), underlining the importance of a description or measurement of these parameters at each site. Landform and

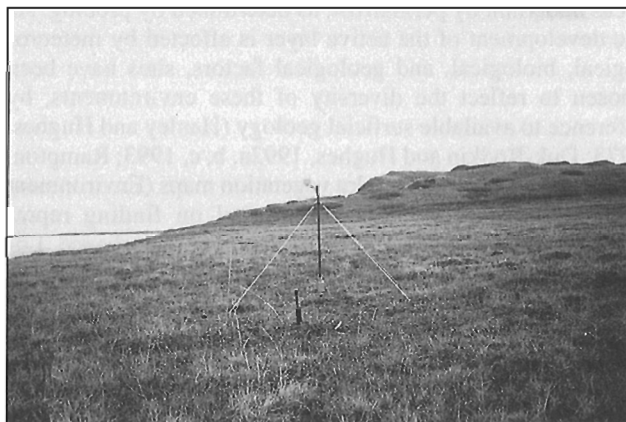


Figure 2. View of site 90 TT 9, Coral Bay, Mackenzie Delta, four years after jet-drilling the hole for the thaw tube with heave scribe (foreground). The ground temperature data logger is buried near the base of the air temperature screen.

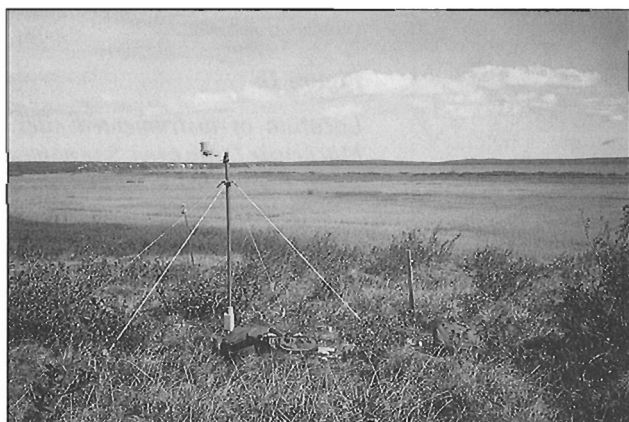


Figure 3. View of site 90 TT 6, Lousy Point, Mackenzie Delta.

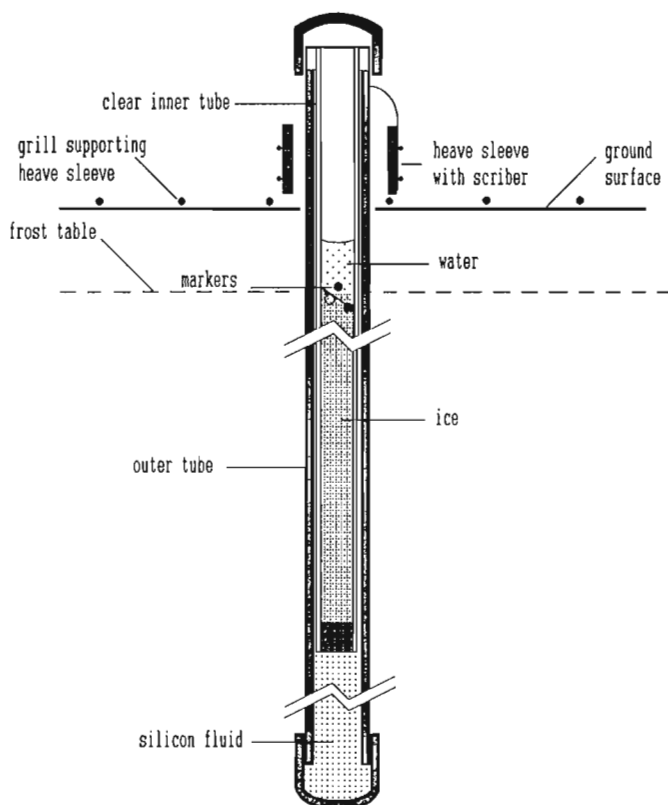
surface morphology were described, slope and aspect were estimated, and elevation was measured with an aneroid barometer relative to the Mackenzie River or sea level. A characterization of vegetation included identification, and estimation of height of shrubs and chest diameter of trees in the immediate vicinity of the installations. Estimates of percentage ground cover were made and plants identified, approximating species level for vascular plants.

Installations of most thaw tubes were made in late June-August 1990-1992. A 1.2 m stainless steel frost probe was used at each site to measure the depth of the active layer at that time and subsequently. A pit was dug to the frost table and the materials were described, and soil samples were taken for laboratory determination of moisture content and texture.

Thaw tubes (TT) and heave/subsidence recorder (48 sites)

Maximum annual depth of thaw is measured using a modified version of a frost tube developed by Mackay (1973). These consist of nested plastic tubes: an outer 2.5 cm diameter PVC tube is anchored in permafrost to a depth of about 4 m below surface, and an inner clear tube containing water and extending below maximum thaw depth, slips into the outer tube and is held at a reference height by a collar (Fig. 4). After the water

Thaw Depth Monitoring Tube



after J. R. Mackay, 1973

Figure 4. Schematic of thaw depth monitoring tube, adapted from Mackay (1973).

Table 1. Location and description of active layer monitoring sites, lower Mackenzie Valley

Site	Location	Installations	Elevation (m)	Situation
Francis Creek (91 TT 21, 22)	65°11'52" 126°27'56"	TT, 1991 AG, 1993	54 m, 51 m	alluvial terrace cut into stony silt till ⁵ , 15 cm and 30 cm organic cover respectively open spruce – sphagnum transition ⁷ , site near river is riparian spruce and tall shrub, complete cover
Norman Wells AES (93 AG 10)	65°17'35" 126°45'40"	AG, 1993		gently sloping till plain between Discovery Ridge and River ⁵ low, open black spruce and hardwoods over moss plus cleared AES compound
Norman Wells, IPL (93 AG 11)	65°17'35" 126°53'08"	AG, 1993		alluvial terrace above modern river ⁵ open black spruce and hardwoods over moss
Norman Wells, KP2 (94 TT 5)	65°17'54" 126°50'43"	TT, 1994	65 m	on low rise in thermokarst lacustrine plain ⁵ , clay under 30 cm organic cover, fair drainage open crown spruce – sphagnum transition ⁷ , 100% cover
Mountain River (91 TT 20)	65°40'29" 128°49'37"	TT, 1991 AG, 1993	38 m	low terrace in stony sand (20) or silt (19) on alluvial plain ⁴ , 15 cm and >35 cm organic cover respectively
(91 TT 19)	65°39'41" 128°46'10"	TT, 1991 AG, 1994	39 m	#19 in open spruce with hardwoods ⁷ , 98% ground cover; #20 under hardwood thicket
Grand View (91 TT 17,18)	66°47'13" 130°07'10"	TT, 1991	22 m, 24 m	alluvial terrace surfaces ¹ near the mouth of small stream, first site in organic silt, well drained, other with 15 cm organic cover, fair drainage #17 in open riparian spruce and hardwood, #18 in open spruce-sphagnum transition ⁷
Arctic Red River, floodplain (91 TT 16)	67°29'03" 133°45'47"	TT, 1991 AG, 1994	14 m	bar surface opposite mouth of Arctic Red River in alluvial silt, well drained open riparian pioneer, 75% ground cover ⁷
Arctic Red River, till plain (92 TT 3)	67°29'44" 133°45'47"	TT, 1992	≈30 m	rolling till cover ² thin at site under 10 cm litter, fair drainage open spruce – sphagnum transition ⁷
Rengleng River mouth (91 TT 14)	67°47'42" 134°07'34"	TT, 1991 AG, 1994	13 m	alluvial plain ³ at mouth of Rengleng River in well drained silty sand tall riparian spruce hardwood, complete ground cover, moderate canopy ⁷
Rengleng Lake (91 TT 15)	67°45'58" 134°04'43"	TT, 1991 AG, 1994	8 m	on margin of alluvial plain ³ in moist silty clay tall open riparian spruce hardwood, 95% ground cover ⁷
Caribou Creek (93 TT 1)	68°06'39" 133°28'29"	TT, 1993	≈30 m	blanket till cover ⁶ open small black spruce over moss ⁷
Inuvik airport (90 TT 15)	68°18'57" 133°25'51"	TT, 1990	83 m	bog between low till ridges ⁶ , organics 2.5 m thick scattered small spruce on polygonized shrub lichen surface ⁷
Havikpak Creek (93 TT 2)	68°19'13" 133°30'48"	TT, 1993	≈80 m	till or colluvium in valley between bedrock and till ridges ⁶ open black spruce over shrub lichen ⁷
Inuvik delta site (90 TT 17)	68°24'59" 133°47'13"	TT, 1990	5 m	delta surface between channel and thermokarst pond, material organic silt, well drained open high shrub on recent alluvium ⁷

Table 1 (cont.)

Site	Location	Installations	Elevation (m)	Situation
Trail Valley Creek (91 TT 11)	68°44'13" 133°29'15"	TT, 1991	53 m	irregular terrace in valley of Trail Valley Creek, fine grained colluvium ⁶ under 10 cm organics upland low shrub ⁷ , complete cover
Reindeer Station (91 TT 12)	68°41'24" 134°06'18"	TT, 1991 AG, 1994	152 m	plateau above Reindeer Station, till plain ⁶ , fine material in frost hummock upland low shrub ⁷ , bare hummock surfaces
Williams Island (91 TT 13)	68°41'03" 134°06'18"	TT, 1991 AG, 1994	5 m	delta surface on bar of East Channel, organic silt to 85 cm, well drained high shrub on recent alluvium ⁷
YaYa Lake (90 TT 3,4)	69°08'44" 134°42'45"	TT, 1990 AG, 1994	40 m, 10 m	hill top and basin on ice contact sand and gravel upland low shrub ⁷ , 80% cover
Swimming Point (91 TT 1)	69°06'30" 134°23'56"	TT, 1991	8 m	#1 on outwash terrace ⁶ sand with 10 cm organic cover, fair drainage; #2 on floodplain over outwash, fair drainage, and #3 on slope of ice contact ⁶
(91 TT 2)	69°06'35" 134°22'50"	TT, 1991	3 m	sand covered by 30 cm organics, well drained
(91 TT 3)	69°06'31" 134°20'53"	TT, 1991	11 m	#1+3 under upland low shrub vegetation with complete cover; #2 covered by high shrub on recent alluvium
Lousy Point (90 TT 5)	69°13'06" 134°17'05"	TT, 1990 AG, 1994	39 m	hill tops and ridges varying distances from East Channel on ice contact sands ⁶
(91 TT 5)	69°14'27" 134°25'52"	TT, 1991	53 m	upland low shrub ⁷ , complete cover
(91 TT 7)	69°14'26" 134°24'13"	TT, 1991	37 m	
(91 TT 6)	69°14'28" 134°25'09"	TT, 1991	23 m	thermokarst depressions in ice contact terrain ⁶ , lacustrine silt to several metres
(91 TT 9)	69°12'58" 134°17'40"	TT, 1991	16 m	low shrub polygonized wetlands ⁷ , complete cover
(91 TT 8)	69°13'35" 134°20'12"	TT, 1991	≈50 m	hill slope on till ⁶ , material and vegetation similar to ice contact high sites
(90 TT 6)	69°13'01" 134°16'40"	TT, 1990 AG, 1994	9 m	outwash terrace above Mackenzie floodplain ⁶ , 25 cm organics over sand upland low shrub ⁷ , complete cover
(90 TT 7)	69°13'04" 134°16'25"	TT, 1990	1 m	marginal bar on Mackenzie floodplain, silt under shallow water sedge and grass with scattered shrubs on recent alluvium ⁷ , complete cover
Involuted Hill (92 TT 1)	69°28'22" 132°37'37"	TT, 1992 AG, 1994	25 m	top of till-covered ice-cored plateau ⁶ , 20 cm organic, well drained upland low shrub ⁷ , complete cover
(92 TT 2)	69°28'27" 132°38'04"	TT, 1992 AG, 1994	4 m	lacustrine plain in thermokarst basin ⁶ , fine grained material under 10 cm organics wetland low shrub ⁷

Site	Location	Installations	Elevation (m)	Situation
Mason Bay (90 TT 8)	69°31'48" 134°00'57"	TT, 1990	14 m	thermokarst-altered till veneer over thick sand ⁶ , varying distance from coast, coastal site 9 under 90 cm organics
(90 TT 9)	69°31'51" 134°00'21"	TT, 1990 AG, 1994	4 m	
(90 TT 10)	69°31'42" 134°02'15"	TT, 1990		dryas, lichen, low shrub on variable polygonized terrain ⁷ , 75-85% cover on earth hummocks at 8+10, complete at 9
North Point (90 TT 2)	69°39'46" 134°23'07"	TT, 1990	29 m	thermokarst-altered till veneer over thick sand ⁶ , varying elevation and distance from coast, mixture of organics + silt to 45 cm in #2+11, to 80 cm in #12 and to 110 cm in 94-1
(90 TT 11)	69°39'35" 134°22'34"	TT, 1990	16 m	
(90 TT 12)	69°39'25" 134°21'44"	TT, 1990	3 m	
(94 TT 1)	69°29'07" 134°33'43"	TT, 1994		#2+11 dryas, lichen, low shrub on variable polygon terrain; #12 wetland low shrub tundra; 94-1 low shrub with grass and sedge ⁷ , 95% to complete cover
North Head (90 TT 1)	69°42'53" 134°29'02"	TT, 1990	17 m	most northerly coastal situation on thermokarst till veneer over thick sand ⁶ , 35-40 cm organic cover, varying elevation and distance from coast
(90 TT 13)	69°43'18" 134°27'14"	TT, 1990 AG, 1994	~3 m	
(90 TT 14)	69°43'07" 134°26'29"	TT, 1990 AG, 1994	15 m	dryas, lichen, low shrub on varying polygon terrain ⁷ , 75% cover at #14, others complete
Outer Delta (91 TT A)	69°28'53" 134°49'43"	TT, 1991	all <2 m	on low Holocene delta surfaces ⁹ in silt and fine sand variously exposed to the sea
(91 TT B)	69°24'36" 134°50'35"	TT, 1991		A is on flat polygonized wetland under sedge, grass with low shrub, 100% cover; B+C are recent alluvium under high shrubs, 60% cover; E+F are wetlands under grass and sedge with low shrubs ⁷ , covered by shallow water
(91 TT C)	69°22'09" 134°56'55"	TT, 1991 AG, 1994		
(91 TT E)	69°26'34" 135°21'53"	TT, 1991		
(91 TT F)	69°26'55" 135°20'22"	TT, 1991		

¹ (after Duk-Rodkin and Hughes, 1992a)

² (after Duk-Rodkin and Hughes, 1992b)

³ (after Duk-Rodkin and Hughes, 1992c)

⁴ (after Duk-Rodkin and Hughes, 1993)

⁵ (after Hanley and Hughes, 1973)

⁶ (after Rampton, 1987)

⁷ (after Environment Canada, 1974)

in the inner tube freezes to the frost table, above maximum thaw depth, a coloured glass bead 3 mm in diameter is dropped through the water column to rest on the ice surface. As thaw progresses downward, the bead follows the water/ice interface until maximum depth is reached. On refreezing, it is incorporated into the ice and records the maximum depth of thaw that year. Field and laboratory trials with size and density of bead resulted in a choice that resists movement with a freezing front. Next season prior to maximum thaw, the installation is visited and the inner tube raised to measure the depth of the bead and to introduce a bead of different colour (silicone fluid in the outer tube prevents the tubes from freezing together). Observations are made of the bottom of the inner tube to assure expansion due to refreezing of the water column is upward, thus not affecting the position of the bead. Expansion and contraction of the ice column containing a bead, due to extremes of ground temperature experienced near the surface, have been observed and are less than 1 cm. Frost table probing at each visit is compared to the ice/water interface in the tube and is normally within the range or only a few centimetres outside, suggesting that the frost table in the ground and tube correspond.

To measure the maximum ground surface heave and subsidence over the year, a grill supporting a scribing sleeve is set on the ground surface such that it encircles, but is free of, the outer tube that is anchored in permafrost. As the surface moves up or down due to active layer processes, this sleeve scratches a painted section on the outer tube to record maximum heave and subsidence between observations.

Air temperature-ground temperature sensors (AG) (14 sites)

To monitor for direct evidence of climate change, and for future analysis of the air-ground interaction, an air temperature time-series is required. Also, an overall thermal transfer function between air and ground is useful in regional studies requiring an engineering-level quantification of the influence of various vegetation, forest types, and snow cover on the ground thermal regime. One such function, the n-factor, is defined in terms of an air temperature and ground temperature time series; currently, there are few n-factors published for natural areas (Taylor, 1995), as the emphasis has been more on pavements and cleared areas (Lunardini, 1978).

A 6-plate 12 cm diameter radiation shield (R.M. Young, model 41301-5) was mounted 1.5 m above the ground surface at each site. Air temperatures are measured by a thermistor in the shield that is connected to a single-channel miniature data logger (Onset Computer Corp., HOBO model) in the lower part of the mast (Fig. 5). A similar data logger with built-in thermistor is fitted inside a "35 mm" film canister (53 mm x 32 mm), sealed with silicone rubber and buried near the base of the air temperature mast at a nominal depth of 3-7 cm to measure near-surface ground temperatures. This depth of burial is generally within dense peat at most of the installations, and within mineral soil in the outer Mackenzie Delta. The miniature data logger has a range of -37° to 46°C and a resolution of 0.025 K; temperatures are recorded every five hours for a year. This inexpensive design appears to be

sufficiently robust, based on the experience of similar installations made in the upper Mackenzie Valley the previous year. Two Mackenzie Delta installations are shown in Figures 2 and 3.

DISCUSSION

Sites along the entire Mackenzie Valley transect will be revisited at least annually for data collection and servicing: in summer visits, the depth of thaw will be probed and photos taken, and when early spring visits can be made, snow depth will be measured. Changes in site features can be captured in the photographic record of each visit. In a few years, the latitudinal variability of active layer development should be

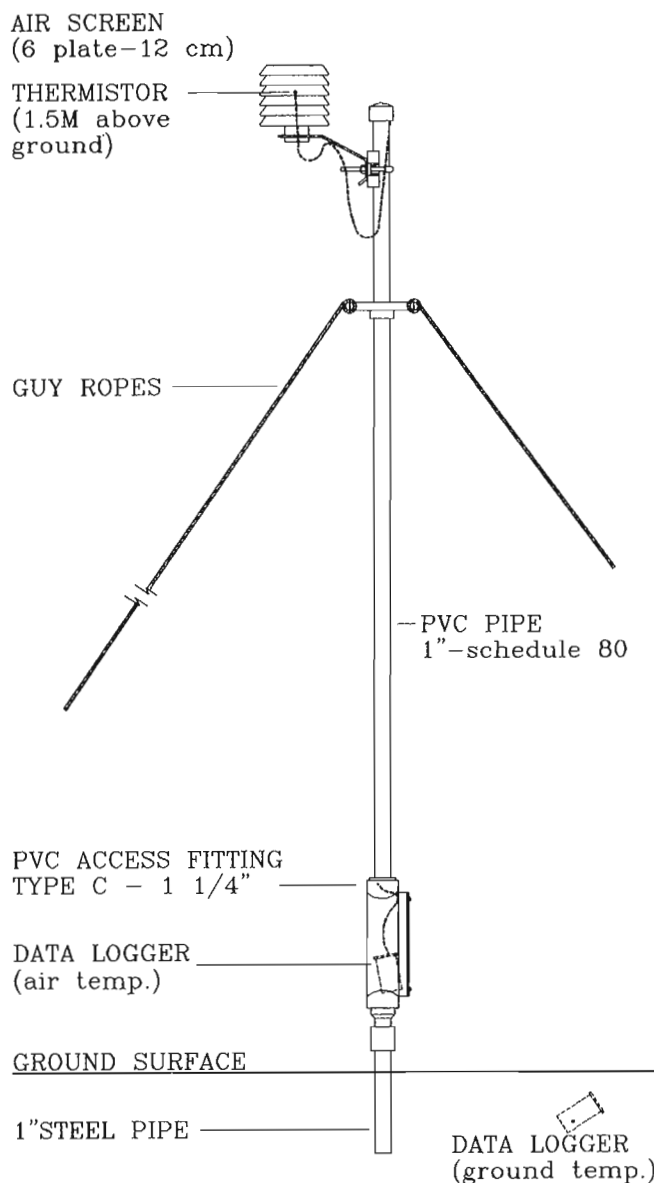


Figure 5. Schematic of air temperature mast and ground surface temperature installation.

established; in later years, any temporal variability should emerge and provide the opportunity to correlate with air temperatures and prediction from global circulation models.

This project is undertaken under the Integrated Research and Monitoring Area program of Terrain Sciences Division, Geological Survey of Canada, and is part of the Mackenzie Basin Impact Study, Environment Canada (Cohen, 1991, in press). Site selection and instrumentation have been coordinated with these and other studies already underway in this region (e.g. Tarnocai and MacInnes, 1993).

CONCLUSIONS

Global circulation models predict that climate warming over the next several decades may be greatest in Arctic regions and other studies predict a substantial impact on the active layer and near-surface permafrost. A 1300 km multi-instrumented transect has been established in natural areas along the Mackenzie River, Northwest Territories, to monitor maximum active layer thickness and the air-ground thermal interaction.

1. Sixty-two sites have been established. Of these, 17 are in the discontinuous permafrost zone of the upper Mackenzie Valley between Fort Simpson and Norman Wells (Nixon and Taylor, 1994), and 45 lie in the discontinuous to continuous permafrost zone of the lower Mackenzie Valley and are described here.
2. The long transect crosses several bioclimatic zones as well as permafrost boundaries, and the sites have been selected to provide maximum variety of natural situations while remaining accessible in this transportation corridor. The active layer is the interface between permafrost and both the atmosphere and biosphere including many human activities. As such, it is important to understand how it varies regionally and how it will respond to environmental change.
3. Instrumentation for the whole transect consists of 57 thaw tubes (TT) and 36 air temperature screens and ground surface temperature sensors with automatic data loggers (AG), most at thaw tube sites. Some additional air and ground temperature records are available for sites shared with other research projects.
4. The variety of instrumentation will contribute to a quantitative analysis of active layer development and processes, and permafrost-climate and permafrost-climate change interaction.

ACKNOWLEDGMENTS

Logistic support was provided by the Polar Continental Shelf Project, Natural Resources Canada, and the Inuvik Scientific Research Centre, Government of the Northwest Territories. Funding was provided by the Geological Survey of Canada under Green Plan, and by Panel on Energy Research and Development, Natural Resources Canada.

REFERENCES

- Burns, R.M.**
1973: The climate of the Mackenzie Valley-Beaufort Sea; Atmospheric Environment Service, Environment Canada, Climatological Studies no. 24, 227 pages.
- Cohen, S.J.**
1991: Regional impacts of projected global warming: a research proposal for the Mackenzie Basin; Proceedings, 2nd Symposium on global change studies, American Meteorological Society.
- Cohen, S.J. (ed.)**
in press: Mackenzie Basin impact study; Environment Canada, Interim Report #2, Downsview, Ontario.
- Duk-Rodkin, A. and Hughes, O.L.**
1992a: Surficial geology, Ontaratie River, District of Mackenzie, Northwest Territories; Geological Survey of Canada, Map 1742A, scale 1:250 000.
1992b: Surficial geology, Arctic Red River, District of Mackenzie, Northwest Territories; Geological Survey of Canada, Map 1746A, scale 1:250 000.
1992c: Surficial geology, Fort McPherson-Bell River, District of Mackenzie, Northwest Territories; Geological Survey of Canada, Map 1745A, scale 1:250 000.
1993: Surficial geology, Sans Sault Rapids, District of Mackenzie, Northwest Territories; Geological Survey of Canada, Map 1784A, scale 1:250 000.
- Edlund, S.A.**
1992: Climate change and its effect on Canadian Arctic plant communities; in Proceedings: Arctic environment, past present and future symposium, (ed.) Ming-ko Woo and Denis J. Gregor; McMaster University, Hamilton, Ontario, Canada, p.121-133.
- Environment Canada**
1974: Vegetation types of the Mackenzie corridor; Environmental-Social Program, Northern Pipelines, Report no. 73-46, Canadian Forestry Service, Environment Canada, 85 p., appendices, maps.
- Hanley, P.T. and Hughes, O.L.**
1973: Surficial geology and geomorphology of Fort Norman, Carcajou Canyon, Norman Wells, and Sans Sault Rapids map areas, District of Mackenzie, Northwest Territories; Geological Survey of Canada, Open File 155, scale 1:125 000.
- Heginbottom, J.A. and Radburn, L.K. (comp.)**
1992: Permafrost and ground ice conditions of northwestern Canada; Geological Survey of Canada, Map 1691A, scale 1:1 000 000.
- Hughes, O.L.**
1986: Quaternary chronology of Yukon Territory and western District of Mackenzie; in Correlation of Quaternary deposits and events around the margin of the Beaufort Sea: Contributions from a joint Canadian-American workshop, April 1984, (ed.) J.A. Heginbottom, and J-S. Vincent; Geological Survey of Canada, Open File 1237, p.13-17.
- Judge, A.S.**
1973: The thermal regime of the Mackenzie Valley: observations of the natural state; Environmental-Social Program, Northern Pipelines, Report no. 73-38, Earth Physics Branch, Energy, Mines, and Resources Canada, 177 p.
1975: Geothermal studies in the Mackenzie Valley by the Earth Physics Branch; Energy, Mines, and Resources Canada, Earth Physics Branch, Geothermal Series no. 2, 12 p.
- Judge, A.S., Pelletier, B.R., and Norquay, I.**
1987: Permafrost base and distribution of gas hydrates; in Marine Science Atlas of the Beaufort Sea - geology and geophysics, (ed.) B.R. Pelletier; Geological Survey of Canada, Miscellaneous Report no. 40, map 39.
- Kane, D.L., Hinzman, L.D., and Zarling, J.P.**
1991: Thermal response of the active layer to climatic warming in a permafrost environment; Cold Regions Science and Technology, v. 19, p.111-122.
- Lunardini, V.J.**
1978: Theory of n-factors and correlation of data; in Proceedings, Third International Conference on Permafrost, Natural Research Council of Canada, v. 1, p. 40-46.
- Mackay, J.R.**
1973: A frost tube for the determination of freezing in the active layer above permafrost; Canadian Geotechnical Journal, v. 10, p.392-396.

Mackay, J.R. (cont.)

1975: The stability of permafrost and recent climatic change in the Mackenzie Valley, N.W.T.; in Report of Activities, Part B; Geological Survey of Canada, Paper 75-1B, p. 173-176.

1976: Ice-wedges as indicators of recent climatic change, western Arctic coast; in Report of Activities, Part A; Geological Survey of Canada, Paper 76-1A, p. 233-234.

Mitchell, J.F.B., Manabe, S., Meleshko, V., and Tokioka, T.

1990: Equilibrium climate change – and its implications for the future; in Climate change, The IPCC Assessment, (ed.) J.T. Houghton, G.J. Jenkins, and J.J. Ephraums; Cambridge Press, New York, p. 131-172.

Nixon, F.M. and Taylor, A.E.

1994: Active layer monitoring in natural environments, Mackenzie Valley, Northwest Territories; in Current Research 1994-B, Geological Survey of Canada, p. 27-34.

Norris, D.K.

1984: Geological map of the northern Yukon and northwest District of Mackenzie; Geological Survey of Canada, Map 1581A, scale 1:5 000 000.

Pollard, W.H. and French, H.M.

1980: A first approximation of the volume of ground ice, Richards Island, Pleistocene Mackenzie delta, Northwest Territories, Canada; Canadian Geotechnical Journal, v. 17, p.509-516.

Rampton, V.N.

1987: Surficial geology, Tuktoyaktuk Coastlands, Northwest Territories; Geological Survey of Canada, Map 1647A, scale 1:500 000.

Tarnocai, C. and MacInnes, K.L.

1993: Soil climates of the Mackenzie Valley, N.W.T., appendix D; in Norman Wells to Zama pipeline permafrost and terrain research and monitoring program: annual progress report to DIAND and IPL, Land Resources Division Internal Report.

Taylor, A.E.

1995: Field measurements of n-factors for natural forest areas, Mackenzie Valley, Northwest Territories; in Current Research 1995-B, Geological Survey of Canada, this volume.

Taylor, A.E., Burgess, M., Judge, A.S., and Allen, V.S.

1982: Canadian geothermal data collection - northern wells 1981; Energy, Mines, and Resources Canada, Earth Physics Branch, Geothermal Series no. 13, 153 pages.

Walter, D.J.

1981: Geological map of the northern Interior Plains, northwestern District of Mackenzie; Geological Survey of Canada, Map 1498A, scale 1:500 000.

Geological Survey of Canada Project 920046LD

Cretaceous and Tertiary fossils discovered in kimberlites at Lac de Gras in the Slave Province, Northwest Territories

W.W. Nassichuk and D.J. McIntyre

Institute of Sedimentary and Petroleum Geology, Calgary

Nassichuk, W.W. and McIntyre, D.J., 1995: Cretaceous and Tertiary fossils discovered in kimberlites at Lac de Gras in the Slave Province, Northwest Territories; in Current Research 1995-B; Geological Survey of Canada, p. 109-114.

Abstract: Fossils from mudstone and siltstone lithoclasts in 13 kimberlite pipes in the Lac de Gras area include well preserved dinoflagellates, pollen, spores, wood, and teleost (ichthyodectid) fish parts. The fossils are indicative of marine and marginal-marine environments for the Cretaceous (Albian-Maastrichtian) interval and nonmarine, possibly lacustrine, environments for the lowermost Tertiary (Paleocene). They are the first evidence that shallow transgressive seas covered much of the Slave Province during Cretaceous time and necessitate revision of paleogeographic maps in northern Canada. Indeed, from middle to Late Cretaceous time, the Western Interior Seaway appears to have extended nearly 400 km farther east than previously shown. The kimberlite pipes were emplaced in early Tertiary time. Thermal maturation of organic matter (spores and wood) from both crater and diatreme facies in several kimberlite pipes suggests that the fossils were exposed to relatively low temperatures following deposition and ultimate incorporation in kimberlite pipes.

Résumé : Des fossiles provenant de lithoclastes de mudstone et de siltstone prélevées dans 13 cheminées de kimberlite dans la région du lac de Gras comprennent des dinoflagellés, du pollen, des spores, des débris ligneux et des parties de téléostéen (ichthyodectidés) bien préservés. Ces fossiles attestent de milieux marins et épicontinentaux pendant l'intervalle du Crétacé (Albien-Maastrichtien) et de milieux non marins, peut-être lacustres, pendant le Tertiaire basal (Paléocène). Ils constituent les premières preuves de la présence de mers transgressives peu profondes qui recouvraient la majeure partie de la Province des Esclaves au Crétacé et ils rendent nécessaire la révision des cartes paléogéographiques du Nord canadien. De fait, depuis le Crétacé moyen jusqu'au Crétacé tardif, le Chenal intérieur de l'Ouest semble avoir été plus étendu, soit près de 400 km plus à l'est qu'indiqué précédemment. Les cheminées de kimberlite sont apparues au début du Tertiaire. La maturation thermique de la matière organique (spores et bois) provenant de faciès tant de cratère que de diatrème dans plusieurs cheminées de kimberlite laisse croire que les fossiles ont été exposés à des températures relativement basses à la suite de leur dépôt et de leur incorporation finale dans les cheminées de kimberlite.

INTRODUCTION

In 1991, diamonds were discovered in a kimberlite pipe at Point Lake in the Slave Province, about 300 km north of Yellowknife. Since then, at least 40 kimberlite pipes, many of them diamondiferous, have been discovered in the area. Most of those kimberlites were discovered by the BHP-Dia Met Joint Venture in the vicinity of Lac de Gras, but discoveries were also made by other companies farther south, just north of the eastern tip of MacKay Lake and farther north, just east of Yamba Lake (Pell, 1994; Fig. 1). The history of diamond discovery in the area, as well as the significance of indicator mineral geochemistry to diamond exploration, have been succinctly reviewed by Fipke et al. (in press).

Diamond exploration in the Slave Province has led to the highly important discovery of Mesozoic (Cretaceous) and Tertiary (Paleocene) fossils preserved within xenoclasts of sedimentary strata in 13 kimberlite pipes. In a report in the Northern Miner (Sept. 20, 1993), the authors first indicated that fossil dinoflagellates, pollen, spores and teleost fish remains, ranging in age from latest Early Cretaceous (Albian) to early Tertiary (Paleocene), were recovered from two pipes in the Lac de Gras area. Thus, the time of emplacement of the pipes had to post-date the youngest fossils in the pipes. In the same Northern Miner report, R.O. Moore from BHP Minerals Canada indicated that rubidium-strontium data from mica (phlogopite) and whole rock samples from a pipe in the Lac de Gras area suggest emplacement 52 ± 1.2 million years ago; that is, in early Tertiary (Eocene) time according to the time

scale of Harland et al. (1990). Accordingly, paleontological and rubidium-strontium data for the time of emplacement of the pipes appear to be mutually supportive. Subsequently, additional fossils (mainly dinoflagellates, pollen, spores) were recovered from mudstone xenoliths in core from other pipes in the Lac de Gras area and from pipes east of Yamba Lake. In both areas, fossil wood was also recovered from both the crater and diatreme facies in a number of pipes.

Fossils in this report were recovered from core provided by the BHP-Dia Met Joint Venture in 1992 and 1993. During the 1994 field season, one of us (WWN) participated in collecting samples for micropaleontological study and fossilized wood from large-diameter drill cuttings at a Joint Venture field camp north of Lac de Gras.

The purpose of this preliminary report is simply to record the presence of marine Cretaceous and nonmarine Tertiary fossils in kimberlites in the Slave Province and to advise that several research activities are currently underway on the fossils and that data will be released in scientific journals. We will identify and classify the fossils and employ them to establish biostratigraphic correlation with Cretaceous and Tertiary successions elsewhere in northern and western Canada. The newly discovered Cretaceous and Tertiary fossils are essential for refining the paleogeography of those systems in northern Canada. Further, we hope to determine, even more precisely, the time of emplacement of kimberlites in the Slave Province to assist in regional geotectonic interpretations. Finally, we will continue to assess the temperature of the kimberlites at the time of emplacement through studies

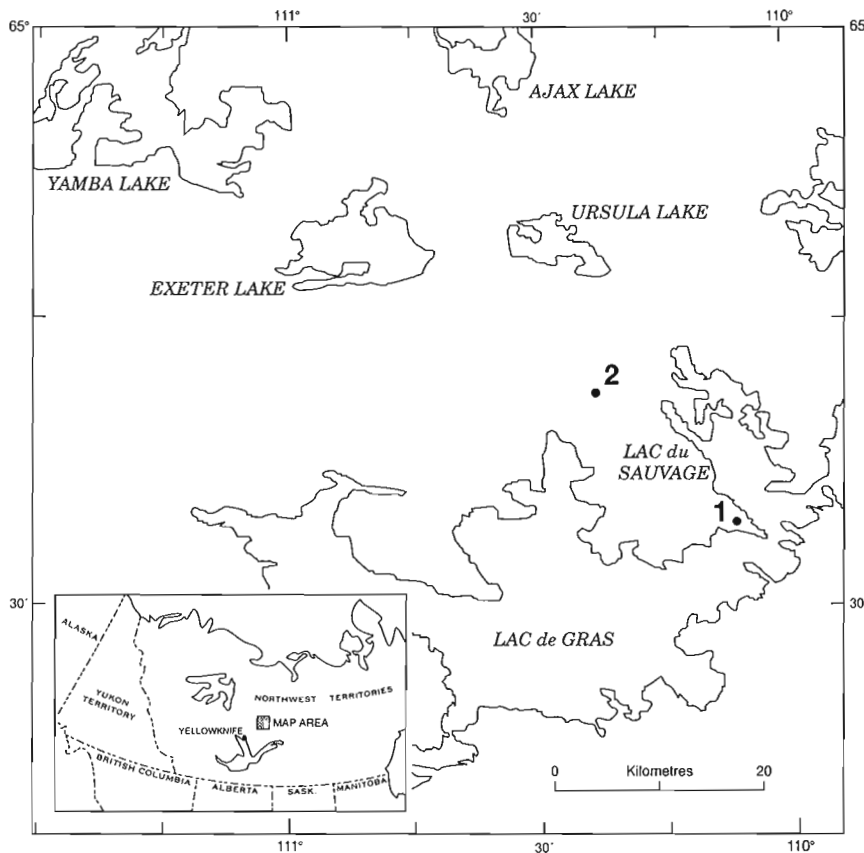


Figure 1.

Map of Lac de Gras area about 300 km northeast of Yellowknife, Northwest Territories, showing position of BHP-Dia Met Joint Venture kimberlite pipes mentioned in this report: 1, Point Lake pipe; 2, "Hawk" pipe.

of the thermal maturation of fossil pollen grains and wood recovered from kimberlite pipes. Some preliminary data were presented by Stasiuk and Nassichuk (1995) who analyzed fossilized wood samples petrographically and concluded that temperatures were less than 104°C in the diatreme facies and about 30°C in the crater facies.

FOSSILS IN KIMBERLITES - GENERAL DISCUSSION

Kimberlites are olivine-rich ultramafic rocks that originated in the upper mantle of the lithosphere. They travelled through carrot-shaped conduits (pipes) or, in some cases, dykes through the crust to the surface and fragments of crustal rock were added to the kimberlite mass as it moved toward the surface. Kimberlites are very rich in volatile materials, such as CO₂, which invariably caused them to erupt at the surface, forming craters. The pipes penetrated, and are presently enveloped by Archean igneous and metamorphic rocks that are more than 2.4 billion years old. They occur within a northwestward-trending belt that is about parallel to a profusion of continental diabase dykes in the Mackenzie dyke-swarm (Fahrig, 1987; LeCheminant and Heaman, 1989).

In the Lac de Gras area, blocks of wall rock, including fossiliferous Cretaceous and Tertiary strata, appear to have fallen into the craters of kimberlite pipes following eruption and were preserved as xenoclasts. Comparable fossil occurrences have not been reported previously from kimberlites or, for that matter, from petrologically similar lamproites in western or northern Canada. However, Paleozoic conodonts and brachiopods of uncertain Ordovician to Devonian age have been recognized in xenoclasts within kimberlites east of Kirkland Lake, Ontario (H. Lee, pers. comm., 1994). Wanless et al. (1968) determined a K-Ar age of 151 ± 8 million years (Late Jurassic) for phlogopites in a kimberlite dyke in the Upper Canada Mine, about 16 km east of Kirkland Lake (Lee, 1968). Paleozoic fossils, possibly of Ordovician or Silurian age, are known from xenoclasts within the Sloan kimberlite pipe in Colorado, which is thought to have been emplaced during Devonian time (J. Carlson, pers. comm., 1994). Curiously, King and McMillan (1975) reported Mesozoic nannofossils from a nonkimberlitic breccia at Ford's Bight, Labrador, that might be part of a diatreme emplaced during an episode of rifting between Labrador and Greenland that began in Jurassic time.

Numerous kimberlites have been discovered in Saskatchewan but we are not aware of any fossils having been recovered from xenoclasts within them. Gent (1992) indicated that the Saskatchewan kimberlites penetrated Lower Cretaceous strata and are probably of Albian or possibly younger Cretaceous age. Indeed, a stratigraphic section drilled at Fort à la Corne, 80 km east of Prince Albert, is available to us and contains abundant reworked (epiclastic) kimberlite grains at several horizons; the section is replete with Cretaceous (late Albian) palynomorphs. Accordingly, since those kimberlite grains were derived from kimberlites

already in place, the Saskatchewan kimberlites must have been emplaced prior to late Albian time and therefore certainly prior to those in the Lac de Gras area.

Elsewhere, abundant fossils have been recovered from the East Siberian or Yakutian kimberlite province in the eastern part of the Siberian Platform. In that area, numerous kimberlites were emplaced during Paleozoic and Mesozoic time (Kushev et al., 1992). Brakhfogel (1984) reported diverse faunas of brachiopods, pelecypods, rugose and tabulate corals, ostracodes, tentaculitids, trilobites, bryozoans, acritarchs, spores, pollen and plant parts in xenoliths ranging from Ordovician to Permian in a number of pipes. He also reported rather abundant Lower Cretaceous carbonaceous wood (*Araucariopitys* sp.) in a number of xenoliths. This is particularly interesting because Cretaceous and/or lower Tertiary wood is common in xenoliths in the Lac de Gras area. Milashev and Shulgina (1959) reported a Late Jurassic to Early Cretaceous belemnite (*Pachyteuthis?* sp.) from an exposed pipe in Siberia. They concluded that Siberian kimberlites occurred in two groups, one of which they thought was emplaced prior to Late Permian time and the other during Cretaceous time.

Kimberlite pipes are abundant in Africa where they are generally thought to have been emplaced during Cretaceous time. We have no record, however, of fossils having been described from xenoliths within the kimberlites. Nevertheless, some reports show fossils in epiclastic sediments that were deposited in crater lakes above kimberlite diatremes; these sediments were derived from the diatremes. Smith (1986) reported Late Cretaceous pelecypods, gastropods, ostracodes, leaf impressions, insect wings, teleost fish and xenopid frog skeletons from a crater lake above a kimberlite diatreme in Bushmanland, South Africa. Fossilized leaves and insects are also known from middle Tertiary strata in a crater lake above the Orapa kimberlite, which is part of a swarm of diamondiferous kimberlites in north-central Botswana (J. Gurney, pers. comm., 1993).

FOSSILS IN LAC DE GRAS KIMBERLITES

Sixty samples of mudstones and siltstones recovered from lithoclasts in 13 kimberlite pipes in the Lac de Gras area have yielded rich and diverse assemblages of dinoflagellates, pollen and spores. Most samples were recovered from within the kimberlitic diatreme facies in the pipes (Fig. 2) at depths between 50 and 150 m. A few samples, however, were recovered from the pyroclastic crater facies, as shallow as 25 m below the surface. The relative positions of "diatreme facies" and "crater facies" in an idealized kimberlite pipe are shown in Figure 2. We have not yet identified diagnostic fossils from epiclastic lake sediments that lie above and post-date kimberlite pipes in the Lac de Gras area.

Samples of wood up to 70 mm long and 30 mm wide occur within the crater facies where they appear rather fresh and are only slightly permineralized. Wood fragments are common but somewhat coalified in the diatreme facies where they are in direct contact with kimberlite grains down to a depth of at least 140 m. Late Cretaceous teleost (ichthyodectid) fish

parts, including parts of skull bones, fin rays, and scales were identified by M.V.H. Wilson (pers. comm., 1993) from heavy mineral separates at a depth of about 140 m in the Point Lake pipe (Fig. 1). We have not yet completed analysis of fossils in all the samples but preliminary results show age ranges from latest Early Cretaceous (Albian) to early Tertiary (Paleocene). The Cretaceous (Albian to Maastrichtian) fossils were deposited in marine to marginal-marine environments, but the Paleocene fossils (pollen and spores) indicate non-marine, possibly floodplain or even lacustrine environments. As expected, lithoclasts appear to have been 'mixed' within pipes, and indeed, in some pipes rather young (Paleocene) fossils occur much deeper in boreholes than considerably older (Albian) fossils. The following three assemblages, from individual xenoliths in a single borehole in the BHP-Dia Met "Hawk" pipe north of Lac de Gras (Fig. 1), are representative of those examined and illustrate a mixing of xenoliths in the pipe; the ages of fossil assemblages appear to decrease with increasing depth. Moreover, the following lists show the diversity of fossils in each of the three samples.

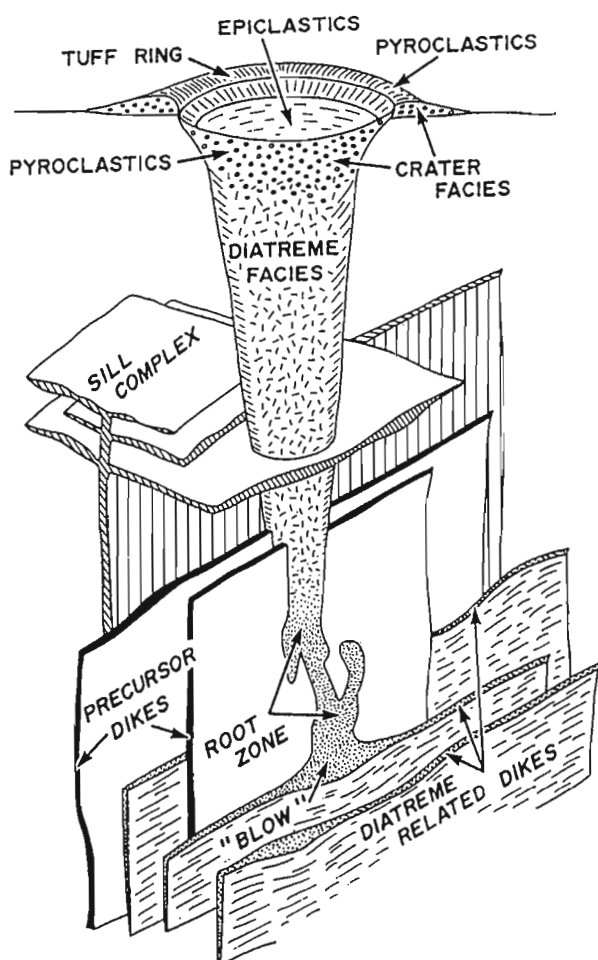


Figure 2. Schematic diagram of kimberlite pipe showing relative position of diatreme facies, crater facies and epiclastic lake sediments; the latter were derived from, and post-date the time of emplacement of, the pipe. Reproduced from Mitchell (1986).

Latest Early Cretaceous (Albian) fossils from drillhole 92-05 (GSC Loc. C-147801) in BHP-Dia Met "Hawk" pipe (Fig. 1) at a depth of 70 m

The sample contains the following abundant dinoflagellates that indicate deposition in a marine environment; pollen and spores are also present but are rare.

- Batioladinium jaegeri* (Alberti) Brideaux
- Chichaouadinium vestitum* (Brideaux) Bujak and Davies
- Cribroperidinium edwardsii* (Cookson and Eisenack) Davey
- Cyclonephelium vannophorum* Davey
- Fromea amphora* Cookson and Eisenack
- Fromea fragilis* (Cookson and Eisenack) Stover and Evitt
- Gingiodinium evittii* Singh
- Leptodinium cancellatum* Brideaux and McIntyre
- Laciniadinium arcticum* (Manum and Cookson) Lentin and Williams
- Luxadinium propatum* Brideaux and McIntyre
- Microdinium opacum* Brideaux
- Odontochitina operculata* (O. Wetzel) Deflandre and Cookson
- Odontochitina singhii* Morgan
- Oligosphaeridium pulcherrimum* (Deflandre and Cookson) Davey and Williams
- Ovoidinium verrucosum* (Cookson and Hughes) Davey
- Palaeoperidinium cretaceum* Pocock emend. Davey
- Pseudoceratium eisenackii* (Davey) Bint

Most species present in the dinoflagellate assemblage are indicative of a late Albian or Cenomanian age. The presence of *Microdinium opacum*, *Leptodinium cancellatum* and *Odontochitina singhii*, however, strongly suggests a Late Albian age.

Late Cretaceous (Turonian) fossils from drillhole 92-05 (GSC Loc. C-147801) in BHP-Dia Met "Hawk" pipe (Fig. 1) at a depth of 74 m

The sample contains a rich dinoflagellate assemblage and abundant amorphous organic materials of marine origin. Among the dinoflagellates are:

- Apteodinium granulatum* Eisenack
- Batioladinium jaegeri* (Alberti) Brideaux
- Caligodinium aceras* (Manum and Cookson) Lentin and Williams
- Coronifera oceanica* Cookson and Eisenack emend. May
- Cribroperidinium exilicristatum* (Davey) Stover and Evitt
- Dinopterygium cladoides* Deflandre
- Florentinia cooksoniae* (Singh) Duxbury
- Hystrichodinium pulchrum* Deflandre
- Kallosphaeridium ringnesiorum* (Manum and Cookson) Helby
- Odontochitina costata* Alberti emend. Clarke and Verdier
- Palaeoperidinium cretaceum* Pocock emend. Davey
- Trithyrodinium* sp.
- Wallodinium luna* (Cookson and Eisenack) Lentin and Williams
- Williamsidinium banksianum* Lentin

The colonial green algae *Palambages* sp. and *Hydrodictyon* sp. are common in this sample. Pollen species include *Rugubivesiculites rugosus* (Pierce), *Parvisaccites radiatus* (Couper), an undescribed tuberculate bisaccate, *Liliacidites dividius* (Pierce) Brenner, *Retitricolpites vulgaris* Pierce, *Retitricolpites* sp. and *Tricolpites* sp. *Williamsdinium bankianum* is absent from pre-Turonian strata and accordingly, the palynoflora is probably of Turonian age.

Early Tertiary (Paleocene) fossils from drillhole 92-05 (GSC Loc. C-147801) in BHP-Dia Met "Hawk" pipe (Fig. 1) at a depth of 75 m

The palynoflora is a mixed assemblage of dinoflagellates, pollen and spores. The dinoflagellates and some of the pollen species also occur higher in this drillhole and, on their own, might indicate a Cretaceous age. The presence of a few species of angiosperm pollen in the samples, however, is especially significant for age determination. Pollen species include *Alnus* sp., *Fraxinopollenites variabilis* Stanley, Castanea-type tricolporate pollen, ?*Celtis* sp., *Momipites* sp. and other types of tricolporate pollen. Pollen species indicate an early Tertiary, Paleocene age. The older (Cretaceous) palynomorphs were probably reworked into the younger (Paleocene) sediments.

Fossils from other pipes

In addition to the fossils mentioned from the "Hawk" pipe, we have recovered fossils from 12 other pipes in the Lac de Gras area. In some of those pipes, rich dinoflagellate assemblages provide definitive evidence for the presence of lower Campanian sediments. These assemblages include *Chatangiella decorosa* (McIntyre) Lentin and Williams, *C. ditissima* (McIntyre) Lentin and Williams, *Dorocysta litotes* Davey, *Ginginodinium ornatum* (Felix and Burbridge) Lentin and Williams, *Isabelidinium microarmum* (McIntyre) Lentin and Williams, *Laciniadinium biconiculum* McIntyre, *L. firmum* (Harland) Morgan, *Spinidinium clavus* Harland and *Trithyrodinium suspectum* (Manum and Cookson) Davey.

Similarly, uppermost Cretaceous (Maastrichtian) assemblages have been identified by the presence of the pollen species *Aquilapollenites augustus* Srivastava, *A. conatus* Norton, *A. reticulatus* (Mchedlishvili) Tschudy and Leopold, *Myrtipites scabratus* Norton, *Siberiapollis montanensis* Tschudy, *Triprojectus magnus* (Mchedlishvili) Stanley and *Wodehouseia spinata* Stanley.

Samples examined from other pipes also contain various angiosperm pollen species which provide additional evidence for the presence of lower Tertiary (Paleocene) nonmarine sediments. Species identified include *Caryapollenites imparalis* Nichols and Ott, *C. veripites* (Wilson and Webster) Nichols and Ott, *C. wodehousei* Nichols and Ott, *Momipites anellus* Nichols and Ott, *M. ventifluminis* Nichols and Ott, *M. wyomingensis* Nichols and Ott and *Pistillipollenites magregori* Rouse.

DISCUSSION AND CONCLUSIONS

Fossils from the Lac de Gras area are of extraordinary importance in defining the distribution of Lower Cretaceous (Albian) to lower Tertiary (Paleocene) strata in northern Canada. Prior to the discovery of kimberlites in the area, no data had ever been presented to prove that Mesozoic and Cenozoic rocks had been deposited above Pre-cambrian rocks in the Slave Province. Indeed, the nearest Cretaceous exposures are about 390 km to the west of Lac de Gras, south of Great Bear Lake in the vicinity of Great Bear Plain (Balkwill, 1971) and in the Cartridge Mountain area (Map 48-1959 in Douglas and Norris, 1959; Douglas et al., 1974). In Douglas et al. (1974), Cretaceous strata are shown on Horn Plateau, about 450 km southwest of Lac de Gras. The age of the Cretaceous strata south of Great Bear Lake has not been established precisely, but on the basis of fossil data available to us, it is most likely in the range of Late Albian to Turonian, similar to other Cretaceous strata exposed elsewhere in the general vicinity of Great Bear Lake. The lower Tertiary (Paleocene) strata nearest to Lac de Gras are exposed at Grizzly Bear Mountain, near Great Bear Lake, about 450 km west.

Now, it is clear that much of the Slave Province must have been covered by a veneer of Cretaceous and lower Tertiary strata long since eroded away by river systems and glacial action. An important idea initiated by McMillan (1973) is that a major anastomosing river system carried sediments from the eastern Cordillera and Canadian shield areas (including the Slave Province) eastward to the Labrador Sea from late Paleocene to Pliocene time. New data supporting this concept of easterly flow in Tertiary time were provided by Duk-Rodkin and Hughes (1994).

As implied earlier, the discovery of marine strata of latest Early Cretaceous and Late Cretaceous age (Albian-Maastrichtian) in the Slave Province necessitates revision to paleogeographic reconstructions of the Western Interior Seaway. A number of authors, including Hills et al. (1994), have reviewed Late Cretaceous connections between the Seaway and the Sverdrup Basin. Lac de Gras data show that Albian-Maastrichtian strata were more widespread than shown earlier and the Cretaceous Seaway was correspondingly wider than previously thought. Particularly from late Albian to Campanian time, marine dinoflagellates were common throughout the entire Seaway, possibly indicative of similar environments. Late Albian dinoflagellate assemblages, similar to those from the kimberlite pipes, occur on Banks Island (Doerenkamp et al., 1976), in the Mackenzie Delta area (Dixon et al., 1985), and in Alberta (Brideaux, 1971; Singh, 1971). Turonian dinoflagellate assemblages from the Lac de Gras area have many similarities with assemblages described from the Arctic Islands (Doerenkamp, 1976; Nunez-Betelu and Hills, 1992), the Mackenzie Delta area (Dixon et al., 1985), and southern Canada (Bloch et al., 1993). Campanian dinoflagellate assemblages from a section along Horton River, Northwest Territories, described by McIntyre (1974), and from Banks Island, described by Doerenkamp (1976), are closely similar to the Lac de Gras Campanian assemblages, which also resemble assemblages from southern Canada.

Teleost (ichthyodectid) fish parts, including fragments of skull bones, teeth, fin rays and scales were recognized by M.V.H. Wilson (pers. comm., 1993) from the diatrema facies in the Point Lake pipe (Fig. 1; Pell, 1994) in the Lac de Gras area. Ichthyodectid fish are known from Turonian strata in the Kanguk Formation, Banks Island and from strata of the same age at Lac des Bois, north of Great Bear Lake, Northwest Territories (Waldman, 1969; Wilson, 1978). Wilson and Chalifa (1989) also described Turonian ichthyodectids from the Kaskapau Formation near Watino, Alberta. M.V.H. Wilson (pers. comm., 1993) suggested that ichthyodectids from the Point Lake pipe might also be Turonian, but require further study.

REFERENCES

- Balkwill, H.R.**
1971: Reconnaissance geology, southern Great Bear Plain, District of Mackenzie; Geological Survey of Canada, Paper 71-11, 47 p. (includes Map 5-1971, Norman, and Camsell River).
- Bloch, J., Schroder-Adams, C., Leckie, D.A., McIntyre, D.J., Craig, J., and Staniland, M.**
1993: Revised stratigraphy of the lower Colorado Group (Albian to Turonian), western Canada; Bulletin of Canadian Petroleum Geology, v. 41, p. 325-348.
- Brakhfogel, F.F.**
1984: Geological aspects of kimberlite magmatism in the northeastern part of the Siberian Platform; Report of the Academy of Sciences of the USSR, Order of Lenin Siberian Department, Yakutsk Branch, Institute of Geology, 128 p.
- Brideaux, W.W.**
1971: Palynology of the Lower Colorado Group, central Alberta, Canada. I. Introductory remarks, geology and microplankton studies; Palaeontographica, Abt. B, Band 135, Liefg. 3-6, p. 53-114.
- Dixon, J., Dietrich, J.R., McNeil, D.H., McIntyre, D.J., Snowdon, L.R., and Brooks, P.**
1985: Geology, biostratigraphy and organic geochemistry of Jurassic to Pleistocene strata, Beaufort-Mackenzie area, Northwest Canada; Canadian Society of Petroleum Geologists, Calgary, Alberta, Course Notes.
- Doerenkamp, A., Jardine, S., and Moreau, P.**
1976: Cretaceous and Tertiary palynomorph assemblages from Banks Island and adjacent areas (N.W.T.); Bulletin of Canadian Petroleum Geology, v. 24, p. 312-417.
- Douglas, R.J.W. and Norris, A.W.**
1959: Horn River Map Area, Northwest Territories; Geological Survey of Canada, Paper 59-11, 23 p.
- Douglas, R.J.W., Norris, A.W., and Norris, D.K.**
1974: Geology, Horn River, District of Mackenzie; Geological Survey of Canada, Map 1372A, scale 1:500 000.
- Duk-Rodkin, A. and Hughes, O.L.**
1994: Tertiary-Quaternary drainage of the pre-glacial Mackenzie Basin; Quaternary International, v. 22/23, p. 221-241.
- Fahrig, W.F.**
1987: The tectonic setting of continental mafic dyke swarms: failed arm and early passive margin; in Mafic Dyke Swarms, (ed.) H.C. Halls and W.F. Fahrig; Geological Association of Canada, Special Paper 34, p. 331-348.
- Fipke, C.E., Gurney, J.J., and Moore, R.O.**
in press: Overview of diamond exploration techniques with an emphasis on indicator mineral geochemistry and Canadian examples; Geological Survey of Canada, Bulletin.
- Harland, W.B., Armstrong, R.L., Cox, A.V., Craig, L.E., Smith, A.G., and Smith, D.G.**
1990: A geologic time scale, 1989; Cambridge University Press, 263 p.
- Hills, L.V., Braunberger, W.F., Núñez-Betelu, L.K., and Hall, R.L.**
1994: Paleogeographic significance of *Scaphites depressus* in the Kanguk Formation (Upper Cretaceous), Axel Heiberg Island, Canadian Arctic; Canadian Journal of Earth Sciences, v. 31, p. 733-736.
- Gent, M.R.**
1992: Diamonds and precious gems of the Phanerozoic Basin, Saskatchewan: preliminary investigations; Saskatchewan Geological Survey, Open File Report 92-2.
- King, A.F. and McMillan, N.J.**
1975: A mid-Mesozoic breccia from the coast of Labrador; Canadian Journal of Earth Sciences, v. 12, p. 44-51.
- Kushev, V.G., Sinitsyn, A.V., Mishnin, V.M., and Natapov, L.M.**
1992: Kimberlite structural environments and their productivity in the East Siberian (Yakutian) Province; Russian Geology and Geophysics, v. 33, no. 10, p. 50-60.
- LeCheminant, A.N. and Heaman, L.M.**
1989: Mackenzie igneous events, Canada: Middle Proterozoic hotspot magmatism associated with ocean opening; Earth and Planetary Science Letters, v. 96, p. 38-48.
- Lec, H.A.**
1968: An Ontario kimberlite occurrence discovered by application of the glauciofocus method to a study of the Munro Esker; Geological Survey of Canada, Paper 68-7, p. 1-3.
- McIntyre, D.J.**
1974: Palynology of an Upper Cretaceous section, Horton River, District of Mackenzie, Northwest Territories; Geological Survey of Canada, Paper 74-14, 56 p.
- McMillan, N.J.**
1973: Shelves of Labrador Sea and Baffin Bay, Canada; in The Future Petroleum Provinces of Canada-their Geology and Potential, (ed.) R.G. McCrossan; Canadian Society of Petroleum Geologists, Memoir 1, p. 473-517.
- Milashov, W.A. and Shulgina, N.I.**
1959: New data on the age of kimberlites on the Siberian Platform; Report of the Academy of Sciences of the USSR, tom. 126, no. 6, p. 1320-1322.
- Mitchell, R.H.**
1986: Kimberlites: mineralogy, geochemistry and petrology; Plenum Press, New York, 442 p.
- Nunez-Betulu, L.K. and Hills, L.V.**
1992: Preliminary palynology of the Kanguk Formation (Upper Cretaceous), Remus Creek, Canadian Arctic Archipelago: I. Marine palynomorphs; Revista Espanola de Paleontologia, v. 7, p. 185-196.
- Pell, J.**
1994: Kimberlites and diamond exploration in the central Slave Province, N.W.T. (75M, N; 76C, D, E, F; 85P; 86A, H); scale 1:500 000 compilation map and margin notes; Indian and Northern Affairs Canada, N.W.T. Geology Division-NAP, Yellowknife, EGS 1994-7.
- Singh, C.**
1971: Lower Cretaceous microfloras of the Peace river area, northwestern Alberta; Research Council of Alberta, Bulletin 44, 322 p.
- Smith, R.M.H.**
1986: Sedimentation and paleoenvironments of Late Cretaceous crater-lake deposits in Bushmanland, South Africa; Sedimentology, v. 33, p. 369-386.
- Stasiuk, V. and Nassichuk, W.W.**
1995: Thermal history of wood and other organic matter in kimberlite pipes at Lac de Gras, Northwest Territories; in Current Research 1995-B; Geological Survey of Canada.
- Waldman, M.**
1969: *Ichthyodectes* and *Holcolepis* from the Cretaceous of Lac des Bois, Northwest Territories, Canada; Canadian Journal of Earth Sciences, v. 6, p. 1316-1319.
- Wanless, R.K., Stevens, R.D., Lachance, G.R., and Edmonds, C.M.**
1968: Age determinations and geological studies, K-Ar isotopic ages, report 8; Geological Survey of Canada, Paper 67-2, Part A, 141 p.
- Wilson, M.V.H.**
1978: Upper Cretaceous marine Teleostei from the basal Kanguk Formation, Banks Island, Northwest Territories; Canadian Journal of Earth Sciences, v. 15, p. 1800-1807.
- Wilson, M.V.H. and Chalifa, Yael**
1989: Fossil marine actinopterygian fishes from the Kaskapau Formation (Upper Cretaceous: Turonian) near Watino, Alberta; Canadian Journal of Earth Sciences, v. 26, p. 2604-2620.

Thermal history and petrology of wood and other organic inclusions in kimberlite pipes at Lac de Gras, Northwest Territories

L.D. Stasiuk and W.W. Nassichuk

Institute of Sedimentary and Petroleum Geology, Calgary

Stasiuk, L.D. and Nassichuk, W.W., 1995: Thermal history and petrology of wood and other organic inclusions in kimberlite pipes at Lac de Gras, Northwest Territories; in Current Research 1995-B; Geological Survey of Canada, p. 115-124.

Abstract: Dispersed peatified to coalified wood and other macerals within the crater and diatreme facies of kimberlite pipes at Lac de Gras have been studied using reflected light microscopy. The coalification levels fall into two categories: i) cellulose-bearing, lignitic peat (≤ 0.20 %Ro); and ii) lignite to sub-bituminous (0.33-0.44 %Ro). The latter are from the diatreme facies whereas most of the low rank samples are from the crater facies. The average temperature of lignitic peat never exceeded 30°C. Huminite from the diatreme facies was subjected to higher temperatures but none of the huminites display microscopic features attributable to pyrometamorphism. If the wood in the diatreme is primary, a short heating event (about 100°C) may have enhanced coalification without altering peat in the crater facies. Alternatively, if huminite in the diatreme represents pre-intrusion burial, coalification and pre-Paleocene erosion may have occurred. The preservation of primary, asphalt bitumen supports a maximum temperature of less than 110°C.

Résumé : Des débris ligneux tourbifiés à houillifiés et d'autres macéraux dispersés au sein des faciès de cratère et de diatrème de cheminées de kimberlite au lac de Gras ont été étudiés au microscope en lumière réfléchi. Les niveaux de carbonification appartiennent à deux catégories : i) tourbe ligneuse, contenant de la cellulose ($\leq 0,20$ % Ro); et ii) lignite à houille sub-bitumineuse (0,33-0,44 % Ro). Cette dernière catégorie s'observe dans le faciès de diatrème tandis que les échantillons de rang inférieur proviennent du faciès de cratère. La température moyenne de la tourbe ligneuse n'excède jamais 30 °C. L'huminite du faciès de diatrème a été soumis à des températures plus élevées mais aucun des huminites ne montre des caractéristiques microscopiques attribuables à un pyrométamorphisme. Si les débris ligneux dans le diatrème sont primaires, un court épisode de chaleur (environ 100 °C) a pu stimuler la carbonification sans altérer la tourbe dans le faciès de cratère. En revanche, si l'huminite dans le diatrème représente un enfouissement pré-intrusif, une carbonification et une érosion pré-paléocènes ont pu se produire. La préservation de bitume asphaltique primaire appuie une température maximale de moins de 110 °C.

INTRODUCTION

Cretaceous and Tertiary fossils (including diverse assemblages of dinoflagellates), pollen and spores, as well as wood and teleost fish parts, have been recovered from xenoclasts in 13 kimberlite pipes that intrude cratonic rocks in the Slave Province in the general vicinity of Lac de Gras (Nassichuk and McIntyre, 1995). Phanerozoic strata are not expressed at the surface. The fossils are the first evidence that marine sediments were deposited in the Slave Province from latest Early Cretaceous (Albian) to latest Cretaceous (Maastrichtian) time. Slightly younger Tertiary (Paleocene) spore and pollen fossils indicate deposition in a nonmarine, possibly lacustrine environment. During late Paleocene or possibly Eocene time, kimberlites, in carrot-shaped pipes, erupted to the surface penetrating the marine Cretaceous and nonmarine Tertiary strata. Subsequently, blocks of Cretaceous and Tertiary strata apparently fell into the ensuing craters and became mixed and incorporated as xenoliths with pyroclastic rocks in the crater-fill facies and with kimberlitic rocks in the somewhat deeper diatreme facies (Nassichuk and McIntyre, 1995, Fig. 2). Whereas much of the Cretaceous strata are of open marine origin, the presence of coaly beds in xenoclasts is indicative of local marginal marine or lagoonal environments as well.

Wood fragments have been recovered from boreholes in the crater and diatreme facies of eight pipes in the Lac de Gras area. They are most abundant at borehole depths less than 50 m in the crater facies but they have also been recovered

from depths exceeding 120 m in the diatreme facies. In the crater facies, wood fragments up to 12 cm long appear "fresh" and internal structures are clearly visible. In the deeper diatreme facies, wood fragments are often in direct contact with kimberlite grains. There, they are generally smaller than fragments in the crater facies, and somewhat more coalified; cellular structures are still clearly discernible.

In this report, we have analyzed five samples of wood and two samples of coaly black shale and mudstone from four different pipes; three of them are directly north of Lac de Gras and one is farther to the northwest, east of Yamba Lake (Fig. 1). Samples were provided through the courtesy of the BHP-Dia Met Joint Venture in the Lac de Gras area and the Tanqueray-Mill City Joint Venture of Yamba Lake. We are particularly indebted to the BHP-Dia Met Joint Venture for assisting one of us (WWN) in field work north of Lac de Gras during 1994.

The purpose of this preliminary report is to provide petrographic information on organic matter recovered from several pipes in the Lac de Gras area and to determine the thermal history of the samples. In particular, we are interested in the maximum temperature (coal rank equivalent) to which the samples were exposed following original deposition and ultimate incorporation in kimberlite pipes. To achieve that end, we analyzed the samples petrographically using incident light microscopy to assess the general maceral composition of the sample and to determine the optical properties in terms of percent reflectance in oil (%Ro) for rank assessment. Our

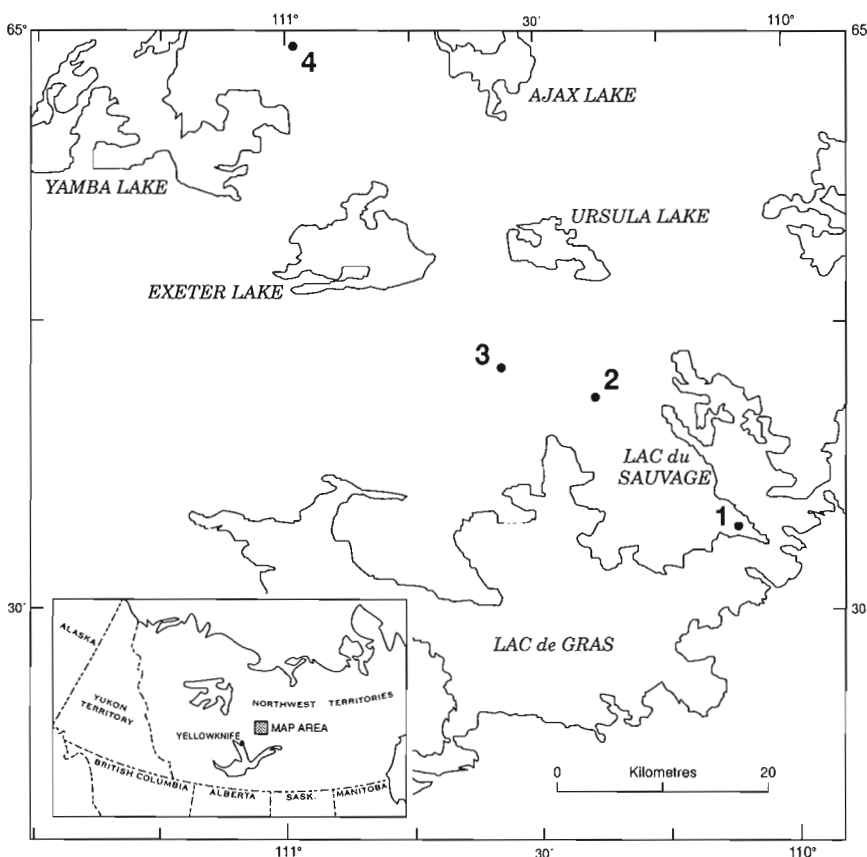


Figure 1.

Map of the Lac de Gras area showing the position of kimberlite pipes that are referred to in this report: 1, Point Lake (BHP-Dia Met); 2, "Hawk" (BHP-Dia Met); 3, Koala Lake (BHP-Dia Met); 4, Torrie (Tanqueray-Mill City).

data are of considerable importance in evaluating temperatures in the crater and diatreme facies of kimberlite pipes in the Slave Province shortly after emplacement.

METHODOLOGY

The samples were prepared following the procedure used for coal maceral analysis by the International Commission of Coal Petrology (ICCP, 1971). Block and particulate samples were set in epoxy-hardener, ground and polished. Brown coal and lignite maceral nomenclature of the ICCP (1971) are used to classify the macerals (dispersed organic constituents) in the samples. Random reflectance in oil (at 546 nm; $n_{oil}=1.518$) of huminite macerals (texto-ulminite A and B, corpohuminite-phlobaphenite) was measured to assess "rank". Fluorescence observations were made using an HBO ultra-violet light source using 365 nm and 400 to 440 nm excitation, a 460 nm beam splitter and a 470 nm barrier filter.

RESULTS OF PETROGRAPHIC ANALYSIS

Description of samples

1. BHP-Dia Met "Point Lake Pipe" (Fig. 1, locality 1; Pell, 1994)

A single sample from the Point Lake Pipe was recovered from the diatreme facies at a borehole depth of 124 m.

Description: Macroscopically, the Point Lake sample is a black, coalified piece of stem-like wood, 6 cm x 1 cm and detrital woody particles in a kimberlite breccia.

2. BHP-Dia Met "Hawk Pipe", 19 km north-northwest of the Point Lake Pipe (Fig. 1, locality 2)

Two samples were recovered from the diatreme facies in this pipe: Hawk A from a borehole depth of 67 m, and Hawk B, 69 m.

Description: Hawk A is a shale or mudstone containing dispersed macerals and subangular quartz grains, some of which contain abundant rutile inclusions. Macerals are dominated by inertodetrinite and fusinite with minor amounts of huminite. Very large fusain particles, some rich in pyrite, are present. A few huminite inclusions (mean 0.45 %Ro) are present, as are trace amounts of biotite.

Hawk B is a shale or mudstone similar to Hawk A that contains angular quartz grains (with rutile inclusions) associated with coaly macerals. Most of the inertinite dominant macerals have chaotic fabric. The inertinites, macrinite, and semi-inertinites have very frayed margins (fissured etc.), indicative of an allochthonous origin for most of the macerals. Most resinites are severely oxidized.

3. BHP-Dia Met "Koala Pipe" (Fig. 1, locality 3; Pell, 1994)

Samples of free wood up to 10 cm long and 3 cm wide were recovered from the crater facies at a depth of 51 m.

Description: Macroscopically, the wood is dark in colour with a "fresh", unaltered exterior appearance with growth rings clearly visible. Internally, it has a "coaly wood" preservation but botanical structures are readily apparent. Some fragments are highly permineralized and infilled with calcite. The ratio of mineral to organic matter ranges from 4:1 to more than 10:1. These fragments are dominated by relatively low-reflecting huminite macerals that are "interweaved" with carbonate matrix and minor amounts of corpohuminite. In other fragments corpohuminite and phlobaphenite are relatively abundant. In these, associated structured "huminite" is relatively anisotropic, typical of wood which still contains cellulose.

4. Tanqueray-Mill City "Torrie Pipe", east of Yamba Lake (Fig. 1, locality 4; Pell, 1994)

Two samples are available from the Torrie Pipe: Torrie A from the crater facies at a depth of 63 m, and Torrie B from the diatreme facies (no depth information available).

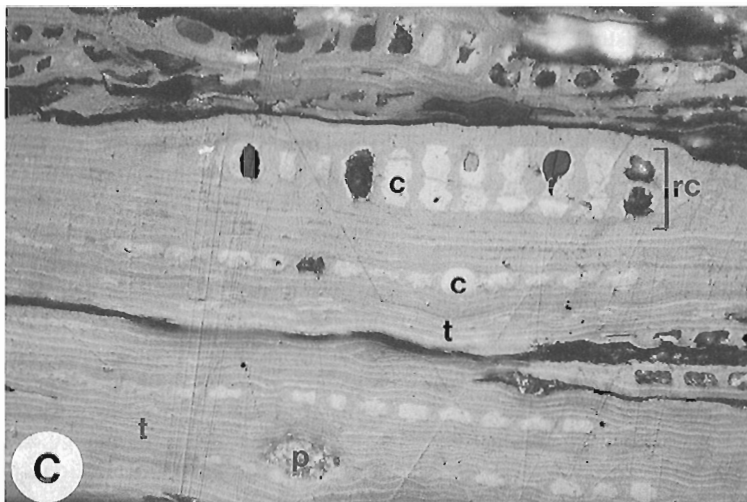
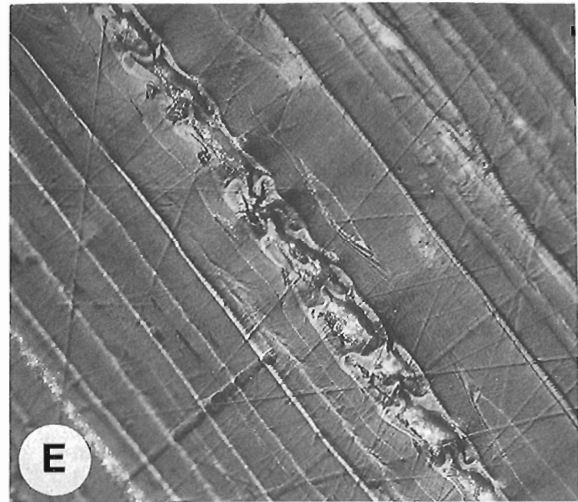
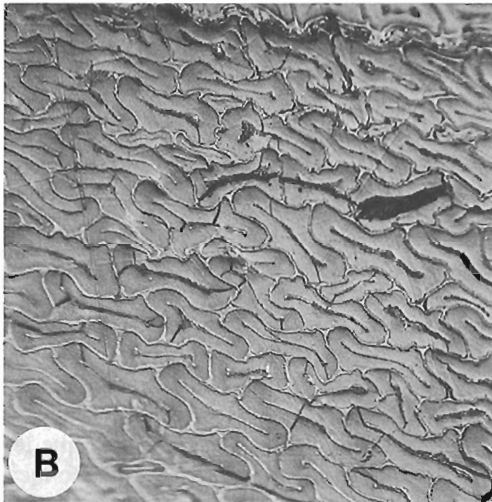
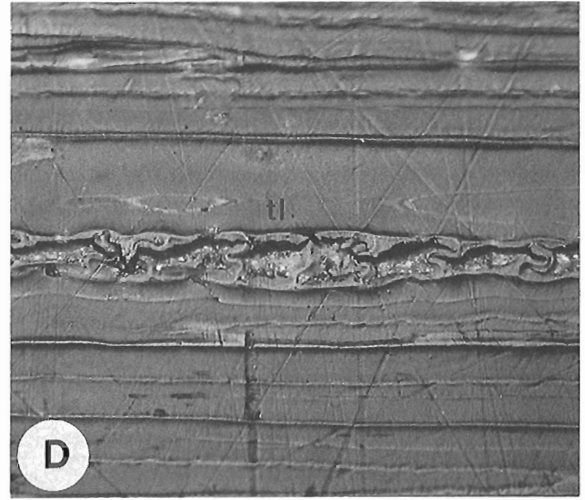
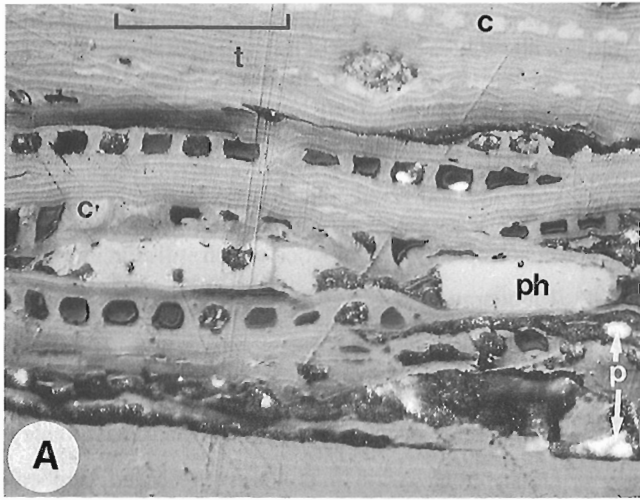
Description: Torrie A is a well preserved, noncoalified wood with minor clay-silica permineralization. The wood shows excellent examples of low reflecting (approx. 0.07 %Ro), thickened, secondary(?) cellular wall-lumens with higher reflecting inner primary(?) cell walls. Also, some samples show cellulose anisotropy in texto-ulminite A (bireflectance=0.04 %Ro). The wood shows well preserved ray cells with up to 12 lumens in a row.

Torrie B is a sample of wood in direct contact with kimberlite grains. The kimberlite host rock has a fine grained matrix that is rich in organic matter. In this regard, it resembles the Point Lake sample, except that organic matter in the latter is somewhat less dispersed. The Torrie B kimberlite also shows some clasts of carbonate rock that contain inclusions of sphalerite and other minerals. The wood in Torrie B is characterized by abundant phlobaphenitic cell infillings, anisotropic texto-ulminite A (0.15 %Ro) and B (approx. 0.18 %Ro mean).

Maceral composition – highlights

Woody material in the majority of samples is dominated by huminite macerals (i.e., those macerals which are derived from lignin and cellulose of terrestrial vascular plants). Samples richest in huminite macerals include: Koala, Torrie A, Torrie B and Point Lake. Huminite macerals in these samples consist almost exclusively of texto-ulminite A (relatively low-reflecting; Fig. 2A), texto-ulminite B (relatively high-reflecting; Fig. 2A, B) and corpohuminite-phlobaphenite (Fig. 2C, D). The higher-reflecting texto-ulminite forms very thin, outer cell walls (<1.25 to 5.0 μm ; Fig. 2A), whereas the low-reflecting B forms thickened cell walls (Fig. 2B). Cellulose is probably represented by the low-reflecting, anisotropic, texto-ulminite A (Fig. 2D, E; see also "Reflectance in Oil" section).

Excellent vascular plant cellular structure is preserved in one diatreme and all crater samples (Torrie B) in the form of ray cells [up to 12 in a row (Fig. 2A)], vascular bundles, cell lumens with secondary infilling, primary and secondary cell



wall thickening, and annual growth rings. The Point Lake sample is significantly more coalified in appearance relative to the other samples and does not have the same details of vascular plant morphology preserved.

Some wood samples from Koala are unique in that the woody remains have been permineralized by carbonate. Trace amounts of sclerotinite (fungal remains; Fig. 3A) were also noted in those samples. The fine grained mineral matrix in the kimberlitic breccia, which hosts the large "woody" stems (in the Torrie B and Point Lake samples), also contains minor amounts of dispersed, commonly contorted huminite (Fig. 3B, C), inertinite and liptinite (mainly pollen) maceral inclusions.

Two of the samples (Hawk A and Hawk B) do not contain large single woody stems but are shales or mudstones that contain rather small detrital macerals within the mineral matrix. All three maceral groups are present in these samples (inertinite>huminite>liptinite). Inertinite is dominated by inertodetrinite with lesser amounts of sclerotinite, fusinite, semifusinite, micrinite, and macrinite; semicoke is also present (Fig. 3C, D, E, 4A). The margins of several of the semifusinite and macrinite macerals are very frayed and fissured (Fig. 3E), suggesting significant reworking. Rare examples of unaltered huminite (telinite) in transition with very fine to fine grained, fissured semicoke (2.19 %Ro_{max}, 1.38 %Ro_{min}) were also noted in the Hawk B sample. Although the majority of the macerals in the Hawk A and Hawk B samples are chaotically distributed within the mineral matrix (highly detrital in habit), there is some evidence for microstratification in the Hawk B sample where inertinite and huminite macerals form a bi-macerite microlithotype (Fig. 3E, 4A).

Liptinite macerals are important in both the Hawk A and Hawk B samples (particularly Hawk B); lesser amounts of liptinites are present in the Torrie A sample. They are dominated by pollen (Fig. 4B) with lesser amounts of sporinite, thin- and thick-walled crassi-cutinite (Fig. 4C), *Palam-bages*(?) alginite (Fig. 4D), traces of dinoflagellates (Torrie A), oxidized resinite (Hawk B) and exsudatinites (fluorescing solid hydrocarbons) infilling mainly inertinite cell voids (Hawk B, Fig. 4E).

Reflectance in oil

Reflectance in oil (%Ro) was determined for the following huminite macerals: textu-ulminite A, textu-ulminite B, undifferentiated huminite (mainly textu-ulminite), and corpohuminite-phlobaphenite (Table 1). Textu-ulminite A and textu-ulminite

B reflectance was determined for the Koala, Torrie A and Torrie B samples; the range is 0.15 to 0.19 %Ro for textu-ulminite A, and 0.19 to 0.26 %Ro for textu-ulminite B (Fig. 5). The textu-ulminites, particularly textu-ulminite B, are anomalously anisotropic (bireflectance averaging 0.04 %Ro), which probably indicates a significant cellulosic component at this level of "coalification-preservation" (Stout and Spackman, 1989).

For the remaining samples, reflectance was determined for "undifferentiated huminite" (Fig. 6A) with the values ranging from 0.19 to 0.44 %Ro. The Point Lake and Hawk A samples contain huminite in the form of large coalified "stems" as well as much smaller huminite particles dispersed in the fine grained matrix of the breccia. The reflectance of the coalified stems in both samples is in the order of 0.06 to 0.11 %Ro higher than the reflectance of the smaller dispersed huminite particles (Table 1). Only one of the samples (Point Lake) exhibited zoned huminite reflectance for a stem (3-5 cm diameter) within the diatreme kimberlite breccia. Huminite in the inner core of this sample is slightly lower (0.38 %Ro) in reflectance than huminite in the outer rim (0.44 %Ro). This difference may in effect be a thick oxidation rim or the effect of waning heat (i.e., the high %Ro rim being a 'metamorphic' aureole).

A bar chart comparing the reflectance of textu-ulminite B with the mean reflectance of undifferentiated huminite reveals two distinct reflectance classes (Fig. 6B). The Hawk and Point Lake samples form a high-reflectance group (Group B; 0.33-0.44 %Ro) while the Koala and Torrie samples form a low-reflectance group (Group A; 0.19-0.26 %Ro).

DISCUSSION

Petrology of coal macerals

The botanical features noted in the low-reflecting Group A samples warrant further investigation to attempt identification. There are, however, some general preliminary inferences which can be made based on reflected light petrographic observations of the woods. Relatively abundant corpohuminite-phlobaphenite cell infillings, as in some fragments of wood in the Koala sample, are commonly attributed to woods derived from coniferous trees (e.g., *Pinus*, *Rhizophora mangle*; ICCP, 1971; Stout and Bensely, 1987). The corpohuminite bodies are derived from condensed tannin (Stout and Bensely, 1987) which are abundant in coniferous

Figure 2. Photomicrographs of macerals from the crater and diatreme kimberlite facies. Polished block, incident white light, oil immersion objective; scale bar=50 μm (all photos to same scale). **A)** Alternating high- and low-reflecting textu-ulminite (t) with cell lumens infilled by large and small corpohuminite (c), phlobaphenite (ph) and pyrite (p); peatified wood; Koala. **B)** Textu-ulminite: low-reflecting, thickened cell walls associated with thin, high-reflecting outer layer; cross-section through peatified wood, compare with longitudinal section in Figure 2D; Torrie B. **C)** Possible ray cells (rc) associated with high- and low-reflecting textu-ulminite (t), corpohuminite (c) and pyrite (p); peatified wood; Koala. **D)** Low-reflecting textu-ulminite representing thickened cell walls (tl); longitudinal section through peatified wood; Torrie B. **E)** Same as for Figure 2D. The stage has been rotated to illustrate the anisotropic nature of the ulminite indicating the presence of cellulose.

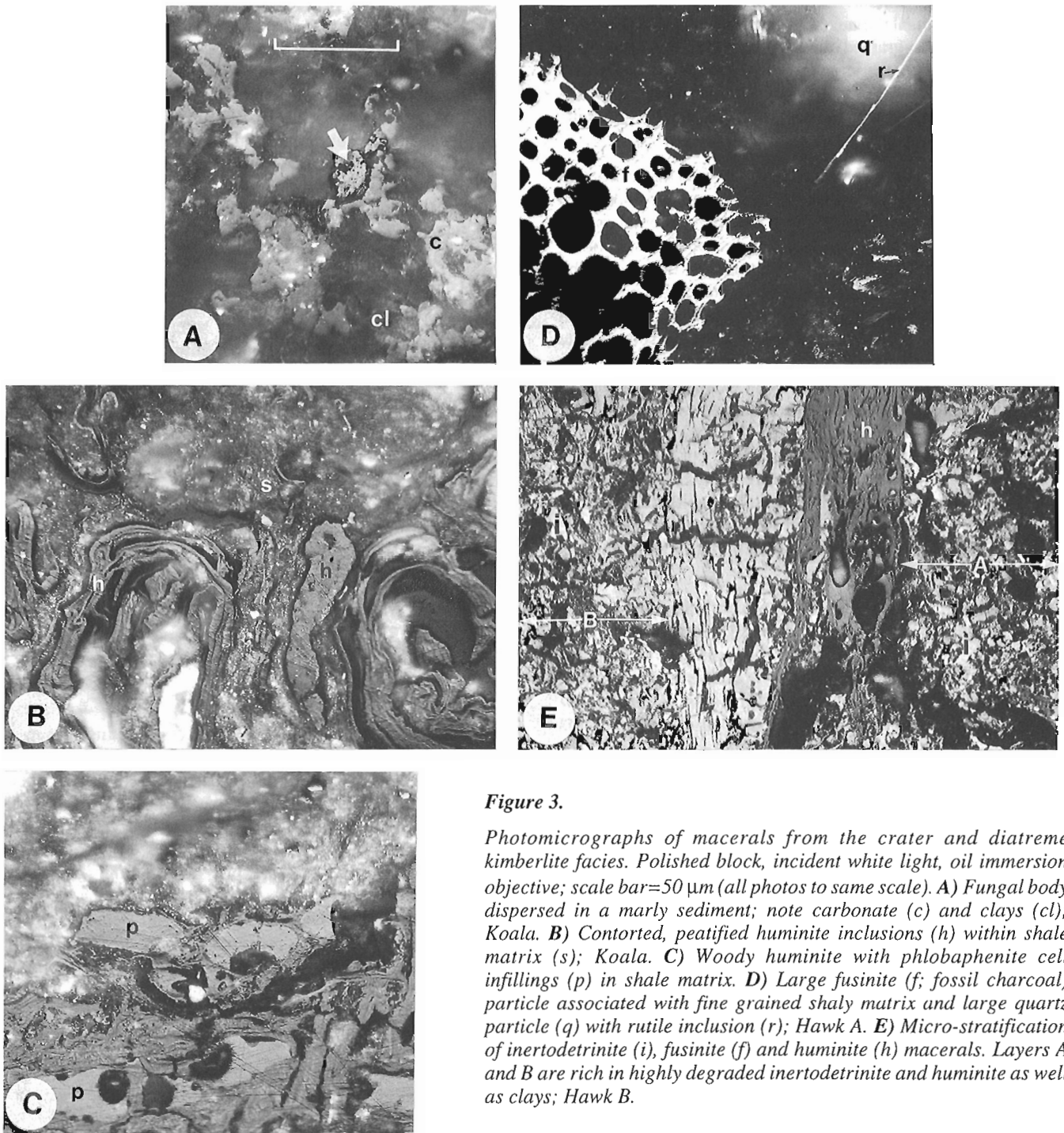


Figure 3.

Photomicrographs of macerals from the crater and diatreme kimberlite facies. Polished block, incident white light, oil immersion objective; scale bar=50 μ m (all photos to same scale). A) Fungal body dispersed in a marly sediment; note carbonate (c) and clays (cl); Koala. B) Contorted, peatified huminite inclusions (h) within shale matrix (s); Koala. C) Woody huminite with phlobaphenite cell infillings (p) in shale matrix. D) Large fusinite (f; fossil charcoal) particle associated with fine grained shaly matrix and large quartz particle (q) with rutile inclusion (r); Hawk A. E) Micro-stratification of inertodetrinite (i), fusinite (f) and huminite (h) macerals. Layers A and B are rich in highly degraded inertodetrinite and huminite as well as clays; Hawk B.

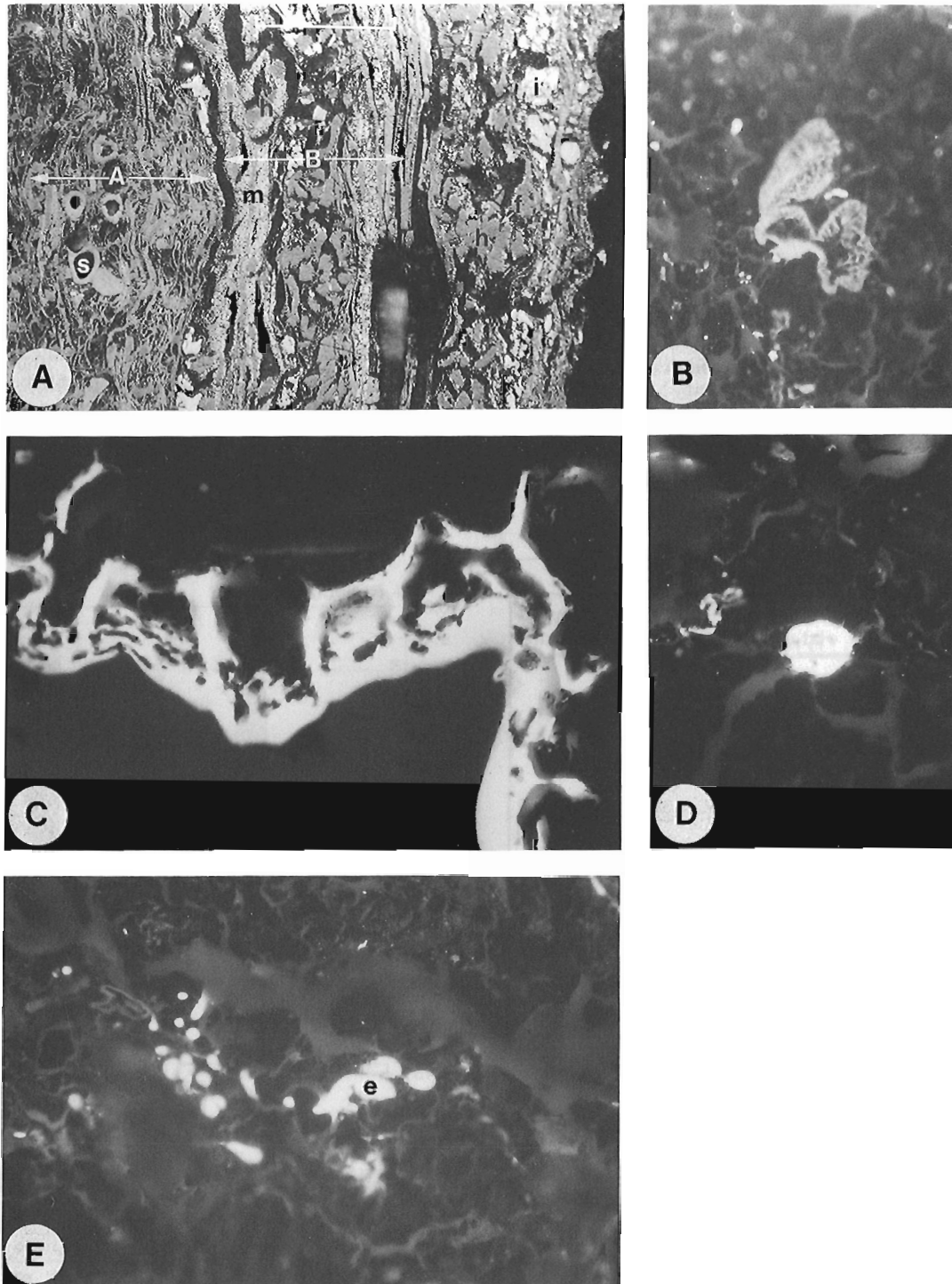


Figure 4. Photomicrographs of macerals from the crater and diatreme kimberlite facies. Polished block, incident white (A) and fluorescent light (B-E), oil immersion objective; scale bar=50 μm (all photos to same scale). See Figure 2A. **A)** Micro-stratification of inertodetrinite (i), sclerotinite (s) and degraded huminite (h) macerals. Layer A is extremely rich in different varieties of sclerotinite macerals (fungal remains). In layer B some of the huminite has been severely oxidized (oxidation fissures: f) and degraded into granular micrinite (m); Hawk B. **B)** Pollen grain from Hawk B; fluorescent light excitation. **C)** Thick-walled crassi-cutinite in Hawk B sample. **D)** Palambages sp. (?) alginite, Hawk B sample. **E)** Yellow-fluorescing exsudatinitite (e) infilling cell lumens in fusinite. The exsudatinitite is soluble in immersion oil under fluorescent light excitation; Hawk B.

trees. Sample Torrie B, on the other hand, was not enriched in corphominite-phlobaphenite, but was characterized by more ray cells in the parenchyma (up to 12) than in the Koala sample mentioned above. Further fluorescence observations may establish the presence and/or absence of resins and essential oils, which may be further evidence for a different origin of the woods in these two samples.

The maceral assemblage in the Hawk B sample is dominated by inertinite macerals which form a chaotic fabric in association with a relatively high concentration of angular to subangular quartz. This textural arrangement, inertinite-enrichment, and concentration of sclerotinite are typical of a fluviially-influenced environment (floodplain?; Stach et al., 1982; Harvey and Dillon, 1985) with a high degree of transport, areas of low to variable water table, periodic atmospheric exposure resulting in severe oxidation, and/or forest fire alteration of vegetal matter. The persistent inclusion of

primary, thermally-produced exsudatinites (oily exsudates) within fusinite cell lumens and maceral fissures and fractures may further attest to periodic dry conditions and the influence of fire. Anomalous temperatures in the paleoenvironment are also suggested by the preservation of the progressive transformation of low-reflecting telinite (0.30 %Ro) into an anisotropic, fine grained semicoke. The assemblage in this sample also contains persistent liptinite macerals (pollen, cutinite) of highly variable fluorescence (including drastic red shifts within a single liptinite maceral), indicating contemporaneous oxidative degradation rather than reworking from older strata. Despite all of the indications that the macerals are allochthonous, in the Hawk B sample there is evidence for microstratification where at least three alternating lamina ($\leq 30 \mu\text{m}$) of huminite and inertinite appear to be interbedded. The microstratification may be evidence for sediment deposition within a Cretaceous basin.

Table 1. Reflectance of huminite macerals

Sample	Reflectance in oil (%Ro)			Corpo-huminite
	Huminite	txt-ulm A	txt-ulm B	
Hawk A	0.33	-	-	-
Hawk A-1	0.44	-	-	-
Hawk B	0.39	-	-	-
Point Lake	0.38	-	-	-
Point Lake-1	0.44	-	-	-
Torrie A	-	0.15	0.19	0.27
Torrie B	-	0.15	0.19	0.18
Koala	0.19	0.19	0.26	0.30
Koala	0.20	-	-	0.33

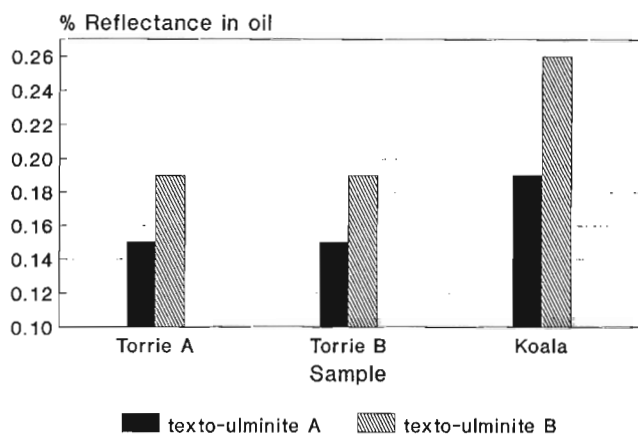


Figure 5. Bar diagram illustrating the difference in reflectance between texto-ulminite A and texto-ulminite B.

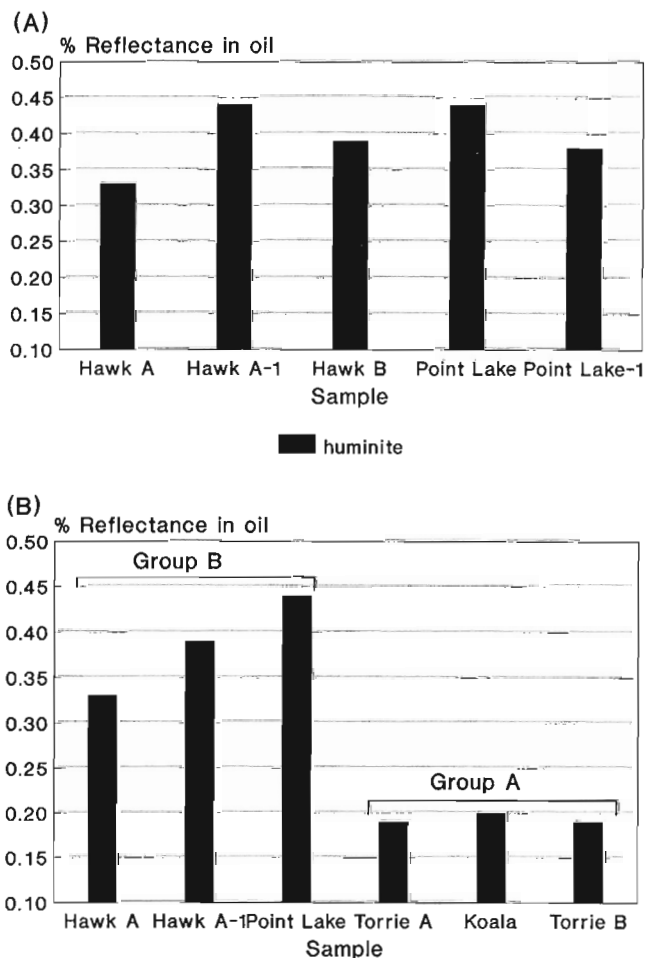


Figure 6. A) Bar diagram illustrating the distribution of reflectance for undifferentiated huminite. B) Bar diagram illustrating the low-reflectance (Group A) and high-reflectance (Group B) huminite populations. All of Group B samples are from the diatreme facies; two of three in Group A are from the crater facies.

"Rank" evaluation based on %Ro

The huminite macerals associated with the kimberlitic intrusions do not show any direct evidence of being severely altered by a pyrometamorphic event (i.e., temperatures $>250^{\circ}\text{C}$). This is not at all surprising since it has been previously proposed that fragments of country rock in Bachelor Lake kimberlite breccias, South Africa, were only metasomatically altered, show no pyrometamorphic effects indicative of relatively high temperatures during or subsequent to their incorporation, and were probably emplaced at low temperatures (Clement, 1975).

The low reflectance values of Group A samples (≤ 0.20 %Ro; Fig. 6B) are typical for values of lignitic (peatified) woods which have only been buried to very shallow depths (Stout and Spackman, 1989). Over a burial time of 50 Ma for Group A samples in the crater facies, the maximum average temperature must have been less than 30°C to maintain the low measured reflectance values (based on time-temperature-reflectance coalification relationship; e.g., Bostick, 1979).

The range of reflectance values for Group B diatreme samples, excluding Torrie B (Fig. 6B), fall within the range of reflectance for coals of lignitic to sub-bituminous "C" rank (Stach et al., 1982). Since the diatreme facies samples have significantly higher reflecting huminite than the crater facies samples (Fig. 6B), two different coalification histories must be involved. Further to this, the petrography suggests that the huminite macerals in the diatreme facies may be primary. This is supported by the lack of oxidation features and the distinct early compactional features (contorted appearance) indicating that the huminites were soft wood at the time of inclusion in the shale clasts. Barring further evidence to the contrary, at this point in the investigation it is assumed that the huminites are primary in the diatreme facies. The petrography also shows that the huminite macerals (coalified woody remains) in Group B samples did not experience pyrometamorphism (i.e., temperatures $>250^{\circ}\text{C}$), otherwise gas release devolatilization structures from the release of CO_2 and CO would be evident (van Heek et al., 1971; W.J. McDougall, pers. comm., 1994). The presence of unaltered, primary asphalt bitumen (exsudatinite) without flow textures in the Hawk B sample (huminite = 0.39 %Ro) suggests that the maximum temperature was less than 104°C , the temperature at which micro-flow begins in asphalt bitumens under atmospheric conditions (Jacob, 1984).

Several thermal history scenarios could account for a lignite to sub-bituminous level of coalification in two of the three diatreme samples. The first possibility is a "cool temperature – maximum burial" history, assuming absolutely no thermal effect emplaced upon the wood during incorporation into the breccia. In this case, all of the coalification post-dates the kimberlite. Thus, to achieve a 0.40 to 0.45 coalification level, an average maximum temperature of 50°C would be required over an effective heating interval of 50 million years. For the case of an average geothermal gradient of $30^{\circ}\text{C}/\text{km}$, a burial depth of 1 km would be required over 50 million years (Bostick, 1979). Significant post-kimberlite burial seems unlikely, otherwise the huminite in the immediately

superjacent crater facies would have achieved the same lignite to sub-bituminous coalification level. However, if the diatreme huminites are older (e.g., Albian; Nassichuk and McIntyre, 1995) than the crater facies huminites (e.g., Paleocene; op. cit.), the lignite to sub-bituminous level of coalification could have been achieved by pre-Paleocene burial.

A second proposal involving a rapid, relatively low temperature heating event during diatreme emplacement could account for the huminite reflectance difference between the diatreme and crater huminites. The heating and duration of the event would be limited to enhancing the coalification of the diatreme huminites but not sufficiently sustained for conductance to, and alteration of, the overlying crater facies. For example, a temperature of 125°C sustained over 300 000 years could effectively coalify huminite to a level equal to 0.40 %Ro (Falvey, 1982). Artificial coalification experiments performed by Davis and Spackman (1964) with modern *Taxodium* wood have shown that the first significant change in the molecular structure of the wood took place between 150° and 175°C after a heating period of only 24 hours (under very high uniaxial pressures). This probably corresponds to the first coalification jump which begins at the sub-bituminous level (Stach et al., 1982), also the rank level of three of four Lac de Gras diatreme samples. At a temperature near 150°C , the duration of heating required to achieve 0.40 %Ro would be near 100 000 years (Bostick, 1979). With a longer heating period, the same 0.40 %Ro level of coalification could be achieved at a lower temperature such as the less than 110°C suggested by the asphalt bitumen. For example, a temperature of 100°C for 2 to 3 Ma could achieve a coalification level of 0.40 %Ro (Bostick, 1979; Falvey, 1982); whether such circumstances could restrict coalification to the diatreme huminites but not the crater huminites is not known. Further investigation is required to better constrain the depositional history of the diatreme huminite and more accurately assess the conditions by which lignite to sub-bituminous levels of coalification were achieved.

ACKNOWLEDGMENTS

The authors thank BHP, Dia Met, Tanqueray and Mill City for samples. The BHP-Dia Met Joint Venture provided field assistance to W.W.N. Thanks to W.J. McDougall for reviewing the manuscript.

REFERENCES

- Bostick, N.H.**
1979: Microscopic measurements of the level of catagenesis of solid organic matter in sedimentary rocks to aid exploration for petroleum and to determine former burial temperatures – a review; Society of Economic Paleontologists and Mineralogists, Special Publication 26, p. 17-23.
- Clement, C.R.**
1975: The emplacement of some diatreme facies kimberlites; in *Physics and Chemistry of the Earth*, v. 9, (ed.) L.H. Ahrens, F. Press, S.K. Runcorn, and H.C. Urey; Pergamon Press, Toronto, p. 51-60.
- Davis, A. and Spackman, W.**
1964: The role of the cellulosic and lignitic components of wood in artificial coalification; *Fuel*, v. 43, p. 215-224.

Falvey, D.A.

1982: Recent advances in burial and thermal geohistory analysis; Australian Petroleum Exploration Association Journal, v. 22, p. 65-81.

Harvey, R.D. and Dillon, J.W.

1985: Maceral distributions in Illinois coals and their paleoenvironmental implications; International Journal of Coal Geology, v. 5, p. 141-165.

International Commission of Coal Petrology (ICCP)

1971: International Handbook of Coal Petrography, 1st supplement to 2nd edition; Centre national de la Recherche scientifique, Paris.

Jacob, H.

1984: Migrabitumen; International Commission of Coal Petrology, Commission II Draft, Calgary, 1984, 11 p.

Nassichuk, W.W. and McIntyre, D.J.

1995: Cretaceous and Tertiary fossils discovered in kimberlites at Lac de Gras in the Slave Province, Northwest Territories; in Current Research 1995-B; Geological Survey of Canada, this volume.

Pell, J.

1994: Kimberlites and diamond exploration in the central Slave Province, N.W.T. (75M, N; 76C, D, E, F; 85P; 86A, H); scale 1:500 000 compilation map and margin notes; Indian and Northern Affairs, Canada, N.W.T. Geology Division NAP, Yellowknife, EGS 1994-7.

Stach, E., Mackowsky, M.Th., Teichmüller, M., Taylor, G.H., Chandra, D., and Teichmüller, R.

1982: Stach's textbook of Coal Petrology; Borntraeger, Stuttgart.

Stout, S.A. and Bensley, D.F.

1987: Fluorescing macerals from wood precursors; International Journal of Coal Geology, v. 7, p. 119-133.

Stout, S.A. and Spackman, W.

1989: Peatification and early coalification of wood as deduced by quantitative microscopic methods; Organic Geochemistry, v. 14, p. 285-289.

van Heek, V.K.H., Jüntgen, H., Luft, K.-F., and Teichmüller, M.

1971: Aussagen zur Gasbildung in frühen Inkohlungsstadien auf Grund von Pyrolyseversuchen; Erdöl und Kohle, v. 24, p. 566-572.

Geological Survey of Canada Project 840081

Mineral occurrences in Middle Devonian carbonates, Salt River and Stony Islands (Slave River) areas, northeastern Alberta¹

M.R. McDonough and H.J. Abercrombie

Institute of Sedimentary and Petroleum Geology, Calgary

McDonough, M.R. and Abercrombie, H.J., 1995: Mineral occurrences in Middle Devonian carbonates, Salt River and Stony Islands (Slave River) areas, northeastern Alberta; in Current Research 1995-B; Geological Survey of Canada, p. 125-130.

Abstract: Three previously known and two new copper occurrences in basal Middle Devonian rocks and Precambrian Shield gneisses at Stony Islands, Alberta, were investigated during the 1994 field season. Interaction between sedimentary derived fluids and the basement is indicated by the presence of copper mineralization in calcite veins cutting basement and sedimentary cover rocks at Stony Islands. Karsted Keg River limestones in the Salt River area show evidence for solution collapse and significant development of gossans and calcite-pyrite veining with associated copper mineralization. These collapse features may have acted as vertical conduits for discharge of metal-enriched sedimentary brines and are therefore viable mineral exploration targets.

Résumé : Au cours de la campagne 1994 sur le terrain, cinq occurrences de cuivre, trois déjà connues et deux nouvelles, dans les roches basales du Dévonien moyen et les gneiss du Bouclier précambrien à Stony Islands, en Alberta, ont été étudiées. L'interaction entre les fluides issus des roches sédimentaires et le socle est révélée par la présence d'une minéralisation cuprifère dans des veines de calcite recoupant le socle et les roches de la couverture sédimentaire à Stony Islands. Les calcaires karstifiés de Keg River dans la région de la rivière Salt fournissent des indices d'un effondrement par dissolution et de la formation importante de chapeaux de fer et de veines de calcite-pyrite avec minéralisation cuprifère associée. Ces effondrements ont peut-être créé des conduits verticaux pour l'écoulement de saumures sédimentaires riches en métal, ce qui en fait, par conséquent, des cibles d'exploration minérale valables.

¹ Contribution to Canada-Alberta Agreement on Mineral Development (1992-1995), a subsidiary agreement under the Canada-Alberta Economic and Regional Development Agreement.

INTRODUCTION

An outlier of basal Middle Devonian strata, resting unconformably on Paleoproterozoic gneisses of the Taltson magmatic zone, is found at Stony Islands, located in the Slave River about 7 km north of Hay Camp, Alberta (NTS 74M/11; Fig. 1). These strata host three copper occurrences that were reported by Godfrey (1986). The setting and nature of these and two previously unreported copper occurrences located nearby were investigated during the 1994 field season. Farther west at Salt River (NTS 74M/13; Fig. 1), karsted Middle Devonian carbonates with gossanous collapse zones were also investigated. Location information for these occurrences are given in Table 1. The implications of these occurrences for the "Prairie-type" disseminated Au-Ag-Cu model (Abercrombie and Feng, 1994a; Feng and Abercrombie, 1994) are discussed.

REGIONAL GEOLOGICAL SETTING

Devonian strata on the eastern edge of the Western Canada Sedimentary Basin lie with profound unconformity on Archean to Paleoproterozoic gneisses of the Taltson magmatic zone (TMZ), a 300 km long, northward-trending belt of gneisses exposed in northeastern Alberta and the District of Mackenzie (Fig. 1). The TMZ is composed of extensive 1.97 to 1.92 Ga S-type granitic gneisses, 2.13 to 2.08 Ga high-grade paragneisses, and 3.2 to 2.14 Ga basement gneisses that are deformed by regional, north-striking, mainly strike-slip shear zones (McDonough et al., 1993; Villeneuve et al., 1993; McNicoll et al., 1994; Bostock and van Breemen, in press; Plint and McDonough, in press). Shear zones are locally mineralized where intersected by east-west brittle faults which may have acted as fluid conduits in the basement.

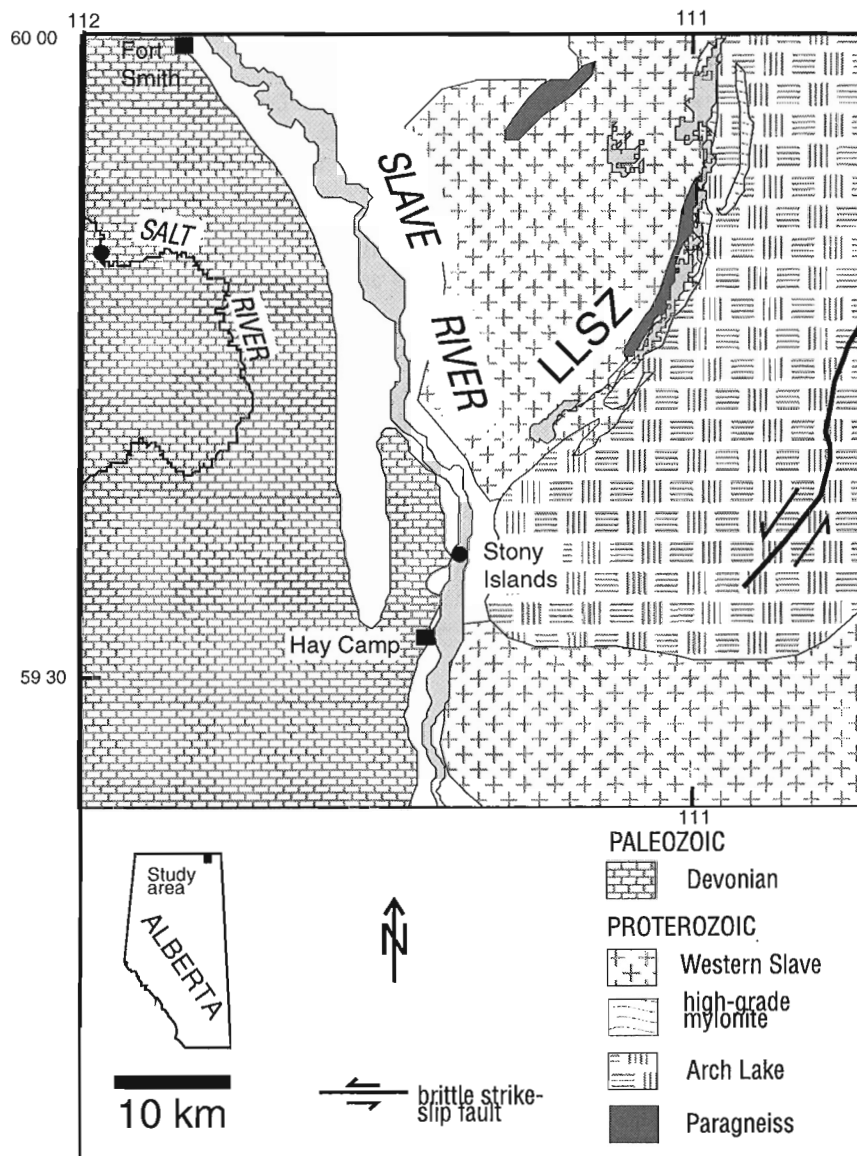


Figure 1.

Generalized geological map of the Fort Smith-Hay Camp area, Alberta (modified from Godfrey, 1986, and McDonough et al., 1993). Salt River and Stony Islands locations are given by solid circles. Western Slave and Arch Lake units are granite and syenogranite plutons, respectively. High grade mylonite comprises granulite to amphibolite grade mylonites in Leland Lakes shear zone (LLSZ).

DEVONIAN STRATIGRAPHY

Stony Islands

Strata overlying the Proterozoic basement at Stony Islands occur in a local trough, east of the eastern margin of the main basin. They are assigned to the La Loche and Fitzgerald formations as defined by Norris (1963).

Devonian rocks at Stony Islands are underlain by weakly deformed Slave granite and by strongly deformed granitic and pelitic gneisses associated with the southwestern extension of the Leland Lakes shear zone (Fig. 1; McDonough et al., 1994). Erosion of the basement surface has produced visible paleotopography having a minimum relief of 3 to 5 m, with Devonian strata onlapping local basement highs (Fig. 2).

A 30 to 50 cm thick, light yellow B-horizon paleosol of presumed Devonian age, which preserves planar Proterozoic fabrics, is developed at the top of the basement surface on the second island (Fig. 2). The paleosol is overlain by a 3 to 15 m thick regolith unit comprising calcareous angular conglomerate, conglomeratic sandstone, and sandy mudstone, and corresponds to the La Loche Formation of Norris (1963). The conglomerate is predominantly clast supported by granitic and semipelitic clasts derived from the basement, and is calcite cemented to locally malachite cemented. Clast size varies from pebble to boulder, with a significant increase in size proximal to basement highs. The La Loche Formation is of presumed Devonian age, as it underlies fossiliferous Devonian strata, and lies unconformably on Proterozoic gneisses.

The La Loche Formation is overlain by the Fitzgerald Formation (Norris, 1963), which consists of a 1 to 2 m thick, nodular-bedded dolomitic limestone unit, and contains a persistent 5 to 10 cm thick, thinly laminated, organic-rich, dark reddish silty shale layer near the base. The red shale is overlain by a well bedded, light grey to tan, micritic to locally sandy, carbonate unit. Fossil assemblages including *Amphipora* suggest a Lower or Middle Devonian age for the Fitzgerald Formation (Norris, 1963).

Table 1. Mineral occurrence location information (UTM Zone 12; NAD27).

Station no.	Easting	Northing	Description
M1264	475897	6605101	Py+Cpy+Mal; Fitzgerald Formation
M1265	476135	6605558	Py+Cpy+Mal; Fitzgerald Formation
M1266	476379	6605499	Mal cement; La Loche Formation
M1269	476132	6605278	Py+Cpy+Mal; Fitzgerald Formation
M1270	476360	6605862	Py; altered Slave granite
M1271	476571	6605269	Mal cement; La Loche Formation
M1276	445770	6631352	Gossanous Keg River limestone

Py=pyrite; Cpy=chalcopyrite; Mal= malachite

Salt River

At Salt River, well bedded to nodular limestones of the Keg River Formation (Norris and Uyeno, 1983) are deformed into a subsidence anticline on the east side of the river (Fig. 2). On the west side of the river, extensive karsting and collapse of Keg River limestones has produced a breccia zone (Fig. 2) approximately 10 m thick. Brecciation is accompanied by the development of gossans and associated calcite-pyrite (limonite) veining.

STONY ISLANDS COPPER OCCURRENCES

Basement

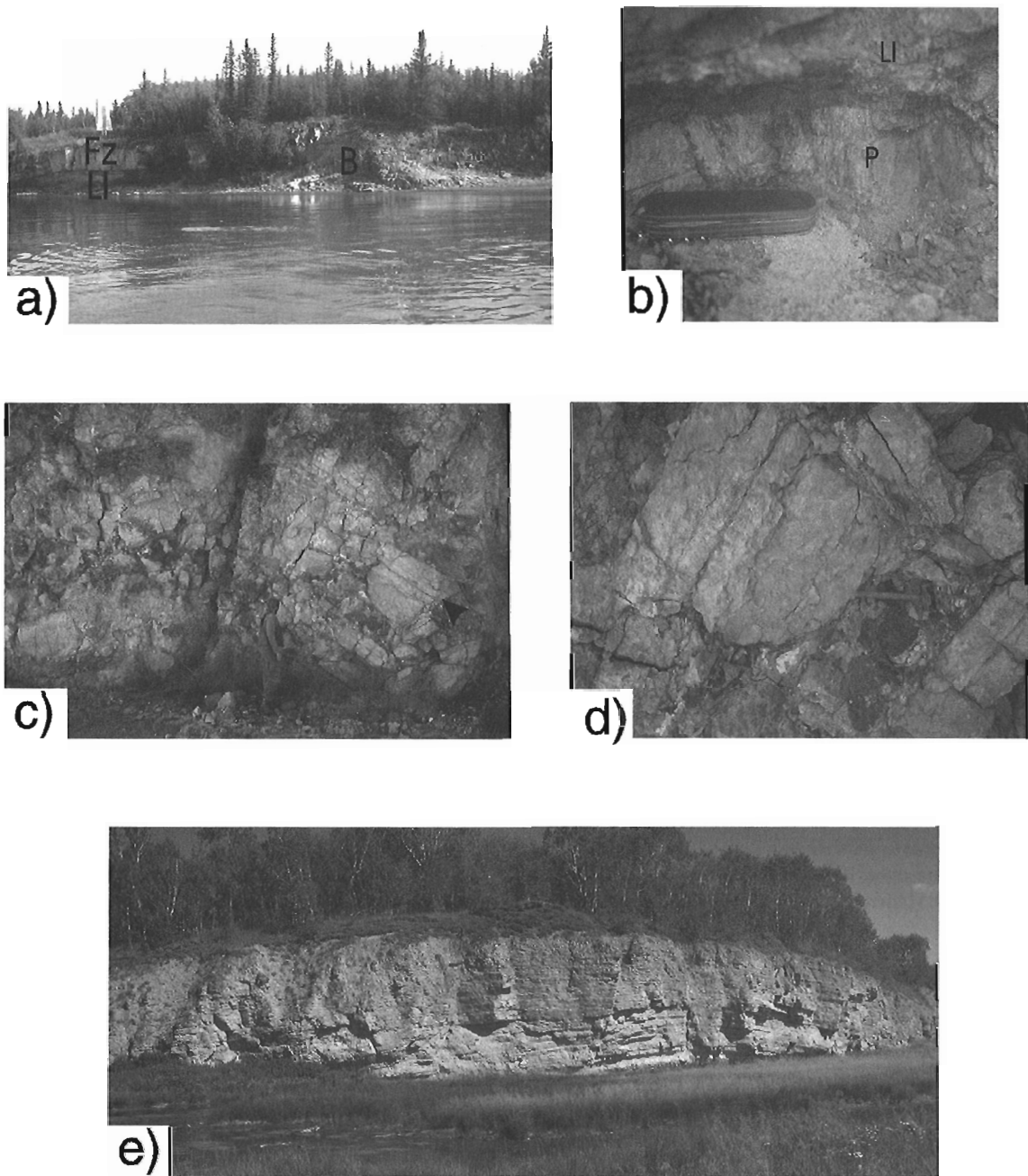
Copper mineralization at Stony Islands includes both vein and disseminated chalcopyrite and malachite, with subordinate amounts of azurite. Chalcopyrite-bearing calcite veins cut basement rocks at a low angle and reach 3 to 5 cm in width (Fig. 3). Chalcopyrite occurs in the middle of the veins and commonly is altered to malachite and azurite. Calcite veining was observed within a few metres of the contact with overlying sediments, where basement rocks are noticeably altered and pass upward into the paleosol described above. Gossanous staining of basement rocks is found in proximity to calcite veining and copper occurrences, and is associated with fine grained retrograde pyrite-chlorite assemblages, probably after biotite, within basement gneisses.

Middle Devonian

Near where calcite veins cut basement gneisses, the overlying La Loche Formation contains poikilotopic calcite cement that is probably of similar origin to the vein calcite. Chalcopyrite nodules are disseminated within the calcite cement and are associated with malachite and azurite staining. In the overlying Fitzgerald Formation, disseminated chalcopyrite is present with pyrite as 1 to 3 mm nodules that typically are coated by malachite, dark oxide, and minor azurite. Disseminated chalcopyrite occurs in a number of thin intervals in the lower part of the Fitzgerald Formation, but is most abundant in bedded limestones immediately above the red shale layer. Estimates of visible copper concentrations range up to 2 per cent.

DISCUSSION

The Stony Islands and Salt River areas are significant because they provide insights into potentially active mineralizing systems at the eastern margin of the Western Canada Sedimentary Basin (WCSB). Disseminated Au-Ag-Cu mineralization to the south in the Fort MacKay region (Abercrombie and Feng, 1994b) is inferred to be related to the discharge of saline brines at the eastern, updip margin of the WCSB (Feng and Abercrombie, 1994). This suggests a regional potential for disseminated Au-Ag-Cu mineralization along the eastern margin of the WCSB, both in the Proterozoic basement and overlying Phanerozoic sediments.



- a) *La Loche (Ll) and Fitzgerald (Fz) formations draping a basement (B) high at Stony Islands;*
- b) *paleosol (P) with preserved Proterozoic planar fabric overlain by La Loche (Ll) conglomerate. Knife is 9 cm long;*
- c) *collapse breccia in Keg River limestones at Salt River. Person for scale, arrow shows location of d);*
- d) *detail of c) showing gossanous material associated with breccia. Hammer is 34 cm long;*
- e) *subsidence anticline in Keg River limestones, east side of Salt River. Outcrop is about 20 m high.*

Figure 2. Outcrop photographs.

Although disseminated Au-Ag-Cu mineralization has been observed in Proterozoic rocks in the Fort MacKay area (Feng and Abercrombie, 1994), evidence for interaction between sedimentary fluids and the basement has only been inferred geochemically. At Stony Islands, clear evidence for interaction between Proterozoic basement gneisses and fluids originating within the sedimentary sequence is shown in the copper-bearing calcite veins that cut the basement and lower parts of the La Loche Formation. Therefore, it is reasonable to suggest that base and precious metals found within Phanerozoic sediments in the region may, in part, have originated through the scavenging of metals from the basement by relatively oxidizing, high salinity brines of sedimentary origin.

Fluid-related deformation, preserved in outcrops examined along the Slave and Salt Rivers, provides evidence for the style of mineralizing systems active in the region. Karsting and collapse of Middle Devonian limestones records the interaction of these rocks with waters of a number of possible origins. Surface-derived waters have undoubtedly contributed to the development of karst in the area. However, the discharge of sedimentary brines associated with the underlying Prairie evaporite occurs to the present day, and may have occurred since Middle Devonian time. Identification of the precise origin of these collapse structures will require further geochemical investigation. Whatever their origin, the collapse structures appear to have acted as vertical conduits



Figure 3. Calcite-chalcopyrite-azurite veins cutting highly altered basement gneiss within 1 m of the sub-Devonian unconformity at Stony Islands.

for the discharge of potentially metal-enriched sedimentary brines and therefore represent attractive targets for mineral exploration.

CONCLUSIONS

Further work is required to assess whether "Prairie-type" disseminated Au-Ag-Cu deposits (Abercrombie and Feng, 1994a; Feng and Abercrombie, 1994) are present in the Stony Islands/Salt River area. The disseminated and vein copper mineralization at Stony Islands, and the presence of gossanous collapse features associated with calcite-pyrite veins in Keg River limestones along the Salt River, indicate that metal-enriched fluids were present in this region. It is probable that these fluids travelled through fracture/vein systems in the basement, and moved upward into the overlying sedimentary column through solution collapse structures. This may provide a previously unrecognized opportunity for mineral exploration in the WCSB and underlying Precambrian basement.

ACKNOWLEDGMENTS

Cheerful assistance in the field by J. Van Ham is greatly appreciated. Critical review by R.W. Macqueen significantly improved the manuscript.

REFERENCES

- Abercrombie, H.J. and Feng, R.**
1994a: Prairie-type disseminated gold-silver-copper mineralization in the Western Canada Sedimentary Basin: Brine-associated native and alloyed metals, chlorides, oxides and carbonates; Geological Society of America, Abstracts with Programs, v. 26, no. 7.
- Abercrombie, H.J. and Feng, R. (cont.)**
1994b: Gold and PGE anomalies in Phanerozoic sedimentary rocks, northeastern Alberta; Program and Abstracts, Calgary Mining Forum, Calgary Mineral Exploration Group, February 10-11, 1994.
- Bostock, H.H. and van Breemen, O.**
in press: Ages of detrital and metamorphic zircons from a pre-Taltson magmatic zone basin at the western margin of Churchill Province; Canadian Journal of Earth Sciences.
- Feng, R. and Abercrombie, H.J.**
1994: Disseminated Au-Ag-Cu mineralization in the Western Canadian Sedimentary Basin, Forth MacKay, northeastern Alberta: a new gold deposit type; in Current Research 1994-E; Geological Survey of Canada, p. 121-132.
- Godfrey, J.D.**
1986: Geology of the Precambrian Shield of northeastern Alberta; Alberta Research Council, Map 1986-1, scale 1:250 000.
- McDonough, M.R., Cooley, M.A., and Schetselaar, E.M.**
1994: Geology, Hay Camp, Alberta (NTS 74M/11); Geological Survey of Canada, Open File 2832, scale 1:50 000.
- McDonough, M.R., Grover, T.W., McNicoll, V.J., and Lindsay, D.D.**
1993: Preliminary report of the geology of the southern Taltson magmatic zone, northeastern Alberta; in Current Research, Part C; Geological Survey of Canada, Paper 93-1C, p. 221-232.
- McNicoll, V.J., McDonough, M.R., and Grover, T.W.**
1994: U-Pb geochronological studies in the southern Taltson magmatic zone, northeastern Alberta; in Alberta Basement Transects Workshop, LITHOPROBE Report #37, (ed.) G.M. Ross; LITHOPROBE Secretariat, University of British Columbia, p. 270-273.
- Norris, A.W.**
1963: Devonian stratigraphy of northeastern Alberta and northwestern Saskatchewan; Geological Survey of Canada, Memoir 313.
- Norris, A.W. and Uyeno, T.T.**
1983: Biostratigraphy and paleontology of Middle-Upper Devonian Boundary Beds, Gypsum Cliffs area, northeastern Alberta; Geological Survey of Canada, Bulletin 313.
- Plint, H.E. and McDonough, M.R.**
in press: $^{40}\text{Ar}/^{39}\text{Ar}$ and K-Ar age constraints on shear zone evolution, southern Taltson magmatic zone, northeastern Alberta; Canadian Journal of Earth Sciences.
- Villeneuve, M.E., Ross, G.M., Thériault, R.J., Miles, W., Parrish, R.R., and Broome, J.**
1993: Tectonic subdivision and U-Pb geochronology of the crystalline basement of the Alberta Basin, western Canada; Geological Survey of Canada, Bulletin 447, 86 p.

Geological Survey of Canada Projects 920076 and 890053

Recent and late Holocene sand dune activity in southwestern Saskatchewan¹

Stephen A. Wolfe, D.J. Huntley², and Jeff Ollerhead³

Terrain Sciences Division, Calgary

Wolfe, S.A., Huntley, D.J., and Ollerhead, J., 1995: Recent and late Holocene sand dune activity in southwestern Saskatchewan; in Current Research 1995-B; Geological Survey of Canada, p. 131-140.

Abstract: This paper attempts to determine the chronology of recent and late Holocene dune activity within the Great Sand Hills region of Saskatchewan. Over the last 50 years, dune activity, as determined from aerial photographs, has varied in accordance with temperature and precipitation trends, increasing during periods of drought. The present trend is towards stabilization although the drought of the 1980s increased activity in several areas to the same level as during the mid 1940s. Optical dates for several dune deposits indicate that dunes have been active in the area within the last millennium. Most dates indicate recent dune activity (<200 years) while others record activity in the early to mid part of the last millennium. We tentatively conclude that a period of dune stability possibly occurred between 200 and 600 years ago and, based on basal deposits, approximately 2600 BP and earlier.

Résumé : Le présent article contient un compte rendu des essais que nous avons réalisés pour déterminer la chronologie de l'activité dunaire durant l'Holocène récent et tardif dans la région des collines Great Sand en Saskatchewan. Au cours des 50 dernières années, l'activité dunaire, établie à partir de photographies aériennes, a varié en fonction des tendances de la température et des précipitations, augmentant durant les périodes de sécheresse. La tendance actuelle est orientée vers une stabilisation même si la sécheresse des années 1980 a accru l'activité dunaire dans plusieurs régions à un niveau équivalent à celui du milieu des années 1940. Les datations optiques de plusieurs dépôts dunaires indiquent que les dunes ont été actives dans cette région au cours du dernier millénaire seulement. La plupart des dates indiquent une activité récente (<200 ans) tandis que d'autres correspondent à une activité datant du milieu du dernier millénaire. Nous concluons donc provisoirement qu'une période de stabilité des dunes a probablement eu lieu il y a entre 200 et 600 ans et, en se basant sur les dépôts de base, il y a environ 2 600 ans et avant.

¹ Palliser Triangle Global Change Contribution no. 18

² Physics Department, Simon Fraser University, Burnaby, British Columbia

³ Mount Allison University, Sackville, New Brunswick

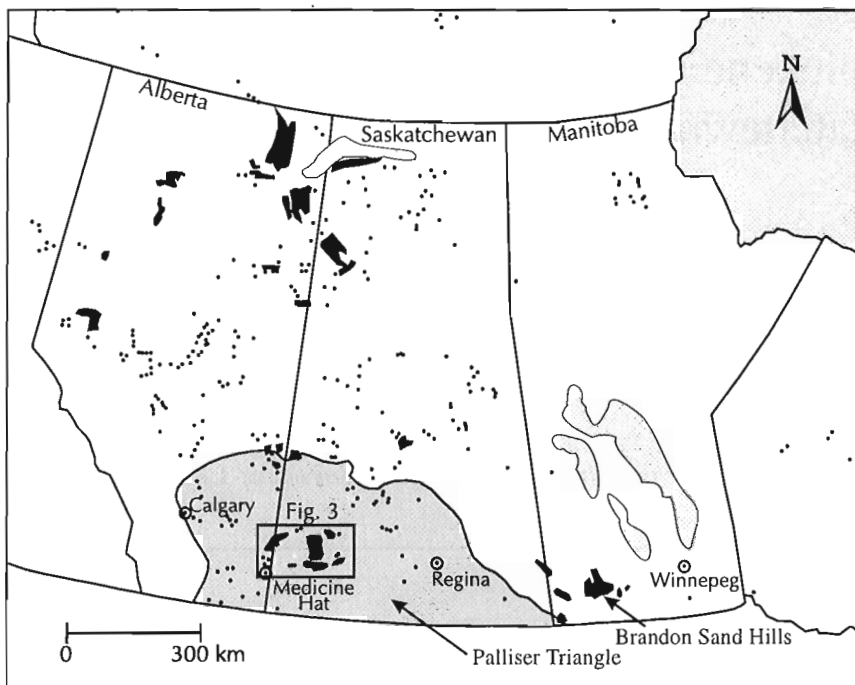


Figure 1.

Sand dunes (black) of the Canadian western prairies, including the Palliser Triangle region (shaded), after David (1989).

INTRODUCTION

In 1991, the Geological Survey of Canada selected the semiarid prairies of southern Alberta, Saskatchewan, and Manitoba as one of three Integrated Research Monitoring Areas (IRMAs) of the Global Change Program (Lemmen et al., 1993; Vance and Last, 1993). Known as the Palliser Triangle (Fig. 1), the region includes nearly all of the grain producing areas of the southern prairies. The regional economy is highly dependent on crop and cattle production, and recurrent droughts result in reduced productivity. Predictions by global circulation models of enhanced aridity combined with an increasing temperature trend for the prairies over the last century (Fig. 2) have also raised concerns over the area's economic future.

In order to help predict the potential geological impact of climate change in the region, relationships between climate and geomorphic processes are being investigated in the Palliser Triangle IRMA. Studies of modern dune activity, morphology, stratigraphy, and chronology are being conducted in the Great Sand Hills region of southwestern Saskatchewan, shown on Figure 3, in order to elucidate the effects of climatic variations upon the eolian system.

BACKGROUND AND STUDY AREA

Eolian processes affect much of the landscape in the Palliser Triangle, as evidenced by sand dunes, loess deposits, dust storms, and deflation of cultivated soils (Catto, 1983; Wheaton and Chakravarti, 1990; Wheaton, 1992; David, 1993). Approximately 20 per cent of the dunes in the western prairie provinces (excluding the Lake Athabasca region) are located within the Palliser Triangle (Fig. 1).

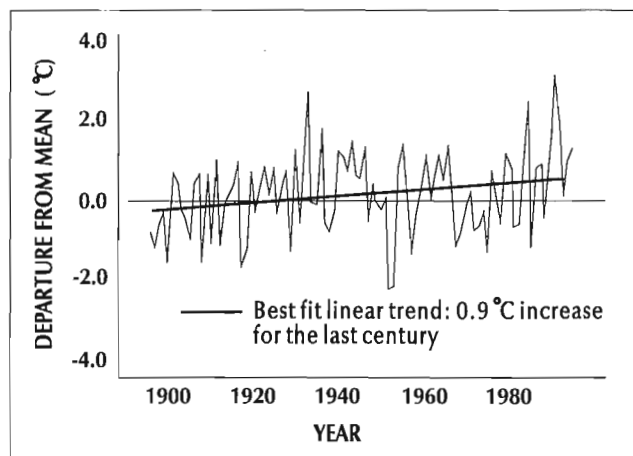


Figure 2. Annual temperature departures from 1951-1980 average for the Canadian prairies for the period 1895-1991 (Gullet and Skinner, 1992).

Although occupying only about 2 per cent of the Triangle, sand dunes nevertheless cover a total area of approximately 3600 km². Most are concentrated near the centre of the Triangle in southwestern Saskatchewan, in the vicinity of the Great Sand Hills.

Great Sand Hills is the largest contiguous dune occurrence in the Canadian Prairies (David, 1977). It is surrounded by numerous smaller dune fields including Tunstall, Bigstick, Seward, and Burstall sand hills, occupying a total area of more than 2000 km² (Fig. 3). The dunes are derived from glaciofluvial, glaciolacustrine, and deltaic sediments deposited during retreat of the Laurentide Ice Sheet. Eolian activity has reworked these deposits into various forms of parabolic dunes, blowouts, and dune crevasses migrating in a general easterly direction.

This area of relatively high dune density is the most arid in the Triangle, with precipitation (~ 300 mm/a) amounting to only 60 per cent of potential evapotranspiration (~ 500 mm/a) in an average year and 40 per cent or less in dry years such as 1987 and 1988 (Environment Canada, 1993). Despite the semiarid climate, nearly all dunes in the region are presently stabilized by sparse vegetation cover. Nevertheless, a few parabolic dunes, blowouts, and small sand sheets are active, especially along the western margin of the Great Sand Hills (Fig. 4).

David (1993) suggested that, under the present-day climate, the long-term trend is towards stabilization of dunes in most parts of the prairies with the lowest rates of stabilization occurring in the Great Sand Hills region. David (1993) further suggested that most larger dunes (higher than 6 to 8 m) probably became active during every period of major or minor aridity in the last three to four millennia because of reduced

vegetation cover due to lower groundwater levels. David (1971) indicated that, outside the Palliser Triangle in the Brandon Sand Hills of Manitoba, major dune activity occurred sometime after 3700, 2100, 1500, 900, and 400 BP as a result of increased dryness in an otherwise subhumid local climate.

As yet there has been no attempt to establish relationships between dune activity and climatic indices in the Palliser Triangle. Furthermore, prior to this study, there were no dates from sand dunes relating to previous eolian activity in the Palliser Triangle. This lack of data has severely limited the possibility of anticipating the potential geomorphic impact of climate change within the region. In the present study we examine recent dune activity and the climatic indices of temperature and precipitation to determine if dune activity has been responsive to climatic variability in the last 50 years.

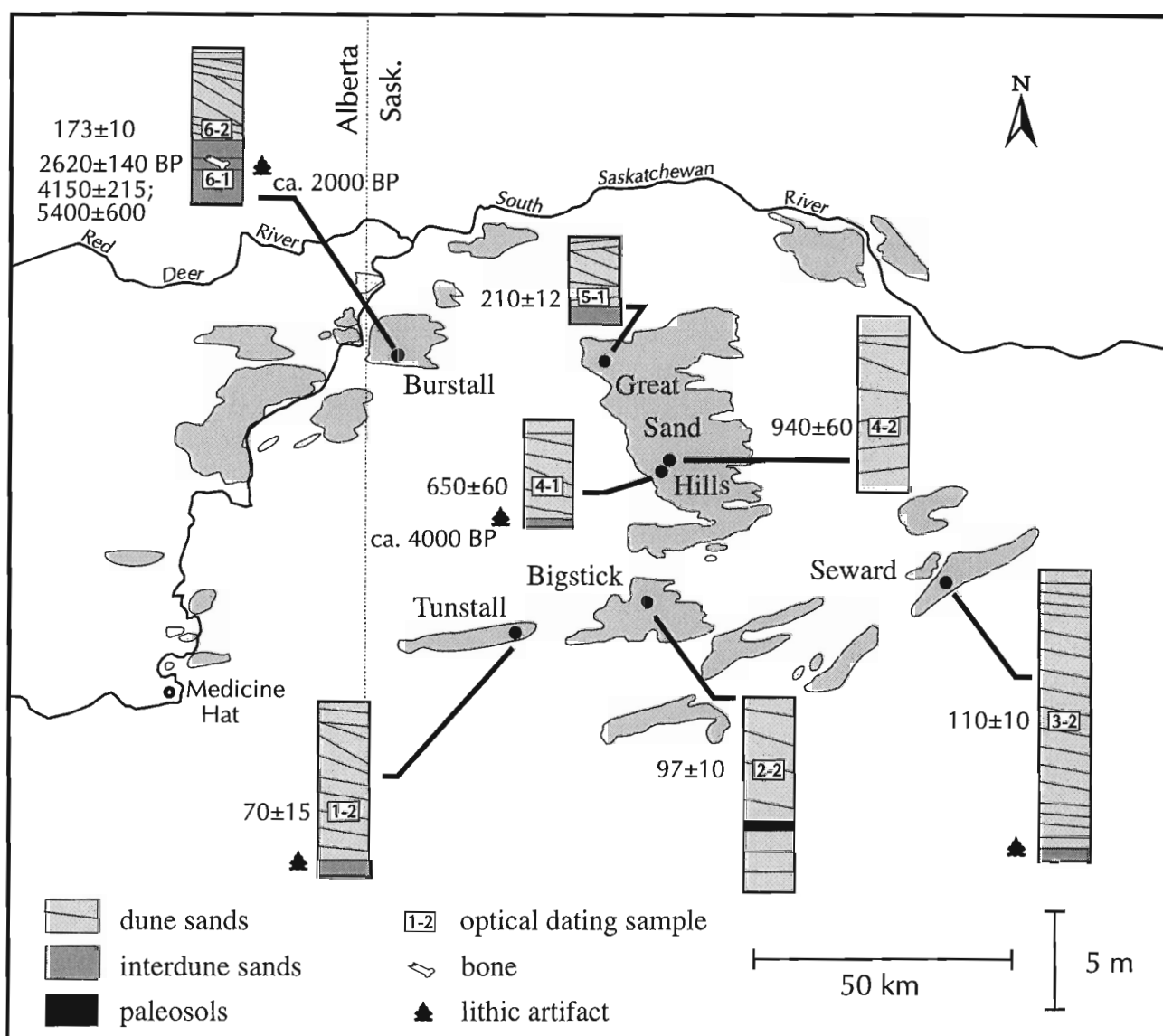


Figure 3. Sample locations, simplified stratigraphy, and dates from the Great Sand Hills region.

Additionally, dune deposits were optically dated to establish chronological control on past dune activity in the Great Sand Hills region.

RECENT DUNE ACTIVITY

In order to obtain a record of recent dune activity in the region, an analysis of aerial photographs dating back to 1944 was undertaken. Aerial photographs were scanned digitally and bare sand areas were subsequently outlined and brought to a common scale using a computer illustration package.

Figures 5 and 6 depict the area of active dunes in the Seward Sand Hills and northwestern Great Sand Hills from 1944 to 1991. For most of this period there has been a general decline in dune activity as marked by a decrease in both the size and number of active dunes. Dune activity in the Seward Sand Hills (Fig. 5) was greatest in 1944 during the period of photographic record. Since then, many of the dunes have decreased in area or stabilized completely resulting in the area of active sand dunes in 1991 being less than 30 per cent of the active area in 1944. Furthermore, very few stabilized dunes reactivated during this period. In the northwestern Great Sand Hills (Fig. 6), dune activity was also greatest in the 1944

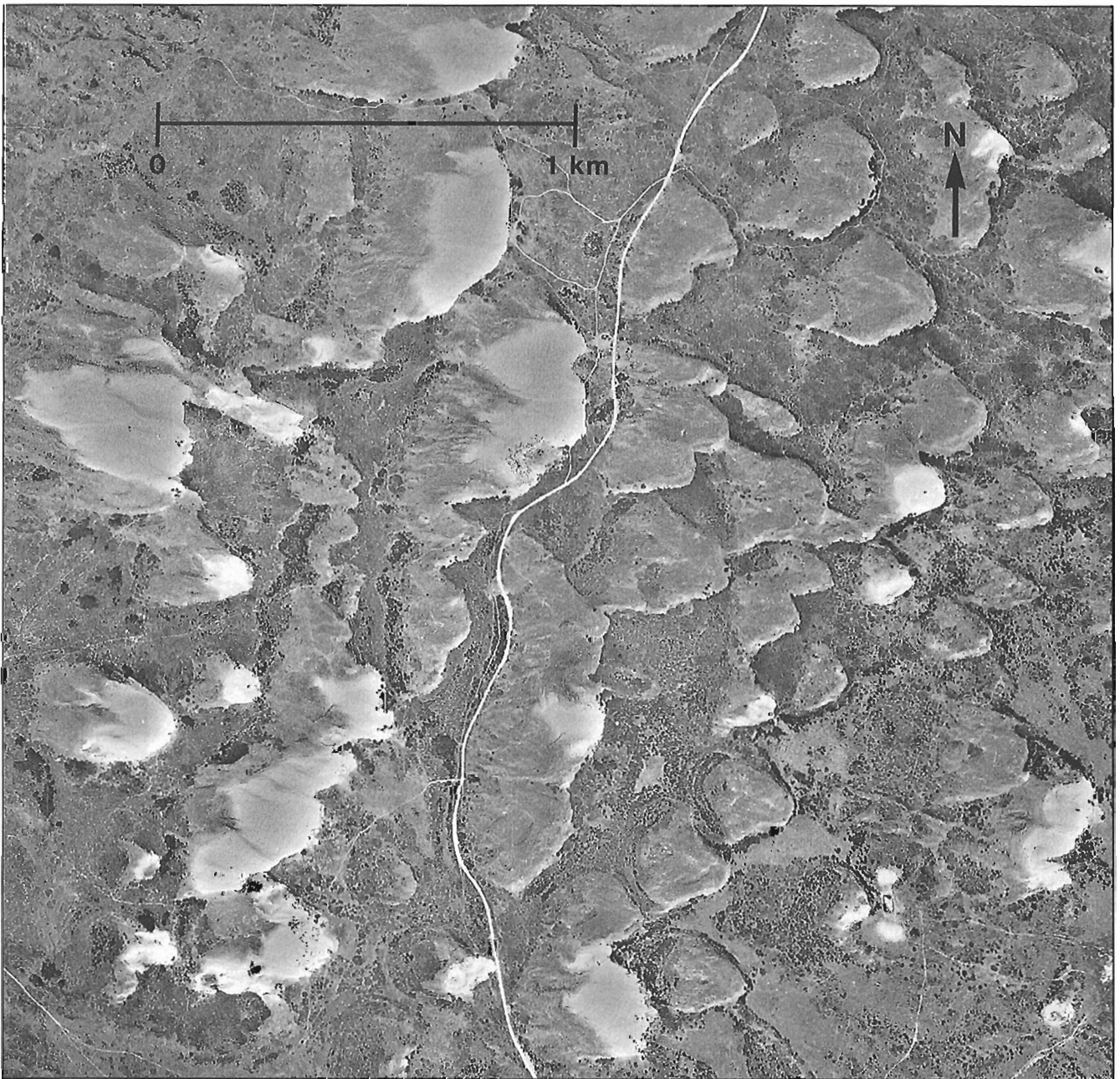


Figure 4. Vertical aerial photograph of easterly migrating active (lightest tone) and stabilized parabolic sand dunes in the northwestern Great Sand Hills. NAPL photo number A21003-101, 1967.

airphoto, with a decrease in active area through to the late 1970s. In 1988 and 1991, however, there was a marked increase in dune activity resulting in a total active area roughly equivalent to that of 1944.

Decreases in dune activity have occurred since 1944, at the same time as an apparent increasing temperature trend in the prairies for the last century (Fig. 2). This is caused, in part, by variability in mean annual temperatures observed in the last 50 years. However, the primary factor controlling dune activity in this semiarid environment is vegetation cover (David, 1993), which responds to moisture availability and temperature. Therefore, dune activity in the region is sensitive to both precipitation and temperature, which define some level of aridity, rather than to temperature alone. In other arid

and semiarid environments, dune activity has been shown to be a function of the ratio of precipitation to potential evapotranspiration (Muhs and Maat, 1993; Lancaster, 1988).

Prairie precipitation trends for the last century indicate that the period encompassing the late 1920s to early 1940s had below average precipitation (Environment Canada, in prep.); coupled with above average temperatures (Fig. 2), this resulted in a period of increased dune activity. The 1940s through to the late 1950s was a period of increased moisture availability accompanied by dune stabilization as observed in Figures 5 and 6. The late 1950s to mid 1960s was a period of below average precipitation and average to above average temperatures. This period is marked by a 10 per cent increase in the area of active dunes in the Seward Sand Hills. Since the

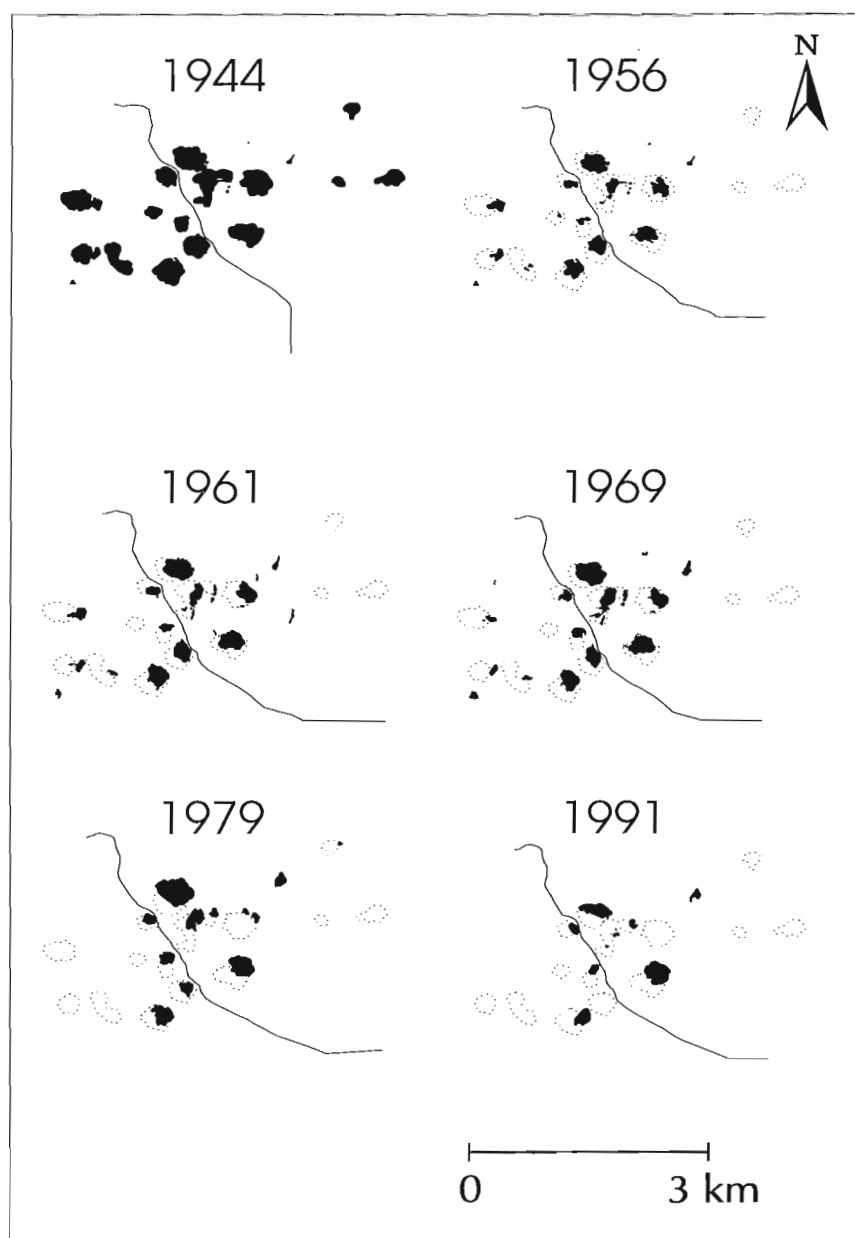


Figure 5.

Active dune areas (black) in the Seward Sand Hills, illustrating change from 1944 (dotted outline) to 1991.

mid 1960s precipitation has generally fluctuated close to the 30-year average from 1951 to 1980, with a marked decrease in precipitation in the 1980s accompanied by average to above average temperatures. In the Seward Sand Hills, dune activity has steadily decreased since the 1960s, whereas in the northwestern Great Sand Hills, dune activity decreased through to 1979 but then increased in 1988 and in 1991. It appears that increased dune activity can be attributed to decreased precipitation and warmer temperatures in the mid to late 1980s. As a result, the area of active dunes in 1991 was equivalent to that in 1944. At the Tunstall Sand Hills, a trend towards dune stability is also apparent with the active area in 1991 only 65 per cent of that of 1944, despite a 10 per cent increase from 1979 to 1991.

Since the level of dune activity is affected by moisture availability, areas such as the northwestern part of the Great Sand Hills, which have a high sand supply and are well drained, are particularly susceptible to drought. In contrast, the Seward Sand Hills, which are poorly drained due to a thin cover of eolian sand, retain more moisture in the ground and are therefore less susceptible to drought. Thus, the change in the area of active dunes in the last 50 years can be attributed to dune activity being a function of precipitation and temperature. The observational record of dune activity and climate on the prairies extends only a short period into the past, however, and it is necessary to rely on proxy sources such as lake cores, archaeological evidence, and various dating methods to build a record of climatic variability and dune activity during the Holocene.

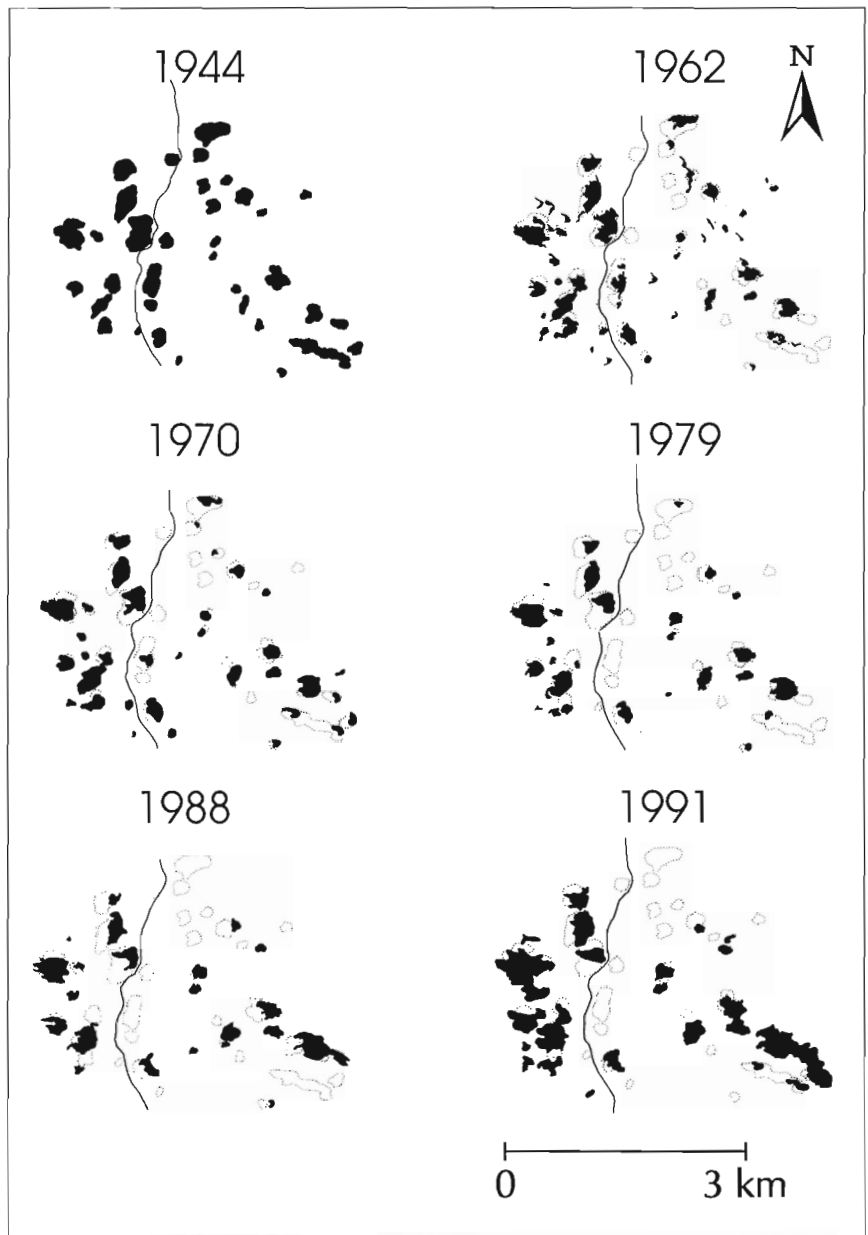


Figure 6.

Active dune areas (black) in the northwestern Great Sand Hills, illustrating change from 1944 (dotted outline) to 1991.

DATING

The paucity of organic matter in eolian deposits makes it difficult to obtain material for conventional radiocarbon or AMS (atomic mass spectrometry) dating. In addition, seeds and other light organics may be reworked in eolian deposits and, therefore, predate the deposit in which they occur. In situ organics such as soil horizons typically indicate periods of dune stability, and hence can only be used to broadly bracket periods of dune activity. Luminescence dating, on the other hand, is ideally suited for dune deposits as it provides a date corresponding to the last time the sediment was exposed to sunlight, and thus can be used to determine a period of eolian activity.

Optical dating, a type of luminescence dating well suited to sediments, was introduced by Huntley et al. (1985). It can be used for quartz, feldspar, or unseparated silt-sized grains; recent reviews have been given by Aitken (1992, in press). Ollerhead et al. (1994) showed that optical dating using 1.4 eV excitation (infrared) on separated K-feldspar grains gave good precision for samples as young as 100 years, although the question of absolute accuracy remained uncertain. It is this method that is used here. The reader should keep in mind that the errors quoted are analytical ones only, and that our knowledge of accuracy is limited, although from comparison done on samples of known age it is probably better than 30 per cent.

Samples were collected from seven sites within the Great Sand Hills region in order to gain a regional perspective on eolian activity within the area. All samples were collected from active blowouts because they exposed older eolian deposits and allowed easy access for sample collection. Sand was collected from major stratigraphic units representing the primary period of dune deposition at each site. Samples were collected from pits dug approximately 1 m into the sections. Additional samples were collected 30 cm above and below each primary sample for moisture contents and dosimetry. A description of the sampling sites is given in Table 1.

The procedures for sample preparation and analysis for optical dating used in this study were similar to those outlined by Ollerhead et al. (1994) except that infrared light, instead of sunlight, was used for the bleaching and the preheat was 16 hours at 120°C.

In situ bison bones were collected from the Burstall Sand Hills 2 m above the base of the blowout. Optical and radiocarbon samples from this section were used to date deposits predating the dune deposits. At the Burstall and the west-central Great Sand Hills sites, archaeological artifacts including projectile points were found on the surface of blowout areas. The age of the points was determined approximately, according to their classification within prehistoric periods.

Table 1. Description of sampling sites in the Great Sand Hills (GSH) region.

Sample	Location	Depth (m)	Water Content (% g.g ⁻¹)	Description
1-2	Tunstall	8.0	3.7	3 m above base of active blowout on a stabilized parabolic dune ridge; finely laminated bedded sands, 5 to 15 cm thick, dipping 10° E
2-2	Seward	8.0	6.2	7 m above base of active blowout at head of a stabilized parabolic dune; crossbedded sand beds to 1 m thick, dipping 17° to 21° E
3-2	Bigstick	4.0	4.4	6 m above base of blowout in an active compound parabolic dune; in sand beds 10 to 15 cm thick, laminae 3 mm to 20 mm, dipping 17° to 28° E
4-1	Central GSH	3.0	4.8	2.5 m above base of backslope of an active parabolic dune; subparallel sand beds dipping 12° to 17° E, laminae 3 mm to 5 mm, occasional convex structures; lithic artifacts found on blowout surface
4-2	Central GSH	6.0	6.3	3 m from base of blowout surface in active blowout of a compound parabolic dune in larger stabilized parabolic dune ridge; sub-parallel sand beds dipping 3° W, laminae 20 mm, occasional convex structures 20 mm thick and 15 cm wide
5-1	Northwest GSH	4.0	6.8	0.5 m from base of blowout surface in large active blowout upwind of active parabolic dune; subparallel, discontinuous convex sand beds dipping 3° to 7° NW, laminae 20 mm thick
6-1	Burstall	6.5	5.8	1.5 m above base of blowout in active blowout dune on a stabilized parabolic dune ridge; mottled sand oxidized stains, root casts, bison bone, and lithic artifacts
6-2	Burstall	3.0	5.1	5 m from base of blowout in same blowout as 6-1; crossbedded sands, beds to 40 cm thick, dipping 15° to 24° E; laminae 10 mm to 50 mm thick, dipping to 64°

Results

All dated samples contained greater than 99.5 per cent sand, the residual being silt. All samples were well sorted with mean grain sizes ranging from 2.15 to 2.71 phi (fine sand). The sand dunes were damp at a depth greater than 15 cm, and moisture contents of the samples ranged from 3.7 to 6.8 per cent ($\text{g}\cdot\text{g}^{-1}$) with an average of 5.4 per cent (Table 1).

Stratigraphy and dates for the sites are shown in Figure 3. At most sites active blowouts had eroded to the base of the eolian sands and revealed underlying sediments. These were typically sands similar in grain size to the dune deposits, but commonly grey and massive to horizontally layered, containing numerous iron oxide stained and cemented root casts. The lower sands represent former surfaces between dunes, and the iron oxide root casts are indicative of a prominent vegetative cover with adequate moisture (Gaylord, 1990). Paleosols are uncommon within the dune deposits themselves, despite the presence of root casts in the underlying interdune strata, and only the Bigstick site contained a soil horizon, indicating a period of dune stability. The lack of paleosols, in general, may be due to poor soil development on stabilized dunes or to the truncation of stabilized surfaces during dune reactivation.

Equivalent doses and dosimetry information for the optical dates are given in Tables 2 and 3, and calculated dates are given in Table 2 and Figure 3. These dates should be considered preliminary, pending further dosimetry measurements, but are unlikely to change by more than 5 per cent. Anomalous fading tests, yet to be performed, could show these dates to be lower limits. As a consistency check, sample 6-1 was also measured using a 5-day 140°C preheat; the result was indistinguishable from that of the 16-hour 120°C preheat (Table 2). For an additional check, a measurement was made

on quartz from 6-1 using 2.4 eV excitation (green) and a 48-hour 150°C preheat; this yielded a somewhat greater age (Table 2) and the accuracy of the ages must be considered uncertain to the extent of the disagreement.

Five dune samples had ages of 200 years or less, and all seven had ages within the last millennium. These young ages are to be expected if the dunes have been active during recent periods of aridity, reworking older deposits. This reworking means that older dune deposits are generally less common than younger ones in areas of present dune activity.

There is typically a considerable age difference between dune deposits and underlying sediment. At four sites, lithic artifacts were found on the surface of the blowout (Fig. 3). In the west-central Great Sand Hills, dune sands dating at 650 ± 60 years overlie sandy interdune deposits containing a projectile point of the Oxbow period from circa 4000 BP. Other artifacts at the same site also indicate later periods of occupation, including an early Prairie-Side Notched point from circa 1200 BP. Cluny Complex ceramic shards were also found on the surface of the blowout, and postdate the dune sands at some time after 300 BP.

At Burstall, dune sands dated at 173 ± 10 years overlie interdune deposits dating to at least 2000 BP. In situ bison bone from the interdune deposit was radiocarbon dated at 2620 ± 140 BP (SRC lab no. S-3553) and Pelican Lake-type projectile points found in the blowout are dated at circa 2000 BP. Sand taken from the same horizon as the bone sample was optically dated at 4150 ± 215 years using feldspar grains and 5400 ± 600 years using quartz grains. The two optical ages are significantly different, with quartz grains giving an older age. An additional sample, taken from the immediate vicinity of the bone, is currently being analyzed in

Table 2. Dose rates, equivalent doses, and optical dating ages of deposits in the Great Sand Hills (GSH) region.

Dune	Sample	Dose rate (mGy a^{-1})	D_{eq} (Gy)	Age (a)
K-feldspar; 1.4 eV excitation, 120°C, 16-hour preheat				
Tunstall	1-2	2.44	0.17 ± 0.03	70 ± 15
Seward	2-2	2.92	0.32 ± 0.02	110 ± 10
Bigstick	3-2	2.58	0.25 ± 0.01	97 ± 10
Central GSH	4-1	2.82	1.82 ± 0.15	650 ± 60
Central GSH	4-2	2.73	2.57 ± 0.11	940 ± 60
Northwest GSH	5-1	2.66	0.57 ± 0.02	210 ± 12
Burstall	6-1	2.62 ± 0.12	10.7 ± 0.8 10.9 ± 0.3	4150 ± 215
Burstall	6-2	2.78	0.48 ± 0.02	173 ± 10
quartz; 2.41 eV excitation, 150°C, 48-hour preheat				
Burstall	6-1	2.00	10.8 ± 0.9	5400 ± 600
140°C, 5-day preheat				

Table 3. Potassium (K), uranium (U), and thorium (Th) contents.

Sample	K ^a			
	Bulk sample (wt.% ± 6%)	K-feldspar fraction (wt.% ± 5%)	U ^b (µg.g ⁻¹ ± 0.09)	Th ^c (µg.g ⁻¹ ± 0.2)
1-2	1.35		0.8	(2.5)
2-2	1.36		1.3	(4.1)
3-2	1.49	7.1	0.9	2.5 ± 0.05
4-1	1.38		1.1	(3.5)
4-2	1.39	7.5	1.0	3.14 ± 0.03
5-1	1.23		1.1	(3.5)
6-1	1.43	7.6	1.3	4.1 ± 0.05
6-2	1.15		1.1	(3.5)

^a Potassium contents from atomic absorption analysis
^b Uranium contents from delayed neutron analysis
^c Thorium contents from neutron activation analysis except those in brackets which are calculated on the basis of a constant Th/U ratio of 3.15 determined from other measured values

an attempt to reconcile the difference between the optical dates and the bone date. At present, an average age of approximately 4800 years is tentatively assigned for exposure of these sediments to sunlight.

Although the age of the lithic artifacts could not be determined at Tunstall and Seward, the presence of artifacts at these sites suggests that a chronological break likely exists between the underlying deposits that contain them and dune sands optically dated at 70 ± 15 and 110 ± 10 years, respectively.

DISCUSSION

Given the limited number of samples, definitive conclusions regarding past eolian activity in the region cannot be made. However, the dates, combined with observations of recent dune activity, suggest that dunes have been active to some extent throughout the last 200 years. The sparsity of earlier dates is probably indicative of extensive, although possibly sporadic, recent dune activity (<200 years) in the Great Sand Hills region.

None of the dates from the Great Sand Hills region record dune activity between 220 and 590 years ago. According to Vance et al. (1992) the period between 100 and 600 BP was one of high water conditions at Chappice Lake, near Medicine Hat approximately 100 km southwest of the Great Sand Hills, coinciding with the Little Ice Age. The lack of dune activity at this time may be the result of increased moisture and dune stabilization between AD 1400 and 1770. The two dune samples from the west-central Great Sand Hills date at 650 ± 60 years and 940 ± 60 years, indicating dune activity in the

early part of the last millennium. The period between 600 and 1000 BP at Chappice Lake was marked by significant droughts (Vance et al., 1992).

The bone date and artifacts at Burstall suggest a period of occupation around 2600 BP with associated sediments tentatively assigned an optical date of about 4800 years. This may indicate that a period of dune stability existed locally at about 2600 BP and earlier. This period of stability conforms to the high water period at Chappice Lake, which occurred between 2600 and 4400 BP. Underlying deposits at most of the other dune sites also include oxidized root casts and associated lithic artifacts. At west-central Great Sand Hills, for example, this association could indicate a period of stability.

CONCLUSIONS

The association between dune activity and aridity during the historic period identified in this study suggests a correlation between eolian activity and climatic indices in this area for the last millennium. Despite the increase in dune activity in the late 1980s and early 1990s, the net trend in the last 50 years appears to be towards dune stabilization. As a consequence, few dunes are active today that were not active in 1944. Since the majority of optical dates for dune sands in the region are less than 200 years, it is reasonable to suggest that dune activity has continued at the present level or greater for the last 200 years. Prior to this, eolian activity likely coincided with aridity, with a period of relative stability possibly occurring between 200 and 600 years ago corresponding with the Little Ice Age, and increased activity occurring in the early part of the past millennium. Although no earlier dune dates are available within the region, deposits underlying dune

sands indicate moister conditions and possibly a period of dune stability occurring at circa 2600 BP in parts of the Great Sand Hills.

The tentative chronology presented here suggests that dune activity does correspond to periods of aridity within the region and could be correlated with fluctuations in precipitation and temperature through the late Holocene. Nevertheless, more detailed chronology of dune activity is required before such correlations can be fully substantiated. Ongoing investigations are focusing on improving the geological and historic record of dune activity and on correlating activity to climatic indices related to precipitation and temperature. With a better understanding of past eolian activity and climatic controls, it will be possible to predict the response of eolian dune activity to various climatic scenarios within the Palliser Triangle.

ACKNOWLEDGMENTS

The authors would like to thank Ian and Irene Forsyth for accommodation during fieldwork in Saskatchewan. Lithic artifacts were identified by Stan Mathison and Brian Gablehouse. Much of the preparation and analysis of samples for optical dating was performed by G.O. Morariu at Simon Fraser University. The authors wish to thank D.S. Lemmen for reviewing the manuscript.

REFERENCES

- Aitken, M.J.**
1992: Optical dating; *Quaternary Science Reviews*, v. 11, p. 127-132.
in press: Optical dating: a non-specialist review; *Quaternary Geochronology*.
- Catto, N.R.**
1983: Loess in the Cypress Hills, Alberta, Canada; *Canadian Journal of Earth Sciences*, v. 20, p. 1159-1167.
- David, P.P.**
1971: The Brookdale road section and its significance in the chronological studies of dune activities in the Brandon Sand Hills of Manitoba; *Geological Association of Canada, Special Paper no. 9*, p. 293-299.
1977: Sand dune occurrences of Canada: a theme and resource inventory study of eolian landforms in Canada; *Indian and Northern Affairs, National Parks Branch, Contract no. 74-230*, 183 pp.
- David, P.P. (cont.)**
1989: Eolian Processes; in Chapter 9 of *Quaternary Geology of Canada and Greenland*, (ed.) R.J. Fulton; Geological Survey of Canada, *Geology of Canada*, no. 1, p. 620-623.
1993: Great Sand Hills of Saskatchewan: an overview; in *Quaternary and Late Tertiary landscapes of southwestern Saskatchewan and adjacent areas*. (ed.) D.J. Sauchyn; *Canadian Plains Proceedings 25*, v. 2, Canadian Plains Research Centre, University of Regina, 114 p.
- Environment Canada**
1993: Canadian climate normals, 1961-90: Prairie Provinces; 266 p.
- Gaylord, D.R.**
1990: Holocene paleoclimatic fluctuations revealed from dune and interdune strata in Wyoming; *Journal of Arid Environments*, v. 18, 123-138.
- Gullet, D.W. and Skinner, W.R.**
1992: The state of Canada's climate: temperature change in Canada 1895-1991; *State of the Environment Report No. 92-2*, Atmospheric Environment Service, Environment Canada, 36 p.
- Huntley, D.J., Godfrey-Smith, D.I., and Thewalt, M.L.W.**
1985: Optical dating of sediments; *Nature (London)*, v. 313, p. 105-107.
- Lancaster, N.**
1988: Development of linear dunes in the southwestern Kalahari, southern Africa; *Journal of Arid Environments*, v. 14, p. 233-244.
- Lemmen, D.S., Dyke, L.D., and Edlund, S.A.**
1993: The Geological Survey of Canada's Integrated Research and Monitoring Area (IRMA) Projects: a contribution to Canadian global change research; *Journal of Paleolimnology*, v. 9, p. 77-83.
- Muhs, D.R. and Maat, P.B.**
1993: The potential response of eolian sands to greenhouse warming and precipitation reduction on the Great Plains of the U.S.A.; *Journal of Arid Environments*, v. 25, p. 351-361.
- Ollerhead, J., Huntley, D.J., and Berger, G.W.**
1994: Luminescence dating of sediments from Buctouche Spit, New Brunswick; *Canadian Journal of Earth Sciences*, v. 31, p. 523-531.
- Vance, R.E. and Last, W.M.**
1993: Paleolimnology and global change on the southern Canadian prairies; in *Current Research 1994-B*; Geological Survey of Canada, p. 49-58.
- Vance, R.E., Clague, J.J., and Mathewes, R.W.**
1992: Holocene paleohydrology of a hyposaline lake in southeastern Alberta; *Journal of Paleolimnology*, v. 8, p. 103-120.
- Wheaton, E.E.**
1992: Prairie dust storms - a neglected hazard; *Natural Hazards*, v. 5, p. 53-63.
- Wheaton, E.E. and Chakravarti, A.K.**
1990: Dust storms in the Canadian Prairies; *International Journal of Climatology*, v. 10, p. 829-837.

Geological Survey of Canada Project 910013

A preliminary assessment of remote sensing as a tool for mapping surficial sediments in the southern Canadian Prairies¹

A. Blais, W.R. Stevens, D.F. Graham², and V.H. Singhroy³
Terrain Sciences Division

Blais, A., Stevens, W.R., Graham, D.F., and Singhroy, V.H., 1995: A preliminary assessment of remote sensing as a tool for mapping surficial sediments in the southern Canadian Prairies; in Current Research 1995-B; Geological Survey of Canada, p. 141-149.

Abstract: As part of the Southern Prairies NATMAP Project, an attempt was made at using remote sensing as a tool for mapping surficial sediments. Three images were processed. One was a radar ERS-1 (SAR) image and by itself, it revealed only a rough outline of the geomorphological features, such as the meandering streams and a kettled till plain. The other two were Landsat TM images (Bands 4, 5, and 7) one taken in the spring and one taken in the late summer. From these, two saturation processed images were produced. These revealed a better outline of the available geomorphological features by delineating them in black. Colour composites of Landsat TM bands combined with ERS-1 (SAR) data showed encouraging results. More image processing is in progress to evaluate the potential use of remote sensing as a tool for mapping surficial sediments in the southern prairies.

Résumé : Dans le cadre du projet des Prairies méridionales du CARTNAT, l'utilisation de la télédétection pour cartographier les sédiments de surface a été mise à l'essai. Trois images ont été traitées. L'une d'elles était une image radar (ROS) saisie par ERS-1 qui, par elle-même, n'a permis qu'une délimitation grossière des éléments géomorphologiques, comme les ruisseaux à méandres et une plaine de till à dépressions fermées. Les deux autres images étaient des images saisies par le TM de Landsat (bandes 4, 5 et 7), l'une prise au printemps et l'autre à la fin de l'été. À partir de celles-ci, deux images saturées ont été produites. Elles révèlent avec plus de précision les différents éléments géomorphologiques en les délimitant en noir. Les compositions colorées des bandes TM de Landsat combinées aux données recueillies par ROS d'ERS-1 ont donné des résultats encourageants. Le traitement d'autres images se poursuit afin d'évaluer le potentiel de la télédétection comme outil de cartographie des sédiments de surface dans les prairies méridionales.

¹ Contribution to the Southern Prairies NATMAP Project

² Remote Sensing Office, Geological Survey of Canada, Ottawa, Ontario

³ Canadian Centre for Remote Sensing, Ottawa, Ontario

INTRODUCTION

Surficial sediment mapping in the southern prairies began in 1992 as part of the Southern Prairies NATMAP Project (Fulton et al., 1994). The purpose of this part of the project is to map the Quaternary surficial sediments of a section of the Virden map area (62F), southwestern Manitoba/southeastern Saskatchewan (Fig. 1). In addition to the traditional method of mapping Quaternary surficial deposits (i.e., air photo interpretation, traversing, till sampling for geochemical analyses and pebble counts for ice flow indicators, searching for paleocurrent indicators in ice marginal sand and gravel deposits, augering for stratigraphic indicators, etc.), an attempt was made at using remote sensing as a method of mapping these deposits. The main objective was to compare two satellite images; one taken in the spring and one in the late summer to look for soil moisture differences inherent in sediment textures and perhaps geomorphological features. The second objective was to evaluate whether an enhanced ERS-1 SAR image could outline the relief and hence, geomorphological features in such flat topography as the southern prairies.

STUDY AREA

Physiography

The study area includes four 1:50 000 scale map areas (NTS 62F/5, 11, 12, 13; Fig. 1), which are located within the Saskatchewan plain of the southern Interior Plains physiographic region (Klassen, 1989). The Saskatchewan plain is separated from the Alberta and Manitoba plains by escarpments with sharp westward rises. These bedrock rises were developed on a preglacial surface. On the western side of the Saskatchewan plain, the bedrock rise is called the Missouri Coteau and it measures about 100 m. On the eastern side, the bedrock rise is called the Manitoba Escarpment and

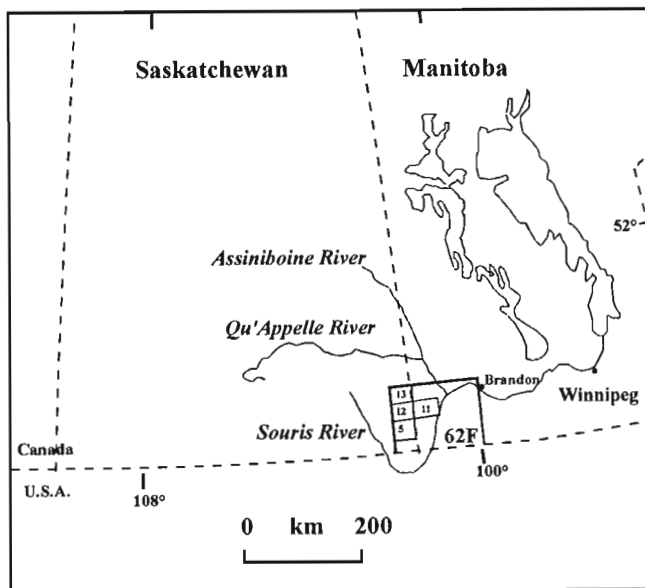


Figure 1. Location map of study area.

it measures about 300 m. Because of these sharp westward rises, the drainage pattern follows a general eastward current towards the Canadian Shield (Klassen, 1989).

Surficial sediments

Regional geomorphology of the sediments reflect the underlying bedrock surface of the southern Canadian Interior Plains (Klassen, 1989). Hence, the general topography in the study area is flat to gently rolling with a sediment cover of 30 to 90 m thickness and virtually no bedrock exposure.

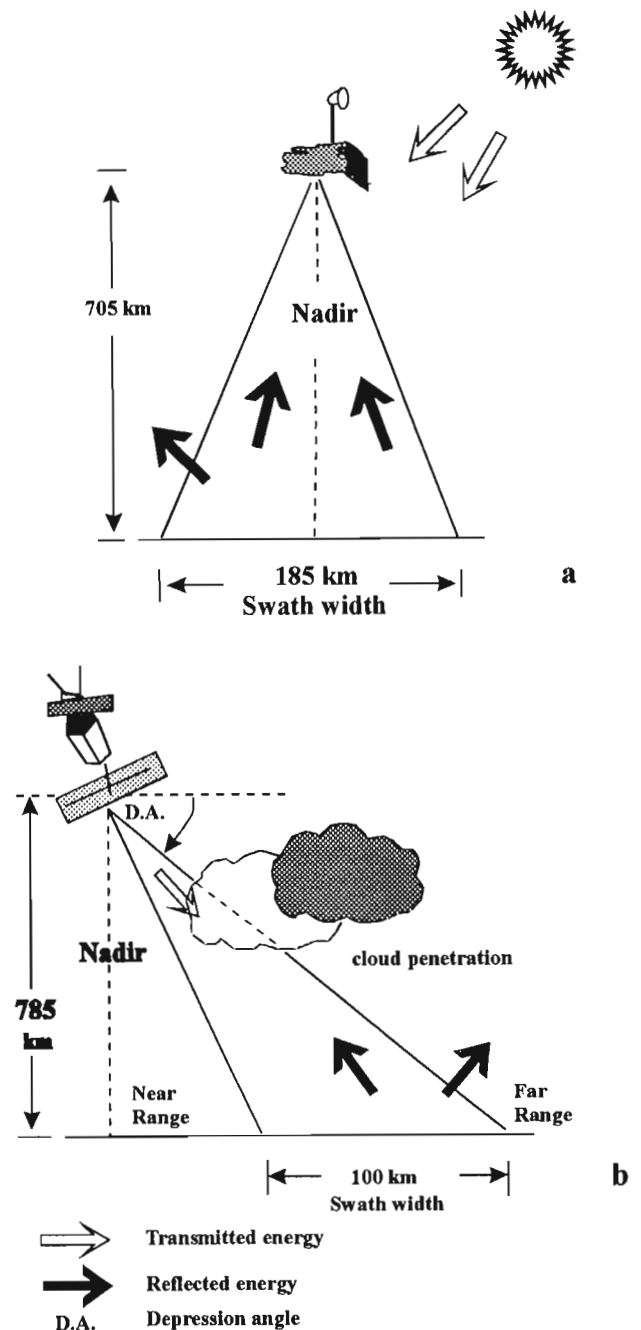


Figure 2. Satellite imaging geometries (not to scale). a) Landsat TM. b) ERS-1 SAR.

Surface sediments of the study area were deposited during and since the last glaciation (Late Wisconsinan-Holocene). The most abundant type of sediment found in the area is till, which was deposited during the last glaciation. It is mainly composed of equal amounts of clay, silt, and sand with minor coarser material. Geomorphological features associated with the surface till deposits are hummocky moraine with knob and kettle topography.

Another type of glacial sediment observed are glaciofluvial deposits, which are composed mainly of sorted, stratified sand and gravel. In the study area, the geomorphological features associated with these glaciofluvial deposits are usually outwash trains.

The non-glacial sediments observed in the study area are modern alluvial and colluvial deposits. The composition of alluvial deposits varies greatly from "washed till" to well sorted, silts, sands, and gravels. Geomorphological features associated with these are meandering drainage patterns defined by modern rivers and streams. Colluvial deposits are mainly composed of fine grained slope washed sediments deposited in temporary bodies of water (kettles).

PREVIOUS WORK

There are very few published articles on mapping surficial sediments in the Canadian Prairies using remote sensing. For example, Sauer (1980) studied the effects of glaciation in southern Saskatchewan and Mollard (1986) evaluated the effects of landscape related to oil and gas exploration. A study by Singhroy et al. (1992; in press) suggested integrating radar images with TM data in order to enhance surficial materials found in areas of low relief, such as The Pas, west-central Manitoba. However, most studies that have been conducted in the Canadian Prairies on surficial materials are related to soil or vegetation assessments (Bannatyne, 1980; Mollard and Robert Janes, 1984; Sauchyn, 1990).

METHODOLOGY

Data sets

Landsat TM

Two digital Landsat data sets (Landsat TM imaging geometry; Fig. 2a) were selected and processed. In order to identify textural differences through moisture variations, TM data sets of early spring (May 14, 1993) and late summer (August 29, 1991) were used. These data sets were geometrically corrected to UTM projections using topographic maps (1:50 000 scale) of the Virden (62F) area.

Landsat TM spring and late summer image contrasts were enhanced for all 7 Bands. After examination of the 7 Bands, TM Bands 4, 5, and 7 were chosen for this study because they highlighted terrain features (drainage and kettles). Satellite image interpretation studies on vegetation have also used these three TM bands (Mollard and Robert Janes, 1984).

Principal component analysis was tested on the late summer TM data because this enhancement technique had been proven useful for highlighting subtle terrain features, such as rock alteration (Ma et al., 1991). However, after comparing principal component enhancements with contrast stretch enhancements, it was observed that the contrast stretch image displayed terrain features better. Therefore, the principal component enhancement technique was not further considered.

ERS-1 SAR

To further enhance surface texture and terrain roughness, an ERS-1 Synthetic Aperture Radar (SAR; dated May 25, 1993) image was introduced as suggested by Singhroy et al. (1992). The ERS-1 (SAR) image is a single band image. This single band is called the C-band (5300 MHz) and it has a beam with a depression angle of 64° to 70° (SAR imaging geometry, Fig. 2b).

Image enhancement techniques

The purpose of image enhancement techniques in remote sensing is to improve the visual impact of the image, so as to facilitate the geological image interpretation (Singhroy et al., in press). The following procedures were conducted on the ERS-1 SAR image and the TM images based on the methods proposed by Harris et al. (1990), Graham and Ciesielski (1994), and Singhroy et al. (in press). The procedures are presented as flow diagrams in Figures 3, 4, and 5.

As mentioned above, the Landsat TM spring and summer images were first enhanced by conducting an image contrast stretch and geometrically correcting them (also called geocoding; Fig. 3).

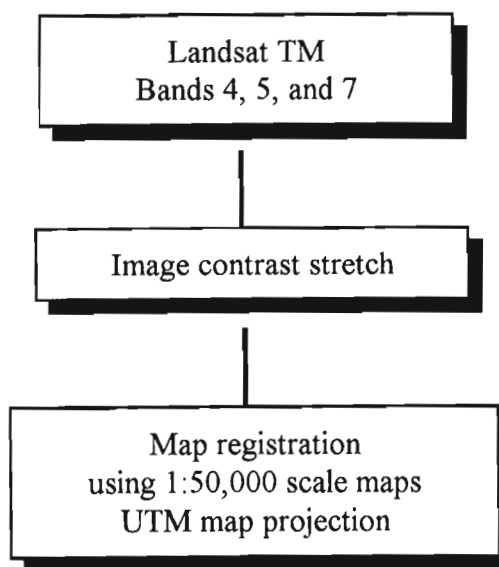


Figure 3. Enhancement flow diagram – Landsat TM.

Based on methods proposed by Singhroy et al. (in press), the ERS-1 SAR image was processed from 16 to 8 bit data compression to facilitate the imagery display. Following this step, the image was filtered to suppress speckle. Reduction of radar speckle improves the interpretability of the radar image. After filtering, the radar image was enhanced with a linear contrast stretch. Finally, the radar image was then registered to the geocoded TM images to improve its geometric quality (Fig. 4).

IHS transform enhancement

The final steps in image enhancements were carried out using what are called IHS transform techniques (Fig. 5). IHS transform is defined by: "three separate, orthogonal, and easily perceived colour attributes, those of intensity, hue, and saturation" (Harris et al., 1990, p. 1631). Intensity is the total energy or brightness of the image. Hue represents the average

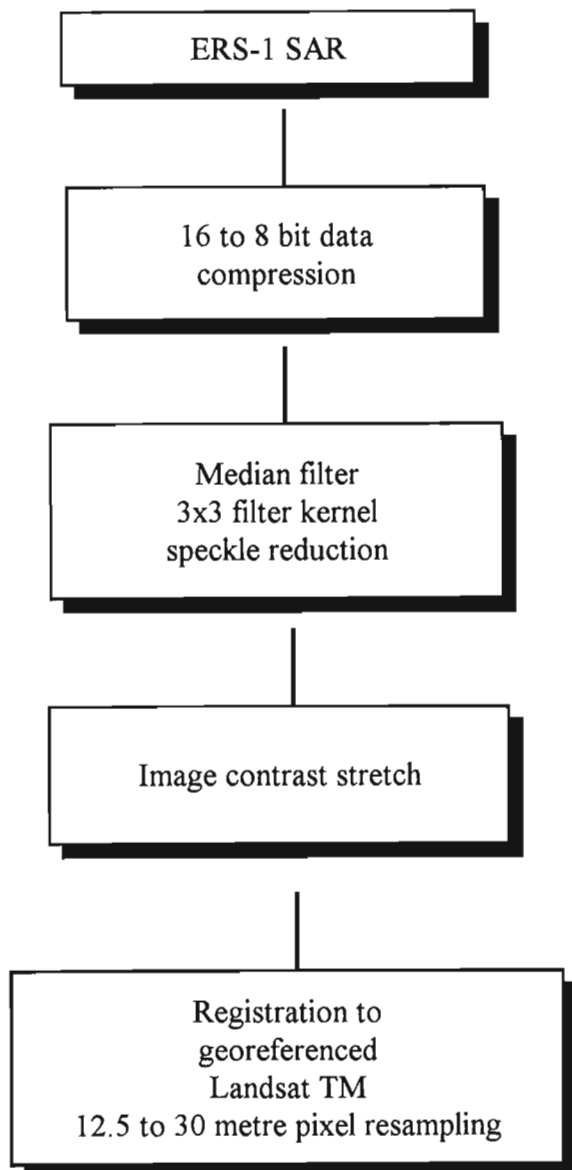


Figure 4. Enhancement flow diagram – ERS-1 (SAR).

wavelength of colour and ranges from blue through green, yellow, red, and purple. Saturation is described as the purity of colour (Harris et al., 1990).

In our case study, one of the red, green, blue (RGB) colour systems has been assigned to one TM Band (Fig. 5). In other words, red (R) was assigned to TM-4 Band, blue (B) to TM-5 Band, and green (G) to TM-7 Band (Fig. 5).

a) Integration of TM and SAR data

Since colour composites of TM and SAR data have been used successfully in geological mapping (Singhroy et al., 1993a,b), we integrated our data sets also. The purpose of using an IHS transform technique in the integration is to maintain the spectral and spatial characteristics (Singhroy et al., in press).

b) Saturation of each TM data set

An IHS transform technique was conducted on each TM image through what is called a saturation technique. The saturation enhances the image so that the variation in the quantity of white light introduced back into the image is at a maximum. The result is a black and white image with varying levels of grey tones. All tones in the image have an assigned digital number value (DN) that varies between 0 (black) and 255 (white) (Harris et al., 1990).

DISCUSSION OF RESULTS

ERS-1 data

The ERS-1 SAR spring image enhancement was used to bring out variations in topography and ground roughness (Fig. 6). In the study area, local topography is controlled by the river channels which cut through the subtle relief of the prairies. Surface roughness is generally man-made in the form of homogeneous crop growth in individual fields or the orientation of furrows in tilled fallow fields. The roughness of a fallow field, as expressed in the ERS-1 image, is a function of the orientation of furrows with respect to the SAR antenna look direction. In Figure 6, only a rough outline of a meandering river basin is shown in dark grey tones with a few dark grey speckles that are probably water filled kettles. In this case, the enhanced ERS-1 SAR, by itself, indicates poor results.

TM data

In the spring and late summer TM images enhanced through saturation, the drainage channel boundaries were highlighted by a darker tone at channel margins (the width of a single pixel; Fig. 7, 8). This indicates locations where all three TM bands have close to the same digital value (DN; grey level).

As a result, the saturation enhanced TM images for the spring (Fig. 7) and late summer (Fig. 8) were the best black and white image enhancements for outlining the geomorphological features available in the area, such as the meandering drainage pattern and the kettled till plain. For reasons still

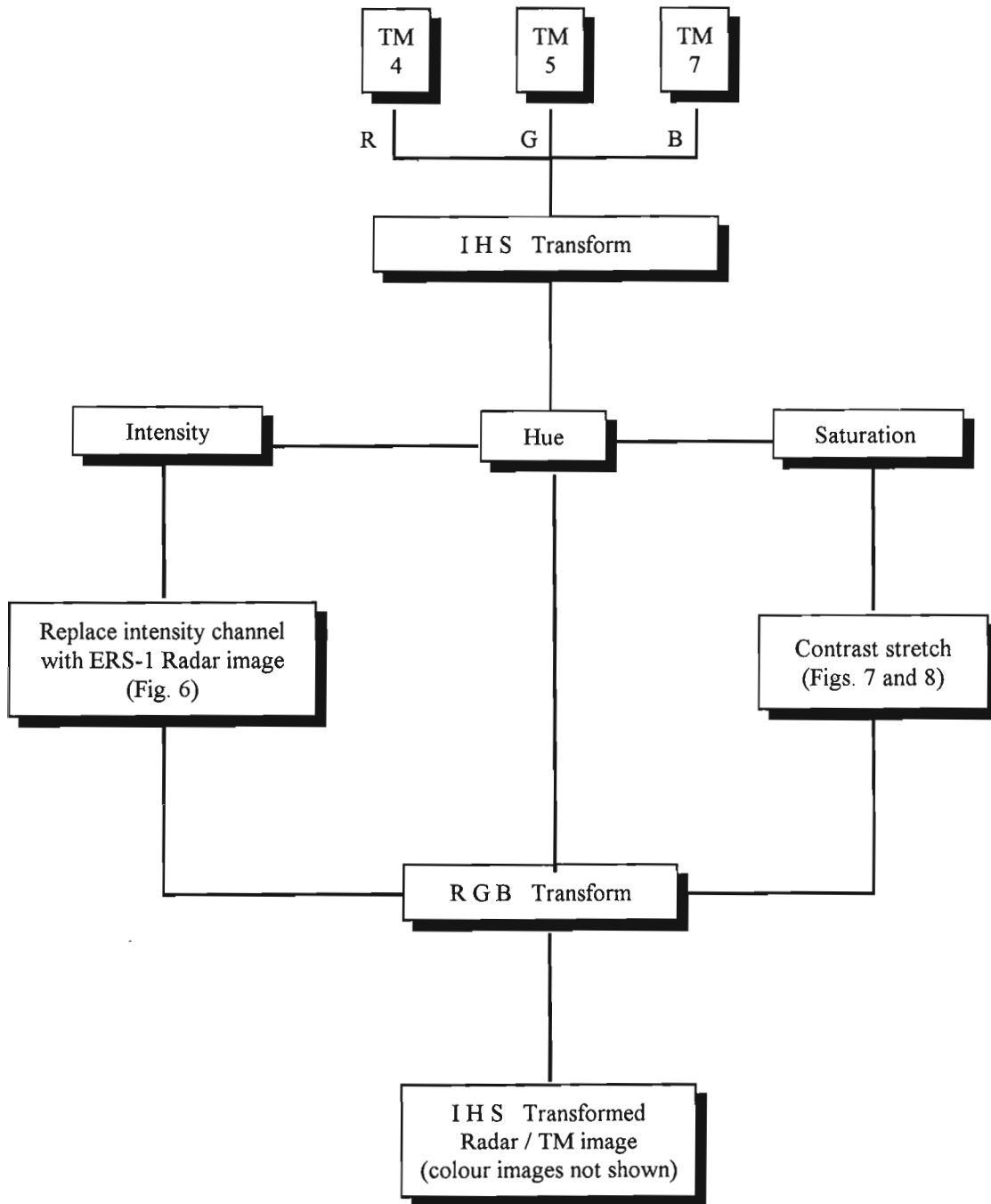


Figure 5. Enhancement flow diagram.

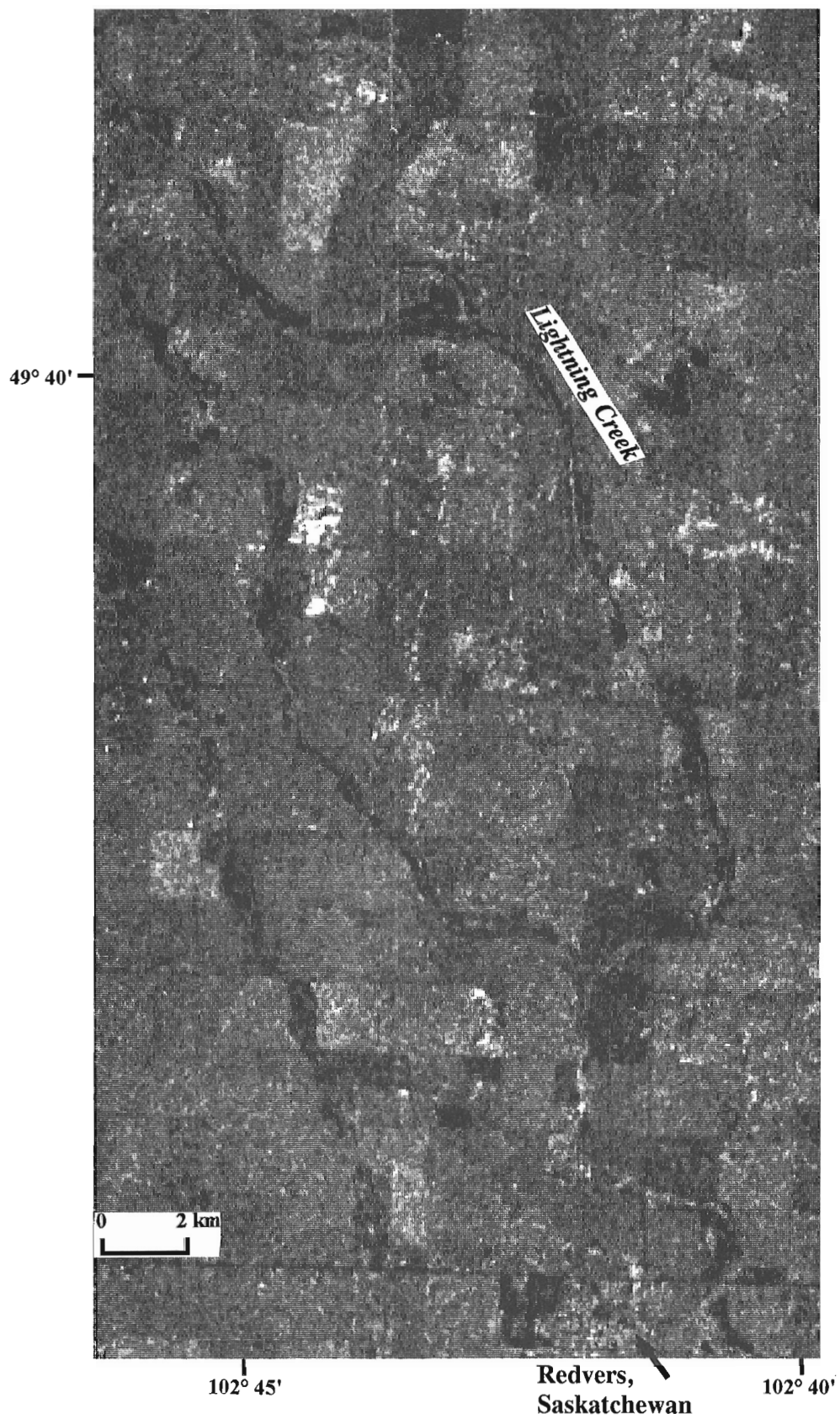


Figure 6. ERS-1 SAR outlining meandering drainage system. Redvers, Saskatchewan is located in the south-central part of NTS 62F/12 map area (Fig. 1).

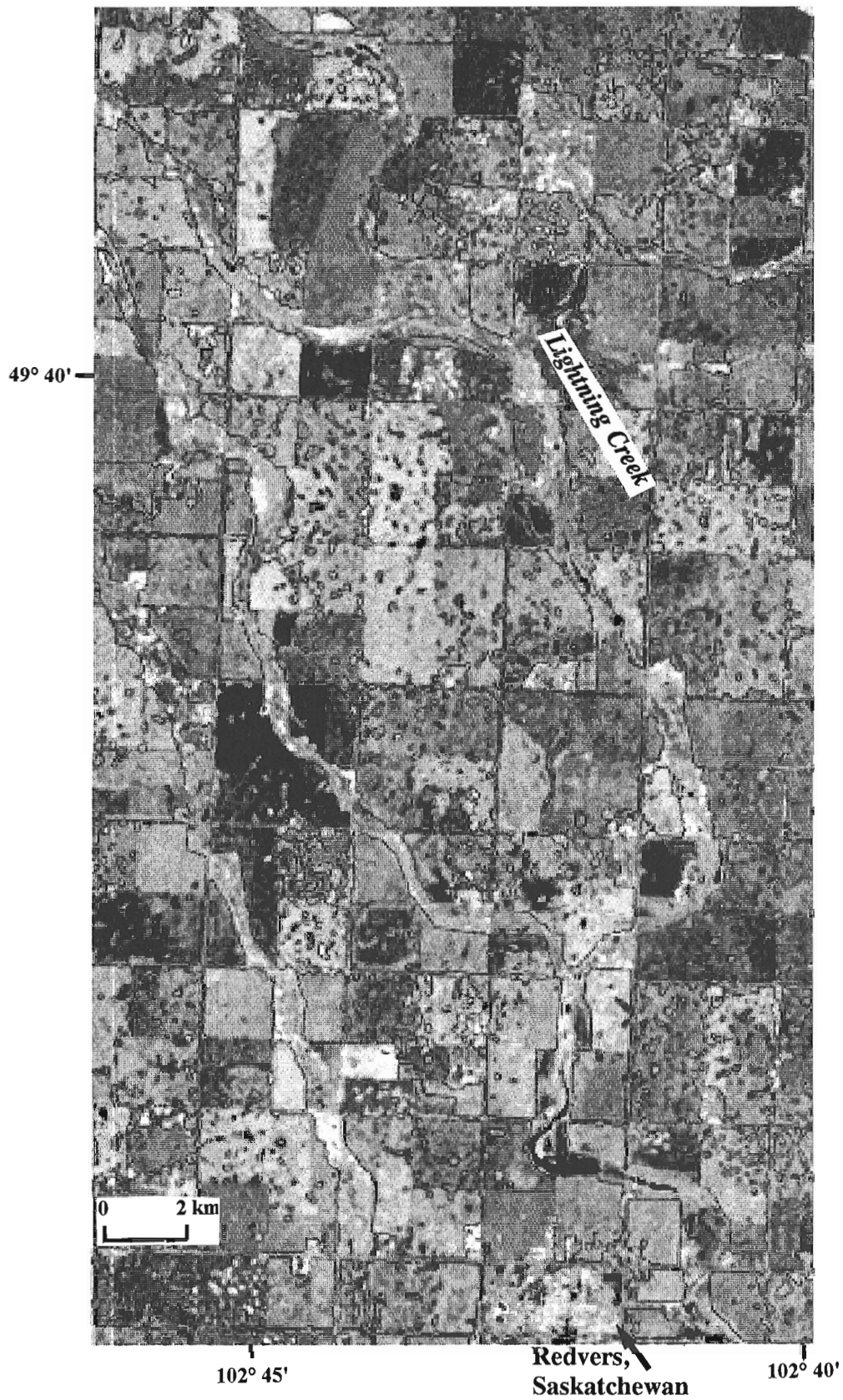


Figure 7. Saturation enhanced spring image of Landsat TM bands 4, 5, and 7. Redvers, Saskatchewan is located in the south central part of NTS 62F/12 map area (Fig.1).

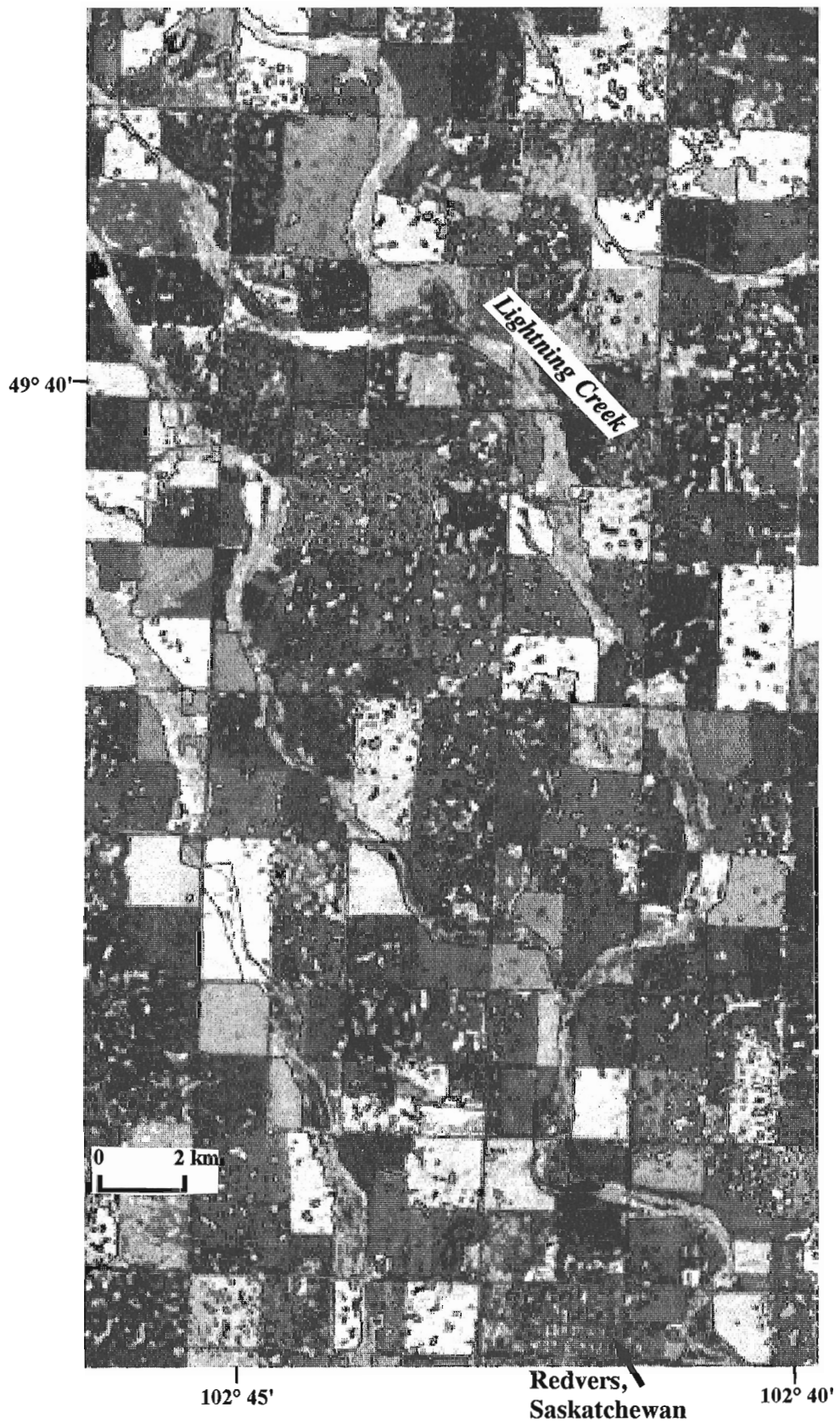


Figure 8. Saturation enhanced late summer image Landsat TM bands 4, 5, and 7. Redvers, Saskatchewan is located in the south central part of NTS 62F/12 map area (Fig.1).

not determined, the late summer saturation enhanced TM image (Fig. 8) seems to delineate the geomorphological features more clearly than the spring saturation file (Fig. 7).

Landsat TM and ERS-1 colour composites

The optimum spring and late summer images that could be used for the detection of soil moisture were generated by integrating TM and ERS-1 (SAR) data and producing enhanced colour composites (Fig. 5). The spectral information from TM of two time periods was complemented by subtle topography and surface roughness information in the ERS-1 (SAR) image. Colour composites of the TM spring and late summer saturation enhanced images with ERS-1 (SAR) showed encouraging results. Due to publication constraints, only black and white image figures are shown.

CONCLUSION

From our preliminary work, it was concluded that the enhanced ERS-1 (SAR) image (Fig. 6) did not reveal many geomorphological features in this flat relief, but only rough outlines of the meandering rivers and some kettled terrain.

The saturation processed TM images (Fig. 7, 8) provide a clearer outline of the meandering streams and kettled till plain represented by black lines on the image. These results were better than the ERS-1 image. The late summer saturation enhancement was superior to the spring image (Fig. 8) for the delineation of geomorphological features (Fig. 7).

Colour composites of ERS-1 and TM data showed encouraging results in outlining geomorphological features. Our objective of comparing moisture differences in the spring and late summer images using image textural differences, which could outline geomorphological features is currently being addressed. This will be realized by future image processing techniques.

ACKNOWLEDGMENTS

Image processing was carried out at the Remote Sensing office operated by the Mineral Resources Division of the Geological Survey of Canada. Discussions with J.R. Bélanger and R.J. Fulton of Terrain Sciences Division have greatly improved the manuscript.

REFERENCES

- Bannatyne, B.B.**
1980: Sphagnum bogs in southern Manitoba and their identification by remote sensing; Manitoba Department of Mines, Resources and Environmental Management, Economic Geology Report ER79-7.
- Fulton, R.J., Thorleifson, L.H., Matile, G., and Blais, A.**
1994: Prairie NATMAP field work and field database structure; in *Current Research 1994-B*; Geological Survey of Canada, p. 69-72.
- Graham, D.F. and Ciesielski, A.**
1994: Combining field observations and remote sensing to map the Grenville Front along the Pascagama River, Québec; in *Current Research 1994-C*; Geological Survey of Canada, p. 343-354.
- Harris, J.R. and Murray, R., and Hirose, T.**
1990: IHS Transform for the integration of radar imagery with other remotely sensed data; *Photogrammetric Engineering and Remote Sensing*, v. 56, no. 12, p. 1631-1641.
- Klassen, R.W.**
1989: Quaternary geology of the southern Canadian Interior Plains; in *Quaternary Geology of Canada and Greenland*, (ed.) R.J. Fulton; Geological Survey of Canada, no. 1, p. 138-174.
- Ma, J., Slaney, V.R., Harris, J.R., Graham, D.F., Ballantyne, S.B., and Harris, D.C.**
1991: Use of Landsat TM data for the mapping of limonitic and altered rocks in the Sulphurets area, central British Columbia; *Proceedings of the 14th Canadian Symposium on Remote Sensing*, p. 419-422.
- Mollard, J.D.**
1986: Correlating natural fracture systems, photolineaments, paleo and modern topography and drainage evolution, groundwater effects in the landscape and oil and gas exploration and exploitation in Saskatchewan and southern Alberta; *Third annual Canadian/American Conference on Hydrogeology*, 55 p.
- Mollard, J.D. and Robert Janes, J.**
1984: Airphoto interpretation and the Canadian landscape; *Energy, Mines, and Resources Canada*, 415 p.
- Sauchyn, D.J.**
1990: Mapping and analysis of soil degradation in southern Saskatchewan; *Challenge of the 1990s*; *Geographic Information Systems Proceedings, National Conference*, Ottawa, p. 107-117.
- Sauer, E.K.**
1980: Air-photo interpretation of glacial stratigraphy and the engineering assessment of terrain in southern Saskatchewan (Canada); *Photogrammetria*, v. 35, p. 207-232.
- Singhroy, V.H., Kenny, F.M., and Barnett, P.J.**
1992: Radar imagery for Quaternary geological mapping in glaciated terrains; *Canadian Journal of Remote Sensing*, v. 18, no. 2., p. 112-117.
- Singhroy, V.H., Lowman, P.D., and Morasse, C.R.**
1993a: Analysis of ERS-1 SAR for structural and surficial mapping in the Sudbury Basin, Canada; *Proceedings 16th Canadian Remote Sensing Symposium*, Sherbrooke, p. 277-282.
- Singhroy, V.H., Slaney, R., Lowman, P.D., Harris, P.J., and Moon, W.**
1993b: RADARSAT and radar geology in Canada; *Canadian Journal of Remote Sensing*, v. 19, no. 4, p. 338-351.
- Singhroy, V.H., Rivard, B., and St-Jean, R., and Guindon, B.**
in press: Guidelines for enhanced SAR image techniques for geological applications; *Proceedings 10th Thematic Conference on Geological Remote Sensing*, San Antonio, Texas, 9 p.

Stress orientation indicators (neotectonic plucking fractures) in bedrock of glacier forefields, southeastern Cordillera, western Canada

J.S. Bell and G.H. Eisbacher¹

Institute of Sedimentary and Petroleum Geology, Calgary

Bell, J.S. and Eisbacher, G.H., 1995: Stress orientation indicators (neotectonic plucking fractures) in bedrock of glacier forefields, southeastern Cordillera, western Canada; in Current Research 1995-B; Geological Survey of Canada, p. 151-159.

Abstract: Polished surfaces of glacier forefields in the southeastern Canadian Cordillera display plucking fractures that are distinctly oblique to glacial striae. They commonly show preferred orientation in each forefield, and formed by basal glacier shearing and opening of extension fractures. We interpret these incipient fractures as signals of stress release during downwasting of glaciers and suggest that they are oriented parallel to S_{Hmax} .

Résumé : Les surfaces polies des avant-champs glaciaires dans la région sud-est de la Cordillère canadienne montrent des fractures de délogement glaciaire qui sont distinctement obliques par rapport aux stries. Elles se sont formées par cisaillement de la base du glacier et par ouverture de fractures de distension et présentent habituellement une orientation préférentielle dans chaque avant-champ. Nous interprétons ces fractures naissantes comme des signes de libération des contraintes au cours de l'amaigrissement glaciaire, et elles seraient orientées parallèlement à S_{Hmax} .

¹ Geologisches Institut, Universität Karlsruhe, Kaiserstrasse 12, D-7500 Karlsruhe, Germany

INTRODUCTION

In 1994, two weeks were spent in the field in Alberta and British Columbia assessing what field methods might be used to gather additional in situ stress data in the Cordillera, since little is known of its stress regime(s) (Adams and Bell, 1991). In particular, we wished to learn whether artificial road cuts and recently deglaciated glacier forefields would yield useful information. This report describes preliminary observations and results from five glacier forefields.

NEAR SURFACE STRESS INDICATORS

Near surface contemporary crustal stress orientation is indicated locally by such features as quarry floor buckles or "pop-ups" (Coates, 1964; Lo, 1978), and by induced bedding plane slip (Schafer, 1979; Bell, 1985). These features form in areas of load removal where geometries and displacements permit a direct inference of stress orientations; Coates (1964) and Adams (1982) also have inferred stress magnitudes from quarry floor buckling. In order for a rock unit to deform in a manner diagnostic of today's lithospheric stress field, recent load removal is required. It is also essential that the rock's response not be affected by its own fabric or by lateral loads such as adjacent steep and extensive slopes. Thus, massive or thickly bedded, isotropic rocks are best suited for this purpose and, furthermore, should be located in areas of low relief or, at least, near valley axes. Many recently excavated rocks have strongly developed planar fabrics (bedding, schistosity) and are cut by numerous multi-generation fractures; therefore, they are essentially destressed and are not able to respond to unloading within a contemporary lithospheric stress field.

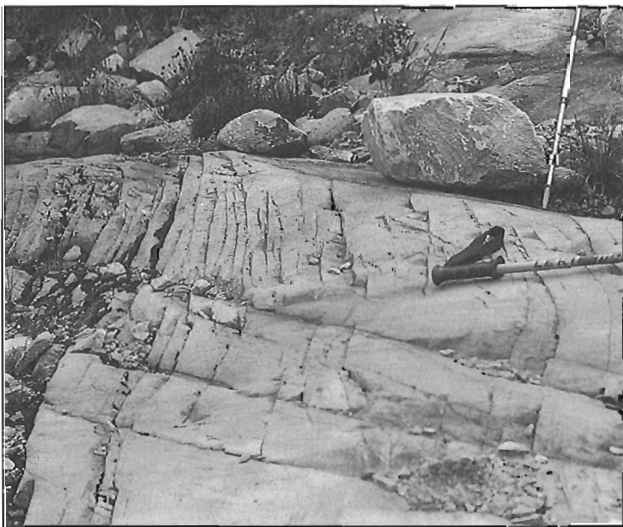


Figure 1. Neotectonic joints in quartzites of the Hamill Group in the Vaux Glacier forefield. Cracks are hairline, discontinuous and have no cementation. They are interpreted as stress relief features parallel to S_{Hmax} .

GLACIAL FOREFIELDS – AREAS OF RECENT LOAD REMOVAL

Most glaciers in the Canadian Cordillera have retreated during the past 150 years and thereby have exposed glacially-eroded forefields in front of their snouts. Bedrock of these forefields has been subject to Holocene glacial erosion and, most importantly, has recently been unloaded. As the glacier snouts thinned by up to several hundreds of metres and thus retreated, a significant ice load was removed above the glacier bed. Elsewhere, earlier workers have recognized the effects of unloading. Gilbert (1904) proposed "dilation from unloading" as one of three possible explanations for the exfoliation of glaciated granite domes in the High Sierra of the western United States, although he did not specifically attribute the unloading to glacial retreat. Fifty years later, Lewis (1954) described up-arching of slabs of gneiss at the snout of the Svellnosbreen glacier and noted that: "the strength of the gneiss presumably enabled it to resist bursting up until the final release of all the superincumbent load on the last retreat of the glacier". He ascribed the up-arching to pressure release and cited Bain's (1931) report of marble bursting during quarrying in Vermont. Both phenomena represent stress-relief buckling (Adams, 1982). Stress relief, however, has a more common manifestation in the form of neotectonic joints (Engelder, 1982; Hancock and Engelder, 1989). These are vertical cracks, parallel to the larger horizontal principal stress (S_{Hmax}) and inferred to form within the upper 0.5 km of the crust due to unloading of differentially stressed rock.

Initially, we anticipated finding stress relief buckles in thin bedded, flat-lying sediments in glacier forefields above which recent glacial retreat had occurred. No such features

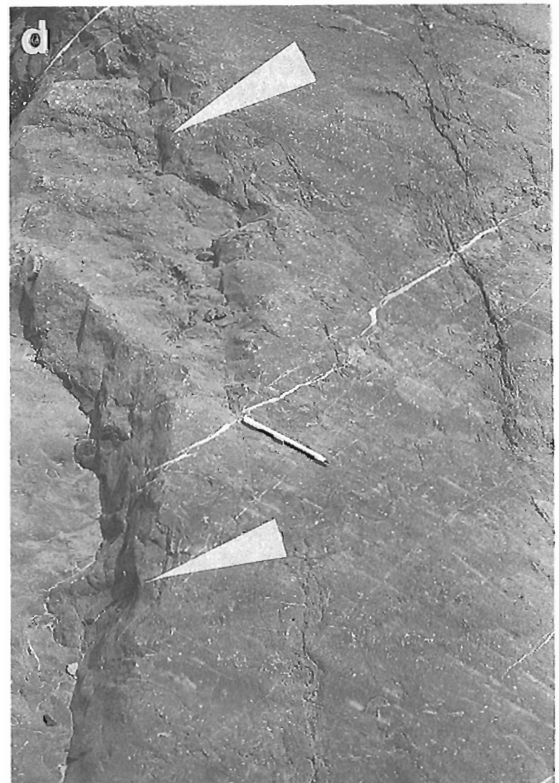
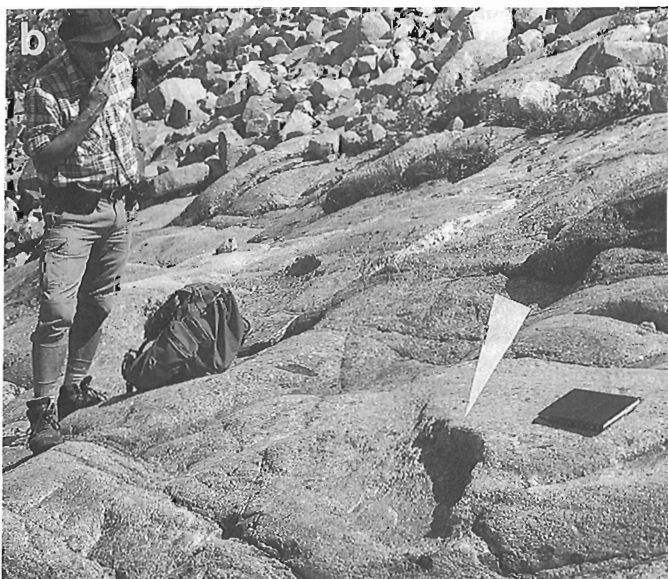
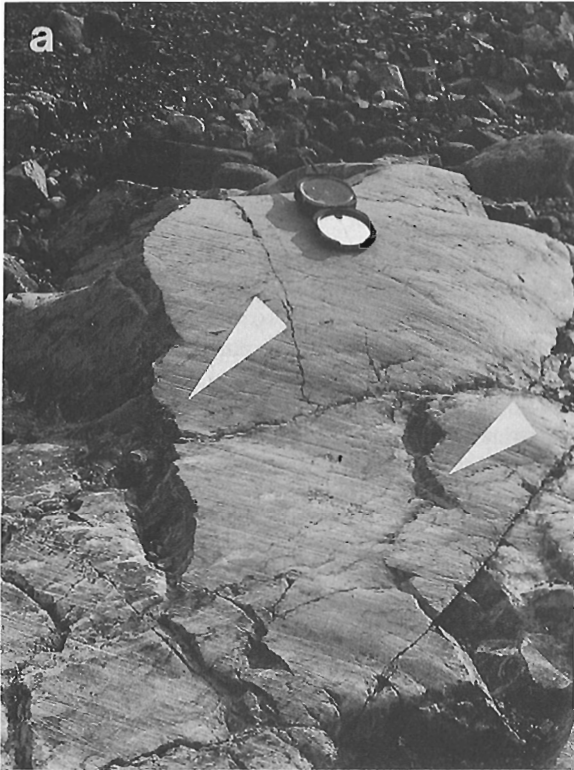
-
- a) Neotectonic plucking fractures in massive limestones in the Athabasca Glacier forefield. Plucking fracture steps, parallel to the Brunton compass, are indicated by the white arrows and are oriented at approximately 50° to the glacial striae. Note the discontinuous hairline fracture to the right of, and parallel to, the largest plucking fracture.
 - b) A plucking fracture (indicated by the white arrow) in granite of the Nelson Batholith in the forefield of the Kokanee Glacier. Glacial striae are parallel to the long axis of the notebook.
 - c) Numerous plucking fractures (parallel to the Brunton compass) oblique to glacial striae in nearly vertically dipping massive limestones. The plucking fracture steps face downstream relative to ice flow in massive Cambrian limestones in the Athabasca Glacier forefield.
 - d) Plucking fracture steps (white arrows) in Takei Formation limestones in the Robson Glacier forefield. Note the parallel microcracks to the right of the plucking fractures. Glacial striae are parallel to the pen.

Figure 2.

were encountered and it soon became apparent that thin bedded rocks were effectively destressed and unable to respond to unloading by buckling. On the other hand, discontinuous hairline fractures with no cementation were found on some polished surfaces (Fig. 1). They exhibited preferred orientations, in common with those described by Hancock and Engelder (1989), and it appeared reasonable to interpret them as diagnostic of the orientation of S_{Hmax} .

Neotectonic Stress-related Plucking Fractures

The most significant findings of this study, however, are what we describe as Neotectonic Plucking Fractures. These occur in rocks that recently have been subject to glacial erosion. They are uneven fracture steps that occur on polished rock surfaces in glacially eroded forefields and, characteristically, they are oriented obliquely to the glacial striae. They record failure by glacial plucking and develop from arrays of short, discontinuous, noncemented hairline fractures that intersect the glacial striae at angles between 20° and 60° (Fig. 2a-d).



Although individual plucking fractures tend to occur as uneven crescentic-shaped steps, the population of plucking fractures exhibits similar strike orientations at a specific site. This preferred orientation suggests that these features may represent a response to stress relief. We attribute their origin to the combined effects of rock stress relief and basal ice shearing during the downwashing stage of glacial retreat (Fig. 3). As a glacier thins and retreats, unloading may generate neotectonic joints in the plane of the vertical principal stress (S_v) and S_{Hmax} at and near the surface of the underlying rocks. If stress relief is not sufficient to generate joints, unloading may weaken the rocks in the S_v - S_{Hmax} plane so that this becomes the preferred axis of rupture. When these rocks are scoured by movement of the glacier above them, chips are plucked from the surface by ice shearing. The moving ice exploits the joints and planes of weakness produced by the unloading and thereby produces arrays of neotectonic plucked fractures with orientations that reflect the underlying rock's stress signature.

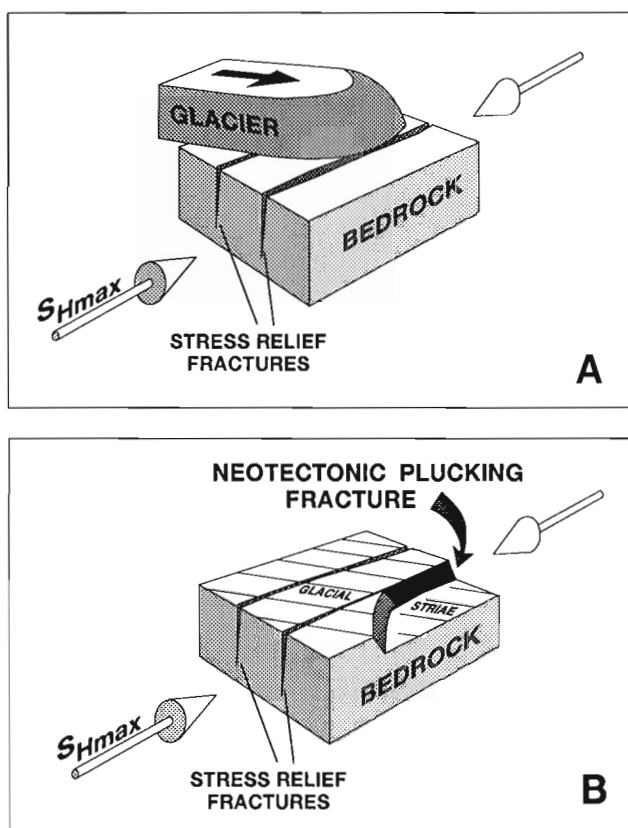


Figure 3. The proposed origin of neotectonic plucking fractures. Initially, as shown in A), stress relief fractures form as the glacier thins and the weight of the ice is reduced. The result of glacial erosion on the underlying rocks is shown in B). A polished surface with glacial striae is produced, while plucking of the underlying rock exploits its stress-relief fabric and gives rise to the ruptured "steps", referred to as neotectonic plucking fractures.

In clearcut cases, such as in the forefield of the Athabasca Glacier, it is easy to identify the neotectonic plucking fractures. They are numerous, their preferred orientation is very apparent and all are oblique to glacial striae. The rocks involved are massive limestones that do not contain weak planar surfaces which could influence the geometry of plucking scars. In other forefields, we encountered rocks containing pre-existing discontinuities such as fissile bedding planes, mineralized joints and schistosity. These fabrics clearly influenced how glacial shearing eroded the rock surfaces. In such cases, it was difficult to recognize plucking fractures that could be clearly diagnostic of in situ stress orientations because of the complex pattern of scars on the polished surfaces.

Our observations suggest that neotectonic plucking fractures should be used to diagnose rock stress orientations only in specific situations, because there are many other factors that influence how rocks will rupture. For plucking scars to reflect in situ stress, the rocks concerned should be massive and not contain any preglacial fabric anisotropy that would influence rupture geometry. In other words, they should be effectively isotropic in their mechanical properties. Furthermore, the polished surfaces should exhibit low relief and low dips. Measurements should be in the central part of a glacial forefield, far from valley walls, so that any lateral loading by adjacent mountainsides does not contribute to the stresses that are relieved by glacial retreat. Finally, the plucking fractures should be oblique to glacial striae; if they are perpendicular to the striae, the possibility exists that they merely record shearing related to the former movement of the glacier.

To our knowledge, oblique neotectonic plucking fractures have not been previously recognized with the genetic connotation that we ascribe to them, although similar features have been described in the literature. Crescentic fractures were recognized by Winchell (1878) on glacialized surfaces in Minnesota, but do not appear to involve plucking. The plucking fractures are more like the chatter marks and crescentic cross fractures which Chamberlin (1888) described as being concave downslope. However, Figure 50 in his paper illustrates a plucked crescentic fracture oblique to the striae on a granitoid rock surface from Victoria, British Columbia. It is very similar to the fractures discussed in this paper. Crescentic fractures, aligned perpendicular to ice movement, were subsequently described by Lahee (1912). Flint (1957), echoing Winchell (1878) and Lahee (1912), noted that crescentic fractures were concave downstream, but did not involve removal of rock. The features most similar to oblique plucked scars that Flint (1957) described were chattermarks that "occur only within large grooves, are concave downstream or are not concave at all, are made by the removal of a chip of rock, and have no fracture that extends deeper than the scar left by the removal of the chip". Unlike Flint's chattermarks, some plucking fractures are associated with fractures that extend deeper than the scar. The cited authors attributed these features to glacial abrasion and quarrying.

LOCALITIES EXAMINED

We examined exposed bedrock in several accessible glacier forefields to determine whether they contain geological indicators of the contemporary stress field. With this objective in view, we concentrated on bedrock forefields where there had been little weathering, and where there was close to 100 per cent outcrop of glacially-polished and relatively massive rock, so that lateral continuity of any observed features could be established. Thin bedded, highly fractured or foliated rocks were avoided, as were areas of pronounced local relief, such as elongate transverse or longitudinal ridges. Both tend to be highly fractured and thus probably dominated by distressed rocks. Data were gathered from relatively massive rocks where topography was smooth, and in parts of the forefields located near valley centres, well away from the potential influence zone of stresses along the toes of steep slopes.

During our study of five bedrock surfaces in the forefields of southeastern Cordilleran glaciers, discontinuous arrays of subparallel, semivertical, clean, hairline cracks with no mineral infilling were observed in massive quartzites of the Vaux Glacier (Fig. 1) and also at Mount Robson. Provisionally, we interpret these cracks as neotectonic joints. They conform to the criteria of Hancock and Engelder (1989) in that they are not stylolites or veins, give no indications of offset by shear, and are the last systematic brittle structures to form in the rocks. They appear to represent stress relief by means of fractures opening in the plane of S_v and S_{Hmax} , as proposed by Hancock and Engelder (1989).

We also observed numerous neotectonic plucking fractures. These features are aligned obliquely to the glacial striae, are not associated with any cemented fractures or with any obvious rock anisotropy, and exhibit a preferred orientation at each site (Fig. 4-8). As inferred above, neotectonic plucking fractures are presumed to have developed through basal shearing below moving ice. Our thesis is that failure, induced

by ice shearing, exploited weaknesses generated by stress relief in the underlying rock. In other words, the glacier plucked off rock weakened by incipient neotectonic fracturing (Fig. 3). We interpret the mean strike of a local population of statistically aligned neotectonic plucking fractures as diagnostic of S_{Hmax} at a specific locality.

1) Robson Glacier forefield (lat. 53.156°N, long. 119.104°W)

Approximately one kilometre north-northwest of the nose of the Robson Glacier, massive limestones of the Middle Cambrian Takei Formation are well exposed over an area of about 0.5 km² within an allochthonous overthrust fault block bounded to the northeast by the Resplendent Fault (Walter, 1980). The Takei Formation limestones strike at 060° to 065° azimuth and dip at 21° to 22° to the southeast. Their polished surfaces are approximately coincident with bedding at this locality. Glacial striae are oriented between 313° and 323° azimuth. Plucking fractures are prominently developed and range in strike from 335° to 035° (Fig. 4). Their mean orientation is 008.3° azimuth with a standard deviation of 13.5° (Mardia, 1972). This is believed to be diagnostic of S_{Hmax} within the allochthonous block underlain by the Resplendent Fault. The cross-sections accompanying the 1:250 000 scale Mount Robson map sheet (Walter, 1980) suggest that the area around Mount Robson may have been subject to Tertiary normal faulting, so the possibility exists that the plucking fractures in the Robson Glacier forefield diagnose stress orientations within a local extensional tectonic province.

2) Athabasca Glacier forefield (lat. 52.208°N, long. 117.235°W)

Numerous neotectonic plucking fractures are displayed on massive bedded Middle Cambrian limestones (Price et al., 1977) that are exposed immediately north of the Athabasca

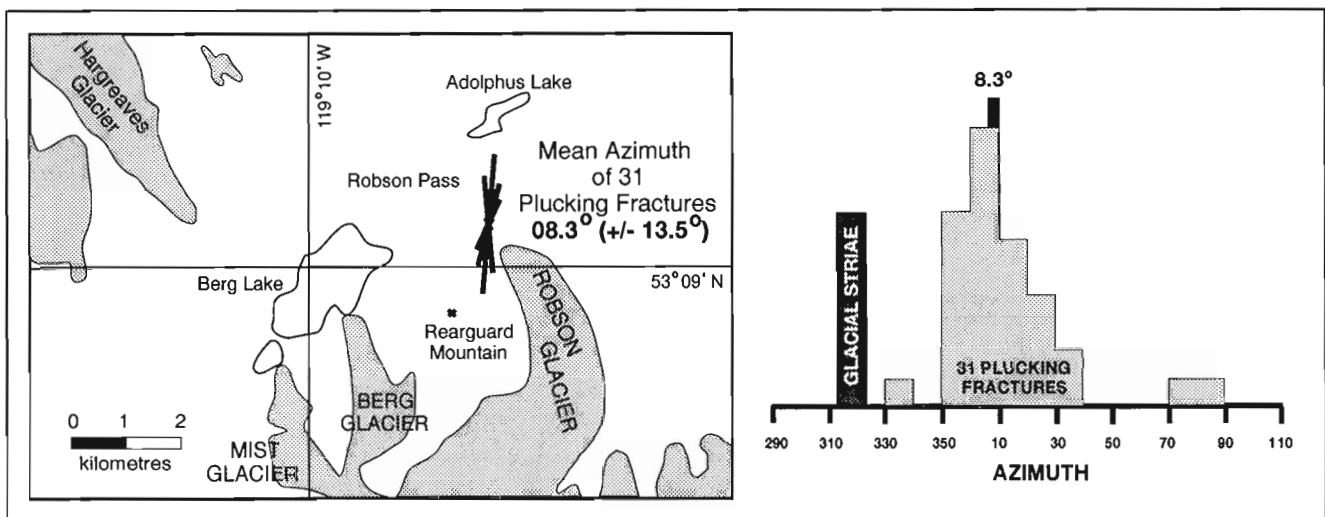


Figure 4. The location of plucking fractures measured in the forefield of the Robson Glacier. The 31 plucking fractures have a mean orientation of 008.3° azimuth. The histogram illustrates the spread of the measurements and their orientations with respect to glacial striae.

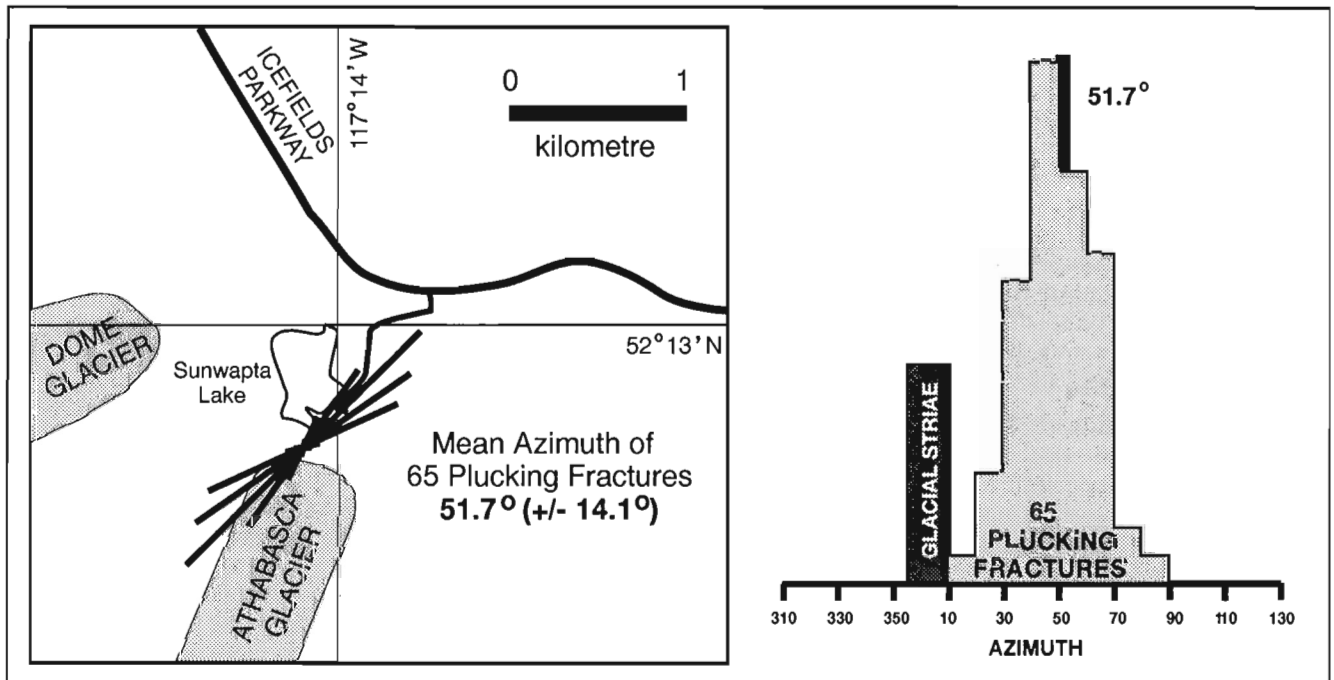


Figure 5. The location of plucking fractures measured in the forefield of the Athabasca Glacier. The 65 plucking fractures have a mean orientation of 051.7° azimuth. The histogram illustrates the distribution of the population.

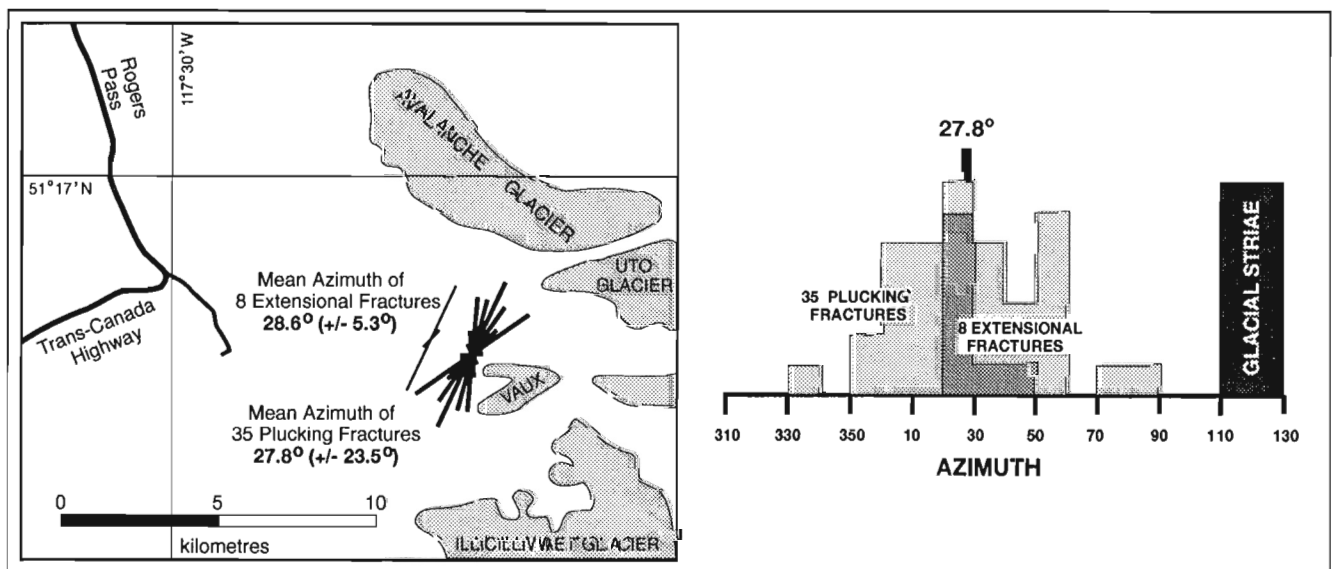


Figure 6. Plucking fractures and extensional fractures measured in the forefield of the Vaux glacier. The mean azimuth of the eight extensional fractures was 028.6° azimuth, very close to the 027.8° azimuth mean orientation of the 35 plucking fractures. All measurements were centred in a location near the origin of the plucking fracture rose diagram. The associated histogram illustrates the spread of the measurements and their orientations with respect to glacial striae.

Glacier between the glacier nose and Sunwapta Lake (Fig. 5). The limestone strikes range from 127° to 138° azimuth (northwest) and dips are steep, varying between 80° to the northwest and 85° to the southeast. The polished surfaces are less inclined, with dips in various directions ranging from 015° to 025° azimuth. They are marked by glacial striae that trend northward; directions vary from 014° to 355° azimuth. Numerous plucking fractures traverse the polished surfaces, oblique to the glacial striae. Plucking fracture strikes range

from 017° to 082° with the majority between 030° and 070° (Fig. 5). Sixty-five readings were made and, as Figure 5 demonstrates, they fall into a normally distributed population with respect to their orientations. According to our interpretation, these plucking fractures imply that S_{Hmax} is oriented at 051.7° azimuth with a standard deviation of 14.1° (Mardia, 1972) at this locality. This azimuth is believed to be representative of in situ stresses within the Simpson Pass thrust sheet underlying the Columbia icefield.

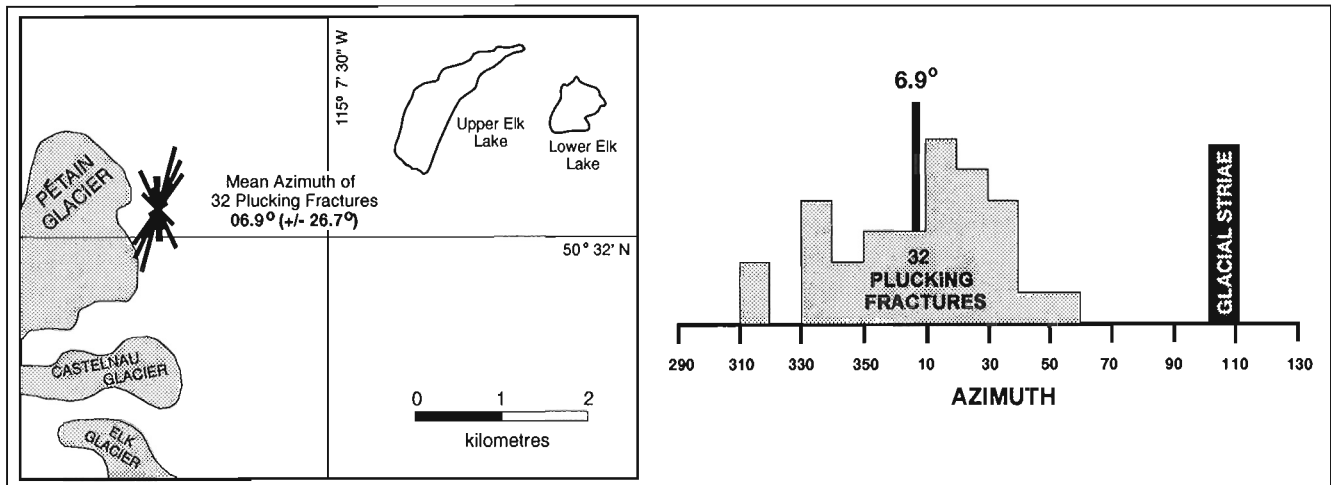


Figure 7. The location of plucking fractures measured in the forefield of the Pétain Glacier. The 31 plucking fractures gave a mean orientation of 006.9° azimuth. The histogram illustrates the spread of the measurements and their orientations with respect to glacial striae.

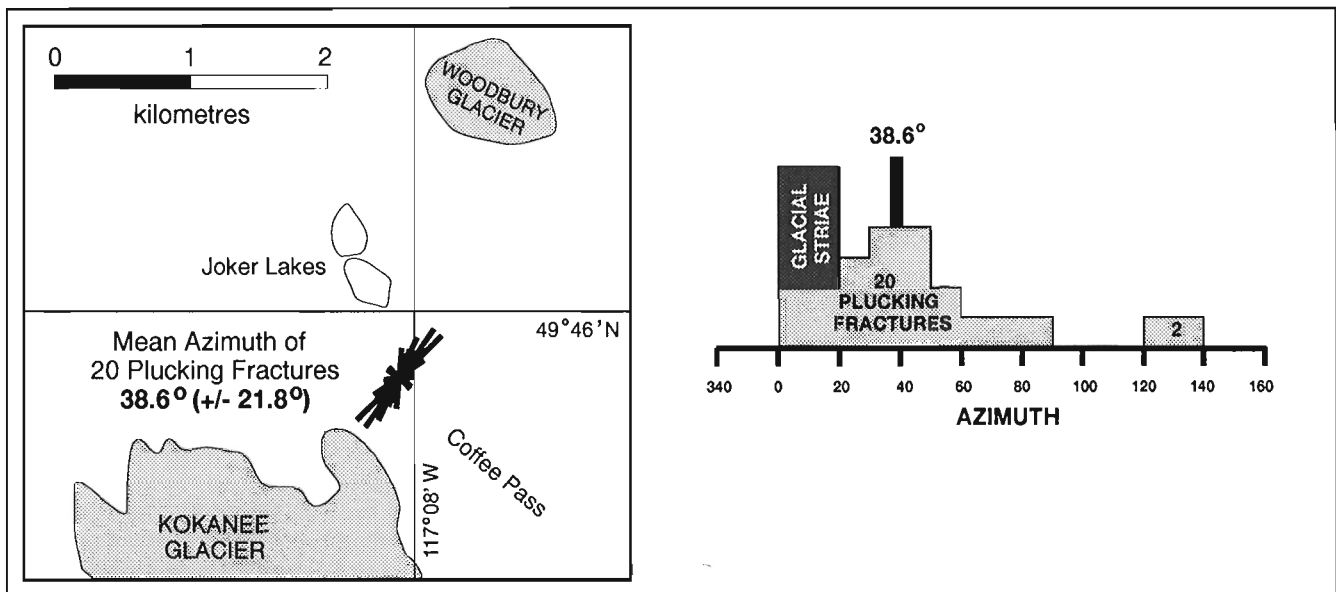


Figure 8. The location of plucking fractures measured in the forefield of the Kokanee Glacier. Twenty-two plucking fractures were measured and fall into two populations as shown by the histogram. The major population exhibits a mean azimuth of 038.6°. The histogram illustrates the spread of the measurements and their orientations with respect to glacial striae.

3) Vaux Glacier forefield (lat. 51.263°N, long. 117.453°W)

The Vaux glacier is a small icefield that was formerly part of the Illicilliwaet Glacier to the north (Fig. 6). The north side of its forefield is underlain by quartzites of the Cambrian Hamill Group (Wheeler, 1963), and these rocks exhibit well-developed plucking fractures. The south side of the Vaux glacier forefield is underlain by thin bedded argillaceous rocks that are highly fractured and foliated. Despite careful examination, we found no clearcut plucking fractures in them. They appear to be effectively destressed.

The massive quartzites in the Vaux glacier forefield strike northwest and exhibit dips ranging from 24° to 45° to the southwest. Polished surfaces either coincide with bedding or have been eroded so that their dip is slightly less (10°-20°). Glacial striae directions range from 310° to 265° azimuth, varying locally according to the topography. Plucking fractures,

especially steps, are well-developed on the polished surfaces and strike obliquely to the glacial striae. As Figure 6 illustrates, 35 strike directions were measured, varying from 337° to 088° azimuth. The mean orientation, interpreted as diagnostic of S_{Hmax} , is 027.8° azimuth with a standard deviation of 23.5° (Mardia, 1972). In addition, eight measurements were made of discontinuous uncemented hairline cracks (Fig. 1), they have a mean strike of 028.6° azimuth ($\pm 5.3^\circ$).

4) Pétain Glacier forefield (lat. 50.543°N, long. 115.161°W)

Massive Mississippian Mount Head Formation limestones are exposed east of the nose of the Pétain Glacier (McMechan, 1993). In the area examined, the beds strike north-northwest and dip at 5° to 10° to the southwest. The bedding surfaces are polished with glacial striae oriented from 281° to 291° azimuth. Plucking fractures are abundant and their strikes range in orientation from 311° to 55° azimuth. The mean direction was 6.9° azimuth with a standard deviation of 26.7° (Fig. 7). Provisionally, this orientation is believed to be diagnostic of S_{Hmax} within the Bourgeau thrust sheet in the region.

5) Kokanee Glacier forefield (lat. 49.769°N, long. 117.137°W)

The Kokanee Glacier rests on porphyritic granites of the Nelson Batholith (Little, 1980). A forefield slope, dipping at 25° to 35° to the north-northwest, was examined south of Joker Lakes (Fig. 8). The orientations of glacial striae range from 000° to 020° azimuth. Plucking fractures are present, but are not prominently developed on this surface (Fig. 2b). We measured 22 examples (Fig. 8). Twenty of them fall into a population with a mean strike of 038.6° azimuth (standard deviation 21.8°). Two plucking fractures are oriented differently (125° and 139°), approximately at right angles to the main group. Provisionally, we interpret S_{Hmax} orientation in this area as 038.6 \pm 21.8° azimuth.

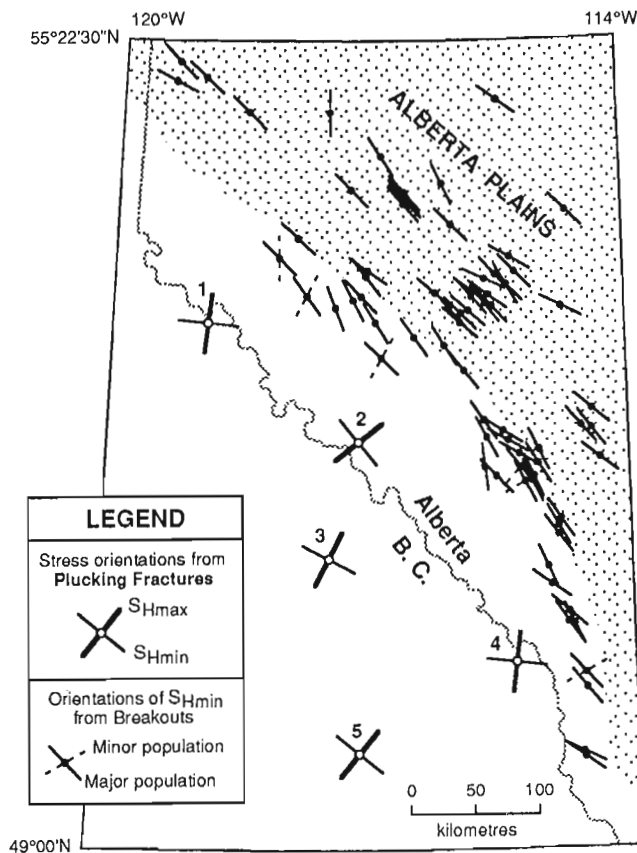


Figure 9. Stress orientations inferred from plucking fracture measurements in the forefields of (1) Robson Glacier, (2) Athabasca Glacier, (3) Vaux Glacier, (4) Pétain Glacier, and (5) Kokanee Glacier. Also shown are S_{Hmin} orientations derived from mean breakout azimuths measured in wells in the Rocky Mountain Foothills and Alberta Plains (Bell and Babcock, 1986). Note that the plucking fracture orientations are reasonably compatible with the breakout axes.

DISCUSSION AND CONCLUSIONS

The recognition of plucking fractures on polished surfaces in recently unloaded glacier forefields, and their interpretation as stress-related rupture surfaces, appears to offer a new tool for measuring contemporaneous in situ stress orientations in the field. The measurements yield mean orientations that are compatible with stress axes in adjacent areas that have been measured with wellbore breakouts (Fig. 9). The interpreted S_{Hmax} orientations are reasonable, particularly those from sites 2, 3 and 5 (Fig. 9). Our fieldwork has demonstrated that consistent measurements can be made, provided massive, nearly isotropic rocks are sampled, and care is taken to ensure that preglacial planes of weakness are not responsible for generating the fractures. Plucking fractures may be widespread on recently unloaded glaciated surfaces and, if so, they

could be an excellent tool for mapping contemporary stress orientations in regions of Canada where no other sources of data are available. Since the phenomenon appears to be developed in massive rocks only, plucking fractures may be present in rocks of the Canadian Shield in areas where little is known of the stress regime, provided that erosion has not destroyed them. Recent extensional fractures may also provide supportive orientations.

Our field studies suggest that it will be necessary to gather 30 to 50 strike measurements of plucking fractures at a specific site in order to assess the S_{Hmax} orientation. Typically, there is considerable directional scatter which is due in part to the crescentic shape of many plucking fractures. Before more studies are undertaken, however, it is necessary to validate the method. The authors believe this could be achieved most effectively by sampling a series of closely located forefields, such as those around one particular ice field, to compare readings from closely spaced localities which had been scoured by glaciers moving in different directions. If common plucking fracture orientations occur in all localities, this would strongly support the fractures being diagnostic of the regional stress regime. Confirmation might also be provided by flat-jack tests at specific sites (Froidevaux et al., 1980), or by hydraulic fracturing in shallow boreholes (J. R. Enever, pers. comm., 1994). Given successful validation, it is proposed to examine more glacial forefields in the Canadian Cordillera to augment our current understanding of the contemporary stress regime(s); there is little of this information available in much of the mountain belt.

It should be emphasized that only preliminary interpretations of the orientation of S_{Hmax} are presented here. Plucking fractures tell us nothing about the relative magnitudes of the principal stresses. A thrust regime ($S_{Hmax} > S_{Hmin} > S_v$) or strike-slip regime ($S_{Hmax} > S_v > S_{Hmin}$) could be present, or a specific site could be in a tectonically extensional setting ($S_v > S_{Hmax} > S_{Hmin}$). Nor is it clear whether the interpreted stress orientations obtained from plucking fractures in the southeastern Cordillera apply to the entire upper lithosphere, or refer only to the allochthonous units in which they were measured. Future work is expected to shed light on this issue.

ACKNOWLEDGMENTS

J.W.H. Monger encouraged the undertaking of this study as part of a collaborative effort within the Geological Survey of Canada to compile a Cordilleran Stress Map, which he is coordinating. G. S. Stockmal and R. W. Macqueen reviewed the manuscript and we are grateful for their suggestions for improving it. H. Geldsetzer and G. Osborn guided the authors to suitable glacial forefields.

REFERENCES

- Adams, J.**
1982: Stress-relief buckles in the McFarland Quarry, Ottawa; Canadian Journal of Earth Sciences, v. 19, p. 1883-1887.
- Adams, J. and Bell, J.S.**
1991: Crustal Stresses in Canada; in Neotectonics of North America, (ed.) D.B. Slemmons, E.R. Engdahl, M.D. Zoback, and D.D. Blackwell; Geological Society of America, Decade Map Volume 1, p. 367-386.
- Bain, G.W.**
1931: Spontaneous rock expansion; Journal of Geology, v. 39, p. 715-735.
- Bell, J.S.**
1985: Offset boreholes in the Rocky Mountains of Alberta, Canada; Geology, v. 13, p. 734-737.
- Bell, J.S. and Babcock, E.A.**
1986: The stress regime of the Western Canadian Basin and implications for hydrocarbon production; Bulletin of Canadian Petroleum Geology, v. 34, p. 364-378.
- Chamberlin, T.C.**
1888: The Rock Scourings of the Great Ice Invasions; in Seventh Annual Report of the United States Geological Survey 1885-1886, Washington, Government Printing Office.
- Coates, D.F.**
1964: Some cases of residual stress effects in engineering work; in State of Stress in the Earth's crust, (ed.) W.R. Judd; New York, Elsevier, p. 679-688.
- Engelder, T.**
1982: Is there a genetic relationship between selected regional joints and contemporary stress within the lithosphere of North America? Tectonics, v. 1, p. 161-177.
- Flint, R.F.**
1957: Glacial and Pleistocene Geology; Wiley, New York, 553 p.
- Froidevaux, C., Paquin, C., and Souriau, M.**
1980: Tectonic stresses in France: In situ measurements with a Flat Jack; Journal of Geophysical Research, v. 85, p. 6342-6345.
- Gilbert, G.K.**
1904: Domes and Dome Structure of the High Sierra; Geological Society of America Bulletin, v. 15, p. 29-36.
- Hancock, P.L. and Engelder, T.**
1989: Neotectonic Joints; Geological Society of America Bulletin, v. 101, p. 1197-1208.
- Lahee, F.H.**
1912: Crescentic Fractures of Glacial Origin; American Journal of Science, v. 33, p. 41-44.
- Lewis, W.V.**
1954: Pressure release and glacial erosion; Journal of Glaciology, v. 2, p. 417-422.
- Little, H.W.**
1980: Nelson Map-Area, West Half, British Columbia (82F W1/2); Geological Survey of Canada, Memoir 308, 205 p.
- Lo, K.Y.**
1978: Regional distribution of in situ horizontal stresses in rocks of southern Ontario; Canadian Geotechnical Journal, v. 15, p. 371-381.
- Mardia, K.V.**
1972: Statistics of directional data: probability and mathematical statistics; Academic Press, New York, 357 p.
- McMechan, M.E.**
1993: Geology of the Rocky Mountain Foothills and Front Ranges in Kananaskis Country, southwest of Calgary, Alberta; Geological Survey of Canada, Open File 2642.
- Price, R.A., Stott, D.F., Campbell, R.B., Mountjoy, E.W., and Ollerenshaw, N.C.**
1977: Athabasca River, Alberta - British Columbia, Sheet 83; Geological Survey of Canada, Map 1339a.
- Schafer, K.**
1979: Recent thrusting in the Appalachians; Nature, v. 280, p. 223-226.
- Walter, D.J.**
1980: Geology, Mount Robson, west of sixth meridian, Alberta - British Columbia; Map 1499A, scale 1:250 000.
- Wheeler, J.O.**
1963: Rogers Pass Map-Area, British Columbia and Alberta (82N W1/2); Geological Survey of Canada, Paper 62-32, 32 p.
- Winchell, N.H.**
1878: The Drift; in The Geological and Natural History Survey of Minnesota, The Sixth Annual Report, for the year 1877, Smith and Harrison, Minneapolis, p. 104-109.

AUTHOR INDEX

Abercrombie, H.J.	125	McDonough, M.R.	125
Allen, V.S.	99	McIntyre, D.J.	109
Alt, B.T.	71	Nassichuk, W.W.	109, 115
Beauchamp, B.	1, 9, 19, 29, 37, 47, 57, 65	Nixon, F.M.	99
Bell, J.S.	151	Ollerhead, J.	131
Blais, A.	141	Sherry, C.T.	37
Bourgeois, J.C.	71	Singhroy, V.H.	141
Desrochers, A.	37, 47, 57, 65	Smith, S.L.	81
Eisbacher, G.H.	151	Stasiuk, L.D.	115
Graham, D.F.	141	Steel, R.	29
Harrison, J.C.	1, 9, 19, 29, 37, 65	Stevens, W.R.	141
Huntley, D.J.	131	Taylor, A.E.	89, 99
Judge, A.S.	81	Thériault, P.	29
Kells, M.P.	47	Wolfe, S.A.	131
Mayr, U.	1, 9, 19, 29, 37, 65	Wright, F.	99

Geological Survey of Canada Current Research, is released twice a year, in January and July. The four parts published in January 1995 (Current Research 1995- A to D) are listed below and can be purchased separately.

Recherches en cours, une publication de la Commission géologique du Canada, est publiée deux fois par année, en janvier et en juillet. Les quatre parties publiées en janvier 1995 (Recherches en cours 1995-A à D) sont énumérées ci-dessous et sont vendues séparément.

Part A: Cordillera and Pacific Margin
Partie A : Cordillère et marge du Pacifique

Part B: Interior Plains and Arctic Canada
Partie B : Plaines intérieures et région arctique du Canada

Part C: Canadian Shield
Partie C : Bouclier canadien

Part D: Eastern Canada and national and general programs
Partie D : Est du Canada et programmes nationaux et généraux